

# CATALYTIC ACTIVITIES OF VANADIUM, MANGANESE AND COPPER COMPLEXES IMMOBILIZED IN ZEOLITE-Y

## A THESIS

*Submitted in partial fulfilment of the  
requirements for the award of the degree*

*of*

DOCTOR OF PHILOSOPHY

*in*

CHEMISTRY

*by*

**PRIYANKA SAINI**



DEPARTMENT OF CHEMISTRY  
INDIAN INSTITUTE OF TECHNOLOGY ROORKEE  
ROORKEE-247 667 (INDIA)

JULY, 2011

**©INDIAN INSTITUTE OF TECHNOLOGY ROORKEE, ROORKEE 2011  
ALL RIGHTS RESERVED**



# INDIAN INSTITUTE OF TECHNOLOGY ROORKEE ROORKEE

## CANDIDATE'S DECLARATION

I hereby certify that the work which is being presented in the thesis entitled **CATALYTIC ACTIVITIES OF VANADIUM, MANGANESE AND COPPER COMPLEXES IMMOBILIZED IN ZEOLITE-Y** in partial fulfilment of the requirements for the award of the Degree of Doctor of Philosophy and submitted in the Department of Chemistry of the Indian Institute of Technology Roorkee is an authentic record of my own work carried out during a period from January, 2008 to July, 2011 under the supervision of Dr. Mannar R. Maurya, Professor, Department of Chemistry, Indian Institute of Technology Roorkee, Roorkee.

The matter presented in the thesis has not been submitted by me for the award of any other degree of this or any other Institute.

*Priyanka Saini*  
(Priyanka Saini)

This is to certify that the above statement made by the candidate is correct to the best of my knowledge.

Date: *July 12, 2011*

*Mannar R. Maurya*  
(Mannar R. Maurya)  
Supervisor

The Ph. D. Viva-Voce Examination of **Miss Priyanka Saini**, Research Scholar, has been held on *September 07, 2011* .....

*Mannar R. Maurya*  
Signature of Supervisor  
*7.9.2011*

*B. S. Sam*  
Signature of External Examiner

*Chairman SRC*

*Wei*

## ABSTRACT

---

Catalysts have played key role in the development of modern chemical technologies. They activate the chemical reaction at milder conditions through the bonding of reactant molecules with definite functional groups called 'active sites', where they react and finally detach from the catalyst for the next cycle. As large as 95 % processes used in the chemical industries there days are catalyst based technologies. Directly or indirectly catalysts have contributed to more than 20 % GDP of developed nations. Most of the catalytic processes, which are widely used in the manufacture of bulk as well as fine chemicals, are homogeneous in nature. A large amount of waste materials has been produced during these processes which imposed a hazardous impact on the environment. Homogeneous catalysts also face the problem of separation from the substrate and products. Therefore, there is a necessity to create new highly effective industrial processes, which are selective, ecologically safe and consume minimum energy. The efficient use of the solid supported catalysts can go a long way towards achieving these goals. As a consequence of the inherent advantages of the heterogeneous catalytic system over their homogeneous counter part, efforts have been directed towards the development of heterogeneous systems. Various methodologies have been evolved for the immobilization of homogeneous transition metal complexes. Encapsulation of homogeneous catalysts in the super cages of zeolite matrix is one of the important methods for the immobilization. This method has provided opportunity to develop catalytic processes in the synthesis of fine chemicals and being used in various types of catalytic reactions like alkylation, hydrogenation, dehydrogenation, hydro-cracking, cyclization, amination, acylation, isometization, rearrangement and oxidation. The catalytic oxidation of organic substrates has been studied well due to its commercial and synthetic importance of the resulted functionalized molecules. All these encouraged us to design zeolite-Y



encapsulated metal complexes and use them as catalysts for various oxidation reactions.

The thesis entitled “Catalytic activities of vanadium, manganese and copper complexes immobilized in zeolite-Y”, describes the synthesis of vanadium, manganese and copper complexes with potential coordinating organic ligands encapsulated in the nano-cavity of zeolite-Y and their characterization by various physico-chemical techniques. Different types of catalytic oxidation reactions have been carried out and suitable reaction conditions have been obtained for the maximum oxidation of organic substrates. The reaction products have been analyzed by gas chromatograph (GC) and their identities confirmed by GC-MS. For convenience the work presented in the thesis has been divided in the following chapters.

**First chapter** is the introductory one and describes various types of solid inert support that have been used for the immobilization of homogeneous catalysts. Literature on the catalytic applications of various encapsulated metal complexes has also been reviewed.

In **Second Chapter**, complexes  $[\text{Mn}^{\text{III}}(\text{pydx-en})\text{Cl}(\text{H}_2\text{O})]$  (**1.1**)  $[\text{Mn}^{\text{III}}(\text{pydx-1,3-pn})\text{Cl}(\text{CH}_3\text{OH})]$  (**1.2**) and  $[\text{Mn}^{\text{III}}(\text{pydx-1,2-pn})\text{Cl}(\text{H}_2\text{O})]$  (**1.3**) have been prepared by the reaction of  $\text{Mn}^{\text{II}}(\text{CH}_3\text{COO})_2$  with dibasic tetradentate ligands, *N,N'*-ethylenebis (pyridoxylideneiminato) ( $\text{H}_2\text{pydx-en}$ , **I**), *N,N'*-propylenebis(pyridoxylideneiminato) ( $\text{H}_2\text{pydx-1,3-pn}$ , **II**) and 1-methyl-*N,N'*-ethylenebis(pyridoxylideneiminato) ( $\text{H}_2\text{pydx-1,2-pn}$ , **III**), respectively followed by aerial oxidation in the presence of LiCl. Crystal and molecular structures of  $[\text{Mn}(\text{pydx-en})\text{Cl}(\text{H}_2\text{O})]$  (**1.1**) and  $[\text{Mn}(\text{pydx-1,3-pn})\text{Cl}(\text{CH}_3\text{OH})]$  (**1.2**) confirm their octahedral geometry and the coordination of ligands through ONNO(2-) form. These complexes have also been encapsulated in the super cages of zeolite-Y. The encapsulated complexes have been used as catalysts for the oxidation, by  $\text{H}_2\text{O}_2$ , of methyl phenyl sulphide, styrene and benzoin efficiently. Oxidation of methyl phenyl sulphide under the optimized reaction conditions gave ca. 86 % conversion

with two major products methyl phenyl sulfoxide and methyl phenyl sulfone in the ca. 70 % and 30 % selectivity, respectively. Oxidation of styrene catalyzed by these complexes gave at least five products namely styrene oxide, benzaldehyde, benzoic acid, 1-phenylethane-1,2-diol and phenylacetaldehyde with a maximum of 76.9 % conversion of styrene by  $[\text{Mn}^{\text{III}}(\text{pydx-en})\text{Cl}(\text{H}_2\text{O})]\text{-Y}$  (**2.4**), 76.3 % by  $[\text{Mn}^{\text{III}}(\text{pydx-1,3-pn})\text{Cl}(\text{H}_2\text{O})]\text{-Y}$  (**2.5**) and 76.0 % by  $[\text{Mn}^{\text{III}}(\text{pydx-1,2-pn})\text{Cl}(\text{H}_2\text{O})]\text{-Y}$  (**2.6**) under optimized conditions. Similarly, ca. 93% conversion of benzoin has been obtained by these catalysts, where the selectivity of the products followed the order: benzil > benzoic acid > benzaldehyde-dimethylacetal. Tests for the recyclability and heterogeneity of the reactions have also been carried. Neat complexes are equally active. However, the recycle ability of encapsulated complexes makes them better over neat ones.

**Third Chapter** describes the synthesis of zeolite-Y encapsulated oxidovanadium(IV) complexes, abbreviated herein as  $[\text{V}^{\text{IV}}\text{O}(\text{pydx-en})]\text{-Y}$  (**3.4**),  $[\text{V}^{\text{IV}}\text{O}(\text{pydx-1,3-pn})]\text{-Y}$  (**3.5**) and  $[\text{V}^{\text{IV}}\text{O}(\text{pydx-1,2-pn})]\text{-Y}$  (**3.6**), with  $\text{H}_2\text{pydx-en}$ ,  $\text{H}_2\text{pydx-1,3-pn}$  and  $\text{H}_2\text{pydx-1,2-pn}$ , respectively. Neat complexes  $[\text{V}^{\text{IV}}\text{O}(\text{pydx-en})]$  (**3.1**),  $[\text{V}^{\text{IV}}\text{O}(\text{pydx-1,3-pn})]$  (**3.2**) and  $[\text{V}^{\text{IV}}\text{O}(\text{pydx-1,2-pn})]$  (**3.3**) have also been prepared. Spectroscopic studies (IR, UV/Vis and EPR), elemental analyses, thermal studies, field emission scanning electron micrographs (FE-SEM) and X-ray diffraction patterns are used to characterize these complexes. Oxidations of styrene, cyclohexene and methyl phenyl sulfide have been investigated using these complexes as catalyst precursors in the presence of  $\text{H}_2\text{O}_2$  as oxidant. Under the optimized reaction conditions, a maximum of 85.5 % conversion of styrene has been obtained with **3.4**, 84.6 % conversion with **3.5** and 82.9 % conversion with **3.6** in 6 h of reaction time. The selectivity of the various products is similar for the catalyst precursors (i.e. complexes **3.4** to **3.6**) and follows the order: benzaldehyde > 1-phenylethane-1,2-diol > benzoic acid > phenyl acetaldehyde. With cyclohexene, a maximum conversion of 95.9 % has been achieved with **3.4**, 94.5 % with **3.5** and 94.2 % conversion with **3.6**, also in 6 h of reaction time. The

selectivity of the various products is similar for the three catalysts: 2-cyclohexene-1-one > 2-cyclohexene-1-ol > cyclohexane-1,2-diol. The oxidation of methyl phenyl sulfide is achieved with **3.4**, **3.5** and **3.6** in 2.5 h of reaction time with 85.5 %, 82.1% and 80% conversion, with higher selectivity towards sulfoxide. UV-Vis and  $^{51}\text{V}$  NMR experiments with **3.1** confirm the plausible formation of  $\text{V}^{\text{V}}\text{O}(\text{O}_2)\text{L}$  as intermediates in the catalytic oxidations.

Reaction of  $\text{Mn}^{\text{II}}(\text{CH}_3\text{COO})_2$  with tribasic pentadentate ligand,  $\text{H}_3\text{sal-dahp}$  obtained by the condensation of salicylaldehyde and 1,3-diamino-2-hydroxypropane followed by aerial oxidation gives  $[\text{Mn}^{\text{III}}(\text{sal-dahp})(\text{H}_2\text{O})]$  (**4.1**). Its encapsulation in zeolite-Y, abbreviated herein as  $[\text{Mn}^{\text{III}}(\text{sal-dahp})(\text{H}_2\text{O})]\text{-Y}$  (**4.2**), has been achieved by the reaction of Mn(II)-exchanged zeolite-Y with  $\text{H}_3\text{sal-dahp}$  in refluxing methanol, followed by aerial oxidation. Studies on these complexes are described in **Fourth Chapter**. Both the complexes are characterized by various physico-chemical studies. Oxidation of benzoin with  $\text{H}_2\text{O}_2$  has been investigated using  $[\text{Mn}^{\text{III}}(\text{sal-dahp})(\text{H}_2\text{O})]\text{-Y}$  as catalyst as oxidant. Under optimized reaction conditions a maximum of 86.1% conversion of benzoin is achieved in 6 h of reaction time. The selectivity of the various products follows the order: benzoic acid (64.3 %) > benzil (22.3 %) > benzaldehyde-dimethylacetal (13.4 %). Neat complex is equally active and the oxidation products obtained also follow the same order of selectivity. Two possible mechanisms, one via  $\text{Mn}^{\text{IV}}=\text{O}$  containing intermediate compound formation and second via direct interaction of benzoin with manganese have been proposed through which various substrates form.

In **Fifth Chapter**, synthesis of  $[\text{Cu}^{\text{II}}(\text{acpy-oap})\text{Cl}]$  by the reaction of monobasic tridentate ligand,  $\text{Hacpy-oap}$  ( $\text{Hacpy-oap}$  = Schiff base derived from 2-acetylpyridine and o-aminophenol) with  $\text{Cu}^{\text{II}}\text{Cl}_2$  in refluxing methanol is presented. Elemental analysis and spectral (IR and electronic) studies confirm its distorted square planar structure. Complex  $[\text{Cu}^{\text{II}}(\text{acpy-oap})\text{Cl}]$  has also been encapsulated in the nano cavity of zeolite-Y and its encapsulation ensured by various physico-

chemical techniques. Neat as well as encapsulated both complexes are active catalysts for the oxidation of styrene and cyclohexene using tert-butylhydroperoxide (TBHP). Reaction conditions for the maximum oxidation of these substrates have been optimized by considering the concentration of oxidant, amount of catalyst, volume of solvent and temperature of the reaction mixture. Under the optimised conditions styrene gave a maximum of 60.2% conversion in 7 h with mainly two reaction products namely styrene oxide and benzaldehyde. Oxidation of cyclohexene required 6 h to give 61.3% conversion where cyclohexene epoxide, 2-cyclohexene-1-one, 2-cyclohexene-1-ol and cyclohexane-1,2-diol are obtained as major oxidation products. Catalyst  $[\text{Cu}^{\text{II}}(\text{acpy-oap})\text{Cl}]$  does not leach metal ion during catalytic activity and is recyclable.

Finally, summary and over all conclusions based on the achievements are presented.

## *Acknowledgements*

*Its time to thank to all those who have helped me during my research in their own special ways.*

*First and foremost, I express my heartiest gratitude towards my research supervisor, Professor M. R. Maurya. He always holds my hand and pull upwards in the ladder of success. I heartily realize that today whatever I am, this is just because of him. His scientific temperament, invaluable guidance, refreshing ideas, and crucial and rational analyses, which enabled me to accomplish the work embodied herein.*

*I am highly thankful to Prof. S. Head V.K. Gupta and Prof. Kamaluddin former Head, Department of Chemistry, Indian Institute of Technology Roorkee, for providing me essential infrastructural facilities to carry out this research work.*

*I am also thankful to the Head, Institute Instrumentation Centre of our institute for providing me necessary instrumentation facilities for my research work. My sincere thank to Mr. A. Haque, Mr. V.P. Saxena, Mr. H. S. Panwar and, Mr. Madan Pal, for helping me for timely help for my research work. I am also grateful to all the members of Chemistry Department for their cooperation in many ways.*

*I am also thankful to Prof. Joao Costa-Pessoa and Dr. Amit Kumar, Instituto Superior Tecnico, Portugal for carrying out the EPR studies and  $^{51}\text{V}$  NMR spectra of some of my samples. I am also thankful to Prof. Fernando Avecilla, Departamento de Química Fundamental, Facultad de Ciencias, Universidade da Coruña, Spain for carrying out Single crystal data of some of my samples.*

*My heartfelt thanks to my seniors and laboratory colleagues Dr. Umesh Kumar, Dr. Maneesh Kumar, Dr. Aarti, Dr. Aftab Alam Khan, Dr. Manisha Bisht, Ruchi Singh and junior Chanchal, Nawal, Nikita, Sarita, Maninder, Naresh, Saurav and Naveen for their lively company and motivation for the completion of my work.*

*My heartfelt thanks to my friends Nidhi Tyagi, Neeraj Naithani, Manu Sharma, Shweta Sharma, Shilpi Verma, Sushil, Varun and Sweety for their selfless support, affectionate company, cooperation and moral support, guidance, suggestions, vibrant company during the period of my thesis and have a wonderful time along the way.*

*Family was the place from everyone gets the potency. No amounts of thanks can ever repay the great debt that I owe my parents. Family always acts like a catalyst. This thesis is dedicated to My father, who indicated me a way to go. I don't have word to express my gratitude towards my father, I am grateful to my father for his encouragement, inspiration, and time to time suggestions during the complete phase of this task, Maa is the first word in the mouth of every child after birth. My work didn't take present shape without my mother's love, blessing and support. The words are not enough to express all my regards, love and thankfulness to my elder sisters Arti and Alka and jiji Vinod and Devindra and my elder brother Ravindra and Bhabhiji Seema for their blessings, love, encouragement, consistent support and motivation at every moment and throughout my study. Their presence always kept me energetic and full of spirits. I am in dearth of words in expressing my warm feelings to my lovable nephews and nieces Tanmay, Ujjawal and Anjali, Pari.*

*The financial assistance provided by Council of Scientific and Industrial Research (CSIR), New Delhi is gratefully acknowledged.*

*Last but not least I wish to acknowledge all those, whose names have not figured above, but helped me in any form during the entire period of my research work.*

*Priyanka Saini*  
(Priyanka Saini)

## LIST OF PUBLICATIONS

1. M.R. Maurya, **Priyanka Saini**, A. Kumar and J. Costa Pessoa, Oxidovanadium(IV) Complexes of Tetradenatate Ligands Encapsulated in Zeolite-Y as Catalysts for the Oxidation of Styrene, Cyclohexene and Methyl phenyl sulfide *Eur. J. Inorg. Chem.*, Under revision.
2. M.R. Maurya, **Priyanka Saini** and F. Avecilla, Synthesis, characterisation and catalytic activities of manganese (III) complexes of pyridoxal-based ONNO donor tetradenatate ligands, *Polyhedron*, Under revision.
3. M.R. Maurya and **Priyanka Saini**, Synthesis of manganese (III) complex of tribasic pentadentate ligand, its encapsulation in zeolite-Y, characterization and catalytic activity, In preparation.

## Papers presented in Symposia / Conferences

1. M.R. Maurya and **Priyanka Saini**, Synthesis, characterisation and catalytic activities of manganese (III) complexes of pyridoxal-based ONNO donor tetradenatate ligands, 1<sup>st</sup> CRSI ZONAL MEETING, National Chemical Laboratory Pune(India), May 13-14, 2011.
2. M.R. Maurya, **Priyanka Saini** and F. Avecilla, Manganese (III) complexes of pyridoxal based tetradentate ligands encapsulated in zeolite-Y as catalyst for the oxidation of methyl phenyl sulfide and styrene, 4<sup>th</sup> Conference on Recent Trends in Instrumental Methods of Analysis, IIT, Roorkee, February 18-20, 2011, P-85.

\*\*\*\*\*

# CONTENTS

	Page No.
CANDIDATE'S DECLARATION	i
ABSTRACT	ii
ACKNOWLEDGEMENTS	vii
LIST OF PUBLICATIONS	ix
CONTENTS	x
LIST OF FIGURES	xiv
LIST OF TABLES	xxi

## CHAPTER 1

### *General Introduction and literature survey*

1.1 Historical	1
1.2 Immobilization of the metal complexes on polymer support	3
1.3 Alumina, silica and other supports for the immobilization of complexes	9
1.4 Encapsulation of metal complexes in Zeolite-Y and their catalytic activities	20
1.5 Objective of the present thesis	36

## CHAPTER 2

### *Synthesis, characterisation and catalytic activities of manganese (III) complexes of pyridoxal-based ONNO donor tetradenatate ligands*

2.1 Introduction	38
2.2 Experimental Section	39
2.2.1 Materials	39
2.2.2 Physical Method and Analysis	40
2.2.3 X-Ray Crystal Structure Determination of [Mn(pydx-en)Cl(H <sub>2</sub> O)] (2.1) and [Mn(pydx-1,3-pn)Cl(CH <sub>3</sub> OH)] (2.2)	40
2.2.4 Preparations	41
2.2.4.1 Preparation of [Mn <sup>III</sup> (pydx-en)Cl(H <sub>2</sub> O)] (2.1)	41
2.2.4.2 Preparation of [Mn <sup>III</sup> (pydx-1,3-pn)Cl(CH <sub>3</sub> OH)] (2.2) and [Mn <sup>III</sup> (pydx-1,2-pn)Cl(H <sub>2</sub> O)] (2.3)	43
2.2.4.3 Preparation of [Mn <sup>II</sup> ]-Y (Manganese Exchanged Zeolite)	43
2.2.4.4 Preparation of [Mn <sup>III</sup> (pydx-en)Cl(H <sub>2</sub> O)]-Y(2.4)	43
2.2.4.5 Preparation of [Mn <sup>III</sup> (pydx-1,3-pn)Cl(H <sub>2</sub> O)]-Y(2.5) and	44



$[\text{Mn}^{\text{III}}(\text{pydx-1,2-pn})\text{Cl}(\text{H}_2\text{O})]\text{-Y}$  (2.6)

2.2.5	Catalytic activity study	44
2.2.5.1	Oxidation of Methyl Phenyl Sulfide	44
2.2.5.2	Oxidation of Styrene	44
2.2.5.3	Oxidation of Benzoin	44
2.3	Results and Discussion	45
2.3.1	Synthesis and solid state characteristics	45
2.3.2	Structure descriptions of $[\text{Mn}^{\text{III}}(\text{pydx-en})\text{Cl}(\text{H}_2\text{O})]$ (2.1) and $[\text{Mn}^{\text{III}}(\text{pydx-1,3-pn})\text{Cl}(\text{CH}_3\text{OH})]$ (2.2)	46
2.3.3	Field-emission-scanning electron micrograph (FE-SEM) and energy dispersive X-ray analysis (EDX) studies	51
2.3.4	Powder X-ray diffraction studies	51
2.3.5	IR spectral studies	52
2.3.6	UV/Vis spectral studies	53
2.3.7	Reactivity of complexes with $\text{H}_2\text{O}_2$	56
2.3.8	Electrochemical studies	57
2.3.9	Catalytic activity studies	60
2.3.9.1	Oxidation of methyl phenyl sulfide	60
2.3.9.2	Oxidation of styrene	66
2.3.9.3	Oxidation of benzoin	73
2.3.10	Test for recyclability and heterogeneity of the reactions	77
2.4	Conclusions	78

## CHAPTER 3

*Oxidovanadium(IV) complexes of tetradenatate ligands encapsulated in zeolite-Y as catalysts for the oxidation of styrene, cyclohexene and methyl phenyl sulfide*

3.1	Introduction	79
3.2	Experimental Section	80
3.2.1	Materials and methods	80
3.2.2	Instrumentation and Characterization Procedures	81
3.2.3	Preparations	81
3.2.3.1	Preparation of $[\text{V}^{\text{IV}}\text{O}(\text{pydx-en})]$ (3.1)	82
3.2.3.2	Preparation of $[\text{V}^{\text{IV}}\text{O}(\text{pydx-1,3-pn})]$ (3.2) and $[\text{V}^{\text{IV}}\text{O}(\text{pydx-1,2-pn})]$ (3.3)	82
3.2.3.3	Preparation of $[\text{V}^{\text{IV}}\text{O}]\text{-Y}$ (oxidovanadium(IV) exchanged zeolite-Y)	82
3.2.3.4	Preparation of $[\text{V}^{\text{IV}}\text{O}(\text{pydx-en})]\text{-Y}$ (3.4)	82
3.2.3.5	Preparation of $[\text{V}^{\text{IV}}\text{O}(\text{pydx-1,3-pn})]\text{-Y}$ (3.5) and	83

[V<sup>IV</sup>O(pydx-1,2-pn)]-Y (3.6)

3.2.4	Catalytic activity	83
3.2.4.1	Oxidation of Styrene	83
3.2.4.2	Oxidation of Cyclohexene	83
3.2.4.3	Oxidation of Methyl phenyl sulfide	84
3.3	Results and Discussion	84
3.3.1	Synthesis and characterization of complexes	84
3.3.2	Thermogravimetric analysis	85
3.3.3	Powder X-ray diffraction studies	86
3.3.4	Field-emission-scanning electron micrograph and energy dispersive X-ray analysis study	86
3.3.5	IR spectral studies	88
3.3.6	Electronic spectral studies	89
3.3.7	EPR studies	91
3.3.8	Catalytic activity studies	94
3.3.8.1	Oxidation of styrene	94
3.3.8.2	Oxidation of cyclohexene	100
3.3.8.3	Oxidation of methyl phenyl sulfide (thioanisole)	106
3.3.9	Tests of recycle ability and heterogeneity of the zeolite-Y encapsulated catalytic reactions	111
3.3.10	Reactivity of complexes and possible catalytic reaction pathway	112
3.4	Conclusions	118

## CHAPTER 4

### *Synthesis of manganese (III) complex of tribasic pentadentate ligand, its encapsulation in zeolite-Y, characterization and catalytic activity*

4.1.	Introduction	120
4.2.	Experimental Section	121
4.2.1	Materials	121
4.2.2	Methods	121
4.2.3	Preparations	121
4.2.3.1	Preparation of H <sub>3</sub> sal-dahp (4.1)	121
4.2.3.2	Preparation of [Mn <sup>III</sup> (sal-dahp)H <sub>2</sub> O](4.1)	121
4.2.3.3	Preparation of [Mn <sup>III</sup> (sal-dahp)H <sub>2</sub> O]-Y(4.2)	122
4.2.4	Catalytic activity study: Oxidation of benzoin	122
4.3	Results and Discussion	123
4.3.1	Synthesis and solid state characteristics	123
4.3.2	IR spectral studies	124
4.3.3	Electronic absorption studies	125
4.3.4	Powder X-ray Diffraction studies	126
4.3.5	Field-Emission-Scanning Electron Micrograph (FE-SEM) and	127

Energy Dispersive X-Ray Analysis (EDX) Studies	
4.3.6 Oxidation of benzoin	128
4.3.7 Reactivity of complexes with H <sub>2</sub> O <sub>2</sub> and possible reaction mechanism	134
4.4. Conclusions	136

## CHAPTER 5

### *Oxidation of styrene and cyclohexene with TBHP catalyzed by copper(II) complex encapsulated in Zeolite-Y*

5.1 Introduction	137
5.2 Experimental	138
5.2.1 Materials and methods	138
5.2.2 Preparations	138
5.2.2.1 Preparation of Hacpy-oap (5.1)	138
5.2.2.2 Preparation of [Cu <sup>II</sup> (acpy-oap)Cl] (5.1)	139
5.2.2.3 Preparation of [Cu <sup>II</sup> ]-Y	139
5.2.2.4 Preparation of [Cu <sup>II</sup> (acpy-oap)Cl]-Y (5.2)	139
5.2.3 Catalytic activity studies	140
5.2.3.1 Oxidation of styrene	140
5.2.3.2 Oxidation of cyclohexene	140
5.3 Results and Discussion	140
5.3.1 Characterization of catalysts	140
5.3.2 Powder X-ray diffraction studies	141
5.3.3 Thermogravimetric analysis	142
5.3.4 IR spectral studies	143
5.3.5 Electronic spectral studies	143
5.3.6 Catalytic activity studies	144
5.3.6.1 Oxidation of styrene	144
5.3.6.2 Oxidation of cyclohexene	150
5.3.7 Possible reaction mechanism	156
5.4 Conclusions	157
SUMMARY AND CONCLUSION	159
REFERENCES	162

## LIST OF FIGURES

- Figure 1.1 Model structure of entrapped [Co(salen)] complex in zeolite-X. Reproduced from reference [48].
- Figure 1.2 3D Model structure of [Fe(hybe)(H<sub>2</sub>O)<sub>2</sub>]<sup>+</sup>.
- Figure 1.3 Dinuclear structure of [{M(fsal)}<sub>2</sub>] complexes; M = Cu(II), Ni(II), Co(II) (56 and 57).
- Figure 2.1 X-ray crystal structure of the [Mn<sup>III</sup>(pydx-en)Cl(H<sub>2</sub>O)] (2.1). Hydrogen atoms are omitted for the clarity.
- Figure 2.2 X-ray crystal structure of the [Mn<sup>III</sup>(pydx-1,3-pn)Cl(CH<sub>3</sub>OH)] (2.2). Hydrogen atoms are omitted for the clarity.
- Figure 2.3 Field emission-scanning electron micrograph (left) of [Mn<sup>III</sup>(pydx-en)Cl(H<sub>2</sub>O)]-Y and the corresponding energy dispersive X-ray analysis plot (right).
- Figure 2.4 XRD patterns of Na-Y (a), [Mn<sup>II</sup>]-Y (b) and [Mn<sup>III</sup>(pydx-en)Cl]-Y (c).
- Figure 2.5 A: Electronic spectra of [Mn<sup>III</sup>(pydx-en)Cl(H<sub>2</sub>O)] (a), [Mn<sup>III</sup>(pydx-1,3-pn)Cl(CH<sub>3</sub>OH)] (b) and [Mn<sup>III</sup>(pydx-1,2-pn)Cl(H<sub>2</sub>O)](c); B: Electronic spectra of [Mn<sup>III</sup>(pydx-en)Cl(H<sub>2</sub>O)]-Y (a), [Mn<sup>III</sup>(pydx-1,3-pn)Cl(H<sub>2</sub>O)]-Y (b) and [Mn<sup>III</sup>(pydx-1,2-pn)Cl(H<sub>2</sub>O)]-Y (c).
- Figure 2.6 UV-Vis spectral changes observed during titration of [Mn<sup>III</sup>(Pydx-en)Cl(H<sub>2</sub>O)] (2.1) with H<sub>2</sub>O<sub>2</sub>. The spectra were recorded after stepwise additions of ten drops portions of H<sub>2</sub>O<sub>2</sub> (0.441 g (3.89 mmol) of 30% H<sub>2</sub>O<sub>2</sub> dissolved in 5 ml of MeOH to 10 ml of 1.0 × 10<sup>-4</sup> M solution in MeOH. In set shows similar spectra recorded with 1.0 × 10<sup>-3</sup> M solution of 2.1 in MeOH.
- Figure 2.7 UV-Vis spectral changes observed during titration of [Mn<sup>III</sup>(Pydx-1,3-pn)Cl (CH<sub>3</sub>OH)] with H<sub>2</sub>O<sub>2</sub>. The spectra were recorded after stepwise additions of one drops portions of H<sub>2</sub>O<sub>2</sub> (0.149 g (1.32 mmol) of 30% H<sub>2</sub>O<sub>2</sub> dissolved in 5 ml of MeOH) to 5 ml of 1.0 × 10<sup>-4</sup> M solution in MeOH. In set shows similar spectra recorded with 1.0 × 10<sup>-3</sup> M solution in MeOH.
- Figure 2.8 Cyclic voltammogram of 1mM solution of [Mn<sup>III</sup>(pydx-en)Cl(H<sub>2</sub>O)] (2.1) in DMF in the presence of 0.1 M tetrabutylammonium perchlorate (TBAP) using Ag/AgCl as reference electrode, glassy-carbon as working electrode and platinum wire as auxiliary electrode; scan rate: 0.1 V/s.

- Figure 2.9 A: Cyclic voltammogram of  $[\text{Mn}^{\text{III}}(\text{Pydx-1,3-pn})\text{Cl}(\text{CH}_3\text{OH})]$  (**2.2**) in DMF solution (1 mM), B: Cyclic voltammogram of  $[\text{Mn}^{\text{III}}(\text{Pydx-1,2-pn})\text{Cl}(\text{H}_2\text{O})]$  (**2.3**) in DMF solution (1 mM). Ag/AgCl as reference electrode and glassy carbon as working electrode, scan rate: 0.1 V/s.
- Figure 2.10 Effect of the amount of  $\text{H}_2\text{O}_2$  on the oxidation of methyl phenyl sulfide as a function of time. Other reaction conditions: methyl phenyl sulfide (1.24 g, 10 mmol),  $[\text{Mn}^{\text{III}}(\text{pydx-en})\text{Cl}(\text{H}_2\text{O})]$ -Y (0.020 g) and acetonitrile (5 ml).
- Figure 2.11 Effect of amount of catalyst on the oxidation of methyl phenyl sulfide as a function of time. Other reaction conditions: methyl phenyl sulfide (1.24 g, 10 mmol),  $\text{H}_2\text{O}_2$  (2.27 g, 20 mmol) and acetonitrile (5 ml).
- Figure 2.12 Effect of amount of solvent on the oxidation of methyl phenyl sulphide as a function of time. Other reaction condition: methyl phenyl sulphide (1.242 g, 10 mmol),  $\text{H}_2\text{O}_2$  (2.27 g, 20 mmol) and  $[\text{Mn}(\text{pydx-en})\text{Cl}(\text{H}_2\text{O})]$ -Y (0.020 g).
- Figure 2.13 Effect of different catalyst on the oxidation of methyl phenyl sulfide. For reaction conditions see text.
- Figure 2.14 Conversion of methyl phenyl sulfide and variation in the selectivity of different reaction products as a function of time using  $[\text{Mn}^{\text{III}}(\text{pydx-en})\text{Cl}(\text{H}_2\text{O})]$ -Y as catalyst: (a) conversion of methyl phenyl sulphide (●), (b) selectivity of methyl phenyl sulfoxide (■) and (c) selectivity of methyl phenyl sulfone (▲).
- Figure 2.15 Effect of the amount of  $\text{H}_2\text{O}_2$  on the oxidation of styrene as a function of time. Other reaction conditions: styrene (1.04 g, 10 mmol),  $[\text{Mn}^{\text{III}}(\text{pydx-en})\text{Cl}(\text{H}_2\text{O})]$ -Y (0.040 g), acetonitrile (5 ml) and temperature (80 °C).
- Figure 2.16 Effect of the amount of catalyst on the oxidation of styrene. Other reaction conditions: styrene (1.04 g, 10 mmol), 30%  $\text{H}_2\text{O}_2$  (2.27 g, 20 mmol),  $\text{CH}_3\text{CN}$  (5 ml) and temp. (80 °C).
- Figure 2.17 Effect of the volume of acetonitrile on the oxidation of styrene. Other reaction conditions: styrene (1.04 g, 10 mmol), 30%  $\text{H}_2\text{O}_2$  (2.27 g, 20 mmol),  $[\text{Mn}^{\text{III}}(\text{pydx-en})\text{Cl}(\text{H}_2\text{O})]$ -Y (0.040 g) and temp. (80 °C).
- Figure 2.18 Comparison of the catalytic potential of zeolite-encapsulated manganese(III) complexes for the oxidation of styrene in the

presence of H<sub>2</sub>O<sub>2</sub> as oxidant.

- Figure 2.19 Conversion of styrene and variation in the selectivity of different reaction products as a function of time using [Mn<sup>III</sup>(pydx-en)Cl(H<sub>2</sub>O)]-Y as a catalyst: (a) conversion of styrene (■), (b) selectivity of benzaldehyde (▲), (c) benzoic acid (◆), (d) styrene oxide (●), (e) phenylacetaldehyde (◄) and (f) 1-phenylethane-1,2-diol (▼).
- Figure 2.20 Effect of amount of H<sub>2</sub>O<sub>2</sub> on the oxidation of benzoin as a function of time. Other reaction conditions: benzoin (1.06 g, 5 mmol), [Mn<sup>III</sup>(pydx-en)Cl(H<sub>2</sub>O)]-Y (0.020 g), methanol (20 ml).
- Figure 2.21 Effect of amount of catalyst on the oxidation of benzoin as a function of time. Other reaction conditions: benzoin (1.06 g, 5 mmol), H<sub>2</sub>O<sub>2</sub> (1.13 g, 10 mmol), methanol (20 ml).
- Figure 2.22 Conversion of benzoin and variation in the selectivity of different reaction products as a function of time using [Mn<sup>III</sup>(pydx-en)Cl(H<sub>2</sub>O)]-Y as a catalyst: (a) conversion of benzoin, (b) selectivity of benzil, (c) benzoic acid and (d) benzaldehyde-dimethylacetal.
- Figure 2.23 Comparison of different catalysts on the oxidation of benzoin. Reaction conditions: benzoin (1.06 g, 5 mmol), catalyst (0.020 g), H<sub>2</sub>O<sub>2</sub> (1.13 g, 10 mmol) and methanol (20 ml).
- Figure 3.1 XRD patterns of Na-Y (a), [V<sup>IV</sup>O]-Y (b) and [V<sup>IV</sup>O(pydx-en)]-Y (c).
- Figure 3.2 Field emission-scanning electron micrograph of [V<sup>IV</sup>O(pydx-en)]-Y and the corresponding Energy Dispersive X-ray analysis plot.
- Figure 3.3 Electronic spectra (in methanol) of [V<sup>IV</sup>O(pydx-en)] (3.1) (a), [V<sup>IV</sup>O(pydx-1,3-pn)] (3.2) (b) and [V<sup>IV</sup>O(pydx-1,2-pn)] (3.3) (c).
- Figure 3.4 Electronic spectra of [V<sup>IV</sup>O(pydx-en)]-Y (3.4) (a), [V<sup>IV</sup>O(pydx-1,3-pn)]-Y (3.5) (b), [V<sup>IV</sup>O(pydx-1,2-pn)]-Y (3.6) (c) recorded dispersed in Nujol<sup>®</sup>.
- Figure 3.5 First derivative EPR spectra of frozen (77 K) solutions of (a) [V<sup>IV</sup>O(pydx-en)] (3.1) (4 mM) in MeOH; (b) [V<sup>IV</sup>O(pydx-1,2-pn)] (3.3) (4 mM) in MeOH; (c) [V<sup>IV</sup>O(pydx-1,3-pn)] (3.2) (4 mM) in DMSO.

- Figure 3.6 First derivative EPR spectra at room temperature of zeolite encapsulated complexes (solids) (a)  $[V^{IV}O]-Y$ ; (b)  $[V^{IV}O(\text{pydx-en})]-Y$  (3.4); (c)  $[V^{IV}O(\text{pydx-1,2-pn})]-Y$  (3.6); (d)  $[V^{IV}O(\text{pydx-1,3-pn})]-Y$  (3.5).
- Figure 3.7 Effect of the amount of  $H_2O_2$  on the oxidation of styrene at 80 °C as a function of time. Reaction conditions: Styrene (1.04 g, 10 mmol),  $[V^{IV}O(\text{pydx-en})]-Y$  (0.010 g), acetonitrile (5 ml).
- Figure 3.8 Effect of the amount of catalyst on the oxidation of styrene at 80 °C as a function of time. Reaction conditions: Styrene (1.04 g, 10 mmol),  $H_2O_2$  (2.27 g, 20 mmol) in acetonitrile (5 ml).
- Figure 3.9 Effect of the amount of solvent on the oxidation of styrene at 80 °C as a function of time. Reaction conditions: Styrene (1.04 g, 10 mmol),  $H_2O_2$  (2.27 g, 20 mmol),  $[V^{IV}O(\text{pydx-en})]-Y$  (0.010 g).
- Figure 3.10 Effect of different catalysts on the oxidation of styrene at 80 °C as a function of time. Reaction conditions: Styrene (1.04 g, 10 mmol),  $H_2O_2$  (2.27 g, 20 mmol) and acetonitrile (5 ml).
- Figure 3.11 Conversion of styrene and variation in the selectivity of different reaction products as a function of time using  $[V^{IV}O(\text{pydx-en})]-Y$  as catalyst: (a) conversion of styrene (■), (b) selectivity of benzaldehyde (▲), (c) selectivity of 1-phenylethane-1,2-diol (▼), (d) selectivity of benzoic acid (◆), (e) selectivity of styrene oxide (●), (f) selectivity of other product (◀).
- Figure 3.12 Effect of the amount of  $H_2O_2$  on the oxidation of cyclohexene at 80 °C as a function of time. Reaction conditions: cyclohexene (0.820 g, 10 mmol),  $[V^{IV}O(\text{pydx-en})]-Y$  (0.005 g) and acetonitrile (5 ml).
- Figure 3.13 Effect of the amount of catalyst on the oxidation of cyclohexene at 80 °C as a function of time. Reaction conditions: cyclohexene (0.820 g, 10 mmol), 30 %  $H_2O_2$  (2.27 g, 20 mmol) and acetonitrile (5 ml).
- Figure 3.14 Effect of the amount of solvent on the oxidation of cyclohexene at 80 °C as a function of time. Reaction conditions: cyclohexene (0.82 g, 10 mmol),  $H_2O_2$  (2.27 g, 20 mmol) and  $[V^{IV}O(\text{pydx-en})]-Y$  (0.005 g).
- Figure 3.15 Effect of the different catalyst precursors on the oxidation of cyclohexene at 80 °C as a function of time. Reaction conditions: cyclohexene (0.820 g, 10 mmol),  $H_2O_2$  (2.27 g, 20 mmol), catalyst amount (0.005 g) acetonitrile (5 ml).

- Figure 3.16 Conversion of cyclohexene and variation in the selectivity of the different reaction products as a function of time using  $[V^{IV}O(\text{pydx-en})]-Y$  (4) as catalyst: (a) conversion of cyclohexene (■), (b) selectivity of cyclohexene-1-one (▼), (c) selectivity of cyclohexene-1-ol (▲), (d) selectivity of cyclohexane-1,2-diol (◆) (e) selectivity of cyclohexene oxide (●) and (f) selectivity of other products (◄).
- Figure 3.17 Effect of the amount of  $H_2O_2$  on the oxidation of methyl phenyl sulfide as a function of time. Reaction conditions: methyl phenyl sulfide (1.242 g, 10 mmol),  $[V^{IV}O(\text{pydx-en})]-Y$  (10 mg) and acetonitrile (5 ml).
- Figure 3.18 Effect of catalyst  $[V^{IV}O(\text{pydx-en})]-Y$  on the oxidation of methyl phenyl sulfoxide at room temperature. Reaction conditions: methyl phenyl sulfide (1.24 g, 10 mmol),  $H_2O_2$  (2.27 g, 20 mmol) and acetonitrile (5 ml).
- Figure 3.19 Effect of volume of solvent on the oxidation of methyl phenyl sulfide at room temperature as a function of time. Reaction conditions: methyl phenyl sulfide (1.242 g, 10 mmol),  $H_2O_2$  (2.2 g, 20 mmol) and  $[V^{IV}O(\text{pydx-en})]-Y$  (0.010 g).
- Figure 3.20 Effect of different catalyst on the oxidation of methyl phenyl sulfide at room temperature. Reaction conditions: catalyst (0.010 g), methyl phenyl sulfide (1.242 g, 10 mmol),  $H_2O_2$  (2.27 g, 20 mmol) and acetonitrile (5 ml).
- Figure 3.21 Conversion of methyl phenyl sulfide and variation in the selectivity of the reaction products as a function of time using  $[V^{IV}O(\text{pydx-en})]-Y$  (3.4) as catalyst: (a) conversion of methyl phenyl sulfide (●), (b) selectivity of methyl phenyl sulfoxide (■) and (c) selectivity of methyl phenyl sulfone (▲).
- Figure 3.22 UV-Vis spectral changes observed during titration of  $[V^{IV}O(\text{pydx-en})]$  (3.1) with  $H_2O_2$ . The spectra were recorded upon stepwise additions of five drops portions of  $H_2O_2$  [1.178 g (10.39 mmol) of 30%  $H_2O_2$  dissolved in 5 ml of DMSO] to 10 ml of  $1.6 \times 10^{-4}$  M solution in DMSO. The inset shows similar spectra recorded with ca.  $7.55 \times 10^{-3}$  M solution of 3.1 in DMSO.
- Figure 3.23 UV-Vis spectral changes observed during titration of  $[V^{IV}O(\text{pydx-1,2-pn})]$  (3.3) with  $H_2O_2$ . The spectra were recorded after stepwise additions of five drops portions of  $H_2O_2$  (1.178 g (10.39 mmol) of 30%  $H_2O_2$  dissolved in 5 ml of DMSO) to 10 ml of  $1.6 \times 10^{-4}$  M solution in DMSO. The inset shows similar spectra recorded with



ca.  $1 \times 10^{-3}$  M solution of **3.3** in DMSO.

- Figure 3.24  $^{51}\text{V}$  NMR spectra (a) of a methanolic solution of  $[\text{V}^{\text{IV}}\text{O}(\text{pydx-en})]$  (**3.1**) (ca. 4 mM) the pH is ca. 7.5; (b) solution of (a) after 1 hr; (c) addition of 0.5 equiv. of aqueous 30%  $\text{H}_2\text{O}_2$  (total) to the solution of (b); (d) after addition of 1.0 equiv. of 30%  $\text{H}_2\text{O}_2$  (total) to the solution of (c); (e) after addition of 2.0 equiv. of 30%  $\text{H}_2\text{O}_2$  (total) to the solution of (d) the pH is ca. 6.5; (f) after addition of 3.0 equiv. (30%)  $\text{H}_2\text{O}_2$  (total) to the solution of (e) the pH is ca. 6.5; (g) addition of methyl phenyl sulphide (10 equiv.) to the solution of (f) after 3hr at room temperature.
- Figure 3.25 First derivative EPR spectra of frozen (77 K) solutions of (a) a methanolic solution of  $[\text{V}^{\text{IV}}\text{O}\{(\text{pydx})_2\text{-en}\}]$  (**3.1**) (ca. 4 mM); (b) after addition of 3.0 equiv (30%)  $\text{H}_2\text{O}_2$  (total) to the solution of (a); (c) after 24 h of addition of methyl phenyl sulphide (10 equiv) to the solution of (b). The high field ranges of the spectra are amplified.
- Figure 4.1 Electronic spectrum of  $[\text{Mn}^{\text{III}}(\text{sal-dahp})(\text{H}_2\text{O})]$  (**4.1**).
- Figure 4.2 Electronic spectrum of  $[\text{Mn}^{\text{III}}(\text{sal-dahp})(\text{H}_2\text{O})]\text{-Y}$  (**4.2**)
- Figure 4.3 XRD patterns of Na-Y (a),  $[\text{Mn}^{\text{II}}]\text{-Y}$  (b) and  $[\text{Mn}^{\text{III}}(\text{sal-dahp})(\text{H}_2\text{O})]\text{-Y}$
- Figure 4.4 Field emission-scanning electron micrograph of  $[\text{Mn}^{\text{III}}(\text{sal-dahp})(\text{H}_2\text{O})]\text{-Y}$  and the corresponding energy dispersive X-ray analysis plot.
- Figure 4.5 Effect of amount of  $\text{H}_2\text{O}_2$  on the oxidation of benzoin as a function of time. Other reaction conditions: benzoin (1.06 g, 5 mmol),  $[\text{Mn}^{\text{III}}(\text{sal-dahp})(\text{H}_2\text{O})]\text{-Y}$  (0.020 g) and methanol (20 mL).
- Figure 4.6 Effect of amount of catalyst on the oxidation of benzoin as a function of time. Other reaction conditions: benzoin (1.06 g, 5 mmol),  $\text{H}_2\text{O}_2$  (1.13 g, 10 mmol) and methanol (20 mL).
- Figure 4.7 Effect of amount of solvent on the oxidation of benzoin as a function of time. Other reaction conditions: benzoin (1.06 g, 5 mmol),  $[\text{Mn}^{\text{III}}(\text{sal-dahp})(\text{H}_2\text{O})]\text{-Y}$  (0.020 g) and  $\text{H}_2\text{O}_2$  (1.13 g, 10 mmol).
- Figure 4.8 Conversion of benzoin and variation in the selectivity of different reaction products as a function of time using  $[\text{Mn}^{\text{III}}(\text{sal-dahp})(\text{H}_2\text{O})]\text{-Y}$  as a catalyst: conversion of benzoin (a), selectivity

of benzil (b), benzaldehyde-dimethylacetal (c) and benzoic acid (d).

- Figure 4.9 UV-Vis spectral changes observed during titration of  $[\text{Mn}^{\text{III}}(\text{sal-dahp})(\text{H}_2\text{O})]$  (**4.1**) with  $\text{H}_2\text{O}_2$ . The spectra were recorded after stepwise addition of one drops portions of aqueous 30%  $\text{H}_2\text{O}_2$  (0.227 g, 2.0 mmol) dissolved in 5 mL of MeOH to 5 mL of ca.  $6.8 \times 10^{-4}$  M solution of  $[\text{Mn}^{\text{III}}(\text{sal-dahp})(\text{H}_2\text{O})]$  (**4.1**) in MeOH. In set shows similar spectra recorded with 5 mL of  $1.36 \times 10^{-3}$  M solution of **4.1** in MeOH.
- Figure 5.1 XRD patterns of (a) Na-Y, (b)  $\text{Cu}^{\text{II}}\text{-Y}$  and (c)  $[\text{Cu}^{\text{II}}(\text{acpy-oap})\text{Cl}]\text{-Y}$ .
- Figure 5.2 Effect of TBHP concentration (TBHP : styrene) on oxidation of styrene. Reaction conditions: styrene (1.04 g, 10 mmol), catalyst (0.050 g),  $\text{CH}_3\text{CN}$  (20 ml) and temperature (80 °C).
- Figure 5.3 Effect of amount of catalyst per unit weight of styrene. Reaction conditions: styrene (1.04 g, 10 mmol), TBHP (2.56 g, 20 mmol),  $\text{CH}_3\text{CN}$  (20 ml) and temperature (80 °C).
- Figure 5.4 Effect of temperature on the oxidation of styrene. Reaction conditions: styrene (1.04 g, 10 mmol), catalyst (0.035 g), TBHP (2.56 g, 20 mmol) and  $\text{CH}_3\text{CN}$  (20 ml).
- Figure 5.5 Effect of different catalysts  $[\text{Cu}(\text{acpy-oap})\text{Cl}]$  (**5.1**) and  $[\text{Cu}(\text{acpy-oap})\text{Cl}]\text{-Y}$  (**5.2**) on the oxidation of styrene.
- Figure 5.6 Effect of TBHP concentration (TBHP : cyclohexene) on oxidation of cyclohexene. Reaction conditions: cyclohexene (0.82 g, 10 mmol), catalyst (0.035 g),  $\text{CH}_3\text{CN}$  (20 ml) and temperature (75 °C).
- Figure 5.7 Effect of amount of catalyst on oxidation of cyclohexene. Reaction conditions: cyclohexene (0.82 g, 10 mmol), TBHP (2.56 g, 20 mmol),  $\text{CH}_3\text{CN}$  (20 ml) and temperature (75 °C).
- Figure 5.8 Effect of reaction temperature on the oxidation of cyclohexene. Reaction conditions: cyclohexene (0.82 g, 10 mmol), catalyst (0.035 g), TBHP (2.56 g, 20 mmol) and  $\text{CH}_3\text{CN}$  (20 ml).
- Figure 5.9 Effect of different catalysts  $[\text{Cu}(\text{acpy-oap})\text{Cl}]$  (**5.1**) and  $[\text{Cu}(\text{acpy-oap})\text{Cl}]\text{-Y}$  (**5.2**) on the oxidation of cyclohexene.
- Figure 5.10 UV-Vis spectral changes observed during titration of  $[\text{Cu}^{\text{II}}(\text{acpy-oap})\text{Cl}]$  with TBHP. The spectra were recorded after successive addition of one drop portions of TBHP in minimum amount of methanol to 10 ml of ca.  $10^{-4}$  M solution of  $[\text{Cu}^{\text{II}}(\text{acpy-oap})\text{Cl}]$  in methanol.

## LIST OF TABLES

- Table 1.1 Major catalytic technology developments during 1949 to 1991<sup>a</sup>.
- Table 1.2 Oxidation of alkenes on *cis*-[Mn(bpy)<sub>2</sub>]<sup>+2</sup> in zeolite X and Y at 293 K[71].
- Table 1.3 Conversion of styrene, product selectivity and TOF.<sup>a</sup>
- Table 2.1 Crystal data collection and structure refinement for [Mn<sup>III</sup>(pydx-en)Cl(H<sub>2</sub>O)] (2.1) and [Mn<sup>III</sup>(pydx-1,3-pn)Cl(CH<sub>3</sub>OH)] (2.2).
- Table 2.2 Manganese content and colour of encapsulated complexes.
- Table 2.3 Selected bond lengths (Å) and bond angles (°) for [Mn<sup>III</sup>(pydx-en)Cl(H<sub>2</sub>O)] (2.1) and [Mn<sup>III</sup>(pydx-1,3-pn)Cl(CH<sub>3</sub>OH)] (2.2)<sup>a</sup>.
- Table 2.4 IR spectral data [cm<sup>-1</sup>] of ligands and complexes.
- Table 2.5 Electronic spectroscopic data of ligands and complexes.
- Table 2.6 Conversion percentage of methyl phenyl sulfide in 3.5 h using H<sub>2</sub>O<sub>2</sub> as an oxidant and selectivity of sulfoxide and sulfone.
- Table 2.7 Product selectivity and percent conversion of styrene with H<sub>2</sub>O<sub>2</sub> after 6 h of reaction time.
- Table 2.8 Conversion of benzoin, TOF and selectivity data of products.
- Table 3.1 Chemical composition, physical and analytical data.
- Table 3.2 IR spectral data of ligand, pure and encapsulated complexes.
- Table 3.3 Electronic spectral data of ligands and complexes studied in this work.
- Table 3.4 Spin Hamiltonian parameters obtained [140] by simulation of the experimental EPR spectra.
- Table 3.5 Percentage conversion of styrene, product selectivity and turn over frequency (TOF).
- Table 3.6 Conversion of cyclohexene and selectivity of various oxidation products after 6 h of reaction time.
- Table 3.7 Conversion percentage of methyl phenyl sulfide in 2.5 h and selectivity of sulfoxide and sulfone.

- Table 3.8 EPR spectral data after addition of  $\text{H}_2\text{O}_2$  and  $\text{H}_2\text{O}_2$  followed by methyl phenyl sulphide.
- Table 4.1 IR spectral data of ligand and complexes.
- Table 4.2 Electronic spectral data of ligand and complexes.
- Table 4.3 Conversion of benzoin (1.06 g, 5 mmol) using  $[\text{Mn}^{\text{III}}(\text{saldahp})(\text{H}_2\text{O})]\text{-Y}$  as catalyst in 6 h of reaction time under different reaction conditions.
- Table 4.4 Conversion of benzoin, TOF and selectivity data of products.
- Table 5.1 IR and electronic spectral data of ligand, pure and encapsulated complexes.
- Table 5.2 Conversion of styrene (1.04 g, 10 mmol) using  $[\text{Cu}^{\text{II}}(\text{acpy-oap})\text{Cl}]\text{-Y}$  as catalyst in 7 h of reaction time under different reaction conditions.
- Table 5.3 Percent conversion of styrene along with TOF and selectivity of different reaction products after 7 h of reaction time.
- Table 5.4 Conversion of cyclohexene (0.82 g, 10 mmol) using  $[\text{Cu}^{\text{II}}(\text{acpy-oap})\text{Cl}]\text{-Y}$  as catalyst in 6 h of reaction time under different reaction conditions.
- Table 5.5 Effect of different catalysts on the oxidation of cyclohexene and product selectivity.

# *CHAPTER 1*

## **General introduction and literature survey**

### **1.1. Historical**

Berzelius first introduced the word catalysis in 1835. Later Ostwald, a Noble prize winner in 1905, defined the catalyst as “a substance that changes the rate of chemical reaction without itself appearing into the final products”. Normally, a catalytic reaction proceeds through the bonding of reactant molecules to the catalyst, where they react and finally products detach from the catalyst leaving the catalyst for the next cycle. The catalytic reaction occurs at the specific sites called “active site” and rate of the reaction can be significantly improved by enhancing the surface area of the catalyst which in turn enhances the availability of the active sites. The speed of the catalytic reaction is presented in terms of a “Turn-over Rate” (TOF), which is defined as number of moles of substrate converted on an ‘active site’ or on a unit catalytic surface area per second at a given condition.

In 20<sup>th</sup> century catalysts have played a vital role as today about 95 % processes used in the chemical industries are catalysts based technologies. Directly or indirectly catalysts have contributed more than 20% GDP of developed nations. Major catalyst based technologies starting 1949 to 1991 are given in Table 1.1 chronologically.

Amongst the variety of catalytically active species known, the transition metal complexes catalyze a wide range of chemical reactions such as oxidation, hydrogenation, polymerization etc. Transition metal complexes based catalysts are generally homogeneous and are soluble in solvents and therefore produce large amount of side waste materials and impose serious hazardous impact on the surrounding environment [2]. One of the major drawbacks of the homogeneous catalysts is their separation from the reaction mixture at the end of the process. The possible contaminations of catalysts in the product also restrict their use in industry while important properties of the industrial catalysts are the substantial

working life and the retention of their effectiveness. There is, therefore, a need to find more efficient catalytic system, especially for fine chemicals industry and also to meet the environmental challenges. Many efforts have been directed in the past two decades towards the development of heterogeneous processes and the heterogenization of active homogeneous catalysts [3]. The heterogenization of homogeneous catalysts can be achieved by immobilization, grafting, anchoring or encapsulating them in an inert solid like organic polymer or inorganic support.

**Table 1.1.** Major catalytic technology developments during 1949 to 1991<sup>a</sup>

Year	Process	Catalyst
1949	Monometallic reforming	Pt-Al <sub>2</sub> O <sub>3</sub>
1957	Polymerization	Zeigler-Natta
1962	Steam reforming	Ni-K- Al <sub>2</sub> O <sub>3</sub>
1964	Zeolite catcracking	X,Y-zeolites
1967	Bimetallic reforming	Pt-Re / Pt-Ir
1968	Selectoreforming	Erionite
1972	Low pressure CH <sub>3</sub> OH	Cu-Zn- Al <sub>2</sub> O <sub>3</sub>
1974	Acetic acid (carbonylation)	Rh-I
1976	Auto emission control	Pt- Al <sub>2</sub> O <sub>3</sub>
1980	Gasoline from methane	ZSM-5
1982	Auto emission; stack gas	Pt-Rh; V <sub>2</sub> O <sub>5</sub> -TiO <sub>2</sub>
1988	Selective oxidation	Ti-silicates
1988	Chiral catalysts	Cinchonidine-Pt; BINAP
1991	Polymerization	Metallocenes

<sup>a</sup> Adopted from ref. [1].

Various types of organic polymers or inorganic solids like zeolites/molecular sieves, silica, alumina, other metal oxides, and carbon have

been used for the heterogenization of homogeneous catalysts. Some of these methods are discussed below:

## **1.2. Immobilization of the metal complexes on polymer support**

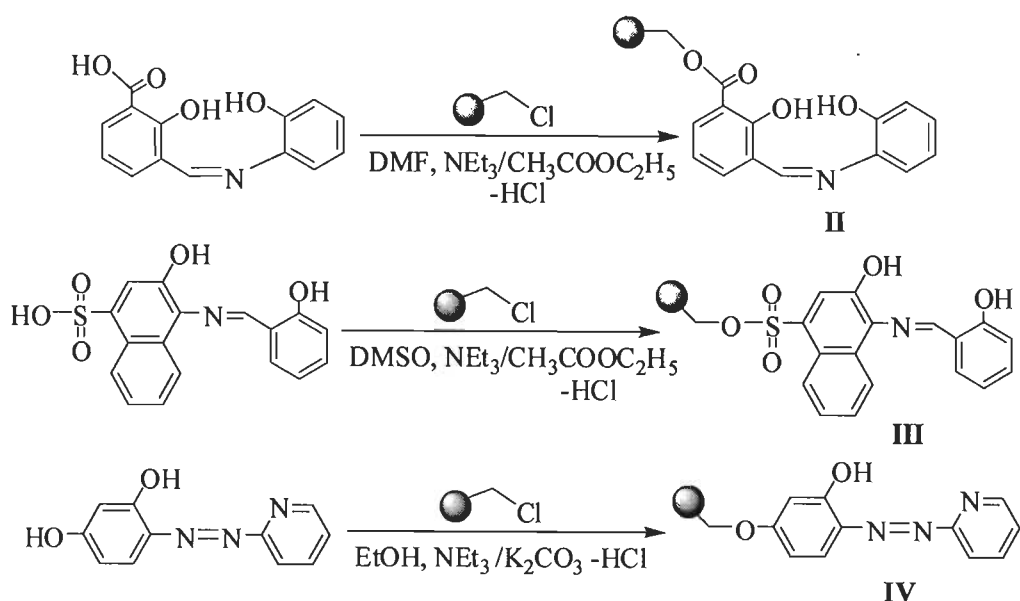
Various polymers such as polystyrene, polyvinylchloride, polyvinylpyridine, polyaniline, polyallyl, polyaminoacid, acrylic polymer, cellulose, silicate can be modified with functional groups.

The functionalized polymers react with organic reagents (more specifically called ligands) to yield the polymer-bound reagents or ligands having available coordination sites to bind metal ions. The polymer-anchored reagents or ligands then react with suitable metal precursors to give the polymer-anchored complexes [4]. Merrifield in 1963 [5] made use of chloromethylated polystyrene for the synthesis of polypeptide chains. Maurya et al. have recently reported wide range of polymer-supported metal complexes and used them as catalysts for various catalytic reactions [6,7]. Earlier works of Sherington et al. are also much appreciated [8,9].

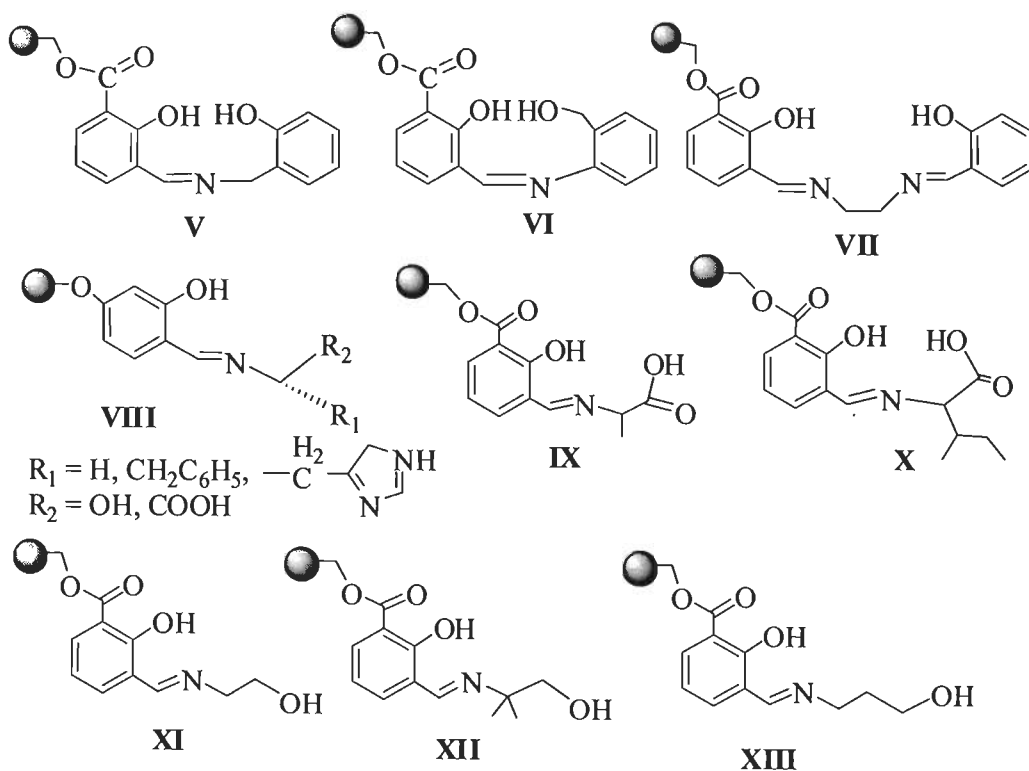
Carboxylic acid and sulfonic acid functions present on various ligand systems may react with  $-\text{CH}_2\text{Cl}$  of Merrifield resin (chloromethylated polystyrene cross-linked with divinyl benzene) in mild basic conditions to give polymer-anchored ligands.  $\text{N}(\text{CH}_2\text{CH}_3)_3$  in ethylacetate has been often used to abstract the HCl produced in the reaction; Scheme 1.1 [10]. In many cases it is required to carry out the reaction at  $90\text{ }^\circ\text{C}$  for effective anchoring. The functionalised polymers (cross-linked as well as straight chain) have widely been used as support for homogeneous catalysts through covalent bonding and to prepare many polymer-anchored ligands.

Some of the polymer-anchored ligands synthesized by this method are presented in Scheme 1.2 [11-16].



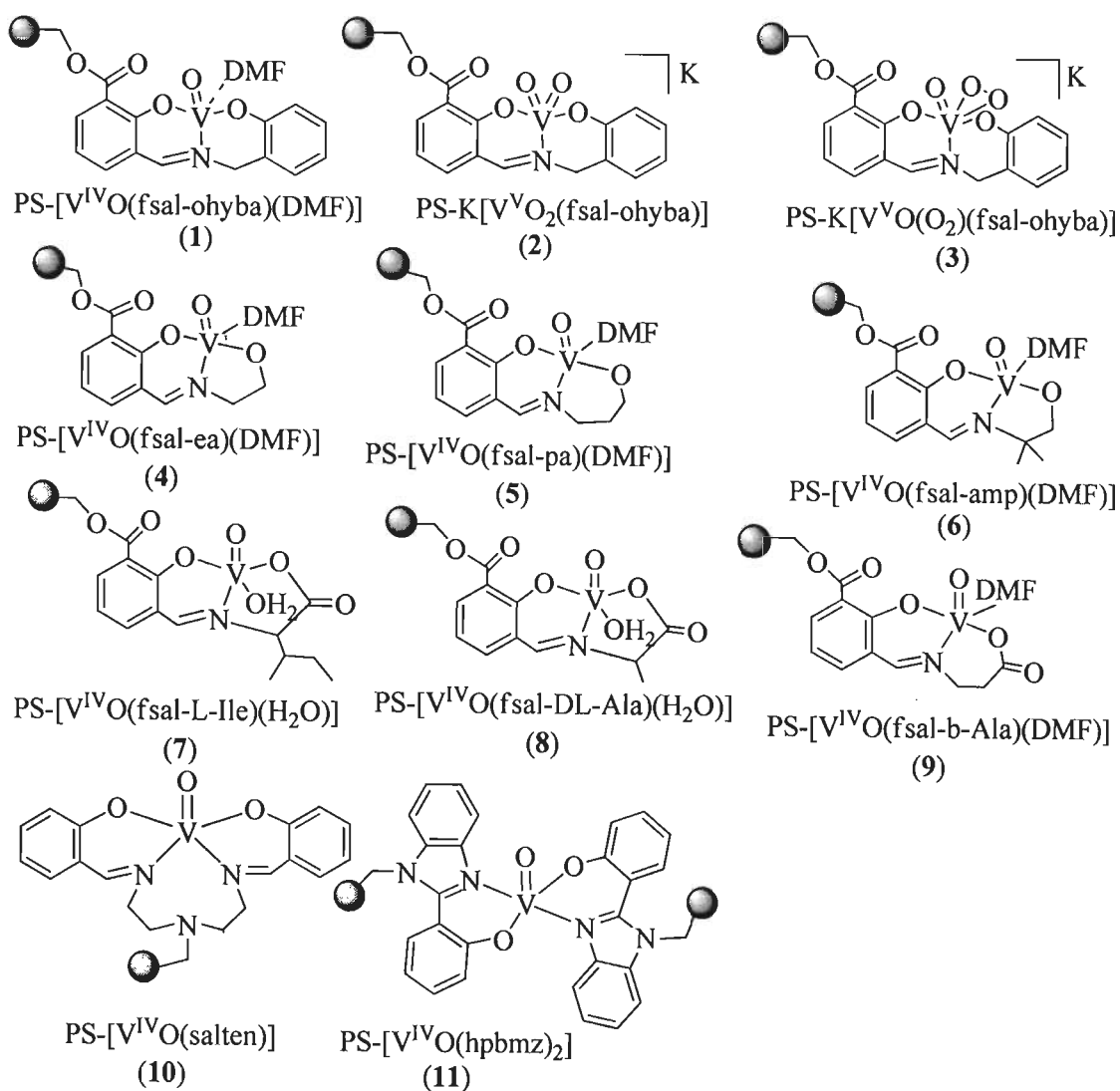


**Scheme 1.1.** Examples of reactions to establish covalent bonds between ligands and PS-Cl. The ball represents the backbone of chloromethylated polystyrene (abbreviated as PS-Cl).



**Scheme 1.2.** Examples of polymer-anchored ligands.

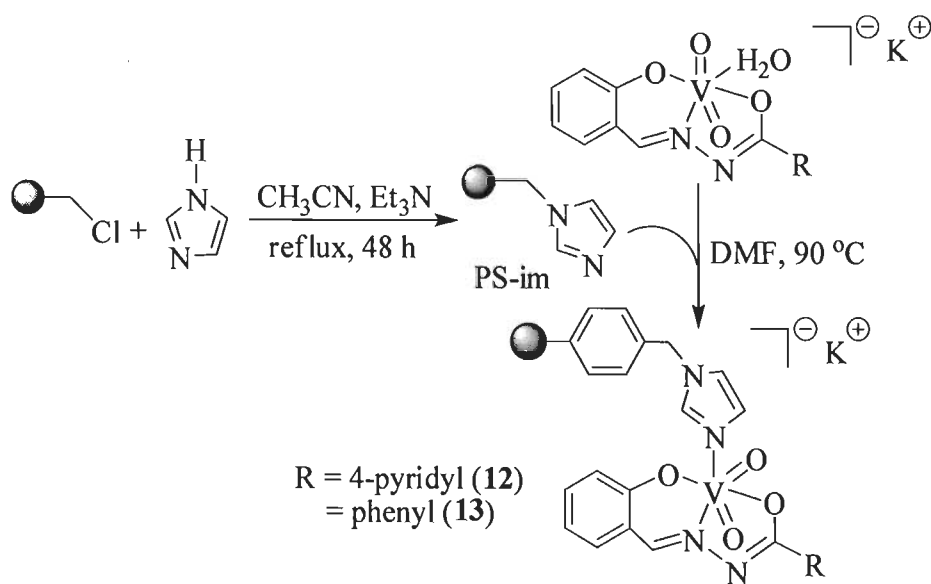
These polymer-anchored ligands on reaction with suitable metal precursors in solvents give the corresponding metal complexes. Some of the isolated and characterized vanadium complexes are grouped in Scheme 1.3. These complexes are used as catalysts for oxygen transformation reactions.



**Scheme 1.3.** Polystyrene bound vanadium complexes.

Metal complexes as such may form covalent bonds if a suitable coordinating site is present on the functional group attached to polymer. Thus, reaction of imidazolomethylpolystyrene (PS-im) with dioxidovanadium(V) complexes

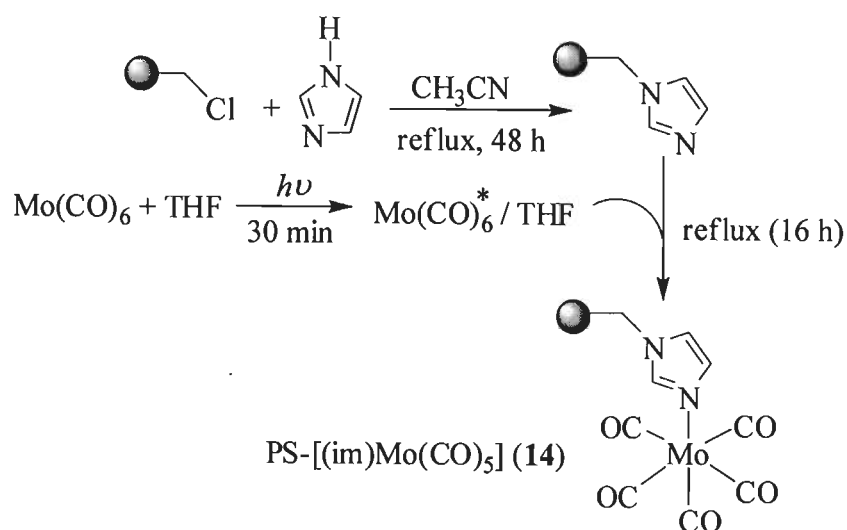
$K[V^VO_2(\text{sal-inh})]\cdot H_2O$  and  $K[V^VO_2(\text{sal-bhz})]\cdot H_2O$  dissolved in DMF gave the imidazolomethylpolystyrene bound complexes  $PS-K[V^VO_2(\text{sal-inh})(\text{im})]$  (**12**) and  $PS-K[V^VO_2(\text{sal-bhz})(\text{im})]$  (**13**), respectively; Scheme 1.4 [17]. The energy dispersive X-ray (EDX) analyses supported the presence of 1.2 % and 1.0 % vanadium in  $PS-K[V^VO_2(\text{sal-inh})(\text{im})]$  and  $PS-K[V^VO_2(\text{sal-bhz})(\text{im})]$ , respectively.



**Scheme 1.4.** Formation of  $PS-K[V^VO_2(\text{sal-inh})(\text{im})]$  (**12**) and  $PS-K[V^VO_2(\text{sal-bhz})(\text{im})]$  (**13**).

The haloperoxidases activity of these model heterogeneous catalysts has been demonstrated considering salicylaldehyde where oxidative brominated major product 5-bromosalicylaldehyde has been obtained selectively. They also catalyze the oxidation of methyl phenyl sulfide with high selectivity towards methyl phenyl sulfoxide. In general, the catalytic activities of immobilized catalysts are better than their non-immobilized analogues possibly due to their uniform distribution in polymer matrices. Relatively high turn over frequency and not much loss in the catalytic activities on recycling these catalysts demonstrate their practical applications.

Molybdenum hexacarbonyl also reacted directly with imidazole bound polystyrene (2 % cross-linked with divinylbenzene) to give polymer supported molybdenum carbonyl catalyst (PS-[(im) Mo(CO)<sub>5</sub>] (14, Scheme 1.5) [18]. Other polymer supported molybdenum carbonyl catalysts, PS-[(en)Mo(CO)<sub>4</sub>], PS-[(detn)Mo(CO)<sub>3</sub>] and PS-[(pipz)Mo(CO)<sub>6</sub>] with ethane-1,2-diamine (en), N<sup>1</sup>-(2-aminoethyl)ethane-1,2-diamine (detn) and piperazine (pipz) covalently bonded to polystyrene have also been prepared similarly and characterized. [19, 20]. All these complexes catalyze the oxidation of a range of alkenes to respective epoxides in the presence of TBHP in CCl<sub>4</sub>.



**Scheme 1.5.**

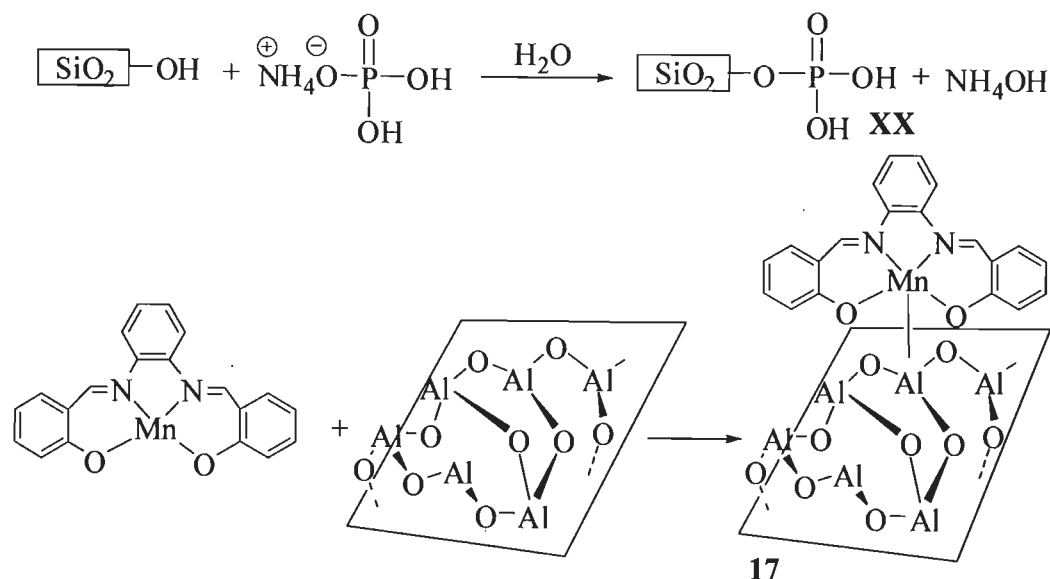
Chavan et al. have designed benzimidazole-functionalized dendrons to immobilize molybdenum complexes [21]. These dendrons react with Mo(CO)<sub>6</sub> and Mo(acac)<sub>2</sub> to give corresponding molybdenum supported complexes (Scheme 1.6) which are oxidatively stable, highly efficient and selective catalysts for the epoxidation of cyclohexene with TBHP as oxidant.

Polybenzimidazole it self has been used for the immobilization of complexes. It has further been modified with 2-(2-aminoethyl)pyridine via epoxidised polybenzimidazole (Scheme 1.7) and used as support for metal complexes [22].



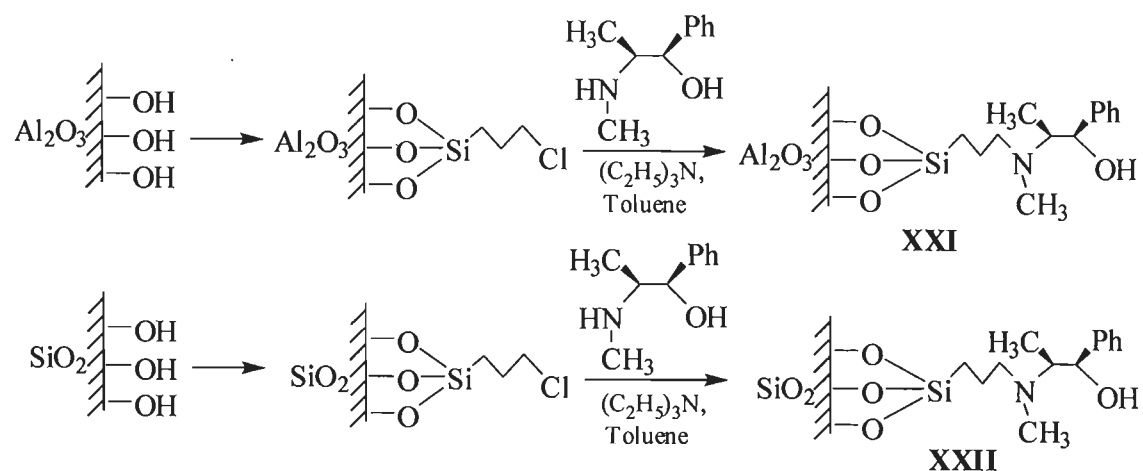
### 1.3. Alumina, silica and other supports for the immobilization of complexes

Alumina and silica have been used for the immobilization of various catalysts by direct reaction of surface hydroxyl groups with reactive species (catalyst); Scheme 1.8 [23-26].



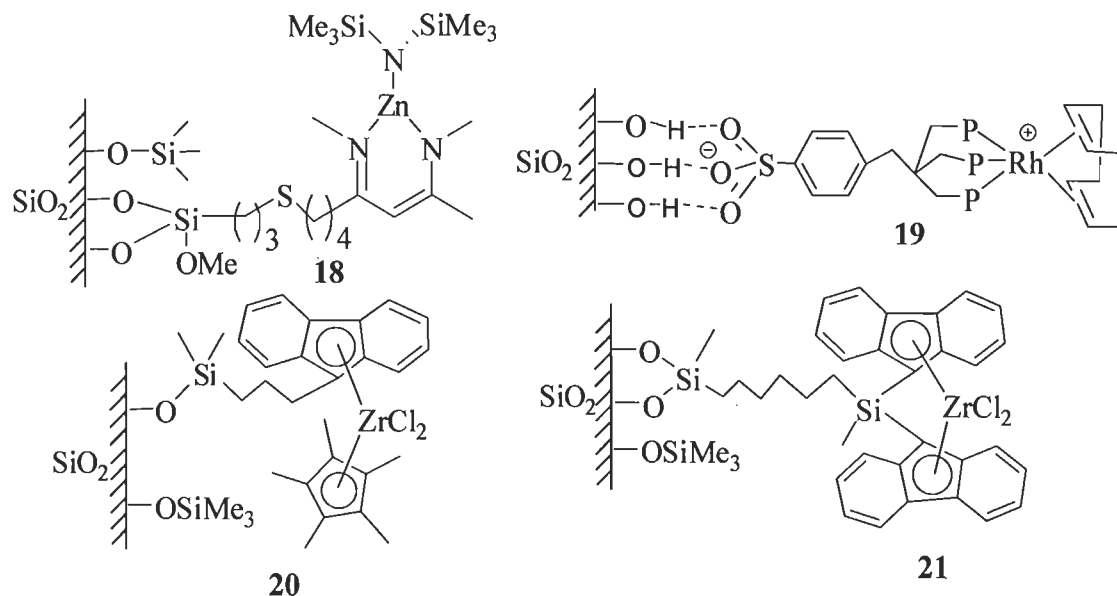
**Scheme 1.8.** Immobilization of catalysts on silica and alumina

Alumina and silica gels have also been modified to immobilize various catalysts by direct reaction of surface hydroxyl groups with reactive ligand(s); Scheme 1.9 [27].



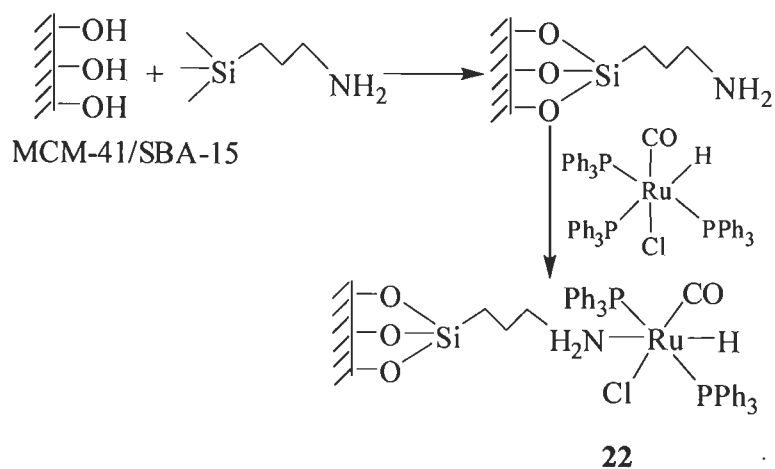
**Scheme 1.9.** Immobilization of catalysts on silica and alumina.

Other examples of silica modified immobilized catalysts are given in Scheme 1.10 [28, 29].

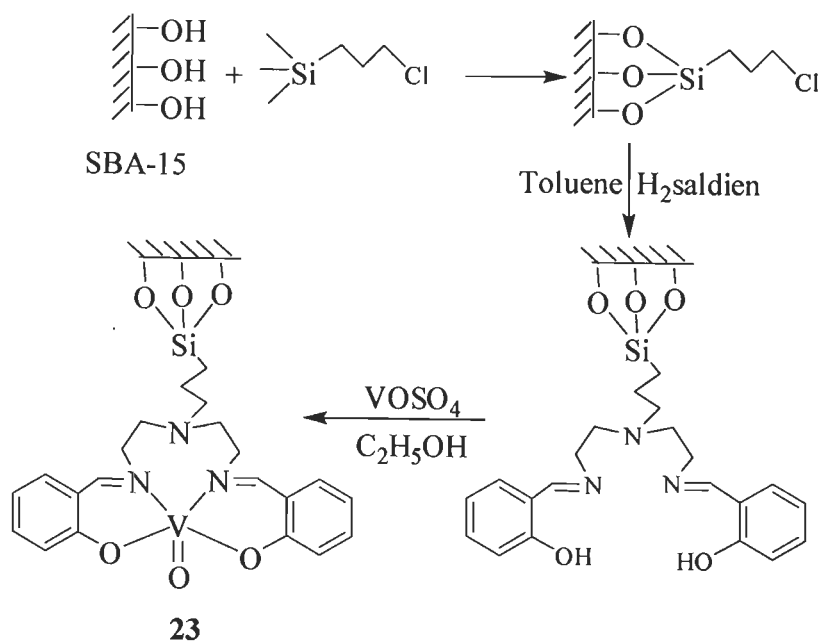


Scheme 1.10.

Halligudi *et al.* have reported the anchoring of  $[\text{RuH}(\text{CO})(\text{PPh}_3)_3\text{Cl}]$  [30] and  $[\text{VO}(\text{saldien})]$  ( $\text{H}_2\text{saldien} = \text{N,N}'\text{-bis}(\text{salicylidene})\text{diethylenetriamine}$ ) on SBA-15 [31] by functionalizing it as shown in Schemes 1.11 and 1.12.

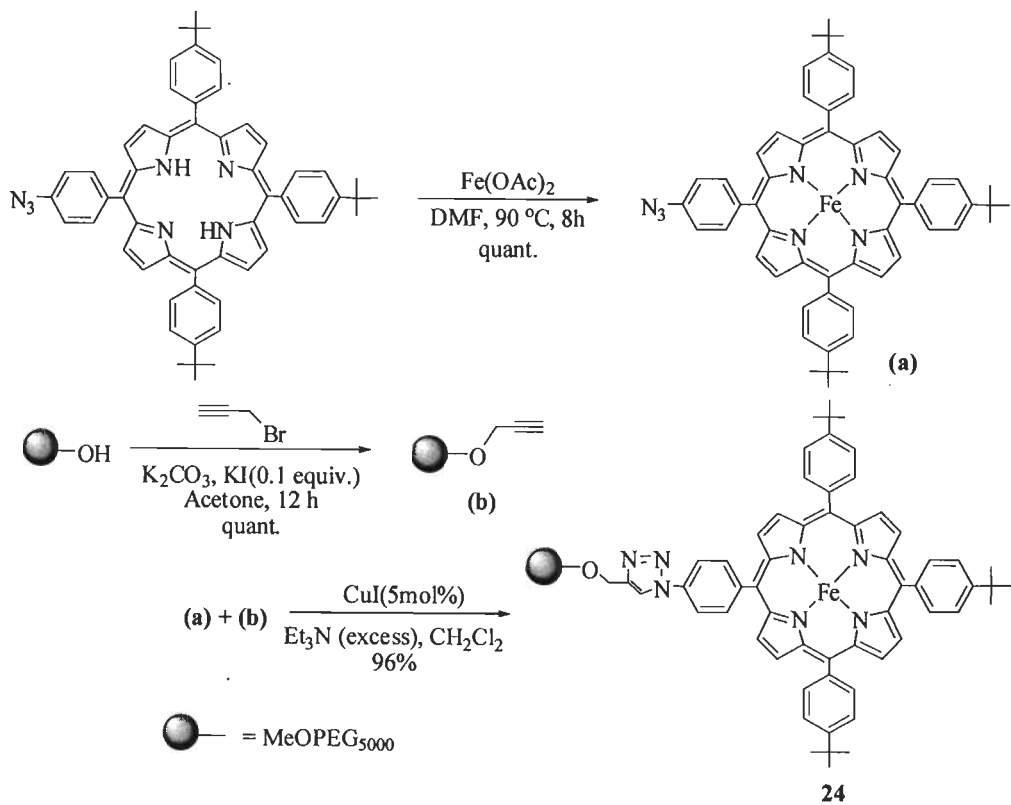


Scheme 1.11.

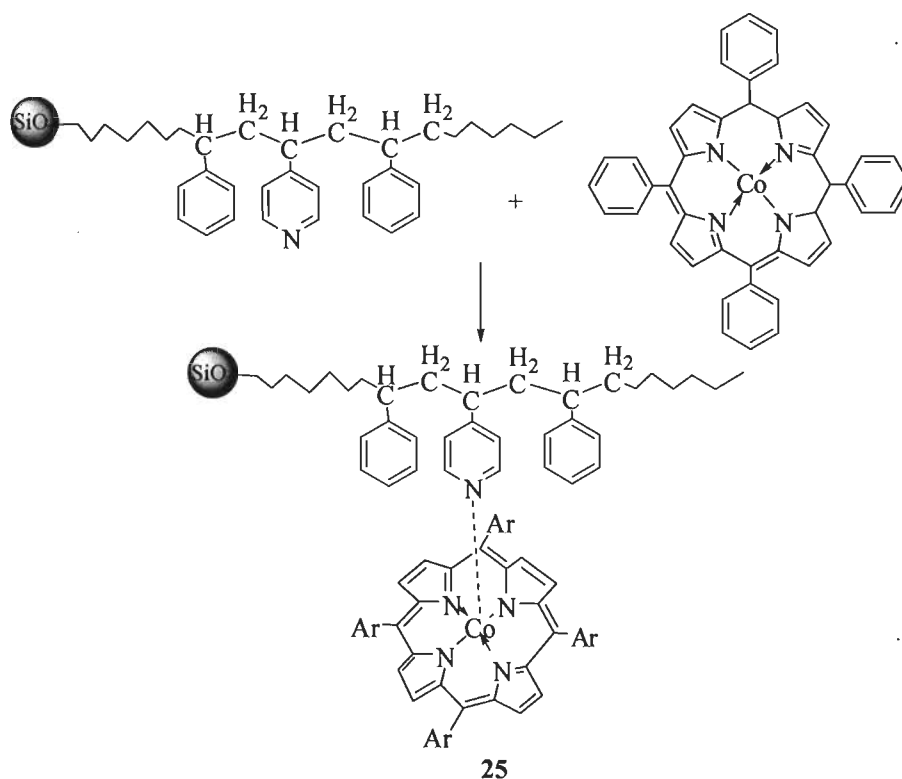


**Scheme 1.12.**

Metalloporphyrins have also been immobilized as shown in Scheme 1.13 [32, 33].

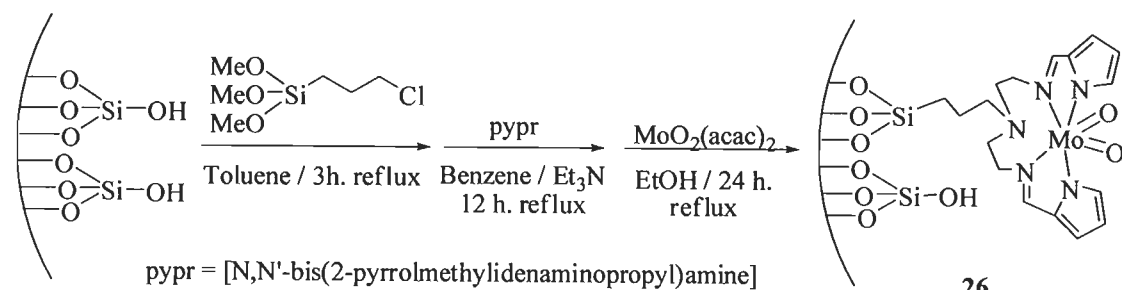






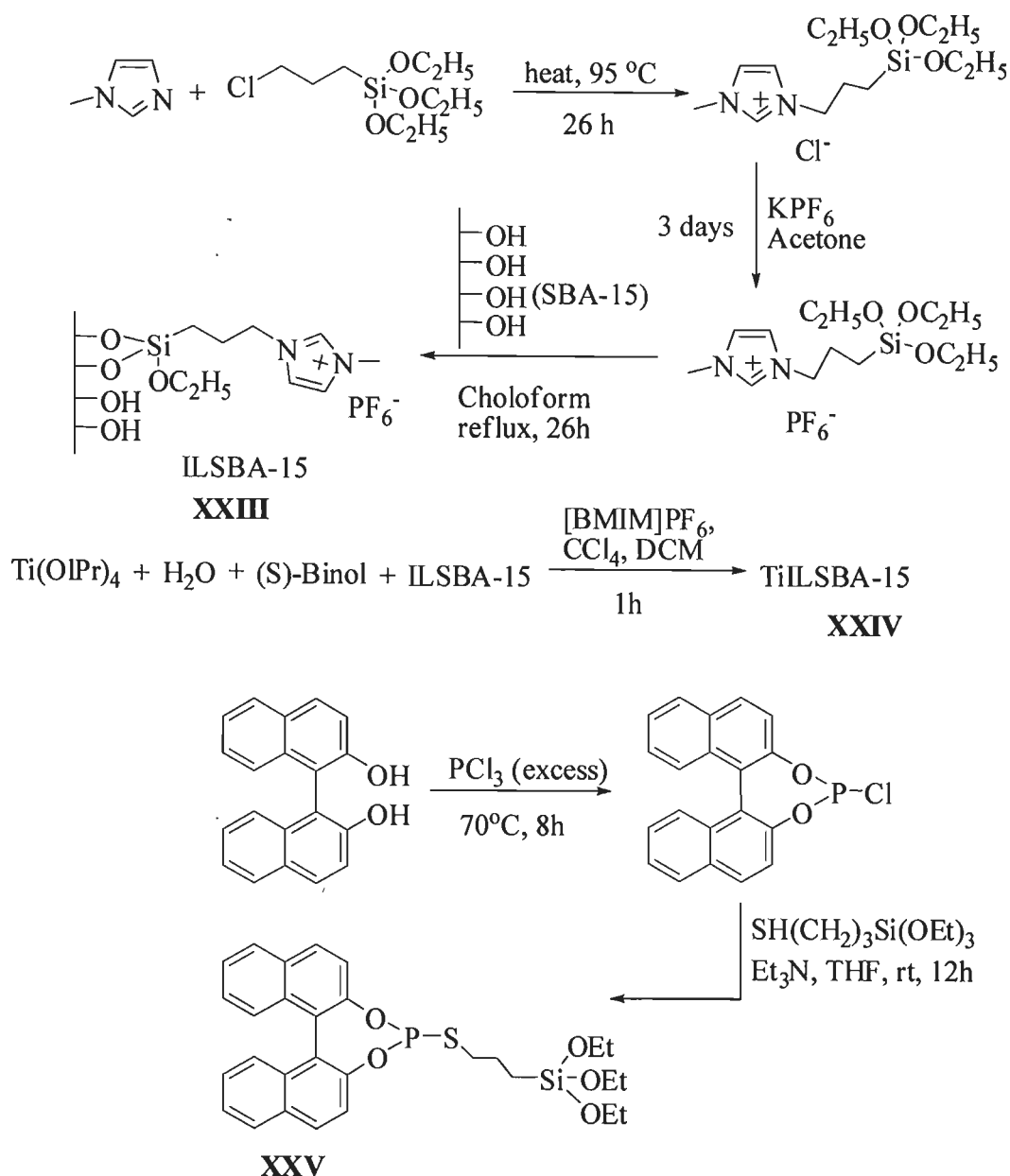
**Scheme 1.13.** Supported porphyrin complexes.

The mesoporous MCM-41 was discovered in 1992 [34]. After that it has attracted attention of various researchers as a solid support for heterogenization of various catalysts. The molecular sieves such as Si-MCM-41 and Si-SBA-15, have free hydroxyl group on the surface and therefore these materials are suitable aspirants for immobilization of catalyst. The dioxidomolybdenum(VI) complex has been immobilized to MCM-41 surface according to the procedure shown in Scheme 1.14 [35, 36].

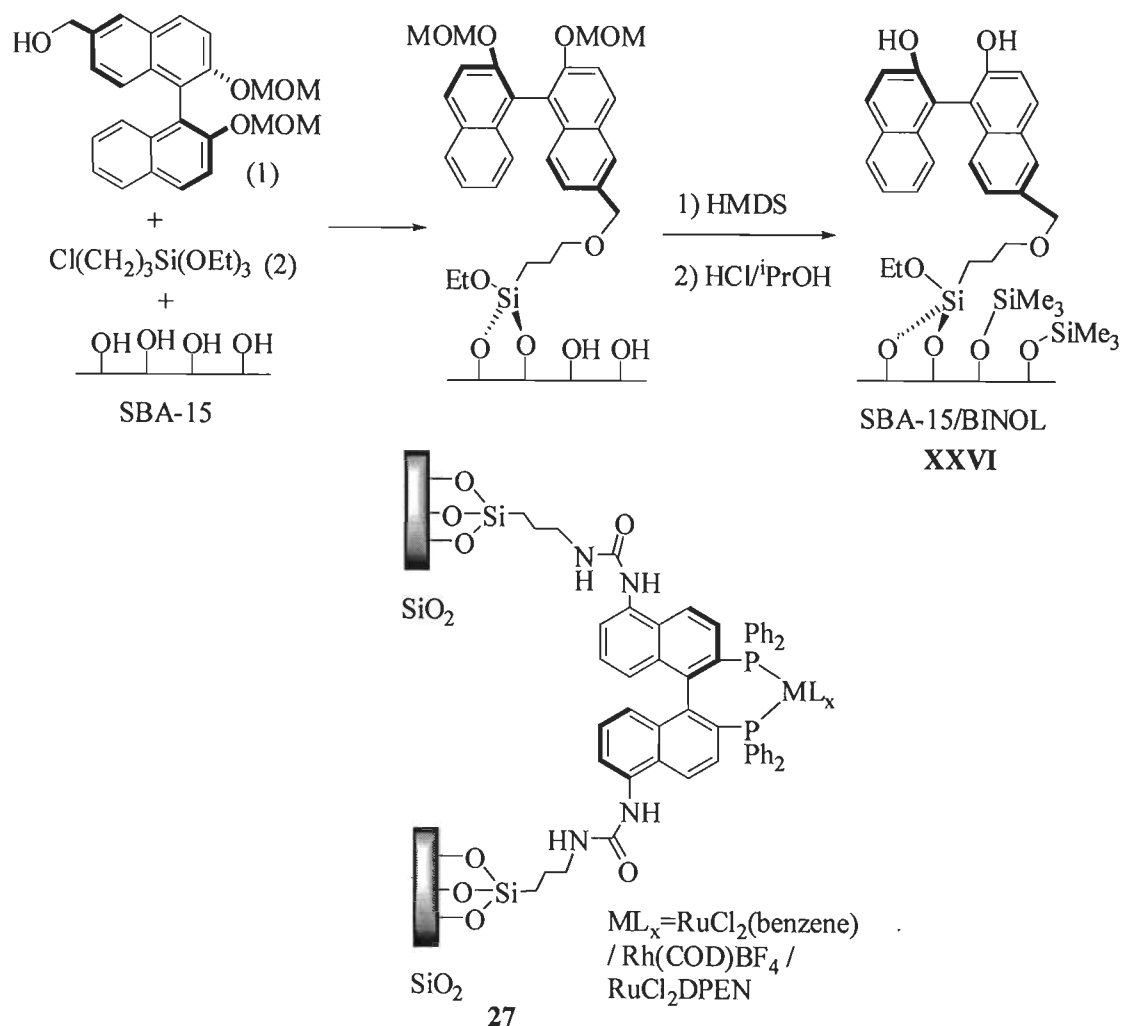


**Scheme 1.14.**

Halligudi *et al.* and others have reported the immobilization of chiral Ti-binol complex onto ionic liquid modified SBA-15 [37-39]. Similarly BINAP (2,2'-bis(diphenylphosphino)-1,1'-binaphthyl)-ruthenium and -rhodium complexes have been immobilized on silica [40] by functionalizing it as shown in Schemes 1.15 and 1.16.



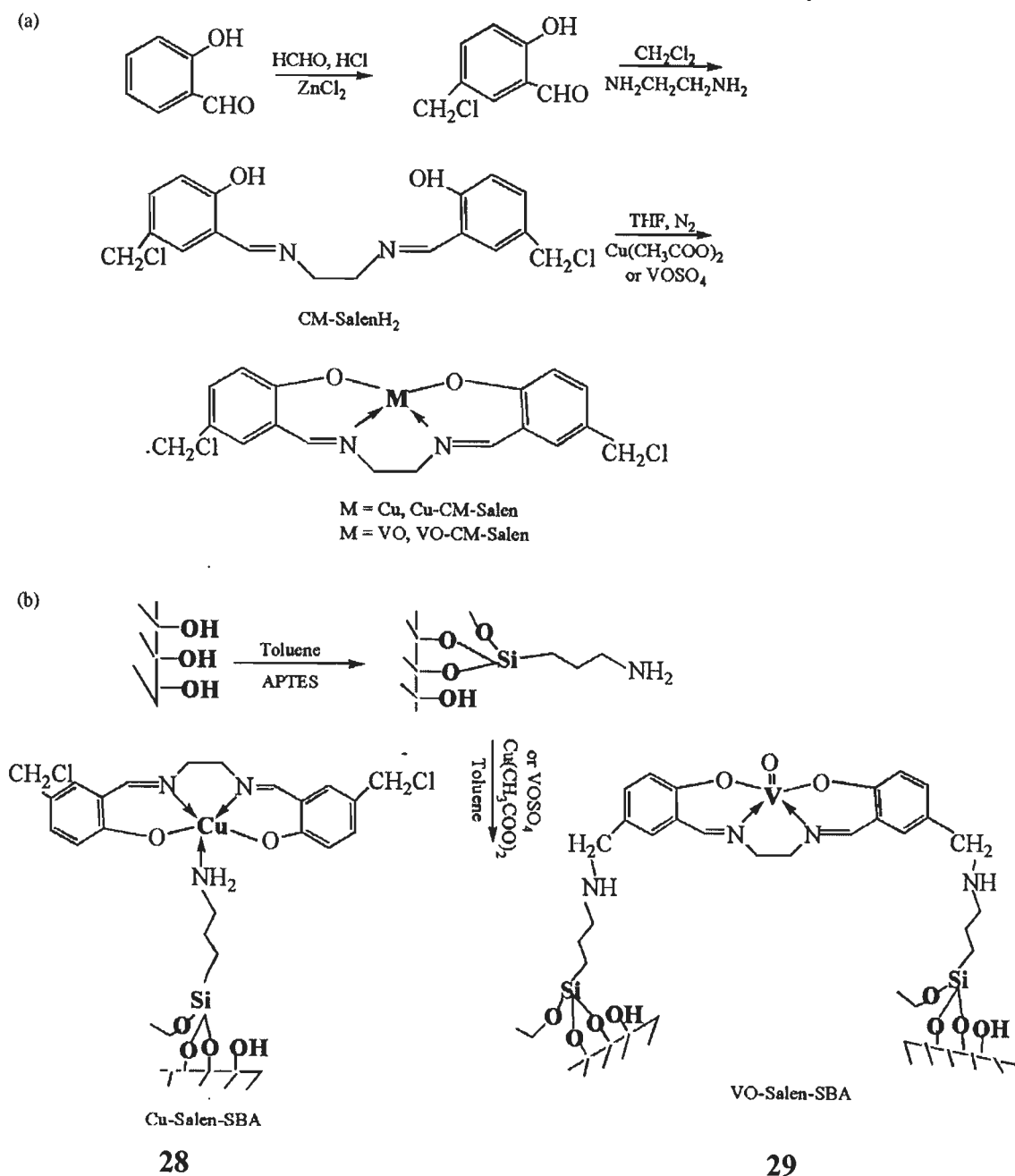
Scheme 1.15.



Scheme 1.16.

Copper(II) and oxidovanadium(IV) Schiff base complexes of type  $[\text{M}(\text{N}_2\text{O}_2)]$  has been directly anchored onto amino-modified SBA-15 materials [41]. The whole synthetic procedures to prepare complexes and their anchoring onto SBA-15 are presented in Scheme 1.17. The copper(II) complex was anchored through the coordination of copper atom with the nitrogen atom of the amino group of the modified SBA-15 while the oxidovanadium(IV) complex was covalently anchored on SBA-15 via the condensation reaction of the chloromethyl group of the Schiff base with the amino group of the modified SBA-15 matrix. The catalytic properties of supported copper(II) and oxidovanadium(IV) complexes in the oxidation of styrene with air or  $\text{H}_2\text{O}_2$  as oxidant were

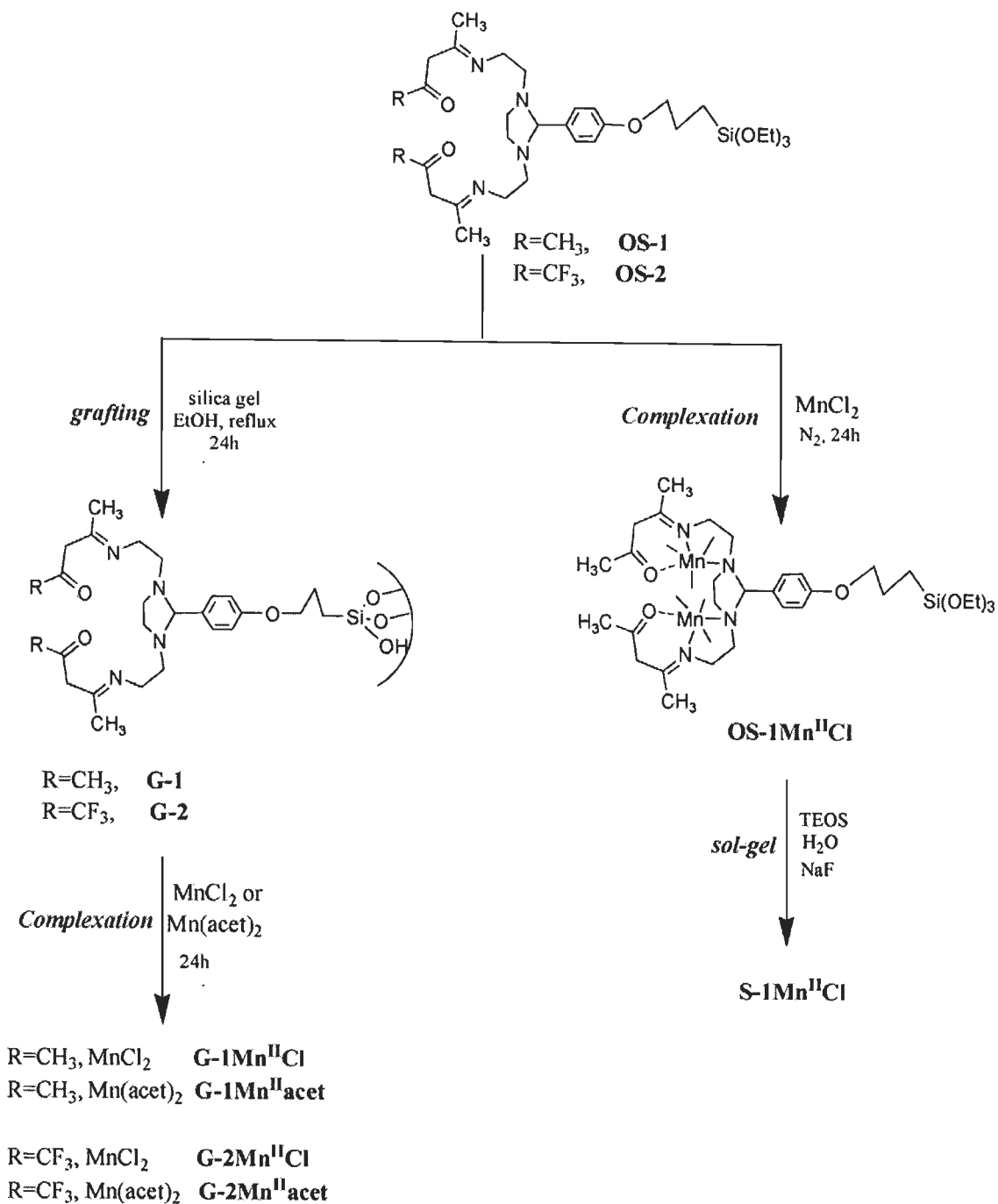
investigated and compared with the properties of their homogeneous analogues. Heterogeneous copper(II) and oxidovanadium(IV) catalysts are more active than their homogeneous analogues and the product selectivity depends upon the oxidants used. The supported oxidovanadium(IV) complex using air as oxidant shows high yield of styrene oxide (56.0%) and good recoverability.



Scheme 1.17. Supported complexes 28 and 29.

Mn(II) complexes of two symmetrical acetylacetonate-based Schiff bases have been immobilized on a silica surface by grafting and sol-gel procedure; Scheme 1.18 [42]. These supported manganese complexes evaluated as heterogeneous catalysts for alkene epoxidation with  $\text{H}_2\text{O}_2$  show remarkable effectiveness and selectivity towards epoxide formation in the presence of ammonium acetate. Moreover, the developed heterogeneous catalysts preserve the coordination and catalytic properties of the active-homogeneous manganese catalysts for alkene epoxidation vs. the competitive  $\text{H}_2\text{O}_2$  dismutation. EPR spectroscopy shows that in heterogeneous manganese catalysts the Mn(II) centers are in a flexible, non-tight, coordination environment, as in the corresponding homogeneous manganese catalysts. However, after a first use of the heterogeneous catalysts, the Mn centers are detached from the ligand and are randomly dispersed on the  $\text{SiO}_2$  surface.

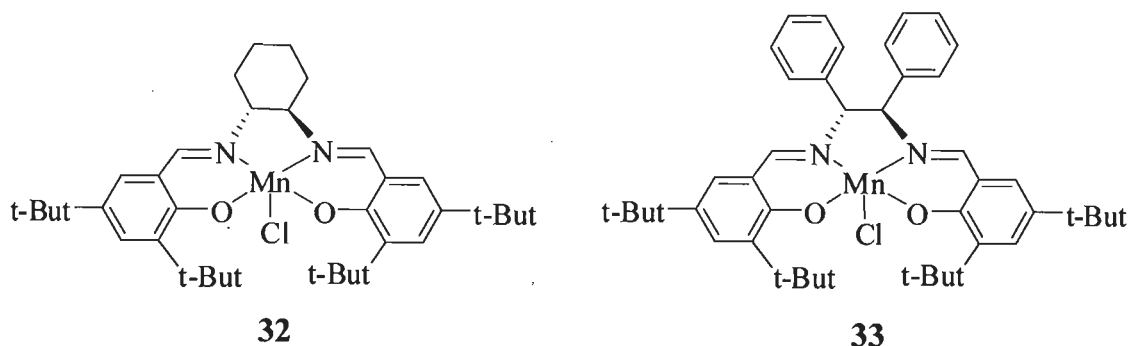
The imidazole-modified silica (SiIm) has been used for immobilization of octabromotetraphenylporphyrinatomanganese(III) chloride  $[\text{Mn}(\text{Br}_8\text{TPP})\text{Cl}]$  and tetraphenylporphyrinatomanganese(III) chloride  $[\text{Mn}(\text{TPP})\text{Cl}]$  as shown in Scheme 1.19 [43]. Imidazole of SiIm coordinates to Mn(III) centre of porphyrines to give heterogeneous catalysts  $[\text{Mn}(\text{Br}_8\text{TPP})\text{Cl}-\text{SiIm}]$  and  $[\text{Mn}(\text{TPP})\text{Cl}-\text{SiIm}]$ . These catalysts catalyze alkene epoxidation and alkane hydroxylation with  $\text{NaIO}_4$  under agitation with magnetic stirring. Ultrasonic irradiation enhanced the catalytic activity of these catalysts in alkene epoxidation and alkane hydroxylation along with shorter reaction times and higher product yields. These new heterogenized catalysts could be reused several times without significant loss of their catalytic activity.



**Scheme 1.18.** Immobilization of Mn(II) complexes on a silica surface by grafting and sol-gel procedure. Reproduced from ref. 42.

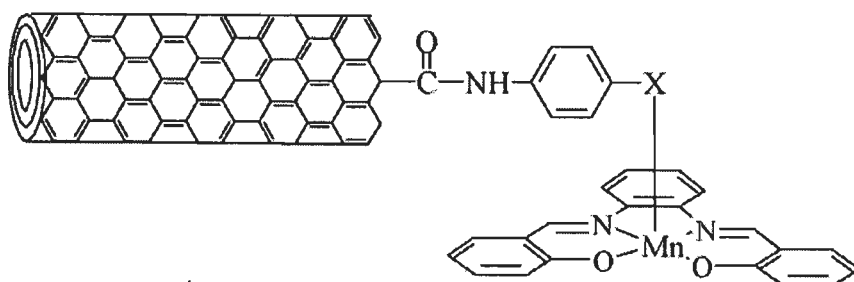


14 eeb %, which is higher than the value found for the homogeneous catalyst under similar conditions. The clay pillars partially collapse after two runs.



**Scheme 1.20.** Mn(III) complexes

Tangestaninejad et al. have reported manganese(III) salophen chloride [Mn(salophen)Cl], supported on functionalized multi-wall carbon nanotubes MWCNTs (Scheme 1.21) [45]. The MWCNT was modified with 1,4-diaminobenzene, 4-aminophenol and 4-aminothiophenol and [Mn(salophen)Cl] was attached to the supports via axial ligation. These new heterogenized catalysts were characterized by elemental analysis, FT-IR and diffuse reflectance spectrometry and scanning electron microscopy. These catalysts are effective for efficient epoxidation of alkenes with NaIO<sub>4</sub> at room temperature. These heterogeneous catalysts were highly reusable in the oxidation reactions and reused several times without significant loss of their catalytic activity.

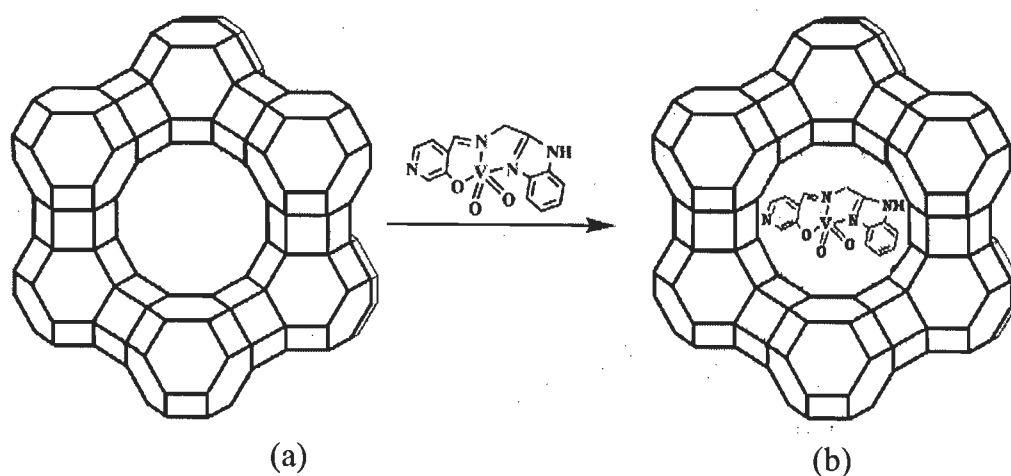


**Scheme 1.21.** Multi-wall carbon nanotube supported Mn(III) complex (34).



#### 1.4. Encapsulation of metal complexes in Zeolite-Y and their catalytic activities

Zeolites are crystalline hydrated aluminosilicates with open framework structures constructed from  $\text{AlO}_4$  and  $\text{SiO}_4$  tetrahedra linked to each other by sharing all oxygen atoms, forming nanocavities and nanochannels of strictly regular dimensions and of different sizes and shapes. **Encapsulation** is a process that does not require interactions between the catalyst and the support, and thus this method mimics the homogeneously catalyzed reactions. However, the important condition for encapsulation is that the catalyst must be larger than the pores of the support material to prevent loss of the catalyst into solution during the course of the reaction, or recovery process [6]. The large size of the encapsulated homogeneous catalysts and their rigidity make them difficult to escape out of the zeolite cages; Scheme 1.22.



**Scheme 1.22.** Structure of zeolite-Y (a) and a metal complex encapsulated in the cavity of zeolite-Y (b).

The super cages of zeolites have attracted attention of researcher for the encapsulation of transition metal complexes. This new class of catalysts is called Zeolite Encapsulated Metal Complexes (ZEMC) or ship-in-bottle complexes. As metal complex is not bonded to the host zeolite cavity, it shares advantageous

features of homogeneous catalyst as well. The pore size of zeolite makes the catalyst shape and size selective.

Romanovskii has reviewed the oxidation of various substrates using metal phthalocyanines as catalyst [46]. Jacobson's catalyst encapsulated in Na-Y has emerged as an important catalyst for the oxidation of olefins [47].

Poltowicz *et al.* have encapsulated whole range of metallosalen complexes (e.g. [Fe(salen)], [Mn(salen)], [Cu(salen)] and Co(salen)]) in Na-X zeolite to study catalytic activity for the oxidation of cyclooctane. A model structure of entrapped [Co(salen)] complex is reproduced in Figure 1.1 [48].

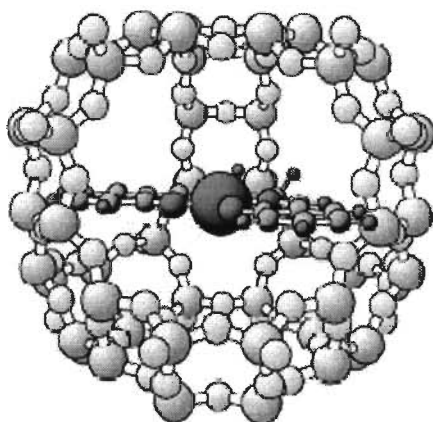
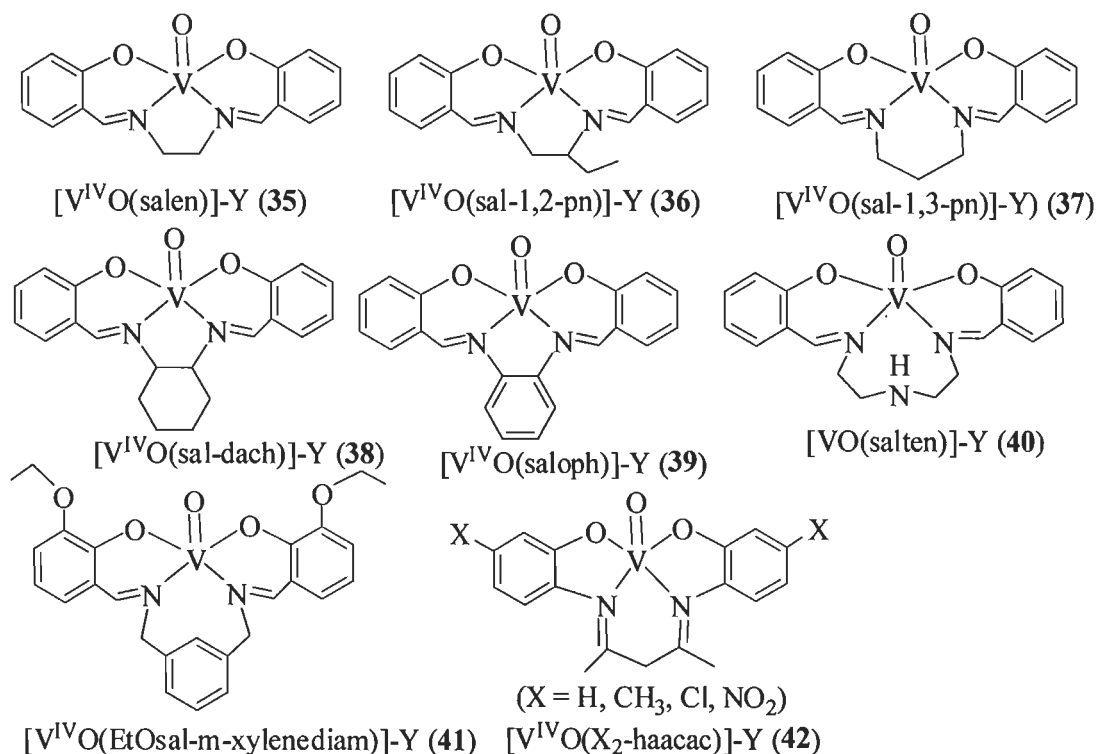


**Figure 1.1.** Model structure of entrapped [Co(salen)] complex in zeolite-X. Reproduced from reference [48].

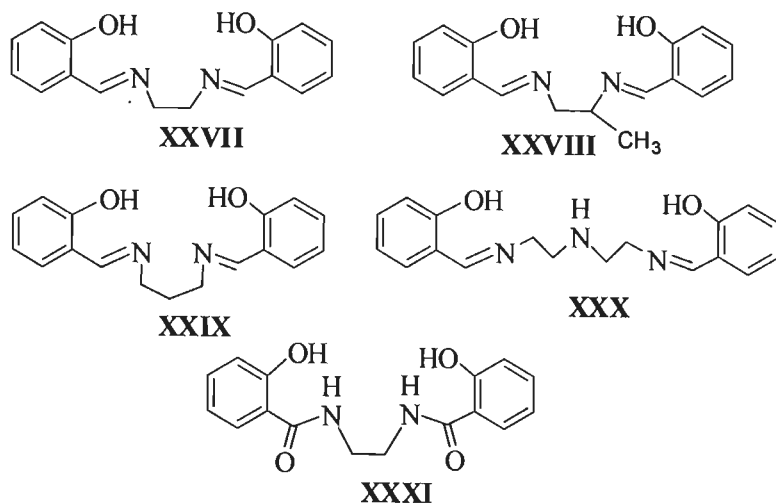
Schemes 1.23 presents some examples of zeolite-Y encapsulated metal complexes (35-42) [49 -54]



**Scheme 1.23.** Proposed zeolite-Y encapsulated vanadium complexes 35-42.

Ratnasamy *et al.* have isolated copper(II) and manganese(III) complexes of salen derivatives encapsulated in the cavity of zeolite-X and zeolite-Y. Cyclic voltammetric studies for manganese(III) complexes indicate that the zeolite matrix facilitates the reduction of Mn(III) to Mn(II) and this suggests that zeolite behaves like electron-withdrawing substituent. The oxidation of styrene under aerobic conditions using tert-butylhydroperoxide gave benzaldehyde, styrene and phenylacetaldehyde. The catalytic efficiency of these encapsulated complexes was much higher than the corresponding neat complexes. Electron withdrawing substituents such as -Cl, -Br, -NO<sub>2</sub> on the aromatic ring enhances the rate of oxidation [55, 56]. These complexes also catalyze the oxidation of phenol and *p*-xylene. Mn(X-sal-1,3-pn)Cl]-X and [Mn(sal-dach)Cl]-X H<sub>2</sub>sal-dach = Schiff derived from salicylaldehyde and 1,2-diaminocyclohexane) at low temperature showed as high as 60 % conversion. Again conversion increased in presence of electron withdrawing group on the aromatic ring [57, 58].

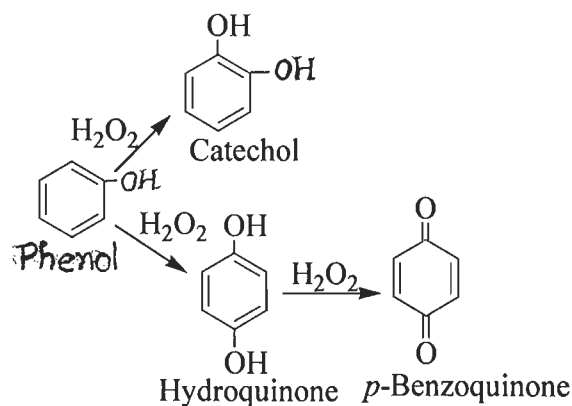
Oxidovanadium(IV) complexes of  $H_2salen$  (XXVII),  $H_2sal-1,2-pn$  (XXVIII),  $H_2sal-1,3-pn$  (XXIX),  $H_2saldien$  (XXX) and  $H_2hybe$  (XXXI) of Scheme 1.24 have been encapsulated in the cavity of zeolite-Y. These complexes catalyse the oxidation of phenol. The oxidation of phenol is one of the industrially important reactions. As the hydroxyl group on phenol is *ortho* and *para* directing, the catalytic oxidation of phenol usually gives two products catechol and hydroquinone. In some cases a further oxidation also occurs to give *p*-benzoquinone as shown in Scheme 1.25. Catechol has been used for pest control, pharmaceuticals, and flavors and aromas. Hydroquinone has mainly been used as photographic developer, polymerization inhibitor, antioxidant and intermediate for numerous dyes. Under the optimized conditions  $[VO(sal-1,3-pn)]-Y$  has shown ca. 34 % conversion while other two complexes,  $[VO(salen)]-Y$  and  $[VO(saldien)]$  register only 33 % conversion. As high as 90 % selectivity of catechol has been observed by later two complexes [59]. Oxidation of cyclohexane has also been carried out by similar complexes [60, 61].



Scheme 1.24.

$Mn(X-salen)$  ( $X = H, Cl, Br$  or  $NO_2$ ), have been used as catalysts for the oxidation of phenol [62]. The oxidation products are mainly catechol and hydroquinone. In no cases the formation of 1,4-benzoquinone was detected. Oxidation of phenol has also been reported using copper(II), nickel(II), iron(III), chromium(III), bismuth(III) and zinc(II) complexes of ligands XXVII to XXXI

encapsulated in zeolite-Y. In all cases conditions have been optimized considering effect of amount of catalyst, effect of substrate,  $\text{H}_2\text{O}_2$  concentration and volume of solvent. It was observed that substrates to oxidant ratio of 1:2 worked nicely to effect maximum oxidation. The 3D model structure of  $[\text{Fe}(\text{hybe})(\text{H}_2\text{O})_2]^+$  was created using CS Chem 3D ultra molecular modeling programme to show that zeolite-Y can accommodate the complex in its super cages without any strain; Figure 1.2 [63-66]. Similarly catalyst  $[\text{V}^{\text{IV}}\text{O}(\text{EtOsalph})]\text{-Y}$  had 71% conversion after 2 h with selectivity of 92 % towards catechol, while  $[\text{V}^{\text{IV}}\text{O}(\text{EtOsalnaph})]\text{-Y}$  exhibited 77 % conversion after 6 h with almost identical selectivity to catechol (94 %) [67].



**Scheme 1.25.** Various products of phenol oxidation.

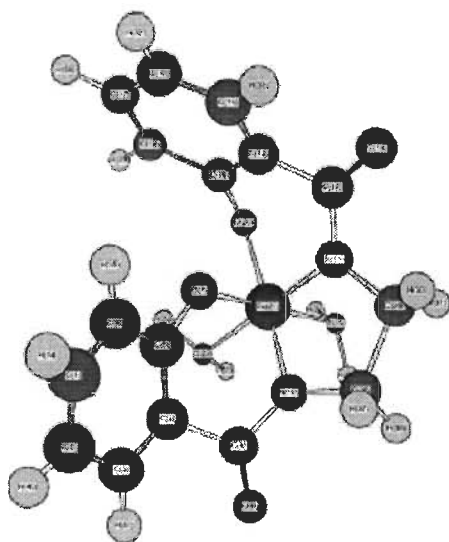
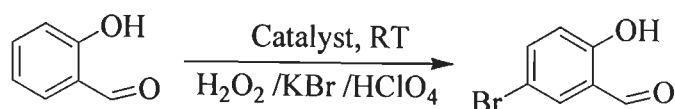


**Figure 1.2.** 3D model structure of  $[\text{Fe}(\text{hybe})(\text{H}_2\text{O})_2]^+$ .

Encapsulation of vanadium phthalocyanine complex in zeolite-Y [ $V^{IV}Pc$ ]-Y (33) was achieved by the “template synthesis method” where the phthalocyanine was prepared using precursors in the presence of zeolite-Y followed by its reaction with  $V^{IV}OSO_4$  [68]. This catalyst also catalyzes the oxidation of phenol.

Under the optimized reaction conditions  $NH_4[V^VO_2(sal-inh)]-Y$  and  $NH_4[V^VO_2(sal-oap)]-Y$  give ca. 26 % conversion of phenol with catechol (85 and 77 % selectivity, respectively) as major product after 6 h [69]. Under similar conditions,  $[V^{IV}O(sal-1,3-pn)]-Y$  showed the highest conversion of 34 % after 6 h,  $[V^{IV}O(salen)]-Y$  and  $[V^{IV}O(saldien)]-Y$  had comparable catalytic activity while  $[V^{IV}O(sal-1,2-pn)]-Y$  had the poorest performance (11 % conversion). All these catalysts are more selective (90%) toward formation of catechol, except  $[V^{IV}O(sal-1,3-pn)]-Y$  which only gave ~68 % selectivity[59].

Oxidative bromination of salicylaldehyde to 5-bromosalicylaldehyde (Scheme 1.26) catalyzed by  $NH_4[V^VO_2(sal-inh)]-Y$  ( $H_2sal-inh$  = Schiff base derived from salicylaldehyde and isonicotinic acid hydrazide), a process also mimicking vanadium bromoperoxidases (VBrPO) enzymes, has been reported by Maurya et al. [70]. By using  $H_2O_2$  as an oxidant in the presence of KBr and  $HClO_4$  the conversions were 27 – 34 % with ca. 87% selectivity after 4 h of reaction time for the major product formed, 5-bromosalicylaldehyde. Comparing with other similar catalyst, their efficiency varied in the order:  $NH_4[V^VO_2(sal-inh)]-Y$  (34%) >  $NH_4[V^VO_2(sal-oap)]-Y$  (26.8%) >  $Na/NH_4V^VO_3-Y$  (22%). The presence of acid was found to be essential for the catalytic oxidative bromination. As zeolite is not affected by small amount of acid used in catalytic experiment due to reexchangeable property of  $Na^+ / NH_4^+$  present in zeolite-Y with  $H^+$  ion, it prevented decomposition of vanadium complexes present in the cavity of zeolite-Y.



**Scheme 1.26.** Oxidation product of salicylaldehyde.

Jacobs *et al.* have reported  $cis$ -[Mn(bipy)<sub>2</sub>]<sup>2+</sup> encapsulated in zeolite X and Y and used them for the oxidation of a series of alkenes and cycloalkenes with H<sub>2</sub>O<sub>2</sub> as oxidant. The percent conversion and selectivity of various products at room temperature are summarized in Table 1.2. The catalytic epoxidation of cycloalkene is followed by acid-catalyzed ring opening. Thus, adipic acid from cyclohexene has also been obtained [71].

Similar iron(II) and manganese(II) complexes of 2,2'-dipyridyl have also been isolated by Niassary *et al.* for the oxidation of cyclic ethers, such as, tetrahydrofuran, tetrahydropyron, 2,3-dihydropyron and 1,4-dioxane using H<sub>2</sub>O<sub>2</sub> and TBHP as oxidant. Mainly cyclic ether-2-ols and cyclic ether-2-ones have been obtained. Minor product, 2,3-dihydro cyclic ether has also been detected in some cases [72].

**Table 1.2.** Oxidation of alkenes on  $cis$ -[Mn(bpy)<sub>2</sub>]<sup>+2</sup> in zeolite X and Y at 293 K [71].

S. No.	Catalyst	Substrate	Time (h)	Conv. (%)	Selectivity (%)		
					Oxide	Diol	Diacid
1	[Mn(bpy) <sub>2</sub> ]-X	1-Hexene	4	2	81	14	--
2	[Mn(bpy) <sub>2</sub> ]-Y	1-Hexene	18	20	50	40	--
3	[Mn(bpy) <sub>2</sub> ]-X	Cyclohexene	4	41	62	32	--
4	[Mn(bpy) <sub>2</sub> ]-Y	Cyclohexene	18	62	6	79	--
5	[Mn(bpy) <sub>2</sub> ]-Y	Cyclohexene	40	100	--	--	80
6	[Mn(bpy) <sub>2</sub> ]-X	1-Dodecene	4	11	74	22	--
7	[Mn(bpy) <sub>2</sub> ]-Y	1-Dodecene	18	20	10	88	--
8	[Mn(bpy) <sub>2</sub> ]-X	Cyclododecene	4	38	78	22	--
9	[Mn(bpy) <sub>2</sub> ]-Y	Cyclododecene	18	56	4	87	--
10	[Mn(bpy) <sub>2</sub> ]-Y	Cyclododecene	40	100	--	--	84

Complexes  $[\text{VO}_2(\text{sal-ambmz})]-\text{Y}$  ( $\text{Hsal-ambmz}$  = Schiff base derived from salicylaldehyde and 2-aminomethylbenzimidazole),  $[\text{V}^{\text{IV}}\text{O}(\text{sal-oaba})(\text{H}_2\text{O})]-\text{Y}$  ( $\text{H}_2\text{sal-oaba}$  = Schiff base derived from salicylaldehyde and o-aminobenzyl alcohol) and  $[\text{V}^{\text{IV}}\text{O}(\text{tmbmz})_2]-\text{Y}$  ( $\text{Htmbmz}$  = thiomethylbenzimidazole) exhibited good/excellent catalytic activity for the oxidation of methyl phenyl sulfide with high turn over frequency (TOF) along with good selectivity towards sulfoxide [73–75].

Catalytic oxidation of styrene using a mild oxidant such as TBHP gives styrene oxide as the main product while a stronger oxidant such as  $\text{H}_2\text{O}_2$  gives rise to several other products. For examples, the zeolite-Y encapsulated complexes  $[\text{VO}(\text{tmbmz})_2]-\text{Y}$ ,  $[\text{VO}(\text{saldien})]-\text{Y}$ ,  $[\text{V}^{\text{V}}\text{O}_2(\text{sal-ambmz})]-\text{Y}$ ,  $[\text{V}^{\text{V}}\text{O}_2(\text{sal-oaba})\text{H}_2\text{O}]-\text{Y}$  and  $[\text{V}^{\text{V}}\text{O}(\text{sal-dach})]-\text{Y}$  catalyzed the oxidation of styrene and gave at least five products [53, 53, 59, 73-75]. Table 1.3 presents conversion and selectivity data for various catalysts used.

**Table 1.3.** Conversion of styrene, product selectivity and TOF.

Catalyst	% Conv.	TOF/ $\text{h}^{-1}$	% Selectivity <sup>b</sup>					
			so	phaa	bza	bzac	phed	Others
$[\text{VO}(\text{tmbmz})_2]-\text{Y}$	96	205	6.1	2.3	68.1	9.6	12.4	1.5
$[\text{VO}_2(\text{sal-ambmz})]-\text{Y}$	97	151	5.4	0.2	54.9	13.2	25.3	1.0
$[\text{VO}_2(\text{sal-oaba})\text{H}_2\text{O}]-\text{Y}$	89	696	6.8	2.1	58.8	6.7	24.1	1.5
$[\text{VO}(\text{sal-dach})]-\text{Y}$	95	328	7.6	4.9	54.2	8.9	22.5	1.9
$[\text{VO}(\text{saldien})]-\text{Y}$	35	2362	35.5	-	11.5	-	-	53.0
$[\text{VO}(\text{saldien})]-\text{Y}^{\text{a}}$	30	-	27.6	-	13.8	-	-	58.6

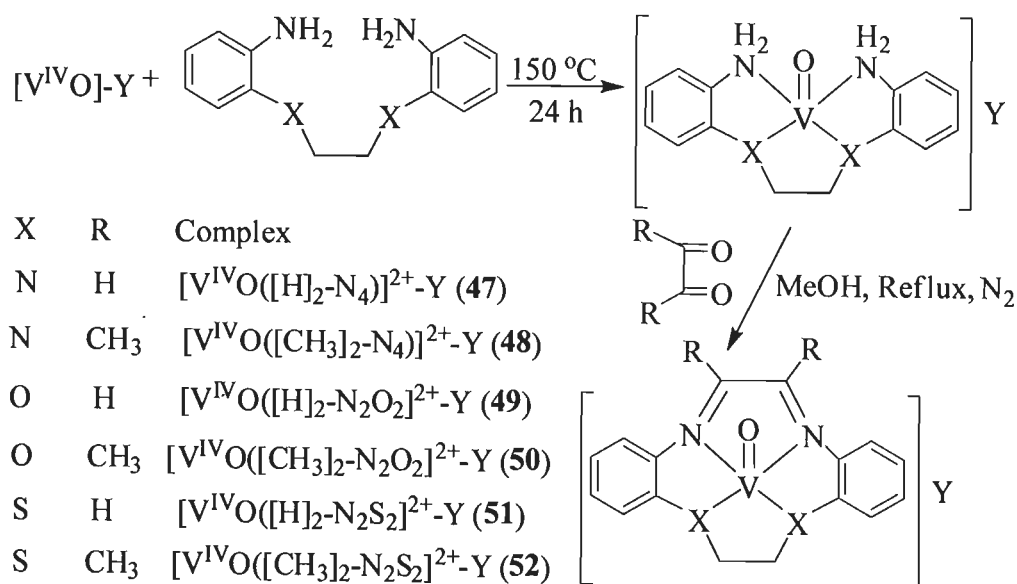
<sup>a</sup> First cycle of used catalyst.

<sup>b</sup>so = styrene oxide, phaa = phenylacetaldehyde, bza = benzaldehyde, bzac = benzoic acid and phed = 1-phenylethane-1,2-diol.



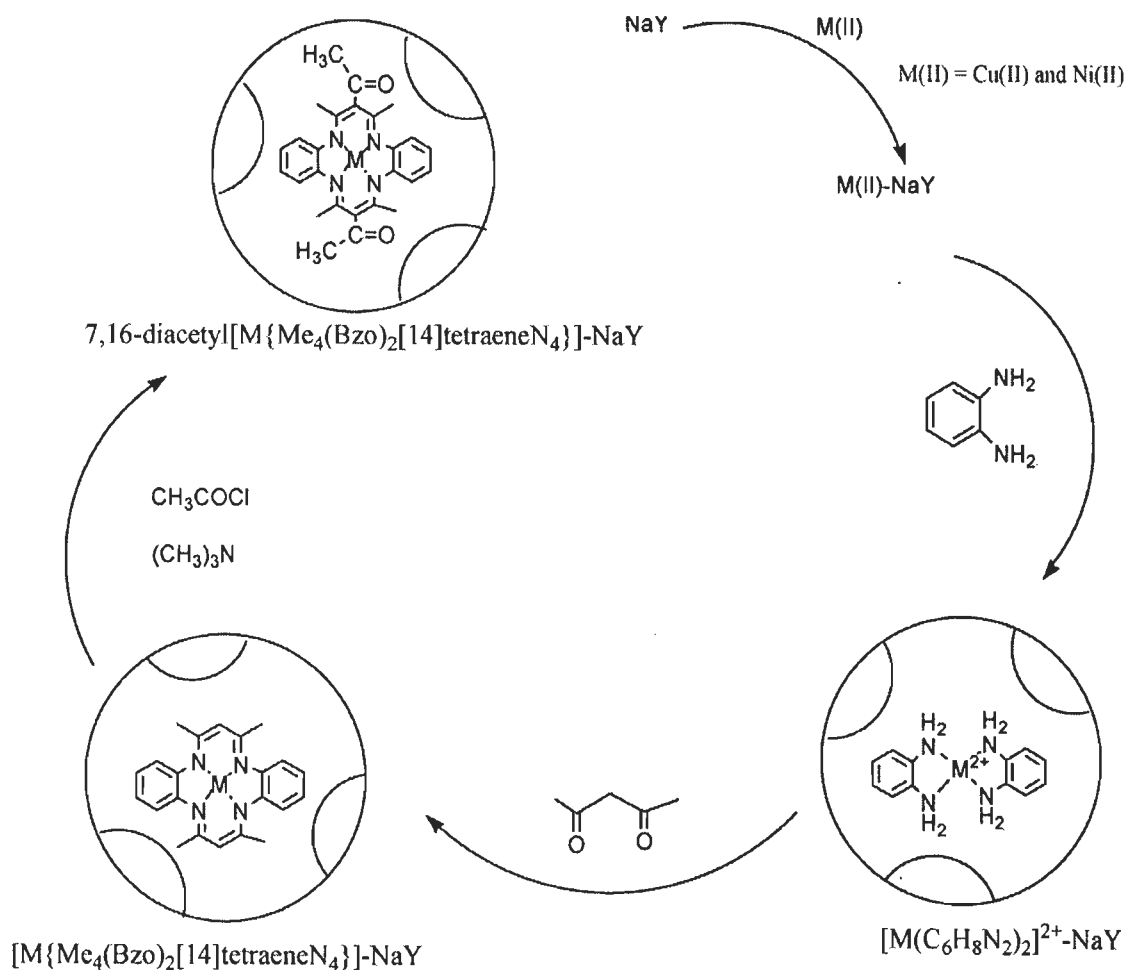


activity on reuse [77, 78]. The corresponding N<sub>4</sub>-macrocyclic oxidovanadium(IV) complexes exhibited slightly lower activity in the oxidation of phenol (20 – 43%) using H<sub>2</sub>O<sub>2</sub> as oxidant. The selectivity of catechol varied between 63 -79 % and was also slightly lower than the corresponding encapsulated ones. Again, conversion of phenol as well as selectivity of catechol both was low with sulfur containing complexes.



**Scheme 1.28.** Synthesis of entrapped zeolite-Y V<sup>IV</sup>O-complexes 47-52 [61].

Oxidation of styrene has also been studied using tetraazamacrocyclic complexes, 7,16-diacetyl[M{Me<sub>4</sub>(Bzo)<sub>2</sub>[14]tetraeneN<sub>4</sub>}], {M= Cu(II) and Ni(II)} encapsulated in the cavity of Zeolite-Y; Scheme 1.29 [79]. These encapsulated tetraazamacrocyclic complexes have been used as a heterogeneous catalyst for the oxidation of styrene and for the solvent free oxidation of benzyl alcohol using hydrogen peroxide as oxidant. The solvent free catalyzed oxidation of benzyl alcohol catalyzed by 7,16-diacetyl[Cu{Me<sub>4</sub>(Bzo)<sub>2</sub>[14]tetraeneN<sub>4</sub>}]<sub>2</sub>-Na-Y gives benzaldehyde as the major product, while that of styrene gives benzaldehyde and styrene oxide as major oxidation products when 7,16-diacetyl[Ni{Me<sub>4</sub>(Bzo)<sub>2</sub>[14]tetraeneN<sub>4</sub>}]<sub>2</sub>-Na-Y is used as catalyst.

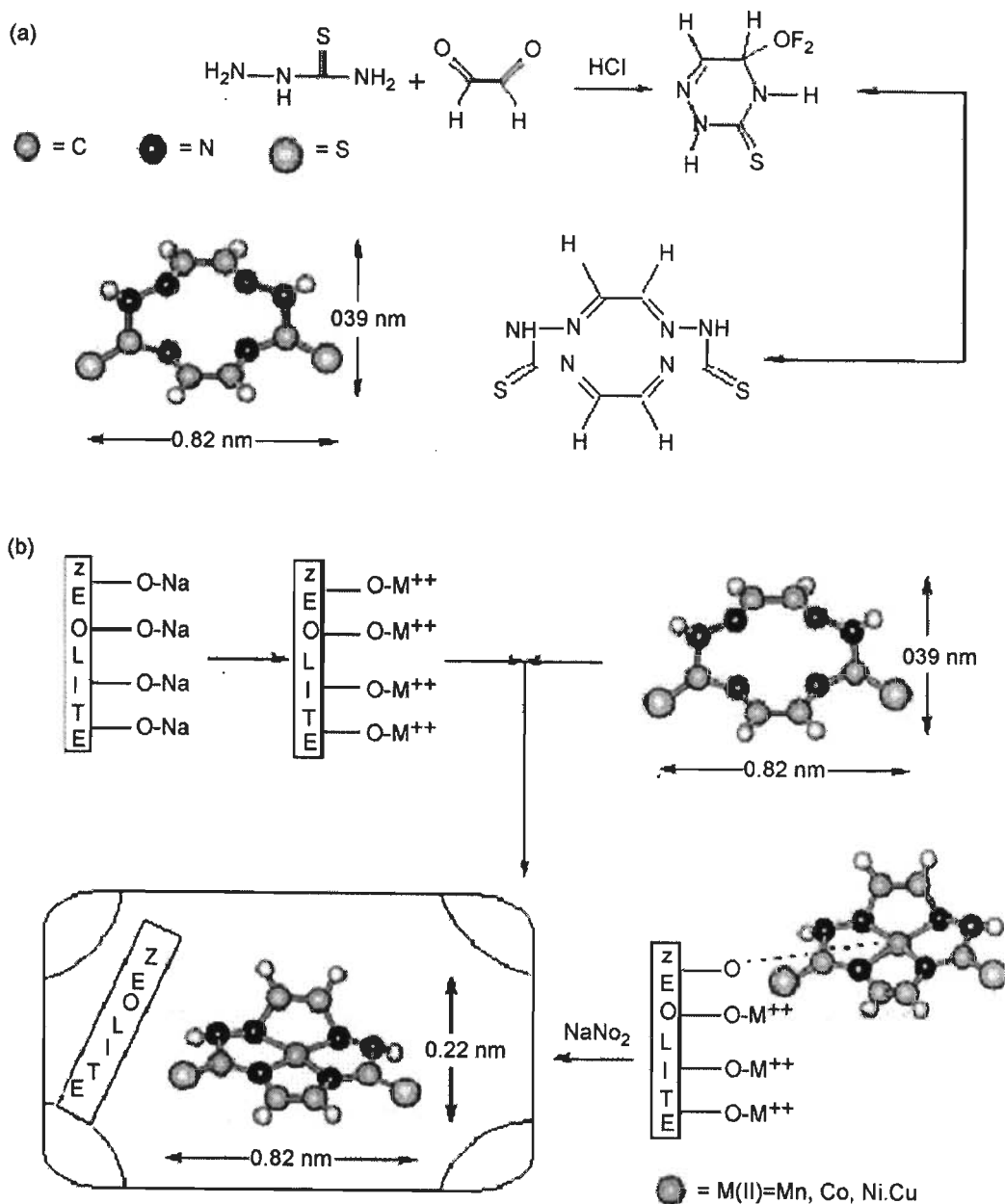


**Scheme 1.29.** Synthetic approach to prepare zeolite-Y encapsulated macrocyclic complexes (M = Cu(II) and Ni(II) (**53** and **54**)).

The Mn(II), Co(II), Ni(II) and Cu(II) complexes of the type [ML] with bis(salicylaldehyde)oxaloyldihydrazone (H<sub>2</sub>L) have been synthesized from the reaction of metal acetate with H<sub>2</sub>L in 1:1 molar ratio in ethanol under reflux. These metal complexes with tetradentate Schiff-base ligand have also been entrapped in the nanocavity of zeolite-Y. The new Host-Guest nano composite Materials has been used as catalyst for oxidation of cyclohexane and their activity compared with the homogeneous analogues [80].

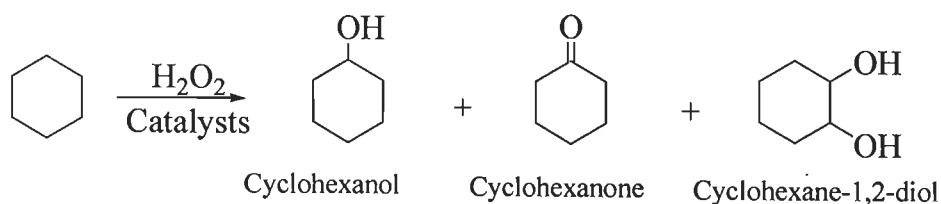
A series of zeolite-Y encapsulated Mn(II), Co(II), Ni(II) and Cu(II) complexes with 12-membered macrocyclic tetradentate ligand, 1,2,5,6,8,11-hexaazacyclododeca-7,12-dithione-2,4,8,10-tetraene (H<sub>6</sub>C<sub>6</sub>N<sub>6</sub>S<sub>2</sub>) have been

synthesized (Scheme 1.30) and characterized. These complexes show good catalytic activity for the oxidation of cyclohexene to 2-cyclohexene-1-one, 2-cyclohexene-2-ol and 1-(*tert*-butylperoxy)-2-cyclohexene. In the presence of *tert*-butylhydroperoxide all catalysts gave 2-cyclohexene-1-one in major yield, though overall conversion has been found low (40–90%) [81].



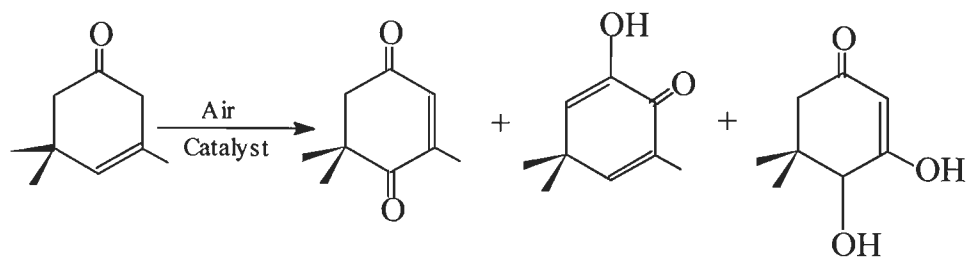
**Scheme 1.30.** Scheme for the preparation of zeolite-Y encapsulated Mn(II), Co(II), Ni(II) and Cu(II) complexes of 1,2,5,6,8,11-hexaazacyclododeca-7,12-dithione-2,4,8,10-tetraene (**55**). Adopted from ref. [81].

Maurya *et al.* reported the oxidation of cyclohexane catalyzed by  $[V^{IV}O(\text{sal-dach})]-Y$  and  $[V^{IV}O(\text{sal-oaba})(H_2O)]-Y$  [53, 74]. After 2 h, a maximum of 21% conversion in  $CH_3CN$  at 70 °C was obtained and the oxidized products were cyclohexanone, cyclohexanol and cyclohexane-1,2-diol (Scheme 1.31) along with an unknown product. The selectivity for cyclohexanol was ca. 93 %.



**Scheme 1.31.** Products of oxidation of cyclohexane

$[Co(\text{salophen})]-Y$  and other derivatives are able to catalyze oxidation of  $\beta$ -isophorone ( $\beta$ IP) to keto isophorone (KIP) along with other minor products (Scheme 1.32) using air as an oxidant at ambient conditions of temperature and pressure [82]. The selectivity for KIP was >95 % at  $\beta$ IP conversion of ~30 % in the beginning which slowly decreased with time to ~60 % selectivity at higher conversion (>95 %) of  $\beta$ IP. The reactivities of these encapsulated catalysts was in the order:  $[Co(\text{Cl-salophen})]-Y > [Co(\text{Br-salophen})]-Y > [Co(\text{NO}_2\text{-salophen})]-Y > [Co(\text{salophen})]-Y$ .



**Scheme 1.32.** Reaction scheme of oxidation of  $\beta$ -isophorone

Cu(II), Ni(II) and Co(II) form dinuclear complexes (Figure 1.3) with 3-formylsalicylic acid ( $H_2fsal$ ) in the cavity of zeolite-Y. These complexes catalyze the oxidation of benzoyl alcohol at 50 °C. The activity was found to vary in the order:  $[Cu(fsalsal)]_2-Y > [Co(fsalsal)]_2-Y > [Ni(fsalsal)]_2-Y$ . It is proposed that an intermediate binuclear oxo complex forms during reaction which ultimately transfers oxygen to the substrate to give product [83].

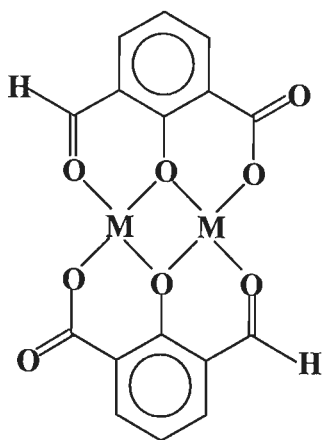
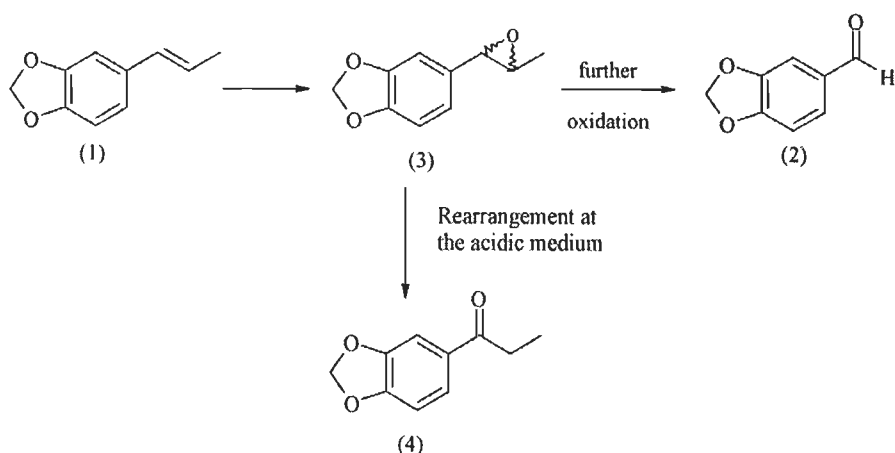


**Figure 1.3.** Dinuclear structure of  $[M(fsalsal)]_2$  complexes; M = Cu(II), Ni(II), Co(II) (56 and 57)

Yusuff *et al.* have reported the catalytic oxidation of ascorbic acid by atmospheric oxygen using  $[Cu(dmpz)]_2-Y$  ( $Hdmpz = 3,5$ -dimethyl-1H-pyrazole) as catalyst. The oxidation of ascorbic acid to dehydroascorbic acid was monitored by continuous measurement of transmittance at 245 nm after exposing deoxygenated methanolic solution of ascorbic acid in air in the presence of catalyst. It is proposed that oxidation proceeds through Cu(I)-ascorbate intermediate [84].

Complex  $[VO(salen)]$  encapsulated in zeolite-Y as well as impregnated on Na-Y have been used for the oxidation of isosafrol (1,2-methylenedioxy-4(1-propenyl)benzene) under microwave; Scheme 1.33.  $VO(salen)-Y$  gave 67 % conversion where selectivity of epoxide (3) was 79 % while that of rearrange

product (4) was 19 %. Though conversion by impregnate sample was low (51 %), the selectivity of epoxide increased to 90 %. Catalyst's surface area and availability of the vanadyl group were the main factors which allowed this superior performance [85].



**Scheme 1.33.**

Reaction of vanadium exchanged zeolite-Y with the ONN donor Hpydx-aepy (Hpydx-aepy = Schiff base obtained by the condensation of pyridoxal and 2-aminoethylpyridine) in methanol followed by aerial oxidation gave zeolite-Y encapsulated dioxidovanadium(V) complex, abbreviated as  $[\text{V}^{\text{V}}\text{O}_2(\text{pydx-aepy})]\text{-Y}$  (58). The encapsulated complex  $[\text{V}^{\text{V}}\text{O}_2(\text{pydx-aepy})]\text{-Y}$  catalyzes the oxidation of styrene, cyclohexene, methyl phenyl sulfide and diphenyl sulfide using  $\text{H}_2\text{O}_2$  as oxidant in good yield. Styrene under optimized reaction conditions gave four reaction products namely, styrene oxide, benzaldehyde, 1-phenylethane-1,2-diol and benzoic acid while organic sulfides gave the corresponding sulfoxide as the major product. Cyclohexene gave cyclohexene epoxide, 2-cyclohexene-1-one, 2-cyclohexene-1-ol and cyclohexane-1,2-diol. Neat complex  $[\text{V}^{\text{IV}}\text{O}(\text{acac})(\text{pydx-aepy})]$  has been used as catalyst precursor to compare its catalytic activities with the encapsulated one [86].

Similarly, ligands Hpydx-aebmz and Hpydx-ambmz [ONN donor Schiff bases obtained by the condensation of pyridoxal and 2-aminoethylbenzimidazole (Hpydx-aebmz) or 2-aminomethylbenzimidazole (Hpydx-ambmz)] in refluxing methanol, followed by aerial oxidation resulted in the formation of the encapsulated  $V^V O_2$ -complexes,  $[V^V O_2(\text{pydx-aebmz})]-Y$  (**59**) and  $[V^V O_2(\text{pydx-ambmz})]-Y$  (**60**) [87], respectively. Under the optimised reaction conditions for the oxidation of styrene with  $H_2O_2$  in acetonitrile, a maximum of 68 % conversion of styrene (with  $[V^V O_2(\text{pydx-aebmz})]-Y$ ) and 65 % (with  $[V^V O_2(\text{pydx-ambmz})]-Y$ ) has been achieved in 6 h of reaction time. The selectivity of the various products is similar for both catalysts and follows the order: benzaldehyde (ca. 55 %) > 1-phenylethane-1,2-diol > benzoic acid > styrene oxide > phenyl acetaldehyde. Speciation of the systems and plausible intermediates involved in the catalytic oxidation processes have been established by UV-Vis, EPR,  $^{51}V$  NMR and DFT studies.

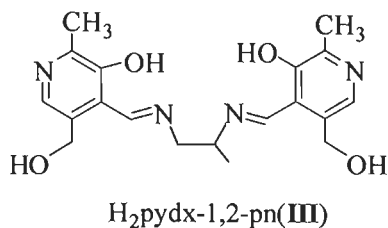
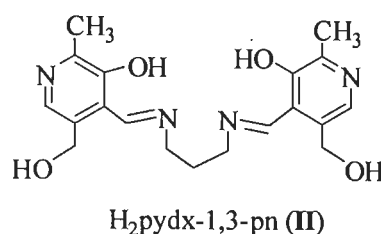
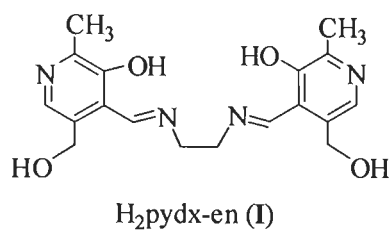


#### 1.4. Objective of the present thesis

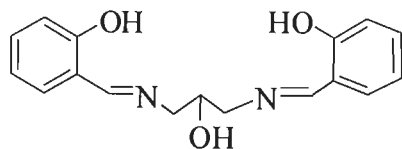
It is evident from the review of the literature that zeolite encapsulated metal complexes have provided opportunities to develop catalytic system for various industrial processes. For the oxidation reactions, specifically, contributions of these catalysts are widely documented. As we go through the oxidation reactions we observe that, in spite of considerable research, optimization of reaction conditions have not been set out in most papers. It was, therefore, reasonable to under take systematic study on the synthesis and characterization of new zeolite-Y encapsulated catalysts and to explore their catalytic potential for the oxidation of organic substrates under optimized reaction conditions.

The present study is aimed to describe the syntheses of zeolite-Y encapsulated and neat vanadium, manganese and copper complexes with the following ligands:

- (i) Dibasic tetradentate ONNO donor ligands, *N,N'*-ethylenebis(pyridoxylideneiminato) ( $H_2$ pydx-en, **I**), *N,N'*-propylenebis(pyridoxylideneiminato) ( $H_2$ pydx-1,3-pn, **II**) and 1-methyl-*N,N'*-ethylenebis(pyridoxylideneiminato) ( $H_2$ pydx-1,2-pn, **III**).

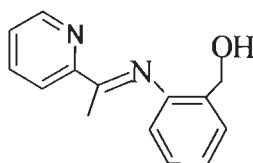


- (ii) Tribasic pentadentate ONONO donor Schiff base derived from salicylaldehyde and 3-hydroxy-1,3-diaminopropane (H<sub>3</sub>sal-dahp, IV).



H<sub>3</sub>sal-dahp (IV)

- (iii) Monobasic tridentate ONN donor Schiff base derived from 2-acetylpyridine and *o*-aminophenol (Hacpy-oap, V).



Hacpy-oap (V)

Thus, neat as well as zeolite-Y encapsulated manganese (III) complexes with ligands I, II, III and IV, oxidovanadium(IV) complexes with ligands I, II and III, and copper(II) complex with ligand V have been prepared and characterized by chemical, spectral (IR and electronic) and thermal studies, XRD patterns, scanning electron micrographs and single crystal X-ray studies (of some manganese complexes). Catalytic potential of both types of complexes have been explored for the following reactions:

- (i) Oxidation of styrene
- (ii) Oxidation of cyclohexene
- (iii) Oxidation of methyl phenyl sulfide
- (iv) Oxidation of oxidation of benzoin

Reaction conditions for all these catalytic reactions have been optimized to get best performance of the catalysts.

# *CHAPTER 2*

## **Synthesis, characterisation and catalytic activities of manganese (III) complexes of pyridoxal-based ONNO donor tetradentate ligands**

### **2.1. Introduction**

Coordination chemistry of manganese has been studied extensively [88,89] due to its occurrence in the active site of several enzymes involved in the chemistry of reactive oxygen species [90-93]. EXAFS studies for the oxygen evolving complex (OEC) [94] and crystal structure of the manganese peroxidase (isolated from *Phanerochaete chrysosporium*) [95] show that manganese center is surrounded by O- or N-donor ligands. Manganese complexes having tetradentate ONNO donor ligands are found to be artificial mimics of some of these enzymes [1]. In addition, they also act as catalysts for important reactions [96, 97].

Despite success of homogeneous catalysts in the oxidation reactions, there is a clear demand for heterogeneous catalysts that provide advantages such as easy handling and product separation, catalyst recovery and production of a less level of waste [98, 99]. For these reasons, the development of heterogeneous catalysts for oxidation reactions remains a very active field of research [100, 101]. For the development of new chemical technologies, zeolite encapsulated metal complexes (ZEMC) hold a key place amongst heterogeneous catalysts. A molecule encapsulated in the zeolite cages is characterised by steric restriction and if the size of the molecule is comparable to the zeolite cage, the molecule in the cage may show interesting properties, which are not encountered under ordinary conditions. The homogeneous catalysts on encapsulation also enjoy the advantages of solid heterogeneous catalysts while maintaining many of their original characters. The flexible nature of salen-type ( $H_2salen = N,N'$ -bis(salicylidene)ethane-1,2-diamine) ligands has provided opportunities to encapsulate various transition-metal complexes in the nano-cavity of zeolites and to develop catalytic processes for various reactions. Poltowicz et al. have encapsulated a whole range of metallosalen complexes including  $[Mn^{II}(salen)]$  in the zeolite-X to study their catalytic activity for the oxidation of cyclooctane [48]. Ratnasamy and co-workers have used manganese(III) complexes of salen



styrene (Acros Organics. New Jersey, U.S.A.), 1,2-diaminoethane, 1,2-diaminopropane and 1,3-diaminopropane (S.D. fine chemicals) were used as obtained. Zeolite-Y (Si/Al = ca. 10) was obtained from Indian Oil Corporation (R&D), Faridabad, India. All other chemicals and solvents used were of AR grade. Ligands H<sub>2</sub>pydx-en (**2.I**) and H<sub>2</sub>pydx-1,3-pn (**2.II**) and H<sub>2</sub>pydx-1,2-pn (**2.III**) were prepared as described in the literature [106].

### **2.2.2. Physical Method and Analysis**

Elemental analyses of the ligands and complexes were obtained by an Elementar model Vario-E1 III. Electronic spectra of the zeolite-Y encapsulated complexes were recorded in Nujol using Shimadzu 1601 UV-Vis spectrophotometer by layering the mull of the sample to inside of one of the cuvettes while keeping the other one layered with Nujol as reference. Spectra of neat complexes were recorded in methanol. IR spectra were recorded as KBr pellet on a Nicolet NEXUS Aligent 1100 series FT-IR spectrometer after grinding the sample with KBr. Thermogravimetric analyses of the complexes were carried out using Perkin Elmer (Pyris Diamond) instrument in air with a heating rate of 10 °C/min. The field emission scanning electron microscopy (FE-SEM) and energy dispersive X-ray analysis (EDX) of encapsulated complexes were recorded on a FEI Quanta 200 FEG microscope. A thermoelectron gas-chromatograph with a HP-1 capillary column (HP-1, 30 m × 0.25 mm × 0.25 μm) was used to analyze the reaction products. X-ray powder diffractograms of solid catalysts were recorded using a Bruker AXS D8 advance X-ray powder diffractometer with a Cu-Kα target. The identity of the products was confirmed using GC-MS, model Perkin-Elmer Clarus 500 by comparing the fragments of each product with the library that was available.

### **2.2.3. X-Ray Crystal Structure Determination of [Mn(pydx-en)Cl(H<sub>2</sub>O)] (2.1) and [Mn(pydx-1,3-pn)Cl(CH<sub>3</sub>OH)] (2.2)**

Three-dimensional room temperature X-ray data were collected on a Bruker Kappa Apex CCD diffractometer at low temperature for [Mn(pydx-en)Cl(H<sub>2</sub>O)]

(2.1) and at room temperature for [Mn(pydx-1,3-pn)Cl(CH<sub>3</sub>OH)] (2.2) by the  $\phi$ - $\omega$  scan method. Reflections were measured from a hemisphere of data collected from frames each of them covering 0.3° in  $\omega$ . Of the 25075 in 2.1 and 17976 in 2.2 reflections measured, all were corrected for Lorentz and polarization effects and for absorption by multi-scan methods based on symmetry-equivalent and repeated reflections, 3021 in 2.1 and 2706 in 2.2 independent reflections exceeded the significance level ( $|F|/\sigma|F|$ ) > 4.0. Complex scattering factors were taken from the program package SHELXTL [107]. The structures were solved by direct methods and refined by full matrix least-squares on  $F^2$ . Hydrogen atoms were left to refine freely with isotropic thermal parameters, except hydrogen atoms of C(3), O(4A) and O(4B), C(15) and C(17) in 2.1, and C(1W) in 2.2 which were included in calculated positions and refined in the riding mode. Refinement was done with allowance for thermal anisotropy of all non-hydrogen atoms. Further details of the crystal structure determination are given in Table 2.1. CCDC No. 817986 (for 2.1) and 817987 (for 2.2) contains the supplementary crystallographic data for the structure reported in this paper.

#### 2.2.4. Preparations

##### 2.2.4.1. Preparation of [Mn<sup>III</sup>(pydx-en)Cl(H<sub>2</sub>O)] (2.1)

A solution of H<sub>2</sub>pydx-en (0.716 g, 2 mmol) in methanol (40 ml) was treated with Mn(CH<sub>3</sub>COO)<sub>2</sub>·4H<sub>2</sub>O (0.419 g, 2 mmol) dissolved in methanol (10 ml) and the resulting reaction mixture was stirred at 60 °C for 1h. After adding LiCl (0.127 g, 3 mmol) to the reaction mixture and stirring further at 60 °C for 1 h, air was passed through the solution with occasional shaking for 24 h. The volume of solvent was reduced to ca. 20 ml and kept in refrigerator at ca. 10 °C where green crystals of 2.1 separated out within 24 h. This was filtered off, washed with methanol and dried in vacuum. Yield: 43.0% (0.400 g). Green crystals suitable for X-ray diffraction study were obtained from the methanolic solution on slow evaporation at room temperature. Anal. Calc. for C<sub>18</sub>ClH<sub>22</sub>MnN<sub>4</sub>O<sub>5</sub> (464.79): C, 46.52; H, 4.77; N, 12.05%. Found: C, 46.4; H, 4.6; N, 12.1%.

**Table 2.1.** Crystal data collection and structure refinement for [Mn<sup>III</sup>(pydx-en)Cl(H<sub>2</sub>O)] (**2.1**) and [Mn<sup>III</sup>(pydx-1,3-pn)Cl(CH<sub>3</sub>OH)] (**2.2**).

	<b>2.1</b>	<b>2.2</b>
Formula	C <sub>18</sub> H <sub>24</sub> ClMnN <sub>4</sub> O <sub>6</sub>	C <sub>20</sub> H <sub>26</sub> ClMnN <sub>4</sub> O <sub>5</sub>
Molecular weight	481.79	492.84
Crystal system	Monoclinic	Monoclinic
Space group	P2 <sub>1</sub> /c	P2 <sub>1</sub> /m
<i>T</i> /K	100(2)	296(2)
<i>a</i> /Å	14.5521(7)	7.7562(3)
<i>b</i> /Å	13.9046(7)	16.8471(8)
<i>c</i> /Å	10.0188(5)	8.1654(3)
<i>β</i> /°	95.673(3)	103.696(3)
<i>V</i> /Å <sup>3</sup>	2017.29(17)	1036.63(7)
<i>F</i> <sub>000</sub>	996	512
<i>Z</i>	4	2
<i>D</i> <sub>calc</sub> /g cm <sup>-3</sup>	1.586	1.579
<i>μ</i> /mm <sup>-1</sup>	0.831	0.807
<i>θ</i>	2.51-25.12	2.42-30.32
<i>R</i> <sub>int</sub>	0.0482	0.0398
Goodness-of-fit on <i>F</i> <sup>2</sup>	1.171	1.166
<i>R</i> <sub>1</sub> <sup>a</sup>	0.0478	0.0362
<i>wR</i> <sub>2</sub> (all data) <sup>b</sup>	0.1209	0.1226
Largest differences peak and hole (eÅ <sup>-3</sup> )	-0.554 and 1.059	-0.650 and 0.867

$${}^a R_1 = \frac{\sum ||F_o| - |F_c||}{\sum |F_o|} \quad {}^b wR_2 = \left\{ \frac{\sum [w(|F_o|^2 - |F_c|^2)]^2}{\sum [w(F_o^4)]} \right\}^{1/2}$$



#### **2.2.4.2. Preparation of [Mn<sup>III</sup>(pydx-1,3-pn)Cl(CH<sub>3</sub>OH)] (2.2) and [Mn<sup>III</sup>(pydx-1,2-pn)Cl(H<sub>2</sub>O)] (2.3)**

Complexes [Mn<sup>III</sup>(pydx-1,3-pn)Cl(CH<sub>3</sub>OH)] (2.2) and [Mn<sup>III</sup>(pydx-1,2-pn)Cl(H<sub>2</sub>O)] (2.3) were prepared following essentially the same procedure outlined for 2.1.

Data for 2.2: Yield 54.9 % (0.541 g). Anal. Calc. for C<sub>20</sub>ClH<sub>26</sub>MnN<sub>4</sub>O<sub>5</sub> (492.84): C, 48.74; H, 5.32; N, 11.3%. Found: C, 48.5; H, 5.2; N, 11.2%.

Data for 2.3: Yield 50.0 % (0.479 g). Anal. Calc. for C<sub>19</sub>ClH<sub>24</sub>MnN<sub>4</sub>O<sub>5</sub> (478.81): C, 47.66; H, 5.05; N, 11.70%. Found: C, 47.6; H, 5.1; N, 11.6%.

#### **2.2.4.3. Preparation of [Mn<sup>II</sup>]-Y (Manganese Exchanged Zeolite)**

A filtered solution of MnSO<sub>4</sub>.H<sub>2</sub>O (9.0 g, 53.3 mmol) dissolved in 50 ml of distilled water was added to a suspension of Na-Y (15.0 g) in 900 ml of H<sub>2</sub>O and the reaction mixture was heated at 90 °C with stirring for 24 h. The solid was filtered, washed with hot distilled water until filtrate was free from any manganese ion content and dried at 150 °C for 24 h. Yield 12.0 g.

#### **2.2.4.4. Preparation of [Mn<sup>III</sup>(pydx-en)Cl(H<sub>2</sub>O)]-Y(2.4)**

A mixture of [Mn<sup>II</sup>]-Y (3.0 g) and H<sub>2</sub>pydx-en (3.0 g) was mixed in 40 ml of methanol and the reaction mixture was refluxed for 15 h in an oil bath with stirring. The resulting material was suction filtered and then extracted with methanol using Soxhlet extractor until the complex was free from unreacted ligand. After filtering, the solid was suspended in aqueous 0.01M NaCl solution and stirred while passing air for 15 h. It was then filtered, washed with double distilled water till no precipitate of AgCl was observed in the filtrate on treating with AgNO<sub>3</sub>.

#### **2.2.4.5. Preparation of [Mn<sup>III</sup>(pydx-1,3-pn)Cl(H<sub>2</sub>O)]-Y (2.5) and [Mn<sup>III</sup>(pydx-1,2-pn)Cl(H<sub>2</sub>O)]-Y (2.6)**

Complexes [Mn<sup>III</sup>(pydx-1,3-pn)Cl(H<sub>2</sub>O)]-Y (2.5) and [Mn<sup>III</sup>(pydx-1,2-pn)Cl(H<sub>2</sub>O)]-Y (2.6) were prepared following essentially the same procedure outlined for 2.4.

### **2.2.5. Catalytic Activity Study**

#### **2.2.5.1. Oxidation of Methyl Phenyl Sulfide**

Methyl phenyl sulfide (1.24 g, 10 mmol), 30% aqueous H<sub>2</sub>O<sub>2</sub> (1.14 g, 10 mmol) and catalyst (0.020 g) in acetonitrile (5 ml) were stirred at room temperature and the reaction was monitored by withdrawing small aliquots of the reaction mixture at every 30 min and analyzing them quantitatively by gas chromatography. The identities of the products were confirmed by GC-MS. The effects of various parameters, such as amounts of oxidant, catalyst and solvent were studied in order to see their effect on the conversion and selectivity of the reaction products.

#### **2.2.5.2. Oxidation of Styrene**

Oxidation of styrene was carried out in a 50 ml two-neck reaction flask fitted with a water condenser. In a typical reaction, styrene (1.04 g, 10 mmol) and aqueous 30% H<sub>2</sub>O<sub>2</sub> (2.27 g, 20 mmol) were taken in 5 ml of acetonitrile and temperature of the reaction mixture was raised to 80 °C. The catalyst, [Mn(pydx-en)Cl(H<sub>2</sub>O)]-Y (0.040 g) was added to the above reaction mixture and stirred. Oxidized products were analyzed quantitatively by gas chromatography during the reaction. The identities of the products were confirmed as mentioned above.

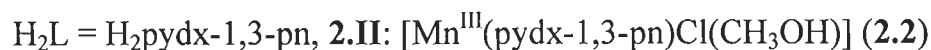
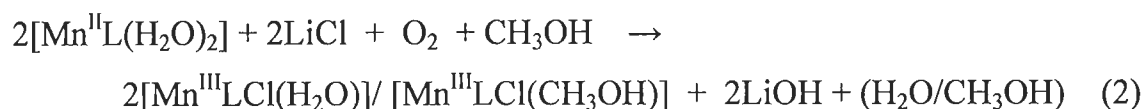
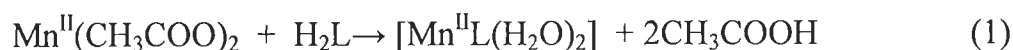
#### **2.2.5.3. Oxidation of Benzoin**

Benzoin (1.06 g, 5 mmol), aqueous 30% H<sub>2</sub>O<sub>2</sub> (1.14 g, 10 mmol) and catalyst (0.020 g) were mixed in methanol (20 ml), and the reaction mixture was heated at 80 °C with continuous stirring. The reaction products were analyzed and identified as mentioned above.

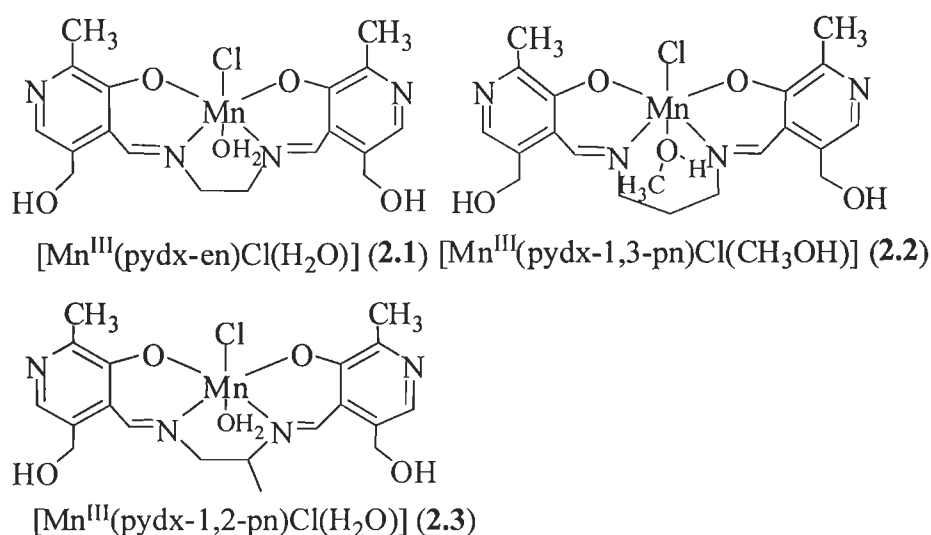
## 2.3. Results and Discussion

### 2.3.1. Synthesis and solid state characteristics

Reaction of  $\text{Mn}^{\text{II}}(\text{CH}_3\text{COO})_2$  with  $\text{H}_2\text{pydx-en}$  (**2.I**),  $\text{H}_2\text{pydx-1,3-pn}$  (**2.II**) and  $\text{H}_2\text{pydx-1,2-pn}$  (**2.III**) [106] in refluxing methanol followed by aerial oxidation in the presence of LiCl yielded  $[\text{Mn}^{\text{III}}(\text{pydx-en})\text{Cl}(\text{H}_2\text{O})]$  (**2.1**),  $[\text{Mn}^{\text{III}}(\text{pydx-1,3-pn})\text{Cl}(\text{CH}_3\text{OH})]$  (**2.2**) and  $[\text{Mn}^{\text{III}}(\text{pydx-1,2-pn})\text{Cl}(\text{H}_2\text{O})]$  (**2.3**), respectively; Equations (1) and (2):



Their structures are presented in Scheme 2.2 and are based on elemental analyses, spectroscopic (IR and UV-Vis) studies, and single crystal X-ray diffraction analyses of complexes  $[\text{Mn}^{\text{III}}(\text{pydx-en})\text{Cl}(\text{H}_2\text{O})]$  (**2.1**) and  $[\text{Mn}^{\text{III}}(\text{pydx-1,3-pn})\text{Cl}(\text{CH}_3\text{OH})]$  (**2.2**).



**Scheme 2.2.** Structures of neat complexes.

Encapsulation of these complexes in the cavity of zeolite-Y involved the following steps: (i) exchange of manganese(II) ion with Na<sup>+</sup> of Na-Y, (ii) the reaction of metal exchanged zeolite-Y with H<sub>2</sub>pydx-en, H<sub>2</sub>pydx-1,3-pn and H<sub>2</sub>pydx-1,2-pn, (iii) the oxidation of formed encapsulated Mn(II) complexes by air to the corresponding Mn(III) complexes in solution, (iv) extraction of the resulting samples with methanol using Soxhlet extraction to remove excess free ligand and neat metal complex formed on the surface of the zeolite, if any, and (v) the exchange of remaining free Mn(III) ions in zeolite-Y encapsulated complexes with aqueous 0.01 M NaCl solution to give finally [Mn<sup>III</sup>(pydx-en)Cl(H<sub>2</sub>O)]-Y (2.4), [Mn<sup>III</sup>(pydx-1,3-pn)Cl(H<sub>2</sub>O)]-Y (2.5) and [Mn<sup>III</sup>(pydx-1,2-pn)Cl(H<sub>2</sub>O)]-Y (2.6). The molecular formula of the complexes is based on the corresponding neat complexes. The manganese content and colours of the encapsulated complexes are presented in Table 2.2. As the prepared complexes were well extracted, the metal content found after encapsulation is only due to the presence of manganese(III) complexes in the super cages of the zeolite-Y. The diagonal dimension of the complexes is about 12 Å (in 2.1 and 2.2), which suggests that they will fit nicely into the super cages of zeolite-Y. These complexes have further been characterized by FE-SEM, X-ray powder diffraction patterns in addition to IR and electronic spectra.

**Table 2.2.** Manganese content and colour of encapsulated complexes.

Compound	Colour	Metal Content	
		Wt.%	mmol/ g
[Mn <sup>III</sup> (pydx-en)Cl(H <sub>2</sub> O)]-Y (2.4)	Light yellow	0.52	0.095
[Mn <sup>III</sup> (pydx-1,3-pn)Cl(H <sub>2</sub> O)]-Y (2.5)	Light yellow	0.40	0.072
[Mn <sup>III</sup> (pydx-1,2-pn)Cl(H <sub>2</sub> O)]-Y (2.6)	White	0.69	0.126

### 2.3.2. Structure descriptions of [Mn<sup>III</sup>(pydx-en)Cl(H<sub>2</sub>O)] (2.1) and [Mn<sup>III</sup>(pydx-1,3-pn)Cl(CH<sub>3</sub>OH)] (2.2)

The solid state structures of compounds [Mn<sup>III</sup>(pydx-en)Cl(H<sub>2</sub>O)] (2.1) and [Mn<sup>III</sup>(pydx-1,3-pn)Cl(CH<sub>3</sub>OH)] (2.2) were determined by single-crystal X-ray

diffraction analyses. Crystal of **2.1** contains  $[\text{Mn}^{\text{III}}(\text{pydx-en})\text{Cl}(\text{H}_2\text{O})]$  where one water molecule is in the asymmetric unit. The hydrogen atoms of this water molecule O(2W) were not localised. The crystal presents a disorder on one of the oxygen atoms, O(4), of the hydroxymethyl group of one pyridoxal ring of the ligand. For this oxygen atom two atom sites have been observed [site occupancy factors O(4A), 0.51437]. Figure 2.1 illustrates its structure, where as bond lengths and angles of the coordination sphere are compiled in Table 2.3. The Mn(III) ion is bound to two imine nitrogen atoms [N(2) and N(3)], two hydroxyl oxygen atoms of the pyridoxal rings [O(2) and O(3)], one chlorine anion [Cl(1)] and one water molecule [O(1W)]. The distances between the Mn(III) ion and these atoms can be considered unequivocal Mn-N<sub>imine</sub>, Mn-O<sub>hydroxyl</sub>, and Mn-Cl bonds. The coordination polyhedron can be best described as a slightly distorted octahedron. The donor atoms of the pydx-en ligand are localized in the equatorial plane. The mean deviation from planarity of the plane containing N(2), N(3), O(2) and O(3) atoms is 0.0428(14) Å and including the Mn atom is 0.0412(14) Å. The Cl(1)-Mn(1)-O(1W) angle is 169.94(8), O(2)-Mn(1)-N(3) is 171.81(12) and O(3)-Mn(1)-N(2) is 175.16(12) and are close to 180°. Likewise, the vectors defined by the metal ion and the axial atoms form angles close to 90° with the vectors containing the metal ion and the equatorial donor atoms, as expected for an octahedral coordination environment. The vectors containing the equatorial donor atoms form angles close to 90° between them, too.

Crystal of **2.2** contains  $[\text{Mn}(\text{pydx-1,3-pn})\text{Cl}(\text{CH}_3\text{OH})]$  complex. The asymmetric unit only contains half molecule of the complex. The molecule lies across a crystallographic symmetry plane, which contains at C(1W), O(1W), Cl(1), C(10) and Mn(1) atoms. The coordination polyhedron can be described as a slightly distorted octahedron. The Mn(III) ion is bound to two imine nitrogen atoms [N(2) and N(2A)], two hydroxyl oxygen atoms of the pyridoxal rings [O(2) and O(2A)], one chlorine anion [Cl(1)] and one CH<sub>3</sub>OH molecule. N(2), N(2A), O(2) and O(2A) occupy the equatorial positions. The mean deviation from planarity of the plane containing the four equatorial donor atoms and the metal ion amounts to 0.0443 Å. Distances and angles found for **2.2** are close to those found

for **2.1** (Table 2.3) and other similar complexes [108–110]. Figure 2.2 shows the structure of the compound **2.2**.

**Table 2.3.** Selected bond lengths (Å) and bond angles (°) for [Mn<sup>III</sup>(pydx-en)Cl(H<sub>2</sub>O)] (**2.1**) and [Mn<sup>III</sup>(pydx-1,3-pn)Cl(CH<sub>3</sub>OH)] (**2.2**)<sup>a</sup>.

Bond lengths for <b>2.1</b>		Bond lengths for <b>2.2</b>	
Mn(1)-O(3)	1.873(3)	Mn(1)-O(2)#1	1.8803(12)
Mn(1)-O(2)	1.885(3)	Mn(1)-O(2)	1.8803(12)
Mn(1)-N(2)	1.973(3)	Mn(1)-N(2)	2.0374(15)
Mn(1)-N(3)	1.987(3)	Mn(1)-N(2)#1	2.0374(15)
Mn(1)-O(1W)	2.236(3)	Mn(1)-O(1W)	2.368(2)
Mn(1)-Cl(1)	2.5970(11)	Mn(1)-Cl(1)	2.5302(7)
N(1)-C(2)	1.323(5)	O(1)-C(6)	1.432(2)
N(1)-C(4)	1.359(5)	N(1)-C(2)	1.332(2)
O(1)-C(6)	1.415(3)	N(1)-C(2)	1.356(2)
C(1)-O(2)	1.328(4)	C(1)-O(2)	1.316(2)
N(2)-C(8)	1.276(3)	N(2)-C(8)	1.292(2)
N(2)-C(9)	1.482(3)	N(2)-C(9)	1.479(2)
O(3)-C(18)	1.315(4)		
N(3)-C(11)	1.289(3)		
N(3)-C(10)	1.477(3)		
N(4)-C(16)	1.327(5)		
N(4)-C(15)	1.351(3)		
O(4A)-C(14)	1.494(6)		
O(4B)-C(14)	1.4313		
Angles for <b>2.1</b>		Angles for <b>2.2</b>	
O(3)-Mn(1)-O(2)	94.69(11)	O(2)#1-Mn(1)-O(2)	88.49(8)

O(3)-Mn(1)-N(2)	175.16(12)	O(2)#1-Mn(1)-N(2)	171.68(6)
O(2)-Mn(1)-N(2)	90.15(12)	O(2)-Mn(1)-N(2)	89.08(6)
O(3)-Mn(1)-N(3)	91.89(12)	O(2)#1-Mn(1)-N(2)#1	89.08(6)
O(2)-Mn(1)-N(3)	171.81(12)	O(2)-Mn(1)-N(2)#1	171.68(6)
N(2)-Mn(1)-N(3)	83.28(12)	N(2)-Mn(1)-N(2)#1	92.19(8)
O(3)-Mn(1)-O(1W)	91.47(11)	O(2)#1-Mn(1)-O(1W)	86.27(6)
O(2)-Mn(1)-O(1W)	91.48(11)	O(2)-Mn(1)-O(1W)	86.27(6)
N(2)-Mn(1)-O(1W)	88.43(11)	N(2)-Mn(1)-O(1W)	85.63(6)
N(3)-Mn(1)-O(1W)	83.48(11)	N(2)#1-Mn(1)-O(1W)	85.63(6)
O(3)-Mn(1)-Cl(1)	93.78(9)	O(2)#1-Mn(1)-Cl(1)	95.94(4)
O(2)-Mn(1)-Cl(1)	96.63(8)	O(2)-Mn(1)-Cl(1)	95.94(4)
N(2)-Mn(1)-Cl(1)	85.61(9)	N(2)-Mn(1)-Cl(1)	92.22(4)
N(3)-Mn(1)-Cl(1)	87.77(9)	N(2)#1-Mn(1)-Cl(1)	92.22(4)
O(1W)-Mn(1)-Cl(1)	169.94(8)	O(1W)-Mn(1)-Cl(1)	176.89(6)

---

<sup>a</sup>Symmetry transformations used to generate equivalent atoms: #1 x,-y+3/2,z.

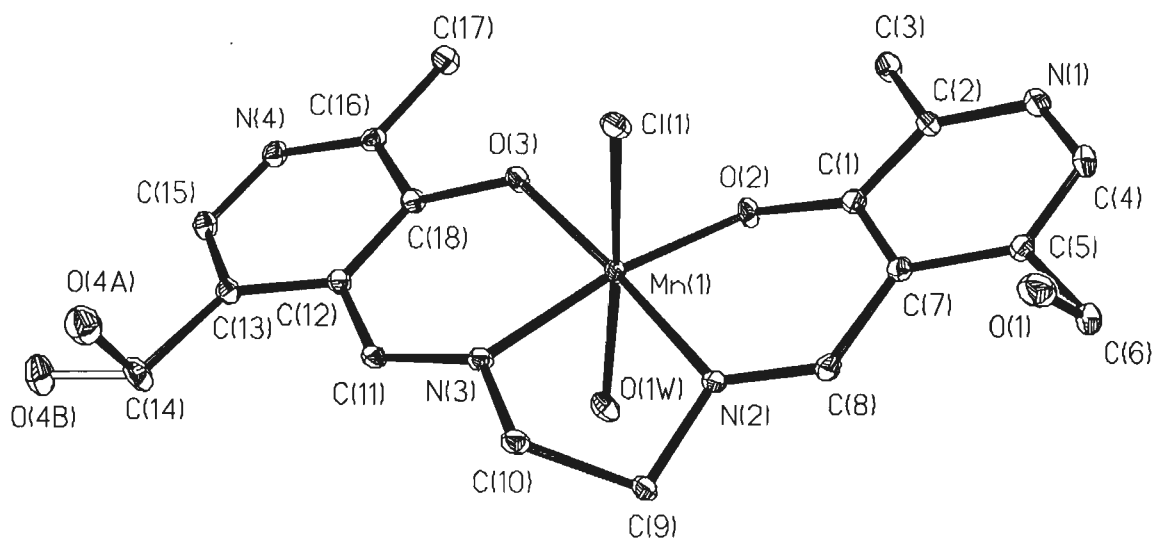


**Figure 2.1.** X-ray crystal structure of the  $[\text{Mn}^{\text{III}}(\text{pydx-en})\text{Cl}(\text{H}_2\text{O})]$  (2.1). Hydrogen atoms are omitted for the clarity.

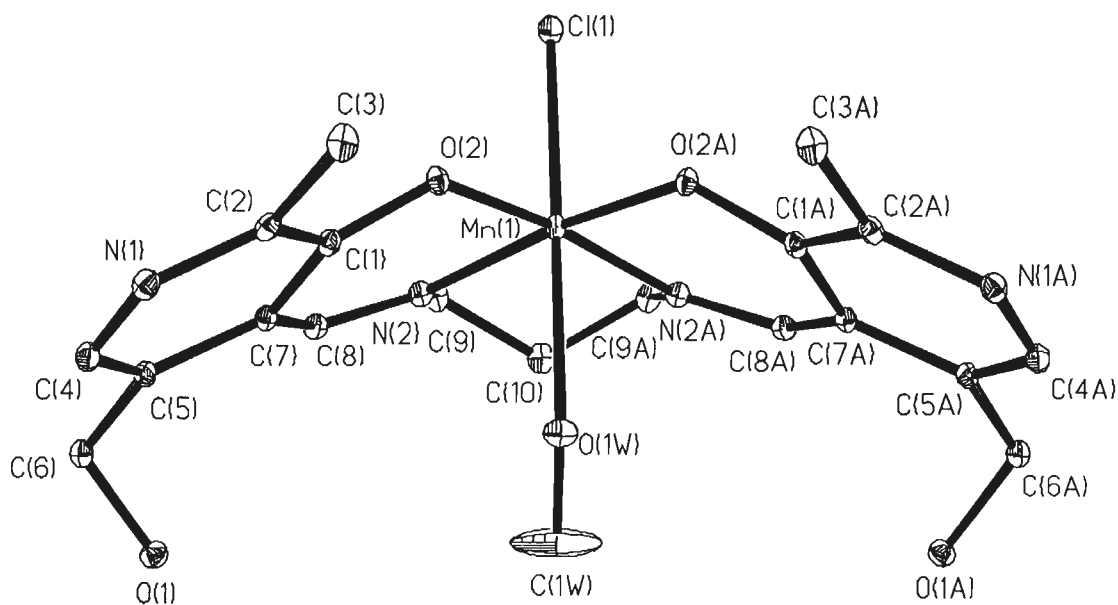


**Figure 2.2.** X-ray crystal structure of the  $[\text{Mn}^{\text{III}}(\text{pydx-1,3-pn})\text{Cl}(\text{CH}_3\text{OH})]$  (2.2). Hydrogen atoms are omitted for the clarity.



### 2.3.3. Field-emission-scanning electron micrograph (FE-SEM) and energy dispersive X-ray analysis (EDX) studies

Scanning electron micrographs of zeolite-entrapped manganese complexes have well-defined crystals, and there is no indication of the presence of any metal ions or complexes on the surface. Energy dispersive X-ray analysis plots support this conclusion as no manganese or nitrogen contents were noted on various spotted surfaces in plots for all three encapsulated complexes. Figure 2.3 presents the field emission-scanning electron micrograph of  $[\text{Mn}^{\text{III}}(\text{pydx-en})\text{Cl}(\text{H}_2\text{O})]\text{-Y}$  and the corresponding energy dispersive X-ray analysis plot. The average percentage of sodium obtained on the spotted surface is about 1.2 % and suggests the exchange of remaining free manganese ions by sodium ions during the re-exchange process (see Experimental Section). No morphological changes on the surface upon encapsulation of the complexes in the cavity are seen because of their poor loading.

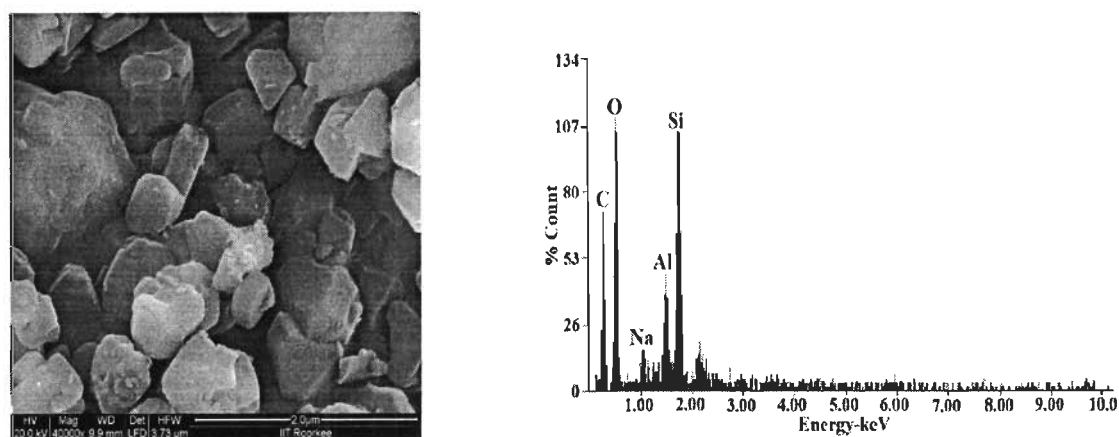


**Figure 2.3.** Field emission-scanning electron micrograph (left) of  $[\text{Mn}^{\text{III}}(\text{pydx-en})\text{Cl}(\text{H}_2\text{O})]\text{-Y}$  and the corresponding energy dispersive X-ray analysis plot (right).

### 2.3.4. Powder X-ray diffraction studies

The powder X-ray diffraction patterns of Na-Y,  $[\text{Mn}^{\text{II}}]\text{-Y}$  and encapsulated metal complexes were recorded at  $2\theta$  values between  $5^\circ$  and  $50^\circ$ . The XRD patterns of Na-Y, manganese exchanged zeolite and a representative zeolite

encapsulated metal complex are presented in Figure 2.4. The diffraction patterns of encapsulated metal complexes,  $\text{Mn}^{\text{II}}\text{-Y}$  and  $\text{Na-Y}$  are essentially similar except a slight change in the intensity of the band in encapsulated complexes. These observations indicate that the framework of zeolite has not undergone any significant structural change during encapsulation i.e. crystallinity of the zeolite-Y is preserved. No new peaks due to complex encapsulated in zeolite were detected possibly due to very low percentage loading of metal complexes.

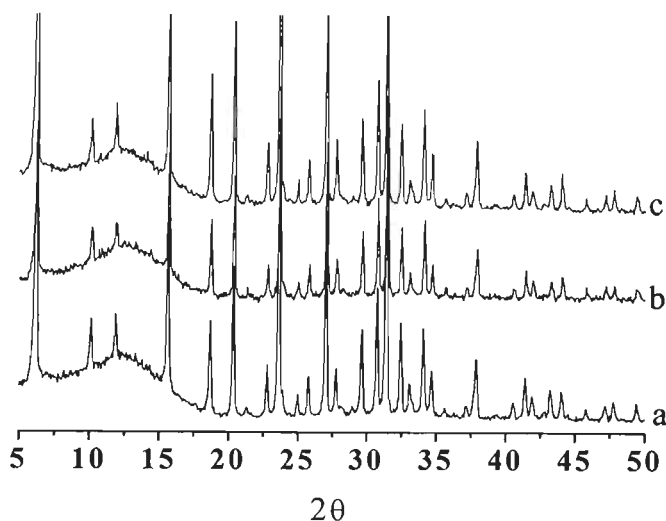


**Figure 2.4.** XRD patterns of Na-Y (a),  $[\text{Mn}^{\text{II}}]\text{-Y}$  (b) and  $[\text{Mn}^{\text{III}}(\text{pydx-en})\text{Cl}]\text{-Y}$  (c).

### 2.3.5. IR spectral studies

A partial list of IR spectroscopic data is presented in Table 2.4. The intensity of the peaks in encapsulated complexes is weak as compared to their neat analogues because of their low concentration in the zeolite matrix. However, the spectra of the encapsulated as well as neat complexes showed essentially similar bands. Comparison of the spectra of these complexes with the respective ligands provides evidence for the coordinating modes of ligands in complexes. A sharp band appearing at  $1630\text{ cm}^{-1}$  (in **2.I**),  $1634\text{ cm}^{-1}$  (in **2.II**) and at  $1631\text{ cm}^{-1}$  (in **2.III**) due to the  $\nu(\text{C}=\text{N})$  (azomethine) shifts to lower wave numbers in complexes, suggesting the coordination of the azomethine nitrogen atom [110]. All (neat as well as encapsulated) complexes exhibit two bands at ca. 518–578 and 463–486

$\text{cm}^{-1}$  in the far IR region due to  $\nu(\text{Mn-O})$  and  $\nu(\text{Mn-N})$ , respectively. In addition, they exhibit a medium intensity band at  $292\text{--}309\text{ cm}^{-1}$  due to  $\nu(\text{Mn-Cl})$  [111]. Several multiple bands of medium intensity covering the region  $2850\text{--}3000\text{ cm}^{-1}$  are observed due to C-H bands. All ligands exhibit a medium intensity band around  $3400\text{ cm}^{-1}$  due to intra-molecular hydrogen bonding. Existence of this band, however, in neat complexes hints towards the presence of hydrogen bonding as well as water of crystallisation. Thus, IR spectral data are compatible with the single crystal X-ray structures of complexes.

**Table 2.4.** IR spectral data [ $\text{cm}^{-1}$ ] of ligands and complexes.

Compound	$\nu(\text{OH})$	$\nu(\text{C=N})$	$\nu(\text{Mn-O})$	$\nu(\text{Mn-N})$	$\nu(\text{Mn-Cl})$
$\text{H}_2\text{pydx-en}$ ( <b>2.I</b> )	3435	1630	-	-	-
$\text{H}_2\text{pydx-1,3-pn}$ ( <b>2.II</b> )	3479	1634	-	-	-
$\text{H}_2\text{pydx-1,2-pn}$ ( <b>2.III</b> )	3475	1631	-	-	-
$[\text{Mn}^{\text{III}}(\text{pydx-en})\text{Cl}(\text{H}_2\text{O})]$ ( <b>2.1</b> )	3359	1621	518	486	292
$[\text{Mn}^{\text{III}}(\text{pydx-1,3-pn})\text{Cl}(\text{CH}_3\text{OH})]$ ( <b>2.2</b> )	3389	1613	528	463	302
$[\text{Mn}^{\text{III}}(\text{pydx-1,2-pn})\text{Cl}(\text{H}_2\text{O})]$ ( <b>2.3</b> )	3416	1613	523	471	301
$[\text{Mn}^{\text{III}}(\text{pydx-en})\text{Cl}(\text{H}_2\text{O})\text{-Y}$ ( <b>2.4</b> )	3432	1637	575	478	309
$[\text{Mn}^{\text{III}}(\text{pydx-1,3-pn})\text{Cl}(\text{H}_2\text{O})\text{-Y}$ ( <b>2.5</b> )	3434	1635	578	473	304
$[\text{Mn}^{\text{III}}(\text{pydx-1,2-pn})\text{Cl}(\text{H}_2\text{O})\text{-Y}$ ( <b>2.6</b> )	3462	1637	575	473	300

### 2.3.6. UV/Vis spectral studies

Electronic spectral data of ligands and complexes are presented in Table 2.5. Electronic spectra of neat complexes (recorded in methanol) exhibit a weak band at 568 nm in  $[\text{Mn}^{\text{III}}(\text{pydx-en})\text{Cl}(\text{H}_2\text{O})]$  (**2.1**), 588 nm in  $[\text{Mn}^{\text{III}}(\text{pydx-1,3-pn})\text{Cl}(\text{CH}_3\text{OH})]$  (**2.2**) and 544 nm in  $[\text{Mn}^{\text{III}}(\text{pydx-1,2-pn})\text{Cl}(\text{H}_2\text{O})]$  (**2.3**) in the visible region (Figure 2.5(A)) and is not affected by the chain length or substituent on the chain of the ligand. For partially distorted  $d^4$  system, such  $d-d$  transition has been assigned to  ${}^5\text{E} \rightarrow {}^5\text{T}$  transition [112-114]. This transition is insensitive of solvent as diffuse reflectance spectra of these complexes also exhibit a weak band

in the same region (Table 2.5). These complexes are also dominated by a medium intensity band at 388-420 nm (a near UV region) attributable to phenolate  $O(p\pi) \rightarrow Mn(d_{\pi^*})$  ligand to metal charge transfer transition. Other UV bands due to ligands in all complexes were obtained well within the expected range reported for salen type complexes [115]. The expected d-d transition for zeolite encapsulated complexes ((recorded in Nujol<sup>®</sup>) could not be obtained because of their poor loading (Figure 2.5(B)). However, charge transfer as well as ligand bands in these complexes were located in the expected places (see Table 2.5) and are similar to those observed for neat complexes.

**Table 2.5.** Electronic spectroscopic data of ligands and complexes.

Compound	Solvent	$\lambda_{max}$ [nm]
H <sub>2</sub> pydx-en ( <b>2.I</b> )	MeOH	336, 254, 215
H <sub>2</sub> pydx-1,3-pn ( <b>2.II</b> )	MeOH	418, 335, 253, 214
H <sub>2</sub> pydx-1,2-pn ( <b>2.III</b> )	MeOH	336, 253, 211
[Mn <sup>III</sup> (pydx-en)Cl(H <sub>2</sub> O)] ( <b>2.1</b> )	MeOH	568, 419, 317, 277, 226
	Solid <sup>a</sup>	509
[Mn <sup>III</sup> (pydx-1,3-pn)Cl(CH <sub>3</sub> OH)] ( <b>2.2</b> )	MeOH	588, 388, 322, 274, 222
	Solid <sup>a</sup>	507
[Mn <sup>III</sup> (pydx-1,2-pn)Cl(H <sub>2</sub> O)] ( <b>2.3</b> )	MeOH	544, 420, 318, 272, 227
	Solid <sup>a</sup>	507
[Mn <sup>III</sup> (pydx-en)Cl(H <sub>2</sub> O)]-Y ( <b>2.4</b> )	Nujol	414, 325, 294
[Mn <sup>III</sup> (pydx-1,3-pn)Cl(H <sub>2</sub> O)]-Y ( <b>2.5</b> )	Nujol	402, 325, 292
[Mn <sup>III</sup> (pydx-1,2-pn)Cl(H <sub>2</sub> O)]-Y ( <b>2.6</b> )	Nujol	410, 325, 294

<sup>a</sup>Defuse Reflectance Spectra.

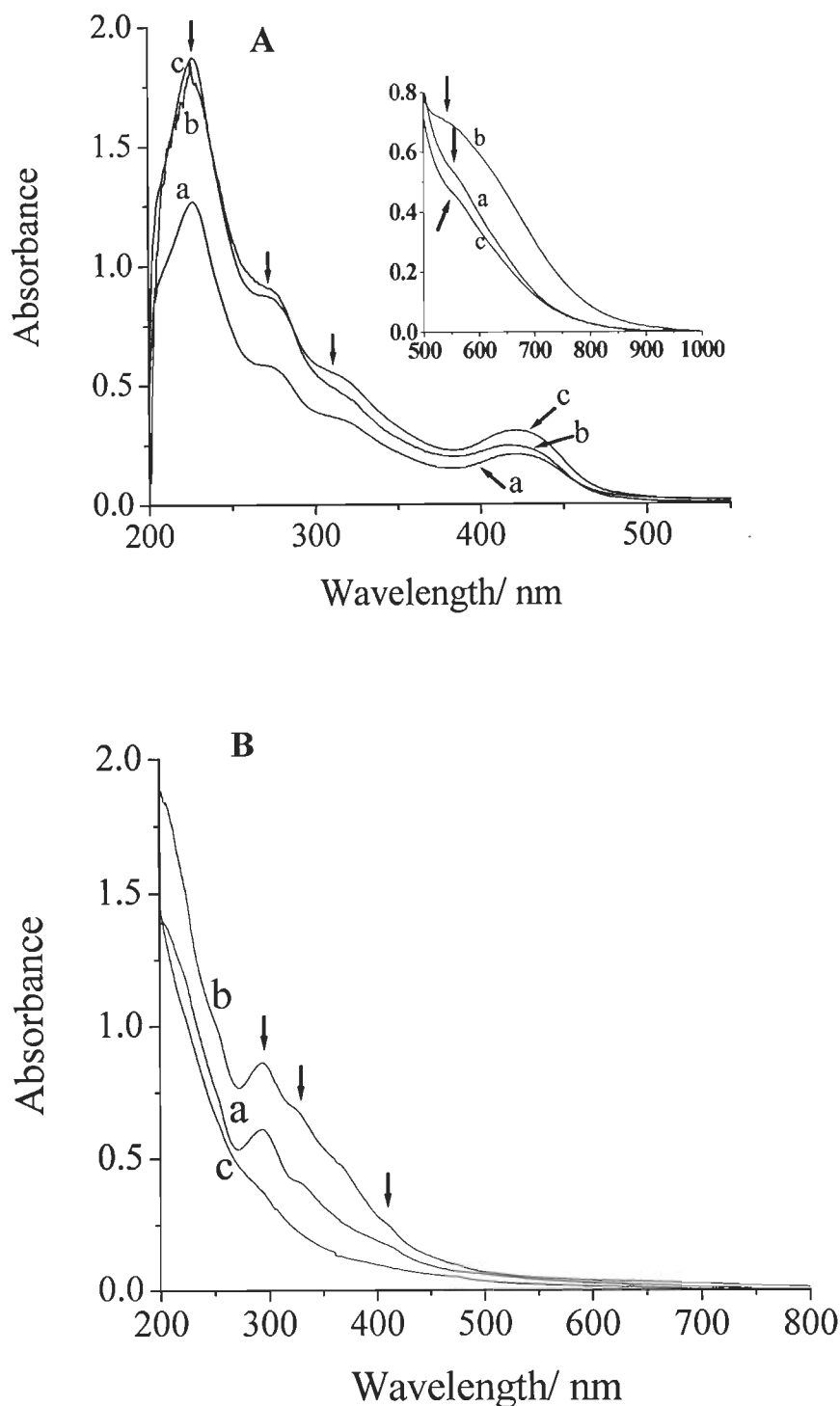


**Figure 2.5. A:** Electronic spectra of  $[\text{Mn}^{\text{III}}(\text{pydx-en})\text{Cl}(\text{H}_2\text{O})]$  (a),  $[\text{Mn}^{\text{III}}(\text{pydx-1,3-pn})\text{Cl}(\text{CH}_3\text{OH})]$  (b) and  $[\text{Mn}^{\text{III}}(\text{pydx-1,2-pn})\text{Cl}(\text{H}_2\text{O})]$ (c); **B:** Electronic spectra of  $[\text{Mn}^{\text{III}}(\text{pydx-en})\text{Cl}(\text{H}_2\text{O})]\text{-Y}$  (a),  $[\text{Mn}^{\text{III}}(\text{pydx-1,3-pn})\text{Cl}(\text{H}_2\text{O})]\text{-Y}$  (b) and  $[\text{Mn}^{\text{III}}(\text{pydx-1,2-pn})\text{Cl}(\text{H}_2\text{O})]\text{-Y}$  (c).

### 2.3.7. Reactivity of complexes with H<sub>2</sub>O<sub>2</sub>

The behavior of the methanolic solutions of manganese(III) complexes with H<sub>2</sub>O<sub>2</sub> added was also monitored by electronic absorption spectroscopy. Thus the stepwise additions of ten drops portions of H<sub>2</sub>O<sub>2</sub> (0.441 g, 3.89 mmol) of 30% H<sub>2</sub>O<sub>2</sub> dissolved in 5 ml of MeOH) to 10 ml of ca.  $1.0 \times 10^{-4}$  M solution of [Mn<sup>III</sup>(Pydx-en)Cl(H<sub>2</sub>O)] in MeOH causes the decrease in intensities of the 419 and 317 nm bands; Figure 2.6. Simultaneously the two UV bands appearing at 277 and 226 nm experience a considerable increase in intensity and finally disappear. The changes in visible region could only be observed with concentrated solution (see in set of Figure 2.6). Thus the d – d band appearing at 568 nm slowly loses its intensity and finally appears as a weak shoulder. This change in spectra has been interpreted as the formation of Mn<sup>IV</sup>=O compound [116, 117]. Similar features have also been observed for complex [Mn<sup>III</sup>(pydx-1,3-pn)Cl(CH<sub>3</sub>OH)] (2.2) (see Figure 2.7). Interestingly, solutions of all complexes acquire original spectral patterns on keeping for long time.

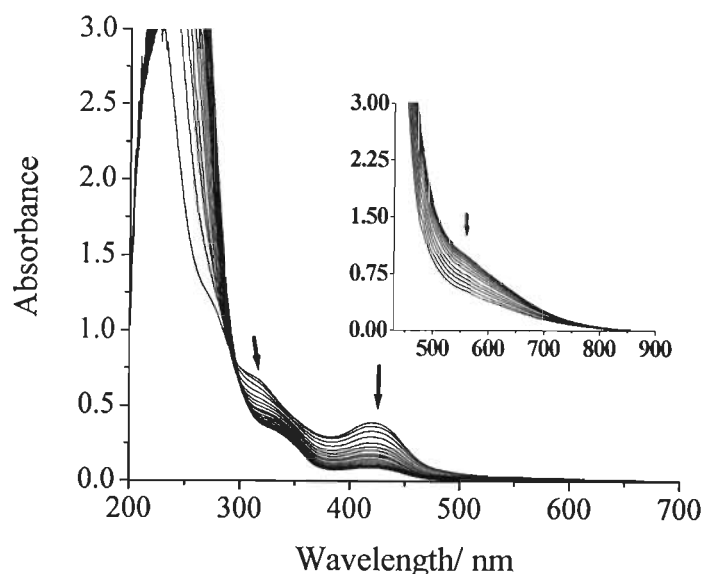


**Figure 2.6.** UV-Vis spectral changes observed during titration of [Mn<sup>III</sup>(Pydx-en)Cl(H<sub>2</sub>O)] (2.1) with H<sub>2</sub>O<sub>2</sub>. The spectra were recorded after stepwise additions of ten drops portions of H<sub>2</sub>O<sub>2</sub> (0.441 g (3.89 mmol) of 30% H<sub>2</sub>O<sub>2</sub> dissolved in 5 ml of MeOH) to 10 ml of  $1.0 \times 10^{-4}$  M solution in MeOH. In set shows similar spectra recorded with  $1.0 \times 10^{-3}$  M solution of 2.1 in MeOH.

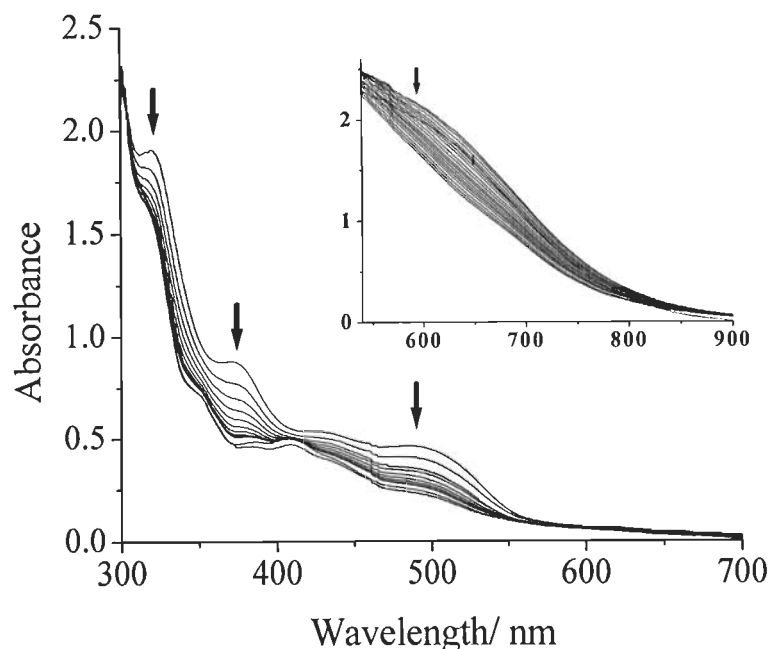


**Figure 2.7.** UV-Vis spectral changes observed during titration of  $[\text{Mn}^{\text{III}}(\text{Pydx-1,3-pn})\text{Cl}(\text{CH}_3\text{OH})]$  with  $\text{H}_2\text{O}_2$ . The spectra were recorded after stepwise additions of one drops portions of  $\text{H}_2\text{O}_2$  (0.149 g (1.32 mmol) of 30%  $\text{H}_2\text{O}_2$  dissolved in 5 ml of MeOH) to 5 ml of  $1.0 \times 10^{-4}$  M solution in MeOH. In set shows similar spectra recorded with  $1.0 \times 10^{-3}$  M solution in MeOH.

### 2.3.8. Electrochemical studies

The cyclic voltammograms (CVs) of complexes  $[\text{Mn}^{\text{III}}(\text{pydx-en})\text{Cl}(\text{H}_2\text{O})]$  (2.1),  $[\text{Mn}^{\text{III}}(\text{pydx-1,3-pn})\text{Cl}(\text{CH}_3\text{OH})]$  (2.2) and  $[\text{Mn}^{\text{III}}(\text{pydx-1,2-pn})\text{Cl}(\text{H}_2\text{O})]$  (2.3) were recorded in the potential range of  $-0.8$  to  $0.8$  V in DMF (dried over molecular sieves), using  $0.1$  M tetrabutylammonium perchlorate (TBAP) as a supporting electrolyte. Voltammograms of these complexes are shown in Figures 2.8 and 2.9. A relatively small peak-to-peak separation ( $\Delta E$ ) of  $0.082$  to  $0.130$  V suggests their quasireversible behaviour while a sharp one-electron redox wave observable by cyclic voltammetry at  $E_{1/2} = -0.038$  to  $-0.071$  V vs. Ag/AgCl corresponds to the  $\text{Mn}^{\text{III}}-\text{Mn}^{\text{II}}$  redox couple [97,109]. Comparable electrochemical

data (i.e., reductive and oxidative peak potentials) for all complexes indicate that the alkyl chain length or methyl group on it has no influence on the manganese nucleus in these complexes. Same conclusion has also been inferred while studying UV-vis spectral studies.

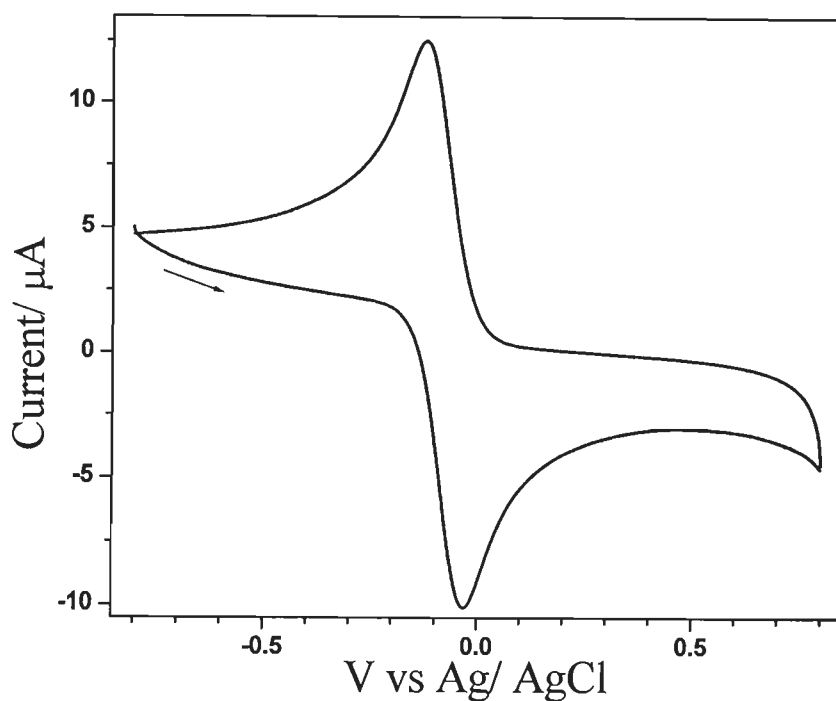


**Figure 2.8.** Cyclic voltammogram of 1mM solution of  $[\text{Mn}^{\text{III}}(\text{pydx-en})\text{Cl}(\text{H}_2\text{O})]$  (2.1) in DMF in the presence of 0.1 M tetrabutylammonium perchlorate (TBAP) using Ag/AgCl as reference electrode, glassy-carbon as working electrode and platinum wire as auxiliary electrode; scan rate: 0.1 V/s.



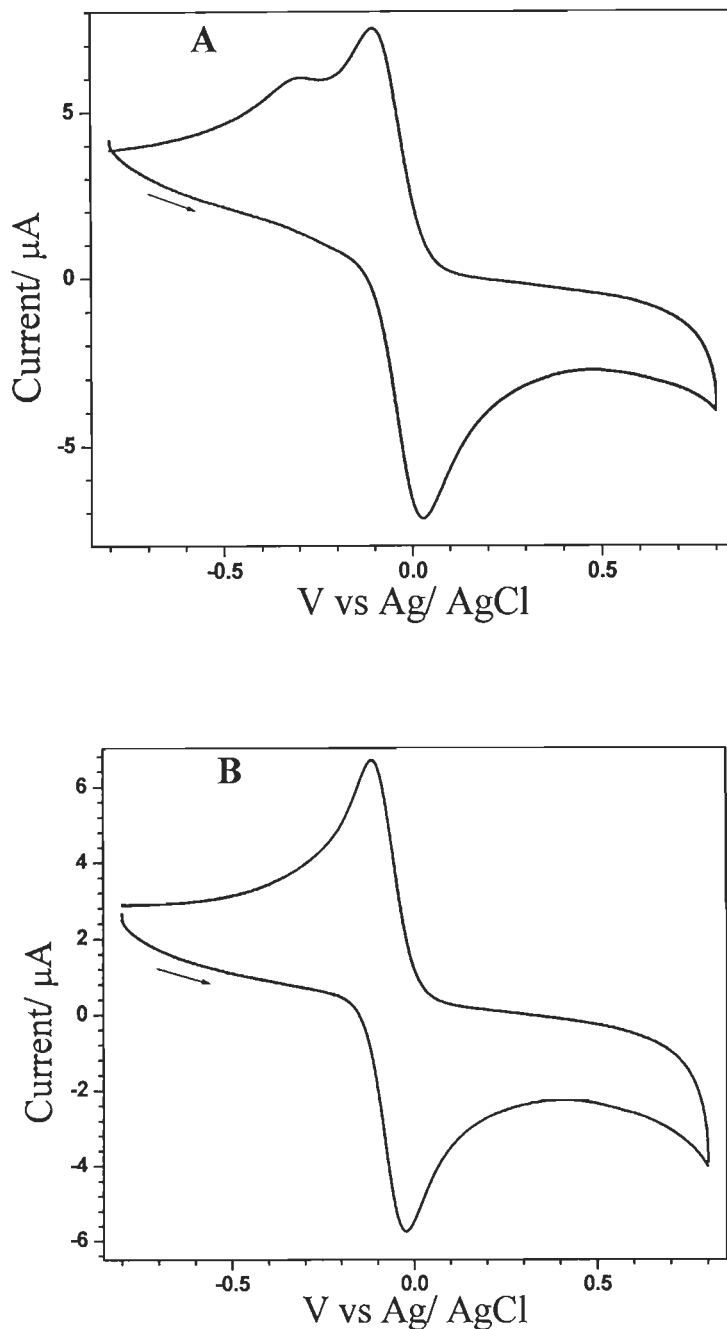


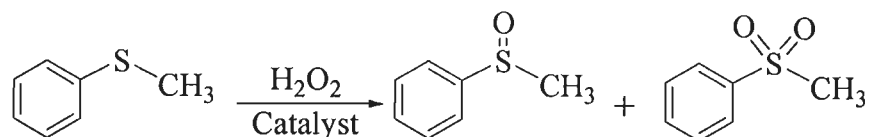
**Figure 2.9.** A: Cyclic voltammogram of  $[\text{Mn}^{\text{III}}(\text{Pydx-1,3-pn})\text{Cl}(\text{CH}_3\text{OH})]$  (**2.2**) in DMF solution (1 mM), B: Cyclic voltammogram of  $[\text{Mn}^{\text{III}}(\text{Pydx-1,2-pn})\text{Cl}(\text{H}_2\text{O})]$

(2.3) in DMF solution (1 mM). Ag/AgCl as reference electrode and glassy carbon as working electrode, scan rate: 0.1 V/s.

### 2.3.9. Catalytic activity studies

#### 2.3.9.1. Oxidation of methyl phenyl sulfide

Oxidation of the sulfur containing compounds is one of the important reactions in pharmaceutical as well as in petroleum industry [118–120]. Such oxidation of methyl phenyl sulfide was tested with the zeolite-Y encapsulated  $Mn^{III}$  complexes prepared in this work. Oxidation of methyl phenyl sulfide in the presence of  $H_2O_2$  gave two products, namely methyl phenyl sulfoxide and methyl phenyl sulfone, as shown in Scheme 2.3.



**Scheme 2.3.**

The catalytic potential of these catalysts has been optimised for the maximum oxidation of methyl phenyl sulfide by studying three different parameters viz. the effect of amount of oxidant (moles of  $H_2O_2$  per mole of styrene) and catalyst (amount of catalyst per mole of methyl phenyl sulfide), and solvent volume of the reaction mixture in detail. Thus,  $[Mn^{III}(pydx-en)Cl(H_2O)]-Y$  (2.4) was taken as a representative catalyst, and the amount of oxidant was varied at a fixed amount of methyl phenyl sulfide (1.242 g, 10 mmol) and catalyst (0.020 g) in acetonitrile (5 ml), and the reaction was carried out at ambient temperature; Figure 2.10. At an aqueous substrate/  $H_2O_2$  ratio of 1:2, a maximum of 87.5% conversion was achieved in 3.5 h of reaction time. Lowering the substrate/  $H_2O_2$  ratio to 1:1 lowers the conversion of methyl phenyl sulfide considerably. However, no obvious increase in percent conversion was observed on increasing this ratio to 1:3, though time period in over all conversion was reduced to 3 h.

The effect of catalyst  $[Mn^{III}(pydx-en)Cl(H_2O)]-Y$  was studied considering three different amounts viz. 0.015, 0.020 and 0.030 g while keeping methyl

methyl phenyl sulfide (1.24 g, 10 mmol) and 30%  $\text{H}_2\text{O}_2$  (2.27 g, 20 mmol) in acetonitrile (5 ml). As mentioned in Figure 2.11, increasing the catalyst amount from 0.015 g to 0.020 g improved the conversion from 77.7% to 87.5% but further increment of catalyst to 0.030 g resulted in the lower conversion. The reason for reduced activity at higher catalyst amount may be adsorption/ chemisorption of the two reactants on separate catalyst particles, thereby reducing the chance to interact. Therefore, it is clear that 0.020 g of catalyst is adequate to obtain an optimum methyl phenyl sulfide conversion of 87.5% in 3.5 h of contact time.

The amount of solvent also has influence on the oxidation of methyl phenyl sulfide. It was concluded (Figure 2.12) that 5 ml  $\text{CH}_3\text{CN}$  was sufficient to effect maximum conversion under above optimized reaction conditions.

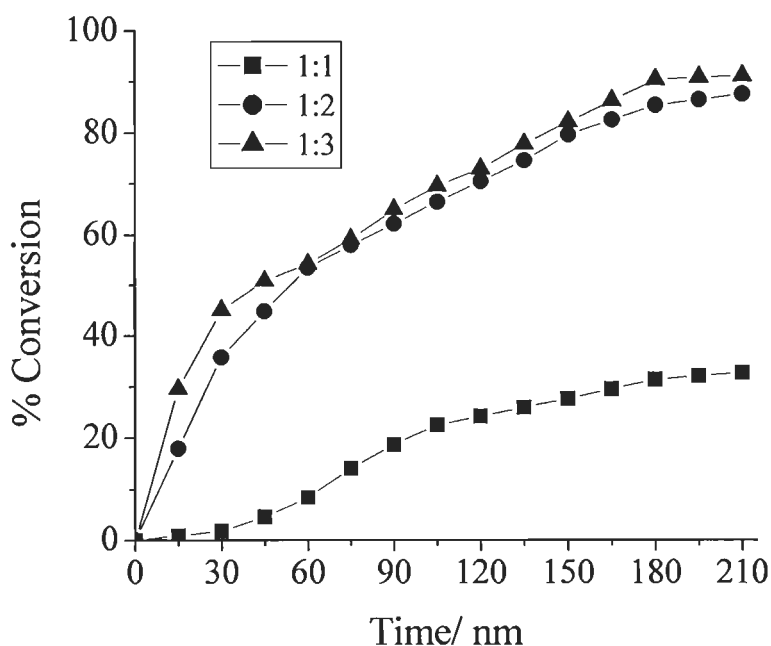


**Figure 2.10.** Effect of the amount of  $\text{H}_2\text{O}_2$  on the oxidation of methyl phenyl sulfide as a function of time. Other reaction conditions: methyl phenyl sulfide (1.24 g, 10 mmol),  $[\text{Mn}^{\text{III}}(\text{pydx-en})\text{Cl}(\text{H}_2\text{O})]\cdot\text{Y}$  (0.020 g) and acetonitrile (5 ml).

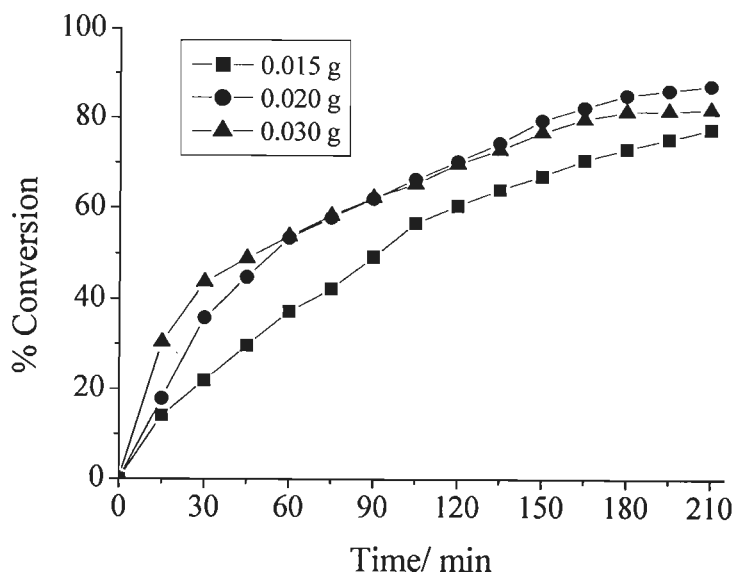


**Figure 2.11.** Effect of amount of catalyst on the oxidation of methyl phenyl sulfide as a function of time. Other reaction conditions: methyl phenyl sulfide (1.24 g, 10 mmol),  $\text{H}_2\text{O}_2$  (2.27 g, 20 mmol) and acetonitrile (5 ml).

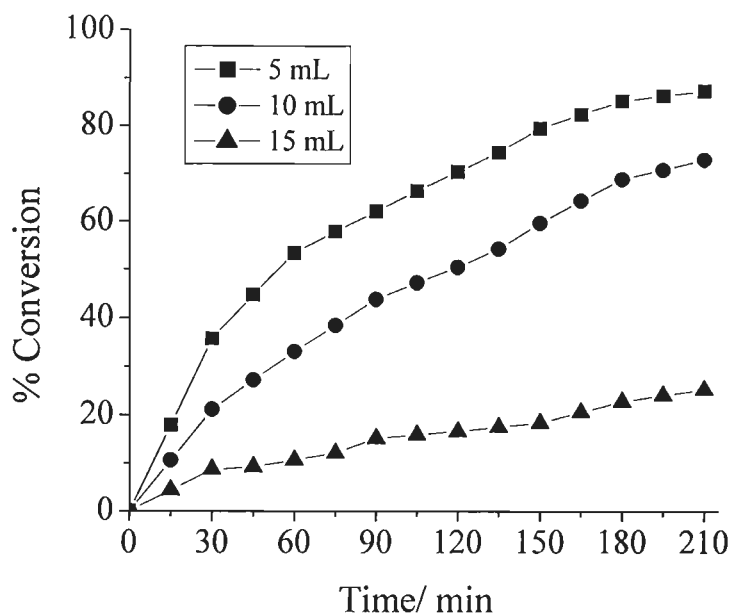


**Figure 2.12.** Effect of amount of solvent on the oxidation of methyl phenyl sulphide as a function of time. Other reaction condition: methyl phenyl sulphide (1.242 g, 10 mmol),  $\text{H}_2\text{O}_2$  (2.27 g, 20 mmol) and  $[\text{Mn}(\text{pydx-en})\text{Cl}(\text{H}_2\text{O})]\text{-Y}$  (0.020 g).

Thus, from these experiments, the best reaction conditions for the maximum oxidation of methyl phenyl sulfide were considered to be: catalyst (0.020 g), methyl phenyl sulfide (1.24 g, 10 mmol), 30% H<sub>2</sub>O<sub>2</sub> (2.27 g, 20 mmol) and acetonitrile (5 ml). Under these reaction conditions catalyst [Mn<sup>III</sup>(pydx-1,3-pn)Cl(H<sub>2</sub>O)]-Y (2.5) and [Mn<sup>III</sup>(pydx-1,2-pn)Cl(H<sub>2</sub>O)]-Y (2.6) were also tested and results are compared in Figure 2.13 while Table 2.6 provides selectivity details.

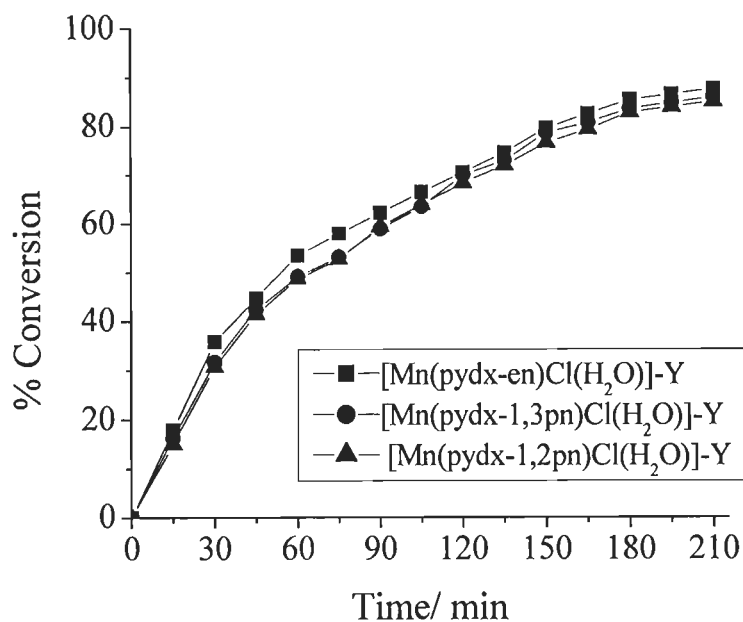


**Figure 2.13.** Effect of different catalyst on the oxidation of methyl phenyl sulfide. For reaction conditions see text.

It is clear from the table that the catalytic potentials of all three catalysts are comparable. However, the percentage conversion of methyl phenyl sulfide varied in the order: [Mn<sup>III</sup>(pydx-en)Cl(H<sub>2</sub>O)]-Y (87.5 %) > [Mn<sup>III</sup>(pydx-1,3-pn)Cl(H<sub>2</sub>O)]-Y (85.8%) > [Mn<sup>III</sup>(pydx-1,2-pn)Cl(H<sub>2</sub>O)]-Y (84.9%). Amongst the two products obtained, the selectivity of the major product i.e. sulfoxide is very close but varies in the order: [Mn<sup>III</sup>(pydx-en)Cl(H<sub>2</sub>O)]-Y (74.7 %) > [Mn<sup>III</sup>(pydx-1,2-pn)Cl(H<sub>2</sub>O)]-Y (70.9%) > [Mn<sup>III</sup>(pydx-1,3-pn)Cl(H<sub>2</sub>O)]-Y (70.2%). The corresponding neat complexes have also been tested considering their same mole concentrations as of the encapsulated ones under above reaction conditions and results are also

presented in Table 2.6. Only 37.5 – 43.5% transformation of methyl phenyl sulphide was achieved with these complexes and is much less than the corresponding encapsulated ones. However, the selectivity of sulfoxide was much better with these complexes. Control experiment was carried out without catalyst under above reaction conditions. The reaction mixture gave 22.7 % conversion of methyl phenyl sulfide with 92.7 % selectivity towards sulfoxide, 7.3 % towards sulfone and ca. 0.3 % an unidentified product. Thus, encapsulated catalysts not only improve the conversion of substrates, they alter the selectivity of the products as well. Feng et al. [121] have compared results of the oxidation of several sulfides from the literature and results of these catalysts compare well with other catalysts.

**Table 2.6.** Conversion percentage of methyl phenyl sulfide in 3.5 h using H<sub>2</sub>O<sub>2</sub> as an oxidant and selectivity of sulfoxide and sulfone.

Catalyst	% Conv.	TOF (h <sup>-1</sup> ) <sup>a</sup>	% Selectivity	
			Sulfoxide	Sulfone
[Mn <sup>III</sup> (pydx-en)Cl(H <sub>2</sub> O)]-Y	87.5	1322	74.7	25.3
[Mn <sup>III</sup> (pydx-1,3-pn)Cl(H <sub>2</sub> O)]-Y	85.8	1685	70.2	29.8
[Mn <sup>III</sup> (pydx-1,2-pn)Cl(H <sub>2</sub> O)]-Y	84.9	966	70.9	29.1
[Mn(pydx-en)Cl(H <sub>2</sub> O)]-Y <sup>b</sup>	84.8	-	72.1	27.9
[Mn(pydx-1,3-pn)Cl(H <sub>2</sub> O)]-Y <sup>b</sup>	82.3	-	68.4	31.6
[Mn(pydx-1,2-pn)Cl(H <sub>2</sub> O)]-Y <sup>b</sup>	81.6	-	69.3	30.7
[Mn <sup>III</sup> (pydx-en)Cl(H <sub>2</sub> O)]	43.5	578	85.8	14.2
[Mn <sup>III</sup> (pydx-1,3-pn)Cl(CH <sub>3</sub> OH)]	37.5	528	97.6	2.4
[M <sup>III</sup> (pydx-1,2-pn)Cl(H <sub>2</sub> O)]	41.3	565	91.0	9.0
Without catalyst	22.7		92.7	7.3

<sup>a</sup>TOF [h<sup>-1</sup>] (turnover frequency): mol of substrate converted per mol of metal (in the solid catalyst) per hour.

<sup>b</sup>First cycle of used catalyst.

The conversion of methyl phenyl sulfide and the selectivity of different reaction products with  $[\text{Mn}^{\text{III}}(\text{pydx-en})\text{Cl}(\text{H}_2\text{O})]\text{-Y}$  as catalyst under the optimized reaction conditions have been analyzed as a function of time and are presented in Figure 2.14. It is clear from the plot that the conversion of methyl phenyl sulfide starts immediately after mixing the substrate, catalyst and oxidant in acetonitrile, and reaches 87.5% in 3.5 h of reaction time. The selectivity of the formed methyl phenyl sulfoxide is ca. 91% at 1 h of reaction time but decreases slowly with time and reaches ca. 74.7% after 3.5 h of reaction. The selectivity of methyl phenyl sulfone is 9% after 1 h of reaction time and reaches 25.5% after 3.5 h.

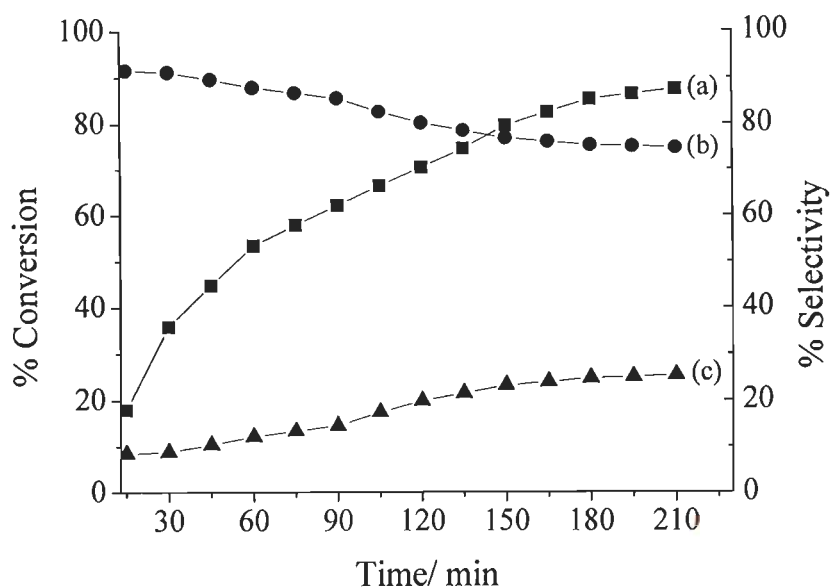
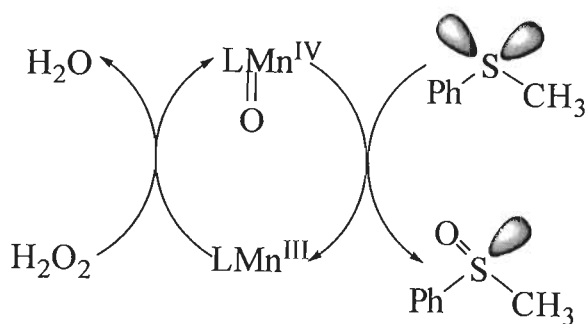


**Figure 2.14.** Conversion of methyl phenyl sulfide and variation in the selectivity of different reaction products as a function of time using  $[\text{Mn}^{\text{III}}(\text{pydx-en})\text{Cl}(\text{H}_2\text{O})]\text{-Y}$  as catalyst: (a) conversion of methyl phenyl sulphide (●), (b) selectivity of methyl phenyl sulfoxide (■) and (c) selectivity of methyl phenyl sulfone (▲).

A probable mechanism for the oxidation of methyl sulphide is shown in Scheme 2.4. This is based on the fact that  $\text{Mn}^{\text{III}}$  complexes react with  $\text{H}_2\text{O}_2$  to give unstable intermediate  $\text{Mn}^{\text{IV}}=\text{O}$  species. The electron-rich sulfur atom of the sulfide undergoes electrophilic oxidation by intermediate  $\text{Mn}^{\text{IV}}=\text{O}$  species to give the sulfoxide and further to sulfone.



Scheme 2.4.

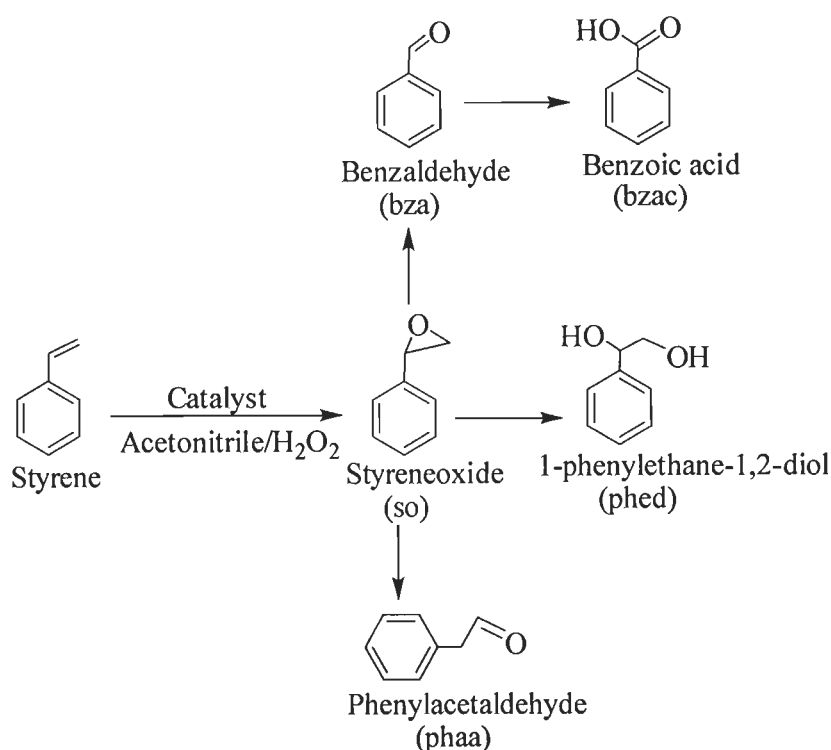
### 2.3.9.2. Oxidation of styrene

The oxidation of styrene, catalysed by  $[\text{Cu}^{\text{II}}(\text{pydx-en})]\text{-Y}$  and  $[\text{Cu}^{\text{II}}(\text{pydx-1,3-pn})]\text{-Y}$  has been reported using  $\text{H}_2\text{O}_2$  and *tert*-butyl hydroperoxide as oxidants, and styrene oxide, benzaldehyde, benzoic acid and phenylacetaldehyde (Scheme 5) along with minor amounts of unidentified products were obtained [110]. We have studied oxidation of styrene, catalysed by zeolite-Y encapsulated manganese complexes,  $[\text{Mn}^{\text{III}}(\text{pydx-en})\text{Cl}(\text{H}_2\text{O})]\text{-Y}$ ,  $[\text{Mn}^{\text{III}}(\text{pydx-1,3-pn})\text{Cl}(\text{H}_2\text{O})]\text{-Y}$  and  $[\text{Mn}^{\text{III}}(\text{pydx-1,2-pn})\text{Cl}(\text{H}_2\text{O})]\text{-Y}$  using  $\text{H}_2\text{O}_2$  as an oxidant and obtained 1-phenylethane-1,2-diol also in addition to all above products as shown in Scheme 2.5. All these oxidation products as observed here were also identified using the zeolite-Y encapsulated complex  $[\text{V}^{\text{IV}}\text{O}(\text{sal-dach})]\text{-Y}$  ( $\text{H}_2\text{sal-dach}$  = Schiff base derived from salicylaldehyde and 1,2-diaminocyclohexane) [122].

In order to achieve suitable reaction conditions for the maximum oxidation of styrene,  $[\text{Mn}^{\text{III}}(\text{pydx-en})\text{Cl}(\text{H}_2\text{O})]\text{-Y}$  was taken as a representative catalyst and three parameters (as mentioned in the preceding section) were again tested. The effect of amount of  $\text{H}_2\text{O}_2$  on the oxidation of styrene as a function of time is illustrated in Figure 2.15. Three different styrene/ $\text{H}_2\text{O}_2$  molar ratios of 1:1, 1:2, and 1:3 were considered, while keeping the fixed amount of styrene (1.04 g, 10 mmol) and catalyst (0.040 g) in 5 ml of  $\text{CH}_3\text{CN}$  at 80 °C. A maximum of 50.8 % conversion of styrene was obtained at a styrene to  $\text{H}_2\text{O}_2$  molar ratio of 1:1. This conversion improved to 76.9 % at a styrene to  $\text{H}_2\text{O}_2$  molar ratio of 1:2. Further



increasing the ratio to 1:3 speeded up the conversion to complete within 5 h but the over all conversion rolled back to 51.5 %. The reason for this may be due to the dilution of the reaction mixture by the presence of larger amount of water molecules in H<sub>2</sub>O<sub>2</sub> solution. It is, therefore, clear that the styrene to H<sub>2</sub>O<sub>2</sub> molar ratio of 1:2 is the best one to obtain the maximum styrene conversion of 76.9 % in 6 h reaction time.



**Scheme 2.5.**

The effect of amount of catalyst on the oxidation of styrene was studied considering three different amounts of [Mn<sup>III</sup>(pydx-en)Cl(H<sub>2</sub>O)]-Y viz. 0.030, 0.040 and 0.050 g while keeping the styrene (1.04 g, 10 mmol) and H<sub>2</sub>O<sub>2</sub> (2.27 g, 20 mmol) in 5 ml of CH<sub>3</sub>CN and the reaction was carried out at 80 °C. As shown in Figure 2.16, a maximum of 51.0% conversion was achieved with 0.030 g of catalyst, whereas 0.040 g of catalyst gave a maximum conversion of 76.9% in 6 h of reaction time. Further increment of catalyst amount (0.050 g) has shown only 60.5% conversion. The reason for reduced activity at higher catalyst amount has been discussed in the previous section.

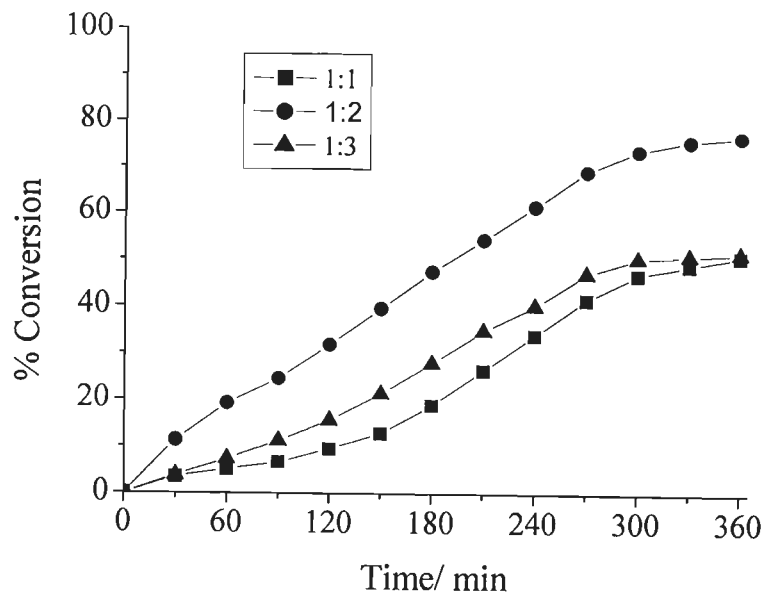


**Figure 2.15.** Effect of the amount of H<sub>2</sub>O<sub>2</sub> on the oxidation of styrene as a function of time. Other reaction conditions: styrene (1.04 g, 10 mmol), [Mn<sup>III</sup>(pydx-en)Cl(H<sub>2</sub>O)]-Y (0.040 g), acetonitrile (5 ml) and temperature (80 °C).

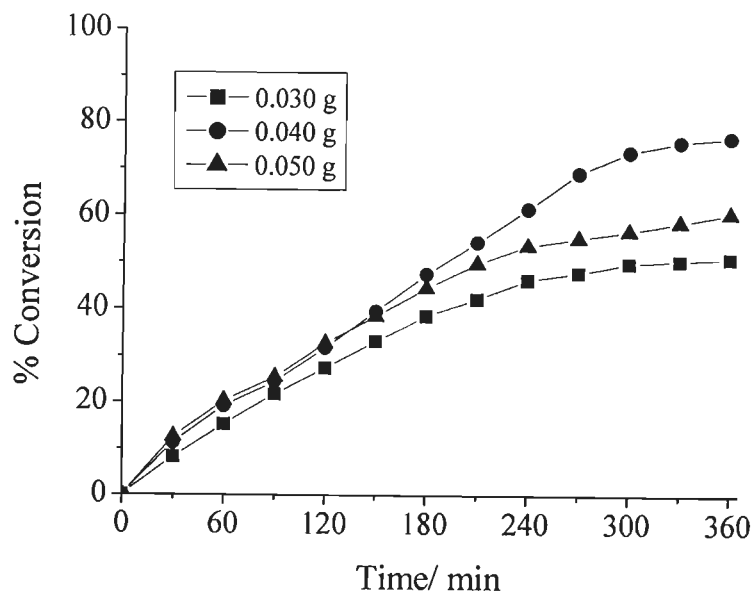


**Figure 2.16.** Effect of the amount of catalyst on the oxidation of styrene. Other reaction conditions: styrene (1.04 g, 10 mmol), 30% H<sub>2</sub>O<sub>2</sub> (2.27 g, 20 mmol), CH<sub>3</sub>CN (5 ml) and temp. (80 °C).

Figure 2.17 illustrates the oxidation of styrene in three different volume of solvent – viz. 5, 10 and 15 ml of acetonitrile, while keeping the optimised conditions of styrene (1.04 g, 10 mmol),  $[\text{Mn}^{\text{III}}(\text{pydx-en})\text{Cl}(\text{H}_2\text{O})]\text{-Y}$  (0.040 g), 30%  $\text{H}_2\text{O}_2$  (2.27 g, 20 mmol) and temperature (80 °C). It was found that conducting the catalytic reaction in 5 ml of acetonitrile is most suitable to maximize the oxidation of styrene.

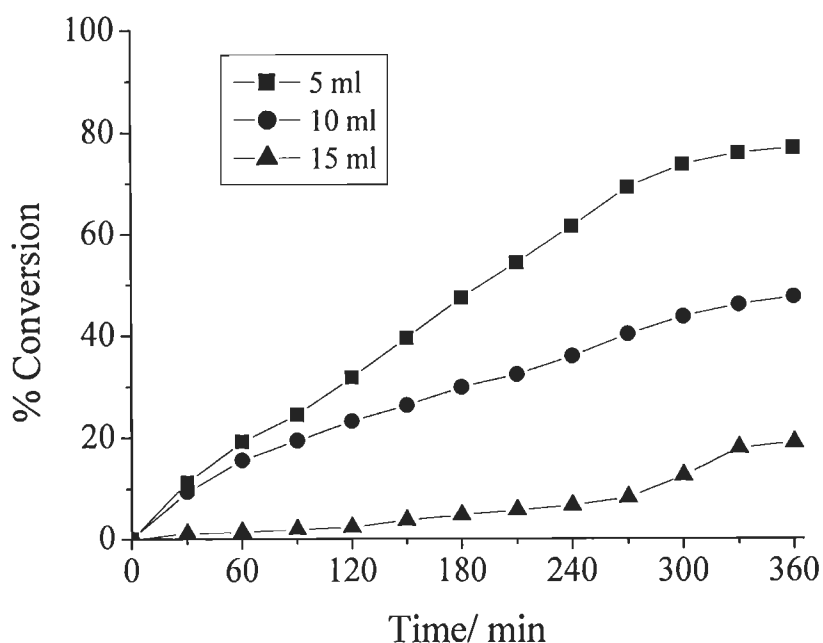


**Figure 2.17.** Effect of the volume of acetonitrile on the oxidation of styrene. Other reaction conditions: styrene (1.04 g, 10 mmol), 30%  $\text{H}_2\text{O}_2$  (2.27 g, 20 mmol),  $[\text{Mn}^{\text{III}}(\text{pydx-en})\text{Cl}(\text{H}_2\text{O})]\text{-Y}$  (0.040 g) and temp. (80 °C).

Therefore, from these experiments, for the maximum oxidation of 10 mmol of styrene, the required conditions as concluded were:  $[\text{Mn}^{\text{III}}(\text{pydx-en})\text{Cl}(\text{H}_2\text{O})]\text{-Y}$  (0.040 g),  $\text{H}_2\text{O}_2$  (2.27 g, 20 mmol),  $\text{CH}_3\text{CN}$  (5 ml) and temperature (80 °C). Under these optimized reaction conditions, the catalytic activities of other zeolite-Y encapsulated complexes were also tested, and the results obtained are illustrated in Figure 2.18 as a function of time. Table 2.7 compares the selectivity of the various products obtained after 6 h of reaction time, along with the percent conversion of

styrene and turnover frequency. It is clear from Table 2.7 and Figure 2.18 that conversion of styrene follows the order:  $[\text{Mn}^{\text{III}}(\text{pydx-en})\text{Cl}(\text{H}_2\text{O})]\text{-Y}$  (76.9%) >  $[\text{Mn}^{\text{III}}(\text{pydx-1,3-pn})\text{Cl}(\text{H}_2\text{O})]\text{-Y}$  (76.0%) >  $[\text{Mn}^{\text{III}}(\text{pydx-1,2-pn})\text{Cl}(\text{H}_2\text{O})]\text{-Y}$  (72.3%). The selectivity of the different reaction products for all complexes are nearly same and follows the order: benzaldehyde >> benzoic acid > styrene oxide > phenylacetaldehyde > 1-phenylethane-1,2-diol. Thus, the selectivity for benzaldehyde is much higher, while the other products are obtained in small amounts.

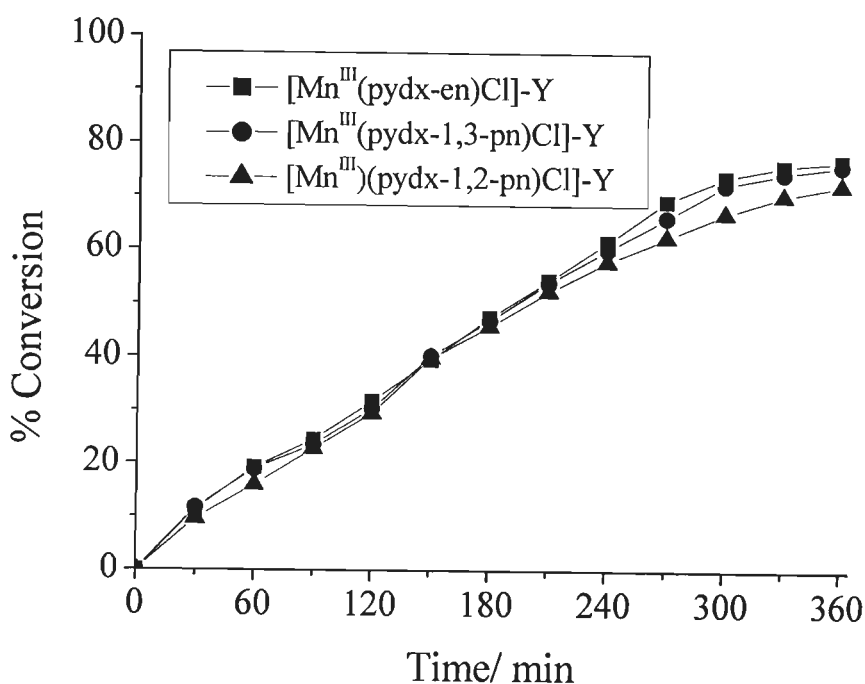


**Figure 2.18.** Comparison of the catalytic potential of zeolite-encapsulated manganese(III) complexes for the oxidation of styrene in the presence of  $\text{H}_2\text{O}_2$  as oxidant.

We have also tested the catalytic activity of the neat complexes for the oxidation of styrene using an equimolar concentration of metal ion as in their respective zeolite-encapsulated  $\text{Mn}^{\text{III}}$  complexes. Table 2.7 also provides the conversion and other details. Under the above reaction conditions, only four products were obtained with the selectivity order: benzaldehyde >> benzoic acid > styrene oxide > phenylacetaldehyde and the conversion obtained (45.7% – 48.6%)

is significantly lower than that shown by the respective encapsulated complexes. Control experiment without catalyst under above reaction conditions gave only 4.0 % conversion.

**Table 2.7.** Product selectivity and percent conversion of styrene with H<sub>2</sub>O<sub>2</sub> after 6 h of reaction time.

Catalyst	% Conv.	TOF (h <sup>-1</sup> )	Selectivity % <sup>b</sup>				
			so	bza	phed	bzac	phaa
[Mn(pydx-en)Cl(H <sub>2</sub> O)]-Y	76.9	339	7.7	78.3	1.5	9.7	2.8
[Mn(pydx-1,3-pn)Cl(H <sub>2</sub> O)]-Y	76.0	435	7.8	77.6	1.9	7.9	4.8
[Mn(pydx-1,2-pn)Cl(H <sub>2</sub> O)]-Y	72.3	240	6.7	75.9	1.7	12.5	3.2
[Mn(pydx-en)Cl(H <sub>2</sub> O)]-Y <sup>a</sup>	73.8	-	5.3	76.5	2.3	10.7	5.2
[Mn(pydx-1,3-pn)Cl(H <sub>2</sub> O)]-Y <sup>a</sup>	72.9	-	7.2	79.6	2.1	7.2	3.9
[Mn(pydx-1,2-pn)Cl(H <sub>2</sub> O)]-Y <sup>a</sup>	71.4	-	6.3	77.4	1.5	8.2	6.6
[Mn(pydx-en)Cl(H <sub>2</sub> O)]	48.6	251	5.4	85.7	-	6.6	2.3
[Mn(pydx-1,3-pn)Cl(CH <sub>3</sub> OH)]	45.7	250	5.2	89.2	-	2.9	2.7
[Mn(pydx-1,2-pn)Cl(H <sub>2</sub> O)]	46.8	249	6.2	87.9	-	3.8	2.1
Without catalyst	4.0		33.3	83.3	-	9.2	2.4

<sup>a</sup>First cycle of used catalyst.

<sup>b</sup>For details of abbreviations see Scheme 2.5.

The conversion of styrene and the selectivity of different reaction products using [Mn<sup>III</sup>(pydx-en)Cl(H<sub>2</sub>O)]-Y as catalyst under the optimized reaction conditions have been analysed as a function of time and are presented in Figure 2.19. It is clear from the plot that the selectivity of the formation of styrene oxide is good (24.6%) in the beginning but it decreases considerably with time and reaches 7.7% in 6 h. A maximum of 75.4% selectivity of benzaldehyde noted after 1/2 h of reaction time, increases only marginally even after 6 h while the formations of benzoic acid, phenylacetaldehyde and 1-phenylethane-1,2-diol start only after ca. 3 h and do not improve much with time. Almost identical trends have also been obtained with the two other catalysts. After 6 h only minor changes have been observed in the selectivity of the different reaction products.

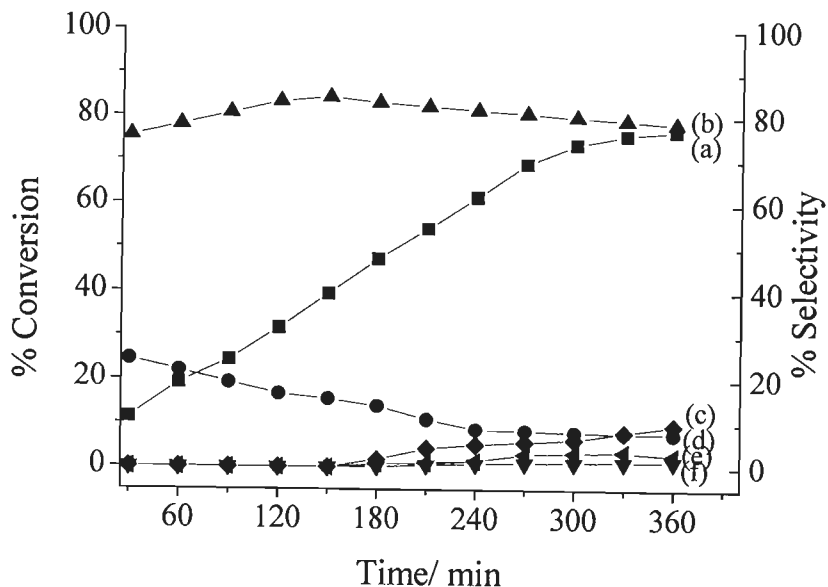
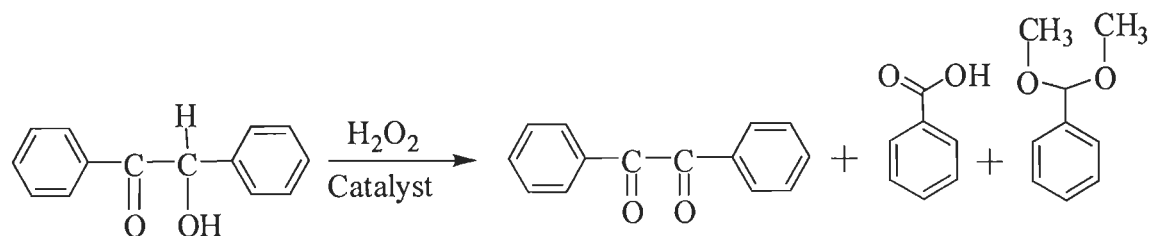


**Figure 2.19.** Conversion of styrene and variation in the selectivity of different reaction products as a function of time using  $[\text{Mn}^{\text{III}}(\text{pydx-en})\text{Cl}(\text{H}_2\text{O})]$ -Y as a catalyst: (a) conversion of styrene (■), (b) selectivity of benzaldehyde (▲), (c) benzoic acid (◆), (d) styrene oxide (●), (e) phenylacetaldehyde (◄) and (f) 1-phenylethane-1,2-diol (▼).

The mechanistic detail for the highest yield of benzaldehyde using *t*-butylhydroperoxide/  $\text{H}_2\text{O}_2$  as oxidant and the formation of different products has been provided in detail in the literature [123–125].  $\text{Mn}^{\text{III}}$  complexes react with  $\text{H}_2\text{O}_2$  to give  $\text{Mn}^{\text{IV}}=\text{O}$  (vide supra) species which ultimately transfer oxygen to the -ene group of styrene to form styrene oxide in the first step. Generally a radical mechanism has been proposed for the oxidation of styrene to benzaldehyde. Thus the formation of benzaldehyde may be facilitated by the direct oxidative cleavage of the styrene side chain double bond by a radical mechanism [124, 126]. A nucleophilic attack of  $\text{H}_2\text{O}_2$  on styrene oxide followed by cleavage of the intermediate hydroperoxystyrene also provides benzaldehyde [127]. Formation of other products such as phenylacetaldehyde is possible through isomerisation of styrene oxide, while the formation of benzoic acid from benzaldehyde is straight forward.

## 2.3.9.3. Oxidation of benzoin

The catalytic efficiency of encapsulated complexes was also tested for the oxidation of benzoin successfully using  $\text{H}_2\text{O}_2$  as oxidant. Oxidation of benzoin, a secondary alcohol, has attracted the attention of researchers because one of its oxidized products, benzil, is a very useful intermediate for the synthesis of heterocyclic compounds and benzilic acid rearrangements [128]. The oxidation products mainly obtained are benzil, benzoic acid and benzaldehyde-dimethylacetal (Scheme 2.6).



Scheme 2.6. Oxidized products of benzoin.

To optimize the reaction conditions for the maximum oxidation of benzoin, the effect of  $\text{H}_2\text{O}_2$  was studied by considering substrate to oxidant ratios of 1:1, 1:2 and 1:3 for the fixed amount of  $[\text{Mn}^{\text{III}}(\text{pydx-en})\text{Cl}(\text{H}_2\text{O})]\text{-Y}$  (0.020 g) and benzoin (1.06 g, 5 mmol) in refluxing methanol (20 ml). About 6 h was required to obtain steady state. Figure 2.20 presents the conversion obtained as a function of time in each case. As shown in figure, the conversion increases from 78.9% to 92.6% on increasing substrate to oxidant ratios from 1:1 to 1:2. Further increment of  $\text{H}_2\text{O}_2$  has no effect on the net oxidation of benzoin.

Similarly, four different amounts of catalysts in the range of 0.020 to 0.040 were considered for the fixed amount of benzoin (1.06 g, 5 mmol) and 30%  $\text{H}_2\text{O}_2$  (1.13 g, 10 mmol) in 20 ml of methanol at the refluxing temperature to see their effect on the conversion of benzoin. As illustrated in Figure 2.21, 0.020 g catalyst was sufficient to effect 92.6% conversion and increasing the amount of catalyst did not show improvement in the oxidation of benzoin except slight reduction in time to reach the steady-state of the reaction. Minimum amount of methanol required for the reaction under above optimized reaction conditions was 20 ml and

further increment of solvent volume has only minor effect on the over all conversion.

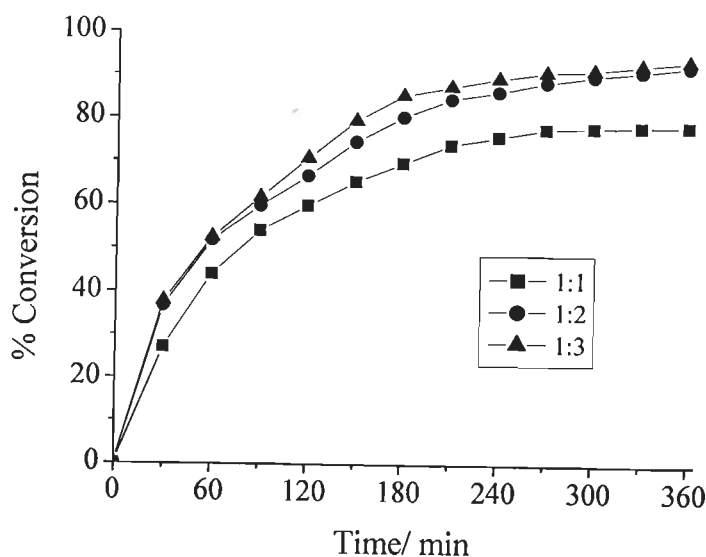


**Figure 2.20.** Effect of amount of  $\text{H}_2\text{O}_2$  on the oxidation of benzoin as a function of time. Other reaction conditions: benzoin (1.06 g, 5 mmol),  $[\text{Mn}^{\text{III}}(\text{pydx-en})\text{Cl}(\text{H}_2\text{O})]\cdot\text{Y}$  (0.020 g), methanol (20 ml).

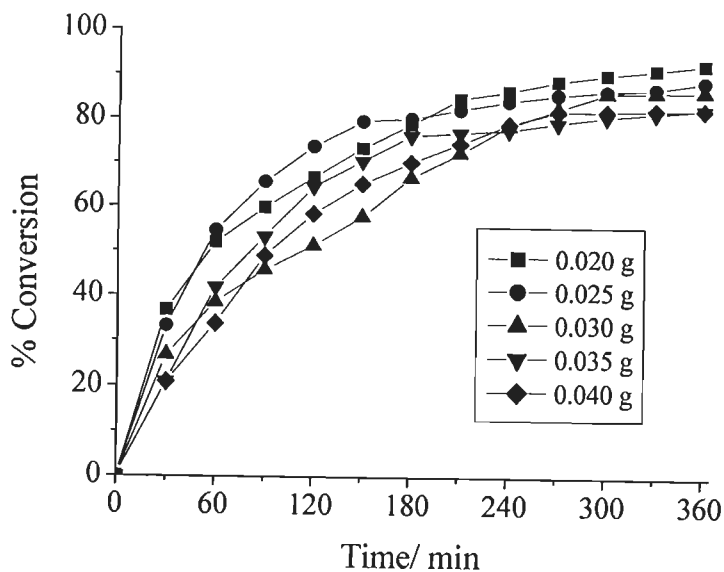


**Figure 2.21.** Effect of amount of catalyst on the oxidation of benzoin as a function of time. Other reaction conditions: benzoin (1.06 g, 5 mmol),  $\text{H}_2\text{O}_2$  (1.13 g, 10 mmol), methanol (20 ml).



Thus, the optimized reaction conditions obtained for the oxidation of benzoin are: benzoin (1.06 g, 5 mmol),  $[\text{Mn}^{\text{III}}(\text{pydx-en})\text{Cl}(\text{H}_2\text{O})]\text{-Y}$  (0.020 g),  $\text{H}_2\text{O}_2$  (1.13 g, 10 mmol) and methanol (20 ml). Figure 2.22 presents the selectivity of various products along with the conversion of benzoin as a function of time for catalyst  $[\text{Mn}^{\text{III}}(\text{pydx-en})\text{Cl}(\text{H}_2\text{O})]\text{-Y}$  under the best suited experimental conditions. It is clear from the plot that only two products (benzil and benzoic acid) form initially. With the highest selectivity of benzil (ca. 40.0%) at the beginning, a continuous but slow decrease of its selectivity with time has been observed which finally reaches 30.8 % after 6 h. The selectivity of benzoic acid also follows the similar trend and reaches 53.2 %. The formation of benzaldehyde-dimethylacetal starts only after 1 h of reaction and slowly increases to 16.0 % at the end of 6 h. Thus, with the maximum benzoin oxidation of 92.6% after 6 h of reaction time, the selectivity of the reaction products varies in the order: benzoic acid (53.2 %) > benzil (30.8 %) > benzaldehyde-dimethylacetal (16.0 %).

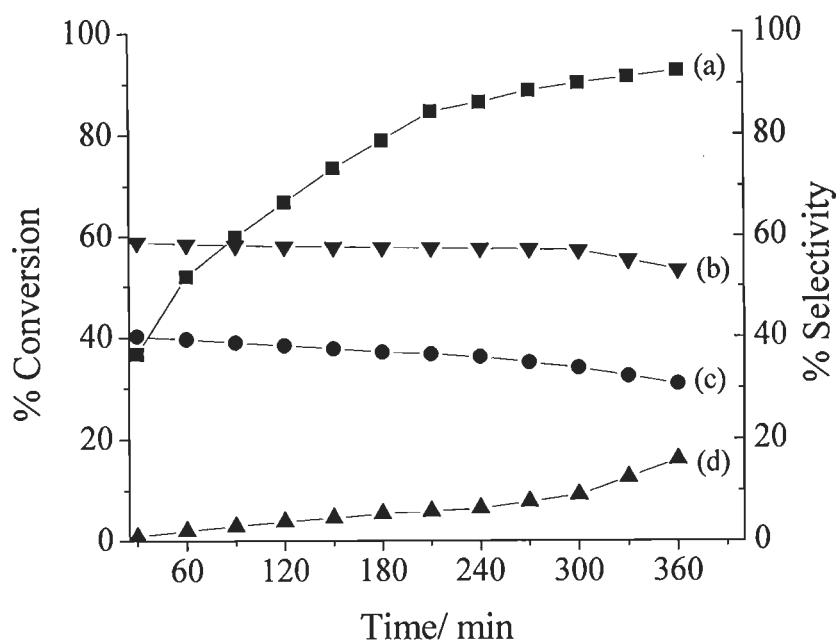


**Figure 2.22.** Conversion of benzoin and variation in the selectivity of different reaction products as a function of time using  $[\text{Mn}^{\text{III}}(\text{pydx-en})\text{Cl}(\text{H}_2\text{O})]\text{-Y}$  as a catalyst: (a) conversion of benzoin, (b) selectivity of benzil, (c) benzoic acid and (d) benzaldehyde-dimethylacetal.

Under the above optimized reaction conditions the oxidation of benzoin, catalyzed by other catalysts, has also been carried out. Figure 2.23 compares the obtained results while Table 2.8 compares the conversions as well as selectivity of products for different catalysts. It is clear that catalysts  $[\text{Mn}^{\text{III}}(\text{pydx-1,3-pn})\text{Cl}(\text{H}_2\text{O})]\text{-Y}$  (2.5) and  $[\text{Mn}^{\text{III}}(\text{pydx-1,2-pn})\text{Cl}(\text{H}_2\text{O})]\text{-Y}$  (2.6) gave 91.9 % and 94.1 % conversions, respectively and are close to the one given by  $[\text{Mn}^{\text{III}}(\text{pydx-en})\text{Cl}(\text{H}_2\text{O})]\text{-Y}$  (2.4). Though, the selectivity of products slightly differs for other catalysts, they essentially follow the same order as obtained for the catalyst 2.4. Control experiment without catalyst under above reaction conditions gave only 8.7 % conversion.

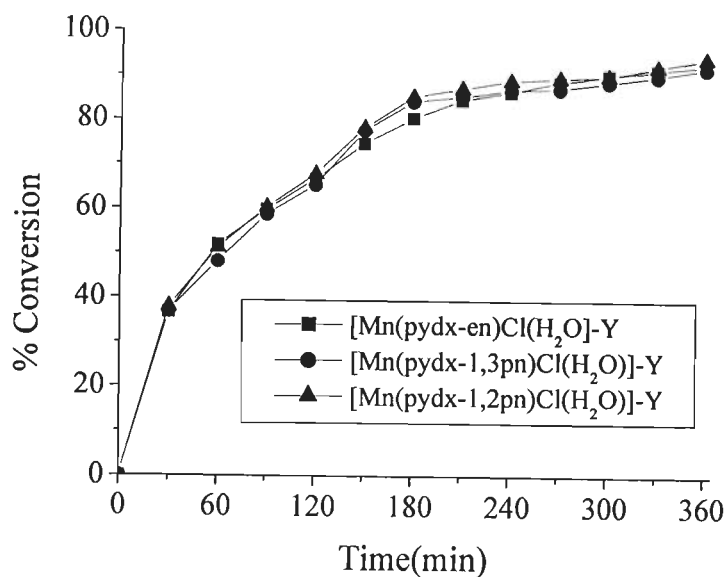


**Figure 2.23.** Comparison of different catalysts on the oxidation of benzoin. Reaction conditions: benzoin (1.06 g, 5 mmol), catalyst (0.020 g),  $\text{H}_2\text{O}_2$  (1.13 g, 10 mmol) and methanol (20 ml).

The performance of neat complexes using the same mole concentrations as used for zeolite-Y encapsulated complexes has also been studied under the above optimized conditions. It was observed that the neat catalysts are also very active and gave 93 - 96% conversion in 6 h of reaction time. Here, the formation of benzaldehyde-dimethylacetal is more but the over all selectivity of products is

again same. However, Moreover, the easy removal of the encapsulated catalysts makes them better compared to their neat analogues.

**Table 2.8.** Conversion of benzoin, TOF and selectivity data of products.

Catalyst	% Conv.	TOF (h <sup>-1</sup> )	% Selectivity		
			Benzil	Dimethyl- aetal	Benzoic acid
[Mn(pydx-en)Cl(H <sub>2</sub> O)]-Y	92.6	409	30.8	11.4	55.8
[Mn(pydx-1,3-pn)Cl(H <sub>2</sub> O)]-Y	91.9	526	31.7	8.9	59.4
[Mn(pydx-1,2-pn)Cl(H <sub>2</sub> O)]-Y	94.1	313	33.9	8.3	57.7
Mn(pydx-en)Cl(H <sub>2</sub> O)]-Y <sup>a</sup>	89.6	-	31.5	10.7	57.8
[Mn(pydx-1,3-pn)Cl(H <sub>2</sub> O)]-Y <sup>a</sup>	87.2	-	29.6	9.4	60.9
[Mn(pydx-1,2-pn)Cl(H <sub>2</sub> O)]-Y <sup>a</sup>	91.5	-	30.7	8.7	60.6
[Mn(pydx-en)Cl(H <sub>2</sub> O)]	93.9	364	31.7	31.1	37.2
[Mn(pydx-1,3-pn)Cl(CH <sub>3</sub> OH)]	96.1	395	33.1	38.9	28.3
[Mn(pydx-1,2-pn)Cl(H <sub>2</sub> O)]	93.2	372	29.2	26.4	44.4
Without catalyst	8.7		65.6	7.1	27.3

<sup>a</sup>First cycle of used catalyst.

### 2.3.10. Test for recyclability and heterogeneity of the reactions

The recyclability of encapsulated complexes [Mn<sup>III</sup>(pydx-en)Cl(H<sub>2</sub>O)]-Y (2.4), [Mn<sup>III</sup>(pydx-1,3-pn)Cl(H<sub>2</sub>O)]-Y (2.5) and [Mn<sup>III</sup>(pydx-1,2-pn)Cl(H<sub>2</sub>O)]-Y (2.6) has been tested for the oxidation of styrene, methyl phenyl sulphide and benzoin. The reaction mixture after a contact time of 6 h was filtered and the separated catalysts were washed with acetonitrile, dried at 120 °C and subjected to further catalytic reactions under similar conditions. No appreciable loss in the activities (see Tables 2.6, 2.7 and 2.8) was found in all cases, indicating that the complexes are still present in the cavity of zeolite-Y. The product distributions with time and selectivity of the reaction products are also nearly preserved as obtained for fresh catalyst within the experimental error. The filtrate collected after separating the used catalyst was placed in the reaction flask and the reaction was continued after adding fresh oxidant for another 4 h. The gas chromatographic

analysis showed no improvement in conversion, and this confirms that the reaction did not proceed upon removal of the solid catalyst. The reaction was, therefore, heterogeneous in nature. IR and electronic spectra of the recovered catalysts are also same to that of the respective neat one and this suggests that nature of complexes remain same after catalytic action.

## 2.4. Conclusions

Manganese(III) complexes  $[\text{Mn}^{\text{III}}(\text{pydx-en})\text{Cl}(\text{H}_2\text{O})]$  (**2.1**) and  $[\text{Mn}^{\text{III}}(\text{pydx-1,3-pn})\text{Cl}(\text{CH}_3\text{OH})]$  (**2.2**) and  $[\text{Mn}^{\text{III}}(\text{pydx-1,2-pn})\text{Cl}(\text{CH}_3\text{OH})]$  (**2.3**) have been prepared with *N,N'*-ethylenebis(pyridoxylideneiminato) ( $\text{H}_2\text{pydx-en}$ , **2.I**), *N,N'*-propylenebis(pyridoxylideneiminato) ( $\text{H}_2\text{pydx-1,3-pn}$ , **2.II**) and 1-methyl-*N,N'*-ethylenebis(pyridoxylideneiminato) ( $\text{H}_2\text{pydx-1,2-pn}$ , **2.III**), respectively and the crystal and molecular structures of two complexes were determined, confirming the ONNO binding mode of the ligands. All the three complexes undergo one electron redox process corresponding to  $\text{Mn}^{\text{III}}-\text{Mn}^{\text{II}}$  redox couple and form unstable oxomanganese(IV) complex on treatment with  $\text{H}_2\text{O}_2$ . These complexes have also been encapsulated in the nano-cavity of zeolite-Y. The encapsulated complexes  $[\text{Mn}^{\text{III}}(\text{pydx-en})\text{Cl}(\text{H}_2\text{O})]\text{-Y}$  (**2.4**),  $[\text{Mn}^{\text{III}}(\text{pydx-1,3-pn})\text{Cl}(\text{H}_2\text{O})]\text{-Y}$  (**2.5**) and  $[\text{Mn}^{\text{III}}(\text{pydx-1,2-pn})\text{Cl}(\text{H}_2\text{O})]\text{-Y}$  (**2.6**) catalyze the oxidation of methyl phenyl sulphide, styrene and benzoin efficiently, using  $\text{H}_2\text{O}_2$  as oxidant. As high as ca. 86 % conversion of methyl phenyl sulphide was obtained with two major products methyl phenyl sulfoxide and methyl phenyl sulfone in the ca. 70 % and 30 % selectivity, respectively. Under the optimized conditions, a maximum of 76.9 % conversion of styrene by **2.4**, 76.3 % by **2.5** and 76.0 % by **2.6** was obtained where major products were styrene oxide and benzaldehyde along with three other minor products benzoic acid, phenylacetaldehyde and 1-phenylethane-1,2-diol. Benzoin gave ca. 93% conversion with three major products, benzil, benzoic acid and benzaldehyde-dimethylacetal. These complexes are recyclable and heterogeneous in nature. Neat complexes also have comparable catalytic activity. Interaction of neat complexes with  $\text{H}_2\text{O}_2$  suggests the formation of  $\text{Mn}^{\text{IV}}=\text{O}$  intermediate species during catalytic reactions.

# *CHAPTER 3*

## **Oxidovanadium(IV) complexes of tetradentate ligands encapsulated in zeolite-Y as catalysts for the oxidation of styrene, cyclohexene and methyl phenyl sulfide**

### **3.1. Introduction**

The advantages of zeolite encapsulated metal complexes (ZEMC) as catalysts in the past two decades have promoted researchers to design such catalysts and investigate their catalytic properties [6, 51, 63, 129-132]. The relatively large size of the encapsulated catalysts and their rigidity make them difficult to escape from the zeolite cages. Thus, zeolite-encapsulated homogeneous catalysts may have the advantages of solid heterogeneous catalysts while retaining most of their original character. The relatively easy preparation, wide variety and flexible nature of salen-type ligands have provided opportunities to encapsulate various transition-metal complexes in the nanocavity of zeolites and to develop catalytic processes for various reactions. Poltowicz et al. encapsulated a whole range of salen complexes e.g. [Fe(salen)], [Mn(salen)], [Cu(salen)] and [Co(salen)] in zeolite-X and studied their catalytic activity for the oxidation of cyclooctane [48]. Ratnasamy and co-workers used copper(II) and manganese(III) complexes of salen derivatives encapsulated in the cavity of zeolite-X and zeolite-Y for the oxidation of styrene under aerobic conditions using *tert*-butylhydroperoxide as oxidant. The catalytic efficiency of these encapsulated complexes was much higher than that of the neat complexes. Electron-withdrawing substituents such as Cl, Br and NO<sub>2</sub> on the aromatic ring were found to enhance the rate of oxidation [55, 56]. These complexes also catalyze the oxidation of phenol and *p*-xylene [57, 58]. Epoxidations of cyclohexene, cyclooctene, 1-hexene and other various types of alkenes, arenes and cycloalkenes, catalyzed by different complexes of salen-type ligands, were also carried out [129, 133-135]. [Co(salophen)]-Y (H<sub>2</sub>salophen = *N,N'*-bis(salicylidene)benzene-1,2-diamine) and related derivatives catalyzed the oxidation of  $\beta$ -isophorone ( $\beta$ IP) to ketoisophorone (KIP) at ambient conditions of temperature and pressure [82]. Liquid-phase oxidation of phenol with H<sub>2</sub>O<sub>2</sub> was

reported using  $\text{Cu}^{\text{II}}$ - and  $\text{V}^{\text{IV}}\text{O}$ -complexes of  $N,N'$ -bis(salicylidene)propane-1,3-diamine ( $\text{H}_2\text{sal-1,3-pn}$ ) and  $N,N'$  bis(salicylidene)diethylenetriamine ( $\text{H}_2\text{saldien}$ ) [59, 63, 66]. Zeolite-Y encapsulated  $\text{Cu}^{\text{II}}$ - and  $\text{V}^{\text{IV}}\text{O}$ -complexes of  $N,N'$ -bis(salicylidene)cyclohexane-1,2-diamine ( $\text{H}_2\text{sal-dach}$ ) catalyze the oxidation of styrene, cyclohexene and cyclohexane efficiently [122]. Similar homogeneous oxidovanadium(IV) complexes derived from 2,2'-dimethylpropanediamine catalyze the oxidation, by tert-butylhydroperoxide, of cyclooctene and styrene [136]. Tris(pyrazolyl)methanesulfonate, [tpms (-)] coordinated vanadium complex even shows good catalytic activity for the oxidation of 3,5-di-tert-butylcatechol [137]. Chiral  $[\text{Mn}^{\text{III}}(\text{salen})]$  type complex immobilized on inorganic-organic hybrid materials—zirconium poly(styrene-phenylvinylphosphonate)phosphate were also used as effective catalyst for asymmetric epoxidation of unfunctionalized olefins [138].

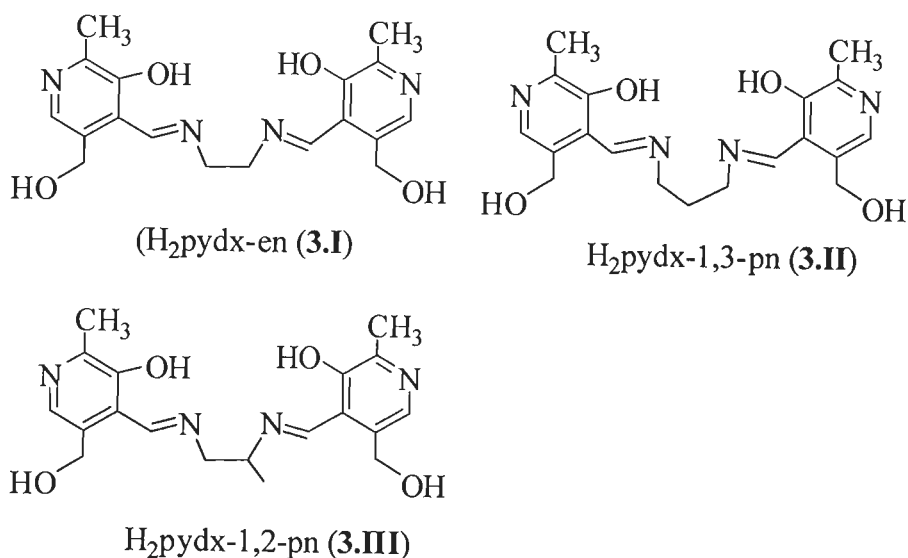
Recently several chiral V-salen and V-salan ( $\text{H}_2\text{salan}$  = reduced Schiff bases) complexes have been prepared and tested as catalysts in the oxidation of styrene, cyclohexene, cumene, and methyl phenyl sulfide using  $\text{H}_2\text{O}_2$  and *t*-BuOOH as oxidants. Overall, the V-salan complexes showed higher activity and normally better selectivity in alkene oxidation and higher activity and enantioselectivity for sulfoxidation than their parent V-salen complexes [139, 140]. The catalytic potential, often with high turn over numbers, of metal complexes encapsulated in the nanocavity of zeolites prompted us to design new zeolite-Y-encapsulated oxidovanadium(IV) complexes of tetradentate ligands **3.I**, **3.II** and **3.III** (Scheme 3.1). We have also prepared the corresponding neat oxidovanadium(IV) complexes of these ligands to compare their catalytic potentials.

## **3.2. Experimental Section**

### **3.2.1. Materials and methods**

Analytical reagent grade oxidovanadium(IV) sulfate was obtained from Loba Chemie, India. Details of other chemicals and solvents are given in Chapter

2. H<sub>2</sub>pydx-en (**3.I**), H<sub>2</sub>pydx-1,3-pn (**3.II**) and H<sub>2</sub>pydx-1,2-pn (**3.III**) were prepared as described in the literature [106].



**Scheme 3.1.** Structures of ligands and abbreviations used in this work.

### 3.2.2. Instrumentation and characterization procedures

EPR spectra were recorded with a Bruker ESP 300E X-band spectrometer. The spin Hamiltonian parameters were obtained by simulation of the spectra with the computer program of Rockenbauer and Korecz [141]. <sup>51</sup>V NMR spectra were obtained on a Bruker Avance III 400 MHz spectrometer with the common parameter settings. NMR spectra were recorded in MeOD-d<sub>4</sub>, and δ (<sup>51</sup>V) values are referenced relative to neat V<sup>V</sup>OCl<sub>3</sub> as external standard. Other instrumental details are presented in Chapter 2.

### 3.2.3. Preparations

#### 3.2.3.1. Preparation of [V<sup>IV</sup>O(pydx-en)] (**3.1**)

A solution of H<sub>2</sub>pydx-en (1.792 g, 5 mmol) in methanol (50 ml) was treated with [V<sup>IV</sup>O(acac)<sub>2</sub>] (1.33 g, 5 mmol) dissolved in 10 ml of methanol and the reaction mixture was refluxed in an oil bath for 4 h. During this period a green solid of [V<sup>IV</sup>O(pydx-en)] slowly separated out. After cooling the mixture, it was



filtered off, washed with methanol and dried. Yield 78.1 %. Anal. Calc. for  $C_{18}H_{20}N_4O_5V$  (423.32): C, 51.07; H, 4.76; N, 13.24%. Found: C, 49.8; H, 4.8; N, 13.4%.

### 3.2.3.2. Preparation of $[V^{IV}O(\text{pydx-1,3-pn})]$ (3.2) and $[V^{IV}O(\text{pydx-1,2-pn})]$ (3.3)

These complexes were prepared similarly using the respective ligand.

$[V^{IV}O(\text{pydx-1,3-pn})]$ (3.2): Yield 88.3%. Anal. Calc. for  $C_{19}H_{22}N_4O_5V$  (437.35): C, 51.18; H, 5.58; N, 11.94%. Found: C, 51.5; H, 5.3; N, 12.2%.

$[V^{IV}O(\text{pydx-1,2-pn})]$ (3.3): Yield 65.4%. Anal. Calc. for  $C_{19}H_{22}N_4O_5V$  (437.35): C, 52.18; H, 5.07; N, 12.81%. Found: C, 51.8; H, 5.0; N, 12.7%.

### 3.2.3.3. Preparation of $[V^{IV}O]-Y$ (oxidovanadium(IV) exchanged zeolite-Y)

A filtered solution of  $V^{IV}OSO_4 \cdot 5H_2O$  (9.0 g, 36 mmol) dissolved in 100 ml of distilled water was added to a suspension of Na-Y (15 g) in 800 ml of distilled  $H_2O$  and the reaction mixture was heated at 90 °C with stirring for 24 h. The light green solid was filtered, washed with hot distilled water until filtrate was free from any  $V^{IV}O^{2+}$  ion content and dried at 150 °C for 24 h. Yield: 14.9 g (99 %). V (ICP-MS): 4.6%.

### 3.2.3.4. Preparation of $[V^{IV}O(\text{pydx-en})]-Y$ (3.4)

A mixture of  $[V^{IV}O]-Y$  (3.0 g) and  $H_2\text{pydx-en}$  (3.0 g) was mixed in 40 ml of methanol and the reaction mixture was refluxed for 15 h in an oil bath with stirring. The resulting material was suction filtered and dried. The crude mass was extracted with methanol using a Soxhlet extractor until the complex was free from unreacted ligand and free metal complex on the surface. After filtering, the free  $V^{IV}O^{2+}$  ions present in the zeolite-Y were removed by stirring with aqueous 0.01 M NaCl solution (200 ml) for 8 h. It was finally washed with distilled water till no precipitate of AgCl was observed in the filtrate on treating with  $AgNO_3$ .

### **3.2.3.5. Preparation of [V<sup>IV</sup>O(pydx-1,3-pn)]-Y (3.5) and [V<sup>IV</sup>O(pydx-1,2-pn)]-Y (3.6)**

Complexes [V<sup>IV</sup>O(pydx-1,3-pn)]-Y (3.5) and [V<sup>IV</sup>O(pydx-1,2-pn)]-Y (3.6) were prepared following a procedure similar to the one described for [V<sup>IV</sup>O(pydx-en)]-Y (3.4).

### **3.2.4. Catalytic activity**

The catalytic potential of the compounds prepared was tested choosing the oxidation of styrene, cyclohexene and methyl phenyl sulfide as model reactions. Thus, [V<sup>IV</sup>O(pydx-en)]-Y (3.4), [V<sup>IV</sup>O(pydx-1,3-pn)]-Y (3.5) and [V<sup>IV</sup>O(pydx-1,2-pn)]-Y (3.6) were used as catalyst precursors. All catalytic reactions were carried out in a 50 ml flask fitted with a water circulated condenser.

The progress of the reactions was monitored by gas chromatography by withdrawing small aliquots at chosen time intervals. The identity of the products was confirmed by GC-MS. For each type of reaction, the effects of various parameters, such as amounts of oxidant and catalyst as well as the temperature of the reaction mixture were studied to check their effect on the conversion and selectivity of the reaction products.

#### **3.2.4.1. Oxidation of styrene**

In a typical reaction, styrene (1.04 g, 10 mmol) and aqueous 30% H<sub>2</sub>O<sub>2</sub> (2.27 g, 20 mmol) were taken in 10 ml of acetonitrile and temperature of the reaction mixture was set to 80 °C. The catalyst (0.010 g) was added to the above reaction mixture with stirring and reaction was considered to begin.

#### **3.2.4.2. Oxidation of cyclohexene**

Aqueous 30% H<sub>2</sub>O<sub>2</sub> (2.27 g, 20 mmol), cyclohexene (0.82 g, 10 mmol) and catalyst (0.005g) were mixed in 5 ml of CH<sub>3</sub>CN and the reaction mixture was heated at 80°C with continuous stirring in an oil bath for ca. 6 h.

### 3.2.4.3. Oxidation of methyl phenyl sulfide

Methyl phenyl sulfide (1.24 g, 10 mmol), aqueous 30% H<sub>2</sub>O<sub>2</sub> (2.27 g, 20 mmol) and catalyst (0.010 g) were taken in 5 ml of CH<sub>3</sub>CN and the reaction mixture was stirred at room temperature for ca. 2.5 h.

## 3.3. Results and discussion

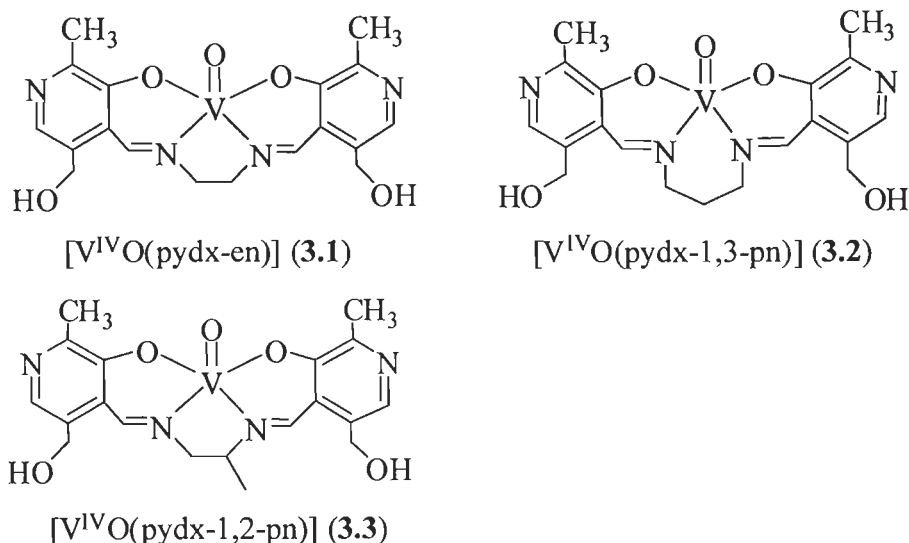
### 3.3.1. Synthesis and characterization of complexes

The reaction between equimolar amounts of [V<sup>IV</sup>O(acac)<sub>2</sub>] and H<sub>2</sub>pydx-en (**3.I**), H<sub>2</sub>pydx-1,3-pn (**3.II**), or H<sub>2</sub>pydx-1-2-pn (**3.III**) (*c.f.* Scheme 3.1) in dry, refluxing methanol yielded the V<sup>IV</sup>O-complexes [V<sup>IV</sup>O(pydx-en)] (**3.1**), [V<sup>IV</sup>O(pydx-1,3-pn)] (**3.2**) and [V<sup>IV</sup>O(pydx-1,2-pn)] (**3.3**) respectively. The general synthetic process may be outlined by Equation (1).



(H<sub>2</sub>L = H<sub>2</sub>pydx-en: **3.1**; H<sub>2</sub>L = H<sub>2</sub>pydx-1,3-pn: **3.2**; H<sub>2</sub>L = H<sub>2</sub>pydx-1-2-pn: **3.3**)

Complexes, **3.1** and **3.2** are soluble in methanol, ethanol, DMSO and DMF. Of these solvents complex **3.3** is soluble in DMSO. Scheme 3.2 presents the structural formulas and binding sets proposed for these complexes, and are based on their spectroscopic characterization (IR, electronic, EPR) and elemental analyses. The coordination of the ligands involves their dianionic (ONNO<sup>2-</sup>) form.



**Scheme 3.2.** Structural formulas of the neat complexes prepared in this work.

Encapsulation of  $[V^{IV}O(\text{pydx-en})]$  (3.1),  $[V^{IV}O(\text{pydx-1,3-pn})]$  (3.2) and  $[V^{IV}O(\text{pydx-1,2-pn})]$  (3.3) in the nano-cavities of zeolite-Y involved as a first step the exchange of  $[V^{IV}O]^{2+}$  with  $Na^+$  of Na-Y in water to form zeolite- $[V^{IV}O]$ -Y species. This is followed by the reaction of the metal exchanged zeolite-Y with 3.I, 3.II or 3.III in methanol to give  $[V^{IV}O(\text{pydx-en})]$ -Y (3.4),  $[V^{IV}O(\text{pydx-1,3-pn})]$ -Y (3.5) and  $[V^{IV}O(\text{pydx-1,2-pn})]$ -Y (3.6). The remaining uncomplexed metal ions in zeolite were removed by ion-exchange with aqueous 0.01 M NaCl solution. Extraction of impurities with methanol was carried out by Soxhlet extraction, thus removing the excess free ligand. As the crude mass was extensively extracted, the metal content found (Table 3.1) after encapsulation is only due to the presence of  $V^{IV}O$ -complexes in the cavities of the zeolite-Y. The diagonal dimension of the closely related complex,  $[Cu^{II}(\text{pydx-en})][110]$  is ca. 12 Å which suggests that they will fit well into the super cages of the zeolite-Y and will not pass through the apertures of ca. 7.4 Å [77].

**Table 3.1.** Chemical composition, physical and analytical data.

Compound	Color	Metal Content	
		Wt. %	Mmol/ g
$[VO(\text{pydx-en})]$ -Y (3.4)	Light green	1.78	0.35
$[VO(\text{pydx-1,2-pn})]$ -Y (3.5)	Light green	0.53	0.10
$[VO(\text{pydx-1,3-pn})]$ -Y (3.6)	Light cream	0.85	0.17

These encapsulated complexes were additionally characterized by thermogravimetric patterns, Field-Emission-Scanning Electron Micrograph (FE-SEM), Energy Dispersive X-Ray analysis (EDX), powder X-ray Diffraction (XRD) Studies and Electron paramagnetic resonance (EPR). The binding modes for these encapsulated complexes are proposed by comparison with the corresponding homogeneous model - complexes.

### 3.3.2. Thermogravimetric analysis

The thermal decomposition of  $[V^{IV}O(\text{pydx-1,3-pn})]$ -Y (3.5) and  $[V^{IV}O(\text{pydx-1,2-pn})]$ -Y (3.6) proceeds in two major steps. An endothermic weight

loss of *ca.* 21% in **3.5** and *ca.* 20% in **3.6** occurs in the temperature range 100 to 300 °C, which is possibly due to the removal of intrazeolitic water. The second step of endothermic weight loss starts immediately after the first one and continues till *ca.* 600 °C to constant weight. A total weight loss of *ca.* 6% in **3.5** and 7% in **3.6** occurs in the temperature range of 300–600 °C due to the slow decomposition of vanadium complexes. The first decomposition step of complex [VO(pydx-en)]-Y (**3.4**) is similar but continues to *ca.* 350 °C with a weight loss of 25%. The second step of endothermic weight loss of *ca.* 16% starts immediately after the first step and consists of several sub steps which continue till *ca.* 650 °C to constant weight. This information suggests the insertion of only a small amount of metal complexes in the cavities of the zeolite-Y. This is in agreement with the low percentage of metal content obtained for encapsulated complexes (*cf.* Table 3.1).

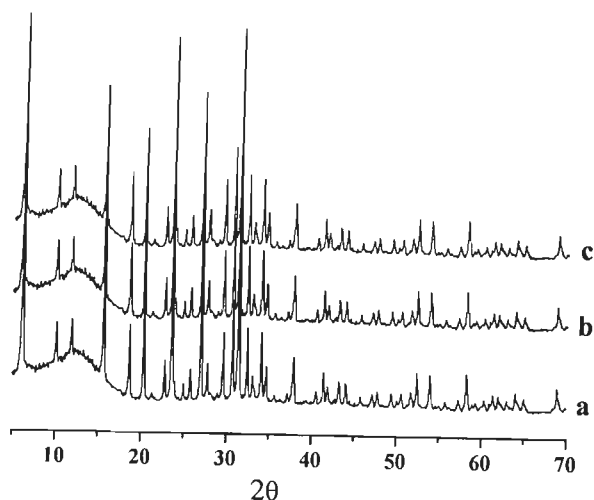
### 3.3.3. Powder X-ray diffraction studies

The powder X-ray diffraction patterns of Na-Y, [V<sup>IV</sup>O]-Y and encapsulated V<sup>IV</sup>O-complexes were recorded at  $2\theta$  values between 5° and 70°. The XRD pattern of representative V<sup>IV</sup>O<sup>2+</sup> exchanged zeolite and the zeolite encapsulated metal complexes, along with Na-Y are presented in Figure 3.1. The diffraction pattern of encapsulated metal complexes, [V<sup>IV</sup>O]-Y and Na-Y are essentially similar except a slight change in the intensity of the bands in encapsulated complexes. These observations indicate that the framework of zeolite did not undergo any significant structural change during encapsulation, i.e. the crystallinity of the zeolite-Y is preserved. No absence or formation of new peaks due to the presence of complexes was detected in encapsulated zeolites.

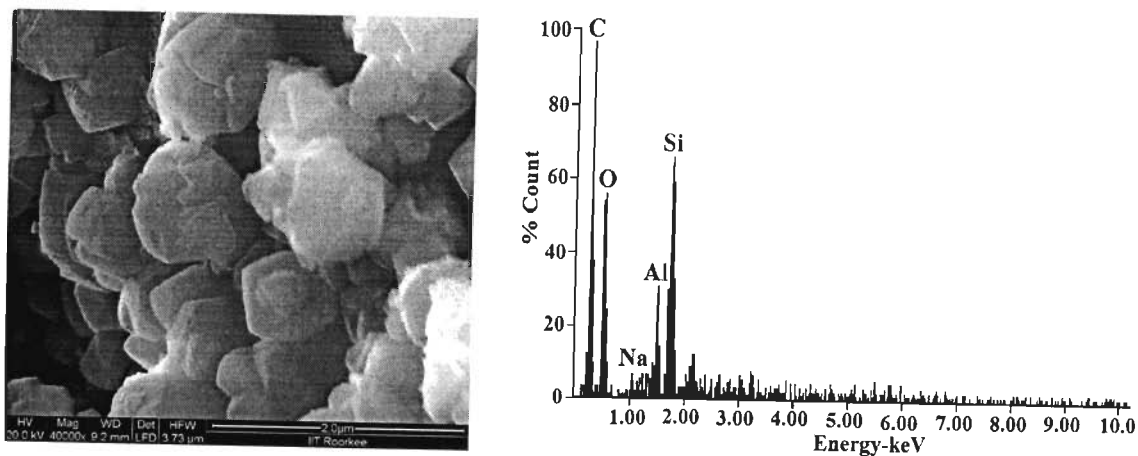
### 3.3.4. Field emission-scanning electron micrograph and Energy-dispersive X-ray analysis study

Figure 3.2 presents the field emission scanning electron micrograph of [V<sup>IV</sup>O(pydx-en)]-Y (**3.4**). It is clear from the micrograph that zeolite-entrapped vanadium complexes have well-defined crystals, and there is no indication of the presence of any metal ions or complexes on the surface. Energy-dispersive X-ray

analysis plots support this conclusion as no vanadium or nitrogen contents were noted on the spotted surfaces in plots. The average silicon and aluminum percentage on the spotted surface, as evaluated semi-quantitatively, were ca. 7.5% and 2.6%, respectively. The finding of ca. 1.1% sodium suggests the exchange of surface free  $V^{IV}O^{2+}$  ions by sodium ions during the re-exchange process (see Experimental Section). Only a small amount of carbon (about 18.4%) but no nitrogen suggests the presence of a trace amount of solvent (methanol) from which it was finally washed after Soxhlet extraction. No morphological changes on the surface upon encapsulation of the complexes in the cavities are noticed. Very similar observations were obtained for other two catalysts.



**Figure 3.1.** XRD patterns of Na-Y (a), [V<sup>IV</sup>O]-Y (b) and [V<sup>IV</sup>O(pydx-en)]-Y (c).



**Figure 3.2.** Field emission-scanning electron micrograph of [V<sup>IV</sup>O(pydx-en)]-Y and the corresponding energy dispersive X-ray analysis plot.

## 3.3.5. IR spectral studies

A partial list of IR spectroscopic data is presented in Table 3.2. Comparison of the spectra of neat complexes with the respective ligand provides evidence for the coordinating mode of ligands in complexes. The intensities of the peaks due to encapsulated complexes are weak because of their low amount in zeolite matrix and the spectra of the encapsulated as well as neat complexes showed essentially similar bands. Ligands as well as complexes exhibit several multiple bands of medium intensity covering the region 2850–3000  $\text{cm}^{-1}$  due to C–H bands. A medium-intensity band around 3000  $\text{cm}^{-1}$  in ligands, mostly due to intramolecular  $\nu(\text{OH})_{\text{phenolic}}$  hydrogen bonding, was not found in the spectra of encapsulated as well as neat complexes, indicating the destruction of the hydrogen bond network followed by the coordination of the phenol oxygen atom after deprotonation. A sharp band appearing at 1630  $\text{cm}^{-1}$  (in **3.I**), at 1634  $\text{cm}^{-1}$  (in **3.II**) and at 1631  $\text{cm}^{-1}$  (in **3.III**) due to the  $\nu(\text{C}=\text{N})$  (azomethine) shifts in complexes, suggesting the coordination of the azomethine nitrogen atom. All neat  $\text{V}^{\text{IV}}\text{O}$ -complexes show a sharp band between 973 - 986  $\text{cm}^{-1}$  due to  $\nu(\text{V}=\text{O})$  [142]. This band was not observed in encapsulated complexes probably due to poor loading of complexes in the zeolite matrix.

**Table 3.2.** IR spectral data of ligand, pure and encapsulated complexes.

Compound	$\nu(\text{C}=\text{N})$	$\nu(\text{V}=\text{O})$
$\text{H}_2\text{pydx-en}$ ( <b>3.I</b> )	1630	-
$\text{H}_2\text{pydx-1,3-pn}$ ( <b>3.II</b> )	1634	-
$\text{H}_2\text{pydx-1,2-pn}$ ( <b>3.III</b> )	1631	-
$[\text{V}^{\text{IV}}\text{O}(\text{pydx-en})]$ ( <b>3.1</b> )	1618	984
$[\text{V}^{\text{IV}}\text{O}(\text{pydx-1,3-pn})]$ ( <b>3.2</b> )	1625	983
$[\text{V}^{\text{IV}}\text{O}(\text{pydx-1,2-pn})]$ ( <b>3.3</b> )	1627	973
$[\text{V}^{\text{IV}}\text{O}(\text{pydx-en})]-\text{Y}$ ( <b>3.4</b> )	1619	-
$[\text{V}^{\text{IV}}\text{O}(\text{pydx-1,3-pn})]-\text{Y}$ ( <b>3.5</b> )	1636	-
$[\text{V}^{\text{IV}}\text{O}(\text{pydx-1,2-pn})]-\text{Y}$ ( <b>3.6</b> )	1637	-



### 3.3.6. Electronic spectral studies

The electronic spectral data of ligands and complexes are presented in Table 3.3. The spectral profiles of neat complexes are reproduced in Figure 3.3 while that of encapsulated ones are in Figure 3.4. The electronic absorption spectra of  $[V^{IV}O(\text{pydx-en})]$  was previously described [106]. The broad band of medium intensity at ca. 380 nm in neat complexes is due to both (i) the ligand to metal charge transfer (phenolate-O to d orbitals of vanadium) band, and (ii) the  $n \rightarrow \pi^*$  transition of the C=N moiety. The bands at ca. 275 nm and ca. 235 nm may be assigned to  $\pi \rightarrow \pi^*$  and  $\phi \rightarrow \phi^*$  transitions, respectively. These are sometimes designated by B-band and K-band, respectively [143]. In addition, two broad bands at ca. 750 and 580 nm (in DMSO) appear in the visible region and are assigned to band I ( $d_{xy} \rightarrow d_{xz}, d_{yz}$ ) and band II ( $d_{xy} \rightarrow d_{x^2-y^2}$ ). All these bands show slight shifts in methanol [144].

**Table 3.3.** Electronic spectral data of ligands and complexes studied in this work.

Compound	Solvent	$\lambda / \text{nm}^a$
$\text{H}_2\text{pydx-en}$ (3.I)	MeOH	336, 254, 215
$\text{H}_2\text{pydx-1,3-pn}$ (3.II)	MeOH	418, 335, 253, 214
$\text{H}_2\text{pydx-1,2-pn}$ (3.III)	MeOH	336, 253, 211
$[V^{IV}O(\text{pydx-en})]$ (3.1)	MeOH	766, 591, 380, 263b, 234
	DMSO	750b, 585, 385, 281b, 262
$[V^{IV}O(\text{pydx-1,2-pn})]$ (3.2)	MeOH	787, 594, 383, 312b, 274b, 239
	DMSO	750b, 590, 385, 280b, 262
$[V^{IV}O(\text{pydx-1,3-pn})]$ (3.3)	MeOH	383, 311b, 274b, 239
	DMSO	774, 538
$[V^{IV}O(\text{pydx-en})]-Y$ (3.4)	Nujol	393, 344, 295, 221
$[V^{IV}O(\text{pydx-1,3-pn})]-Y$ (3.5)	Nujol	415, 340, 273, 228
$[V^{IV}O(\text{pydx-1,2-pn})]-Y$ (3.6)	Nujol	415, 288, 223

<sup>a</sup> b indicates broad band.



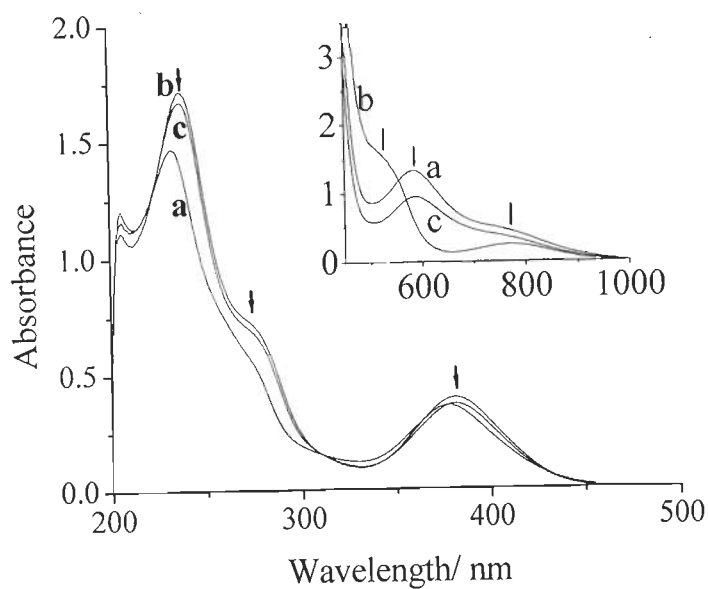


**Figure 3.3.** Electronic spectra (in methanol) of  $[V^{IV}O(pydx-en)]$  (3.1) (a),  $[V^{IV}O(pydx-1,3-pn)]$  (3.2) (b) and  $[V^{IV}O(pydx-1,2-pn)]$  (3.3) (c).

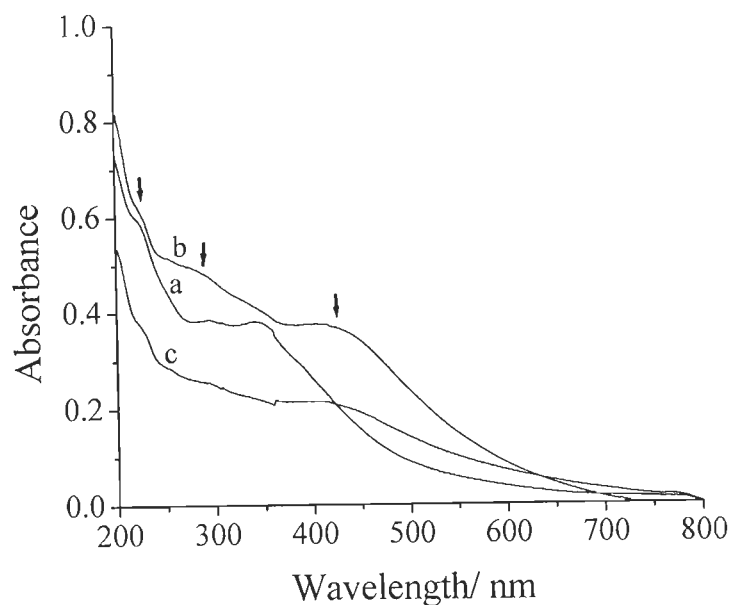


**Figure 3.4.** Electronic spectra of  $[V^{IV}O(pydx-en)]-Y$  (3.4) (a),  $[V^{IV}O(pydx-1,3-pn)]-Y$  (3.5) (b),  $[V^{IV}O(pydx-1,2-pn)]-Y$  (3.6) (c) recorded dispersed in Nujol®.

Due to poor loading of complexes in the nano cavities of zeolite-Y, and their intrinsic low intensity, the bands due to d-d transitions are not observed in  $[V^{IV}O(\text{pydx-en})]\text{-Y}$  (3.4),  $[V^{IV}O(\text{pydx-1,3-pn})]\text{-Y}$  (3.5) and  $[V^{IV}O(\text{pydx-1,2-pn})]\text{-Y}$  (3.6). However, all encapsulated complexes exhibit three bands in the UV region and the band at ca. 400 nm, suggesting the presence of the  $V^{IV}O$ -complexes in the cavities of zeolite-Y.

### 3.3.7. EPR studies

The EPR spectra of “frozen” (77 K) solutions of  $[V^{IV}O(\text{pydx-en})]$  (3.1),  $[V^{IV}O(\text{pydx-1,3-pn})]$  (3.2) and  $[V^{IV}O(\text{pydx-1,2-pn})]$  (3.3) in MeOH or DMSO are depicted in Figure 3.5, and those of solids  $[V^{IV}O(\text{pydx-en})]\text{-Y}$  (3.4),  $[V^{IV}O(\text{pydx-1,3-pn})]\text{-Y}$  (3.5) and  $[V^{IV}O(\text{pydx-1,2-pn})]\text{-Y}$  (3.6) at room temperature in Figure 3.6. The spectra of  $[V^{IV}O(\text{pydx-en})]$  (3.1),  $[V^{IV}O(\text{pydx-1,3-pn})]$  (3.2) and  $[V^{IV}O(\text{pydx-1,2-pn})]$  (3.3) are well resolved while the spectra of  $[V^{IV}O(\text{pydx-en})]\text{-Y}$  (3.4),  $[V^{IV}O(\text{pydx-1,3-pn})]\text{-Y}$  (3.5) and  $[V^{IV}O(\text{pydx-1,2-pn})]\text{-Y}$  (3.6) show broadening and changes in the peak-to-peak line widths due to incomplete rotational averaging of the  $g$  and  $A$  tensors [145]. The spectra were simulated [141] and the obtained spin Hamiltonian parameters  $g_z$  and  $A_z$  agree well with the values estimated using the additivity relationship proposed by Wüthrich [146], and Chasteen [145] with estimated accuracy of  $\pm 3 \times 10^{-4} \text{ cm}^{-1}$ . The spin Hamiltonian parameters obtained by simulation of the experimental EPR spectra are included in Table 3.4, but for the donor groups under consideration their predicted contributions to the parallel hyperfine coupling constant are rather similar  $\{O_{\text{phenolate}} \sim 38.9 \times 10^{-4} \text{ cm}^{-1}; N_{\text{imine}} 39 \pm 2 \times 10^{-4} \text{ cm}^{-1}\}$  [141, 146-150]. Globally the hyperfine features of the spectra of 1-3 are consistent with a binding set involving  $(O_{\text{phenolate}}, N_{\text{imine}}, N_{\text{imine}}, O_{\text{phenolate}})_{\text{equatorial}}$ .

Hydrated zeolite- $[V^{IV}O]\text{-Y}$  was previously reported and its EPR spectrum recorded [151]. It was concluded that the  $V^{IV}O^{2+}$  ions are largely located on type III sites in the large cavities bound to hydroxyl or O atoms, the spin Hamiltonian parameters being:  $g_z = 1.938$  and  $A_z = 178 \times 10^{-4} \text{ cm}^{-1}$ . The EPR spectrum of the prepared zeolite- $[V^{IV}O]\text{-Y}$  (Figure 3.6) shows rather broad lines, thus the spin

Hamiltonian parameters cannot be determined accurately, being  $g_z \sim 1.939$  and  $A_z \sim 176 \times 10^{-4} \text{ cm}^{-1}$ , in good agreement with the data previously reported [151].

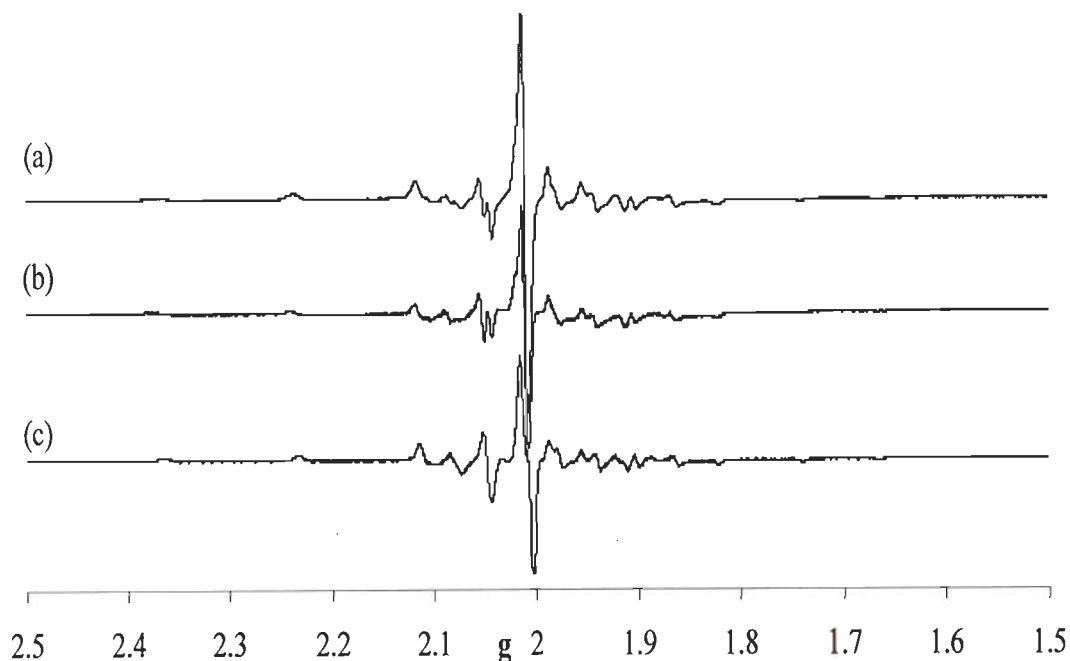


**Figure 3.5.** First derivative EPR spectra of frozen (77 K) solutions of (a)  $[\text{V}^{\text{IV}}\text{O}(\text{pydx-en})]$  (3.1) (4 mM) in MeOH; (b)  $[\text{V}^{\text{IV}}\text{O}(\text{pydx-1,2-pn})]$  (3.3) (4 mM) in MeOH; (c)  $[\text{V}^{\text{IV}}\text{O}(\text{pydx-1,3-pn})]$  (3.2) (4 mM) in DMSO.

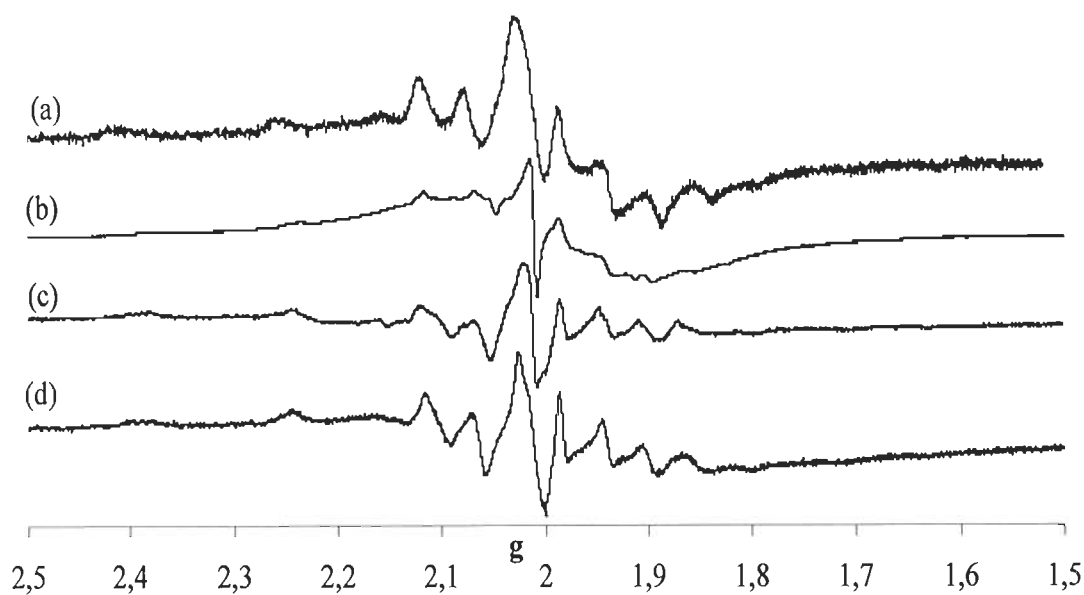


**Figure 3.6.** First derivative EPR spectra at room temperature of zeolite encapsulated complexes (solids) (a)  $[\text{V}^{\text{IV}}\text{O}]\text{-Y}$ ; (b)  $[\text{V}^{\text{IV}}\text{O}(\text{pydx-en})]\text{-Y}$  (3.4); (c)  $[\text{V}^{\text{IV}}\text{O}(\text{pydx-1,2-pn})]\text{-Y}$  (3.6); (d)  $[\text{V}^{\text{IV}}\text{O}(\text{pydx-1,3-pn})]\text{-Y}$  (3.5).

**Table 3.4.** Spin Hamiltonian parameters obtained [140] by simulation of the experimental EPR spectra.

Complex	Species	$g_z$	$A_z$ $\times 10^4 \text{ cm}^{-1}$	$A_x A_y$ $\times 10^4 \text{ cm}^{-1}$	$g_x g_y$
(3.1) 4 mM solution in MeOH		1.957	158.5	55.1	1.979
(3.4) solid	1 <sup>st</sup> species <sup>a</sup>	~1.96	~157	~55	~1.976
	2 <sup>nd</sup> species <sup>a</sup>	~1.96	~159	~60	~1.975
(3.2) 4 mM solution in DMSO		1.956	156.6	48.3	1.985
(3.5) solid		~1.95	~166	~59	~1.981
(3.3) 4 mM solution in MeOH	1 <sup>st</sup> species	1.959	161.7	48	~1.978
	2 <sup>nd</sup> species	1.960	157.9	50	~1.979
(3.6) solid		~1.95	~166	~60	~1.979

<sup>a</sup> Apparently there are two species, but the corresponding  $A$  and  $g$  parameters given are only rough approximations of their correct values.

As mentioned above, encapsulation of  $[\text{V}^{\text{IV}}\text{O}(\text{pydx-en})]$  (3.1),  $[\text{V}^{\text{IV}}\text{O}(\text{pydx-1,3-pn})]$  (3.2) and  $[\text{V}^{\text{IV}}\text{O}(\text{pydx-1,2-pn})]$  (3.3) in zeolite-Y involved the reaction of zeolite- $[\text{V}^{\text{IV}}\text{O}]\text{-Y}$  with  $\text{H}_2\text{pydx-en}$  (3.I),  $\text{H}_2\text{pydx-1,3-pn}$  (3.II) and  $\text{H}_2\text{pydx-1,2-pn}$  (3.III) in methanol, followed by careful and exhaustive extraction procedures to wash out any non-encapsulated vanadium species. The change of the EPR spectrum after introduction of a ligand and its similarity with the corresponding neat complex is a good proof of the encapsulation of the  $\text{V}^{\text{IV}}\text{O}(\text{ligand})$  species inside the pores of zeolite-Y [6].

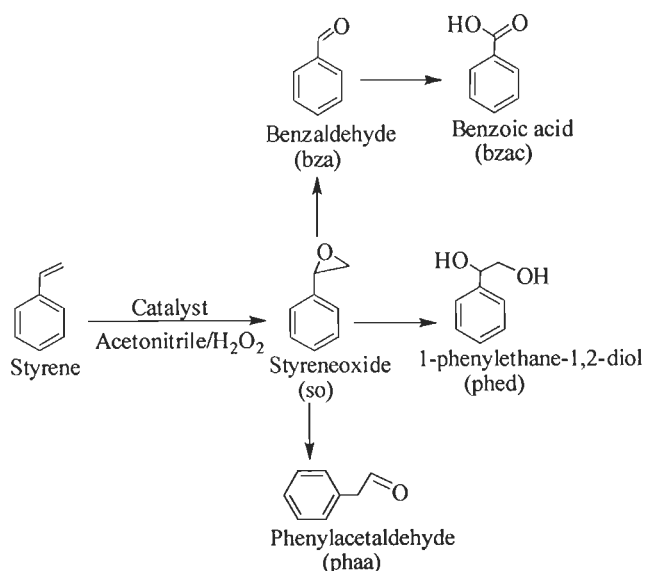
The EPR spectra recorded for  $[\text{V}^{\text{IV}}\text{O}(\text{pydx-en})]\text{-Y}$  (3.4),  $[\text{V}^{\text{IV}}\text{O}(\text{pydx-1,3-pn})]\text{-Y}$  (3.5) and  $[\text{V}^{\text{IV}}\text{O}(\text{pydx-1,2-pn})]\text{-Y}$  (3.6) at 77 K also show relatively broad lines, but differ from the spectrum of zeolite- $[\text{V}^{\text{IV}}\text{O}]\text{-Y}$  used as precursor (Figure 3.6), confirming the change in environment of the  $\text{V}^{\text{IV}}\text{O}$ -centre. It is probable that, besides the binding to the ligands, hydrogen bond interactions are established between the zeolite-OH groups and the  $-\text{CH}_2\text{OH}$  and  $\text{NH}$  moieties of the ligands. Equatorial or axial binding of zeolite-OH groups to  $\text{V}^{\text{IV}}\text{O}$  is also possible and may explain the relatively high  $A_z$  values obtained for 3.5 and 3.6. Notwithstanding,

globally the EPR results for  $[V^{IV}O(\text{pydx-en})]\text{-Y}$  (3.4),  $[V^{IV}O(\text{pydx-1,3-pn})]\text{-Y}$  (3.5) and  $[V^{IV}O(\text{pydx-1,2-pn})]\text{-Y}$  (3.6) confirm the presence of the  $V^{IV}O$ -complexes inside the nanopores of zeolite-Y and are consistent with their formulation, each with a binding set  $(O_{\text{phenolate}}, N_{\text{imine}}, N_{\text{imine}}, O_{\text{phenolate}})_{\text{equatorial}}$ .

### 3.3.8. Catalytic activity studies

#### 3.3.8.1. Oxidation of styrene

To test the catalytic potential of the complexes prepared, the oxidation of styrene was chosen as one of the model reactions. Thus, the oxidation of styrene catalyzed by  $[V^{IV}O(\text{pydx-en})]\text{-Y}$  (3.4),  $[V^{IV}O(\text{pydx-1,3-pn})]\text{-Y}$  (3.5) and  $[V^{IV}O(\text{pydx-1,2-pn})]\text{-Y}$  (3.6) was carried out using aqueous 30%  $H_2O_2$  as an oxidant. It mainly gave styrene oxide, benzaldehyde, 1-phenylethane-1,2-diol, benzoic acid and phenylacetaldehyde along with only minor amounts of other unidentified products, as shown in Scheme 3.3. These products have also been observed when the polymer-supported complex  $PS\text{-}[VO(\text{sal-ohyba})(\text{DMF})]$  ( $H_2\text{sal-ohyba}$  = Schiff base derived from salicylaldehyde and *o*-hydroxybenzylamine) was applied as catalyst [87]. These products of styrene oxidation were previously observed by others as well [124,152-155].



**Scheme 3.3.** Main products obtained upon the catalytic oxidation of styrene by the zeolite encapsulated compounds  $[V^{IV}O(\text{pydx-en})]\text{-Y}$  (3.4),  $[V^{IV}O(\text{pydx-1,3-pn})]\text{-Y}$  (3.5) and  $[V^{IV}O(\text{pydx-1,2-pn})]\text{-Y}$  (3.6).

In the present work our objective was to achieve suitable reaction conditions for the maximum oxidation of styrene. Thus,  $[V^{IV}O(\text{pydx-en})]\text{-Y}$  (3.4) was taken as a representative catalyst and different parameters *viz.* amount of oxidant (moles of  $\text{H}_2\text{O}_2$  per mole of styrene), catalyst and temperature of the reaction mixture were tested.

For three different styrene to aqueous 30 %  $\text{H}_2\text{O}_2$  molar ratios, *viz.* 1 : 1, 1 : 2 and 1 : 3, the amount of styrene (1.04 g, 10 mmol) and catalyst (0.010 g) were taken in  $\text{CH}_3\text{CN}$  (5 ml), and the reaction was carried out at 80 °C. The formation of products was regularly analyzed at similar time intervals. As illustrated in Figure 3.7, increasing the  $\text{H}_2\text{O}_2$ /styrene ratio from 1:1 to 2:1 improved the conversion from ca. 60 % to 86 %. The oxidation improved only marginally upon further increasing this ratio to 1 : 3, which suggested that a higher amount of oxidant does not improve the oxidation of styrene, a 1 : 2 ratio being considered adequate.

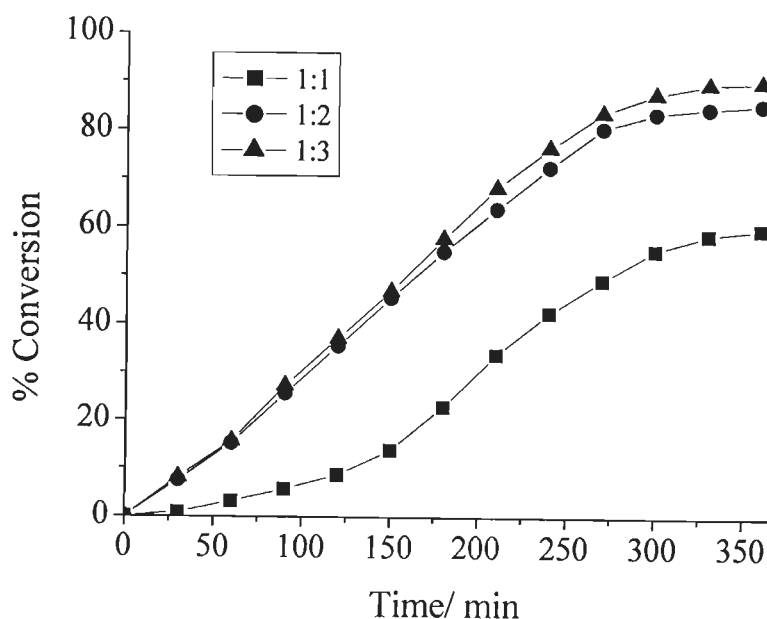


**Figure 3.7.** Effect of the amount of  $\text{H}_2\text{O}_2$  on the oxidation of styrene at 80 °C as a function of time. Reaction conditions: Styrene (1.04 g, 10 mmol),  $[V^{IV}O(\text{pydx-en})]\text{-Y}$  (0.010 g), acetonitrile (5 ml).

Similarly, for three different amounts *viz.* 0.005, 0.010 and 0.015 g of catalyst for the fixed amount of styrene (1.04 g, 10 mmol), H<sub>2</sub>O<sub>2</sub> (2.28 g, 20 mmol), CH<sub>3</sub>CN (5 ml) and temp (80 °C), 0.005 g catalyst gave only 64.4 % conversion (Figure 3.8). A maximum of 85.5 % conversion was achieved on increasing the amount to 0.010 g, while further increments of catalyst amount resulted in lower conversion. Therefore, an amount of 0.010 g catalyst may be considered adequate to obtain the maximum conversion of styrene. The temperature of the reaction mixture also influenced the performance of the catalyst; running the reaction at 80 °C gave much better conversion than at lower temperatures and also reduced the time required to achieve the maximum conversion.

Interestingly 5 ml of acetonitrile was found to be sufficient to effect maximum oxidation of styrene, significantly lower conversions being observed with 10 or 15 ml (Figure 3.9). This may possibly be due to a much higher concentration gradient of reagents between the outside and inside of the zeolite cavities when the volume of solvent is lower.

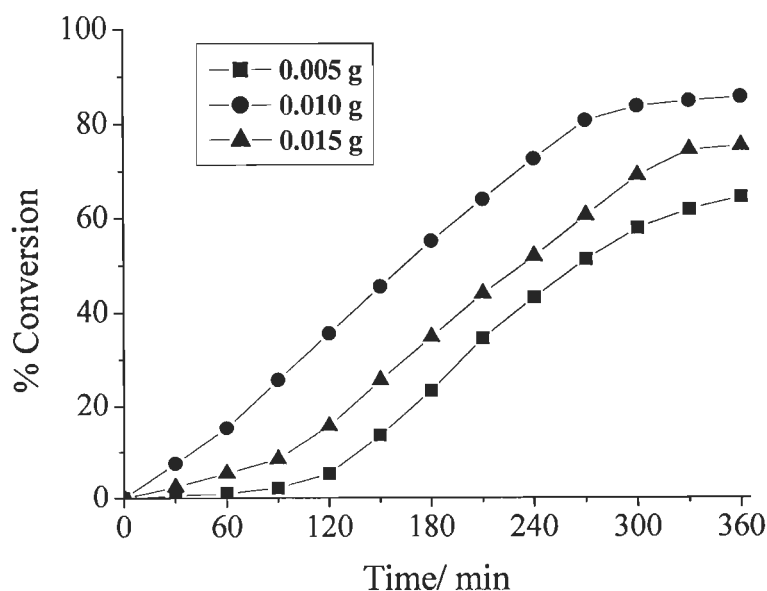


**Figure 3.8.** Effect of the amount of catalyst on the oxidation of styrene at 80 °C as a function of time. Reaction conditions: Styrene (1.04 g, 10 mmol), H<sub>2</sub>O<sub>2</sub> (2.27 g, 20 mmol) in acetonitrile (5 ml).

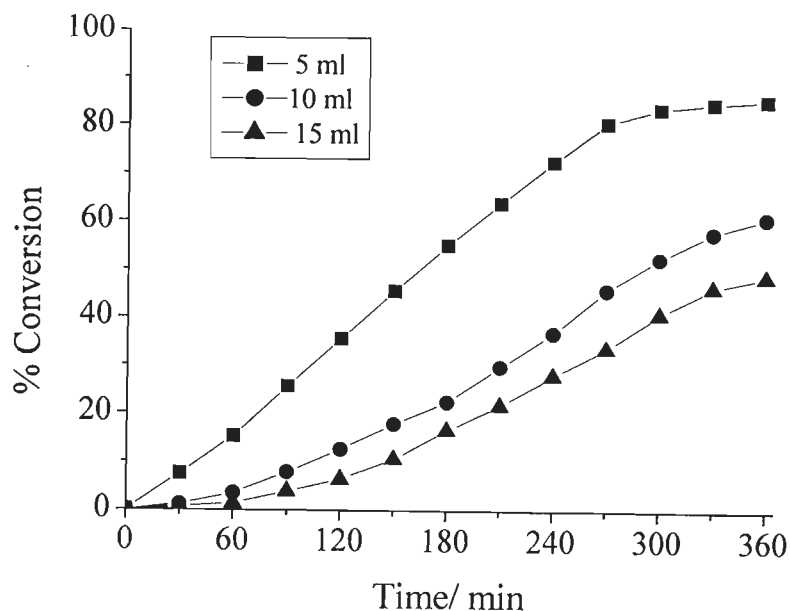


**Figure 3.9.** Effect of the amount of solvent on the oxidation of styrene at 80 °C as a function of time. Reaction conditions: Styrene (1.04 g, 10 mmol), H<sub>2</sub>O<sub>2</sub> (2.27 g, 20 mmol), [V<sup>IV</sup>O(pydx-en)]-Y (0.010 g).

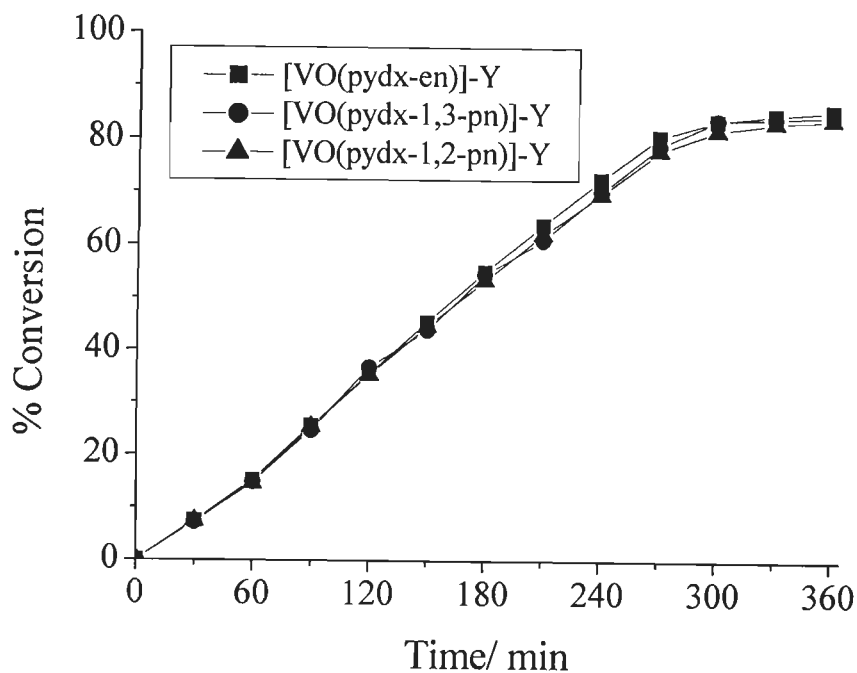


**Figure 3.10.** Effect of different catalysts on the oxidation of styrene at 80 °C as a function of time. Reaction conditions: Styrene (1.04 g, 10 mmol), H<sub>2</sub>O<sub>2</sub> (2.27 g, 20 mmol) and acetonitrile (5 ml).



Thus, for the maximum oxidation of 10 mmol of styrene the following conditions were considered an adequate balance: catalyst (0.010 g), H<sub>2</sub>O<sub>2</sub> (2.27 g, 20 mmol), CH<sub>3</sub>CN (5 ml) and reaction temperature (80 °C). The other catalyst precursors, [V<sup>IV</sup>O(pydx-1,3-pn)]-Y and [V<sup>IV</sup>O(pydx-1,2-pn)]-Y were also tested under the above optimized reaction conditions (Figure 3.10), and the results are presented in Table 3.5. It is clear from the data that all catalysts have very comparable catalytic activity and selectivity. This observation confirms that chain length of the amine residue of ligand has no influence on the performance of the catalyst.

**Table 3.5.** Percentage conversion of styrene, product selectivity and turn over frequency (TOF).

Catalyst	% Conv.	TOF (h <sup>-1</sup> ) <sup>b</sup>	% Selectivity <sup>c</sup>					
			so	bza	phed	bzac	phaa	Other
[V <sup>IV</sup> O(pydx-en)]-Y	85.5	490	3.9	74.7	9.4	6.8	3.4	1.8
[V <sup>IV</sup> O(pydx-en)]-Y <sup>a</sup>	83.4	-	3.7	72.7	9.1	7.2	5.0	2.3
[V <sup>IV</sup> O(pydx-1,3-pn)]-Y	84.6	1628	4.1	74.1	9.3	6.1	2.9	3.5
[V <sup>IV</sup> O(pydx-1,3-pn)]-Y <sup>a</sup>	83.2	-	3.5	73.2	8.6	5.6	6.4	3.7
[V <sup>IV</sup> O(pydx-1,2-pn)]-Y	82.9	995	3.8	76.5	8.2	5.8	2.0	3.6
[V <sup>IV</sup> O(pydx-1,2-pn)]-Y <sup>a</sup>	81.7	-	3.3	75.4	8.0	7.7	2.7	3.9
[V <sup>IV</sup> O]-Y	4.8	-	-	75.0	-	25.0	-	-
[V <sup>IV</sup> O(pydx-en)]	65.3	369	2.3	74.8	4.1	10.6	3.4	4.8
[V <sup>IV</sup> O(pydx-1,2-pn)]	63.2	369	2.6	73.8	3.4	10.2	4.8	5.2
[V <sup>IV</sup> O(pydx-1,3-pn)]	62.7	366	1.8	74.5	3.6	9.6	6.7	3.7

<sup>a</sup> First cycle of used catalyst after recycling.

<sup>b</sup> TOF values calculated at 5 h of reaction time.

<sup>c</sup> so: styrene oxide, bza: benzaldehyde, phed: 1-phenylethane-1,2-diol, bzac: benzoic acid, phaa: phenyl acetaldehyde.

The conversion of styrene and the selectivity of different reaction products using [V<sup>IV</sup>O(pydx-en)]-Y as catalyst under the optimized reaction conditions have

been analyzed as a function of time and are presented in Figure 3.11. It is clear from the plot that a selectivity of 75.5 % of benzaldehyde has been obtained at a conversion of 7.5 % of styrene in 1/2 h of the reaction time. This selectivity slightly improves in the first two hours, then slow decreases with time and reaches 74.7 % with the increase of the conversion of styrene to 85.5 % in 6 h. With 24.5 % at 1/2 h of reaction time, the selectivity of styrene oxide decreases considerably with the conversion of styrene and reaches 3.9 %. The formation of the other three products i.e. benzoic acid, 1-phenylethane-1,2-diol and phenyl acetaldehyde starts only after ca. 2 h and their overall formation is relatively low even after 6 h of the reaction time. After 6 h only minor changes are observed in the selectivity of the different reaction products.

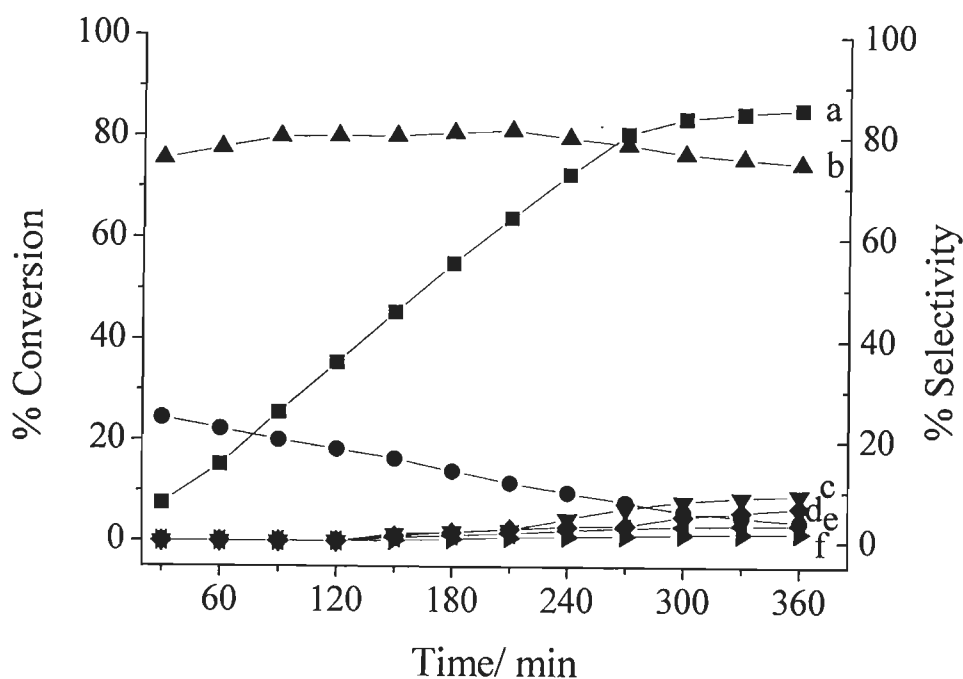


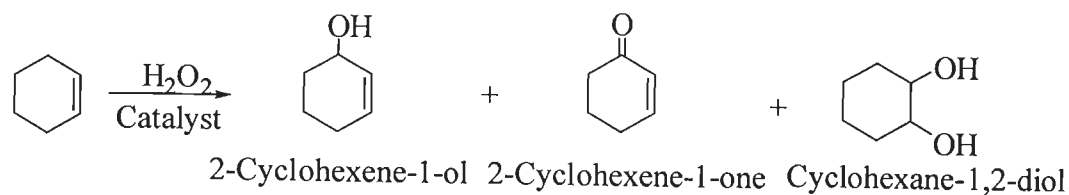
**Figure 3.11.** Conversion of styrene and variation in the selectivity of different reaction products as a function of time using  $[V^{IV}O(pydx-en)]-Y$  as catalyst: (a) conversion of styrene ( $\blacksquare$ ), (b) selectivity of benzaldehyde ( $\blacktriangle$ ), (c) selectivity of 1-phenylethane-1,2-diol ( $\blacktriangledown$ ), (d) selectivity of benzoic acid ( $\blacklozenge$ ), (e) selectivity of styrene oxide ( $\bullet$ ), (f) selectivity of other product ( $\blacktriangleleft$ ).

It is clear from Table 3.5 that the selectivity of the different oxidation products formed varies in the order: benzaldehyde >> 1-phenylethane-1,2-diol > benzoic acid > styrene oxide > phenylacetaldehyde. Upon recycling the activity decreases slightly and the selectivity shows some changes with increase in the formation of phenylacetaldehyde and of the minor non-identified products. Neat complexes are also active and exhibit 62.7 – 65.3 % conversion (Table 3.5). Amongst the products formed, the selectivity of benzoic acid is higher than that of 1-phenylethane-1,2-diol while others follow similar order of selectivity as observed for encapsulated complexes. Blank reaction under above reaction conditions gave ca. 3 % conversion. Thus, neat as well as encapsulated complexes are both good in catalytic activity. However, the recyclable nature and no observed leaching of encapsulated complexes make them better over the neat ones.

Aspects related to the mechanism of reaction are discussed below. Benzaldehyde is clearly the favored product. It may result from the further oxidation of styrene oxide formed in the first step by a nucleophilic attack of H<sub>2</sub>O<sub>2</sub> on styrene oxide followed by cleavage of the intermediate hydroperoxystyrene [6]. The formation of benzaldehyde may also result from direct oxidative cleavage of the styrene side chain double bond via a radical mechanism. The high amount of water present in H<sub>2</sub>O<sub>2</sub> is partly responsible for the possible hydrolysis of styrene oxide to 1-phenylethane-1,2-diol. Other products, e.g. benzoic acid formation through further oxidation of benzaldehyde, only form in low amount in these reactions. Similarly the formation of phenylacetaldehyde through isomerisation of styrene oxide is quite low in all cases.

### **3.3.8.2. Oxidation of cyclohexene**

The oxidation of cyclohexene was also studied using these catalysts. The reaction gave mainly four different products viz. 2-cyclohexene-1-ol, 2-cyclohexene-1-one and cyclohexane-1,2-diol as shown in Scheme 3.4. The formation of the allylic oxidation products 2-cyclohexene-1-one and 2-cyclohexene-1-ol reflects the preferential attack of the activated C-H bond over the C=C bond [156].



**Scheme 3.4.** Oxidation products of cyclohexene.

The different parameters e.g. amount of oxidant, catalyst, solvent and temperature of the reaction mixture were optimized for the maximum oxidation of cyclohexene, again considering  $[\text{V}^{\text{IV}}\text{O}(\text{pydx-en})]\text{-Y}$  (3.4) as a representative catalyst. Three different cyclohexene to aqueous 30%  $\text{H}_2\text{O}_2$  molar ratios viz. 1:1, 1:2 and 1:3 were considered while keeping fixed the amounts of cyclohexene (0.082 g, 10 mmol), catalyst precursor (0.005 g), acetonitrile (5 ml) and temperature at 80 °C. The percent conversion obtained as a function of time is presented in Figure 3.12. A maximum of 90.4 % conversion was achieved at a  $\text{H}_2\text{O}_2$  to cyclohexene molar ratio of 1:1. Increasing this ratio to 1:2 increased this conversion to 95.9 % while 1:3 molar ratios gave 96.9 % conversion. As the 1 : 3 molar ratio of substrate : oxidant did not show significant change in the conversion of cyclohexene, the cyclohexene to  $\text{H}_2\text{O}_2$  molar ratio of 1 : 2 was considered to be adequate.

Similarly, for cyclohexene (0.082 g, 10 mmol), 30 %  $\text{H}_2\text{O}_2$  (2.27 g, 20 mmol) and acetonitrile (5 ml), three different amounts of catalyst viz. 0.003, 0.005 and 0.0075 g were considered and the reactions were monitored at 80 °C. The results obtained as a function of time are presented in Figure 3.13 indicate that 0.005 g of catalyst amount show maximum conversion of 95.9 %, while 0.003 and 0.0075 g catalyst gave lower conversions (ca. 76 and 80 %, respectively) in 5-6 h of reaction time.

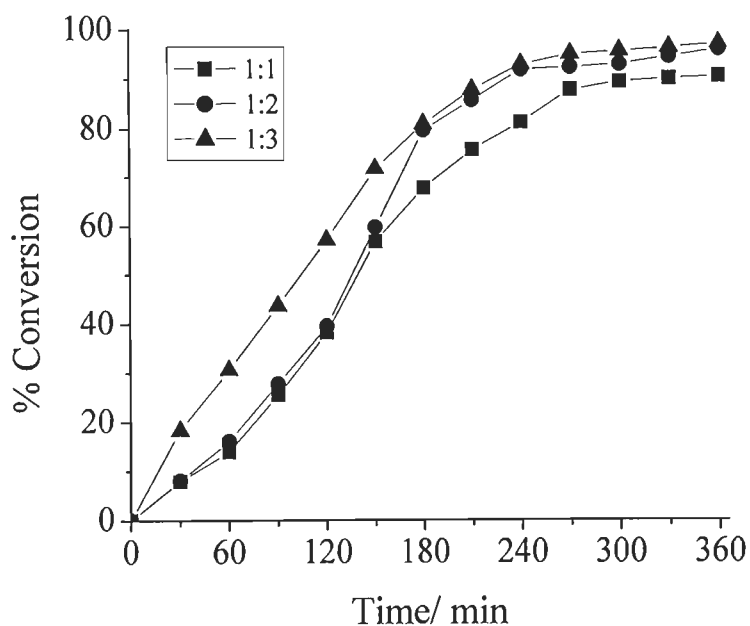


**Figure 3.12.** Effect of the amount of  $\text{H}_2\text{O}_2$  on the oxidation of cyclohexene at  $80^\circ\text{C}$  as a function of time. Reaction conditions: cyclohexene (0.820 g, 10 mmol),  $[\text{V}^{\text{IV}}\text{O}(\text{pydx-en})]\text{-Y}$  (0.005 g) and acetonitrile (5 ml).

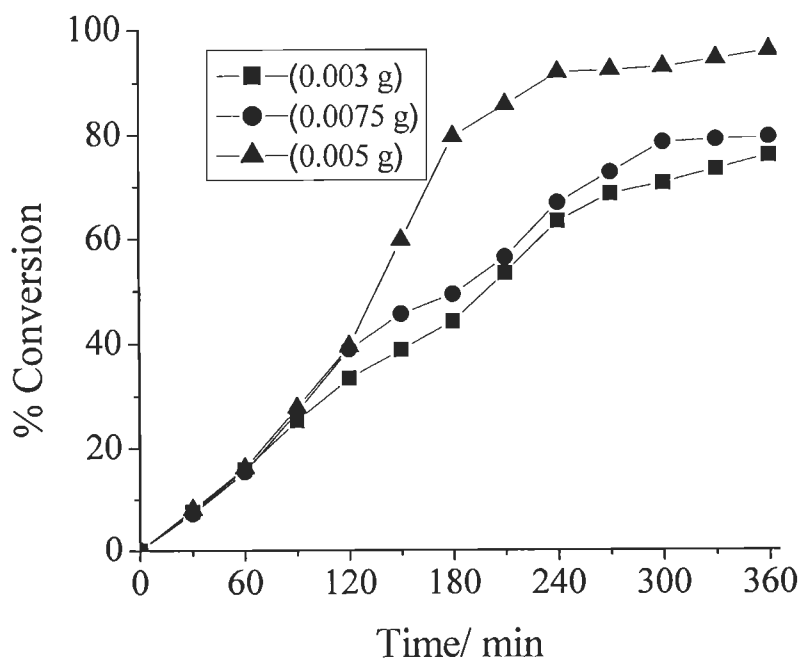


**Figure 3.13.** Effect of the amount of catalyst on the oxidation of cyclohexene at  $80^\circ\text{C}$  as a function of time. Reaction conditions: cyclohexene (0.820 g, 10 mmol), 30 %  $\text{H}_2\text{O}_2$  (2.27 g, 20 mmol) and acetonitrile (5 ml).

As illustrated in Figure 3.14, under the above optimized reaction conditions i.e. cyclohexene (0.82 g, 10 mmol),  $[V^{IV}O(\text{pydx-en})]\text{-Y}$  (0.005 g) and  $\text{H}_2\text{O}_2$  (2.28 g, 20 mmol) in 5 ml of acetonitrile are adequate to effect 95.9 % conversion of cyclohexene at 80 °C. Remarkably, increasing the solvent volume decreases this conversion drastically.

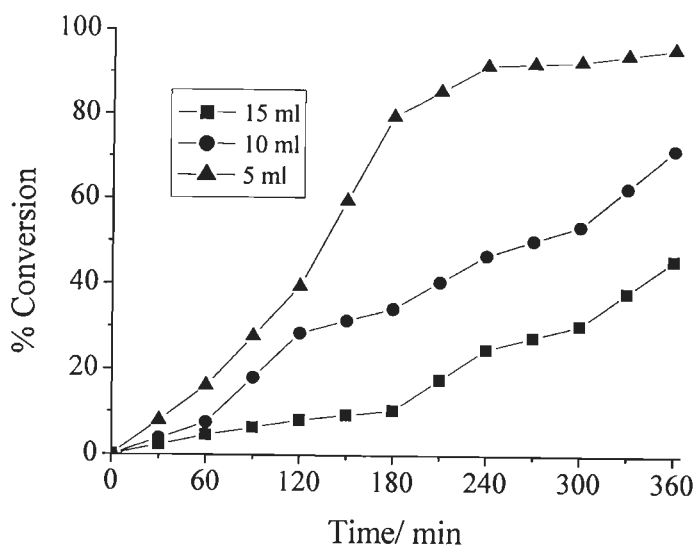


**Figure 3.14.** Effect of the amount of solvent on the oxidation of cyclohexene at 80 °C as a function of time. Reaction conditions: cyclohexene (0.82 g, 10 mmol),  $\text{H}_2\text{O}_2$  (2.27 g, 20 mmol) and  $[V^{IV}O(\text{pydx-en})]\text{-Y}$  (0.005 g).

Thus, under the optimized conditions i.e. cyclohexene (0.82 g, 10 mmol),  $\text{H}_2\text{O}_2$  (2.27 g, 20 mmol), catalyst (0.005 g)  $\text{CH}_3\text{CN}$  (5 ml) and temperature (80 °C), the performance of catalyst precursors **3.5** and **3.6** was also studied. The conversions after 4-6 h of reaction (Figure 3.15) time along with the product selectivity after 6 h are presented in Table 3.6. It is clear that the catalytic performance all encapsulated catalysts are comparable for the oxidation of cyclohexene and the selectivity of the products follows the order: 2-cyclohexene-1-one > 2-cyclohexene-1-ol > cyclohexane-1,2-diol > cyclohexene oxide. After ca. 4h the conversion has almost attained its maximum and only increases marginally between 4 and 6 h of reaction time. Neat complexes exhibit lower conversion along with lower turn over frequency (Table 3.6). Here, the selectivity of different products also differs and follows the order: 2-cyclohexene-1-ol >> 2-cyclohexene-1-one > cyclohexene oxide > cyclohexane-1,2-diol.

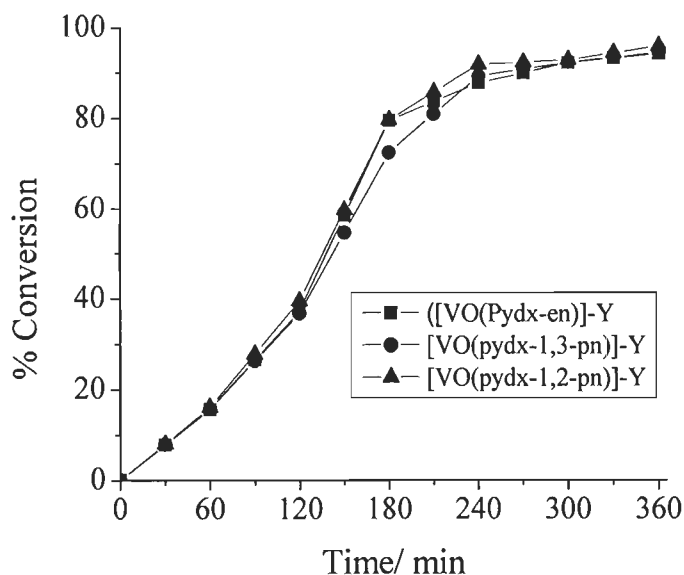


**Figure 3.15.** Effect of the different catalyst precursors on the oxidation of cyclohexene at 80 °C as a function of time. Reaction conditions: cyclohexene (0.820 g, 10 mmol), H<sub>2</sub>O<sub>2</sub> (2.27 g, 20 mmol), catalyst amount (0.005 g) acetonitrile (5 ml).

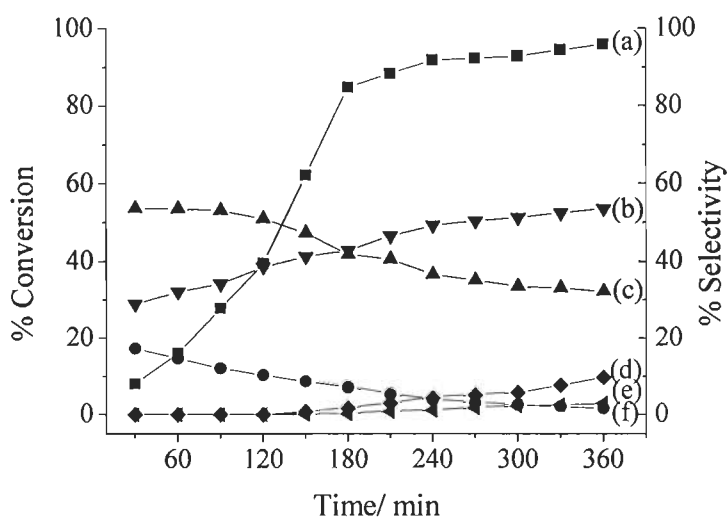


**Figure 3.16.** Conversion of cyclohexene and variation in the selectivity of the different reaction products as a function of time using [V<sup>IV</sup>O(pydx-en)]-Y (4) as catalyst: (a) conversion of cyclohexene (■), (b) selectivity of cyclohexene-1-one (▼), (c) selectivity of cyclohexene-1-ol (▲), (d) selectivity of cyclohexane-1,2-diol (◆) (e) selectivity of cyclohexene oxide (●) and (f) selectivity of other products (◄).

The conversion of cyclohexene and the selectivity of different reaction products using [VO(pydx-en)]-Y (3.4) as catalyst under the optimized reaction conditions have been analyzed as a function of time and are presented in Figure 3.16. The formation of 2-cyclohexene-1-ol started with a selectivity of ca. 60 % which slowly decreased with time and reached ca. 33.6 % at the end of 6 h of reaction. Similarly, the selectivity of cyclohexene oxide started with 17.3% and reached 1.6% while 2-cyclohexene-1-one started with ca. 36 % selectivity and improved to ca. 54.6 %. The formation of cyclohexane-1, 2-diol was initially nearly zero and increased up to 9.8 % after 6 h. The other catalysts gave similar selectivity trends.

**Table 3.6.** Conversion of cyclohexene and selectivity of various oxidation products after 6 h of reaction time.

Catalyst	% Con.	TOF (h <sup>-1</sup> )	% Selectivity <sup>b</sup>				
			a	b	c	d	Others
[V <sup>IV</sup> O(pydx-en)]-Y	95.9	1374	1.6	32.9	50.8	9.7	4.9
[V <sup>IV</sup> O(pydx-en)]-Y <sup>a</sup>	94.2	-	2.8	51.6	43.0	1.6	1.0
[V <sup>IV</sup> O(pydx-1,3-pn)]-Y	92.6	4455	2.5	43.9	46.7	3.9	2.9
[V <sup>IV</sup> O(pydx-1,3-pn)]-Y <sup>a</sup>	90.4	-	3.0	45.4	35.1	13.4	3.1
[V <sup>IV</sup> O(pydx-1,2-pn)]-Y	89.2	2676	2.8	42.9	50.2	3.3	0.1
[V <sup>IV</sup> O(pydx-1,2-pn)]-Y <sup>a</sup>	85.8	-	3.0	47.8	35.0	10.9	3.3
Without catalyst	6.6	-	49.4	10.0	25.0	15.6	-
[V <sup>IV</sup> O(pydx-en)]	28.1	595	9.4	66.8	21.0	2.8	-
[V <sup>IV</sup> O(pydx-1,3-pn)]	32.2	704	5.9	57.3	32.7	4.2	-
[V <sup>IV</sup> O(pydx-1,2-pn)]	23.1	505	10.9	59.1	24.2	5.7	-

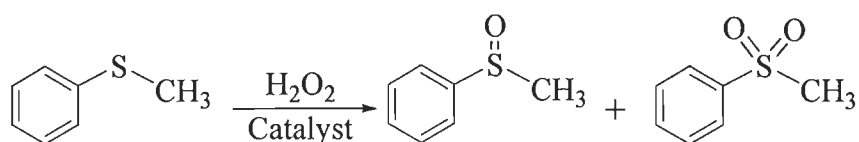
<sup>a</sup> First cycle of used catalyst after recycling.

<sup>b</sup> a: cyclohexene oxide, b: 2-cyclohexene-1-ol c: 2-cyclohexene-1-one and d: cyclohexane-1,2-diol.



### 3.3.8.3. Oxidation of methyl phenyl sulfide

Several vanadium dependent haloperoxidases catalyze sulfoxidations [157–159] where the electron-rich sulfur atom of the sulfide undergoes electrophilic oxidation by  $\text{H}_2\text{O}_2$  to give the sulfoxide and, further, sulfone. Such oxidation of methyl phenyl sulfide was tested with the precursor catalysts i.e.  $\text{V}^{\text{IV}}\text{O}$ -complexes encapsulated in the nano cavities of zeolite-Y. Oxidation of methyl phenyl sulfide in the presence of  $\text{H}_2\text{O}_2$  gave two products: methyl phenyl sulfoxide and methyl phenyl sulfone, as shown in Scheme 3.5.



**Scheme 3.5.** Oxidation of organic sulfides.

Among the three encapsulated complexes studied,  $[\text{V}^{\text{IV}}\text{O}(\text{pydx-en})]\text{-Y}$  (3.4) was chosen again as a representative one and the reaction conditions were optimised considering the amount of catalyst precursor, oxidant and solvent to obtain maximum conversion of thioanisole. The effect of  $\text{H}_2\text{O}_2$  was studied considering substrate to oxidant ratios of 1:1, 1:2 and 1:3 for the fixed amount of catalyst (0.010 g), methyl phenyl sulfide (1.242 g, 10 mmol) in acetonitrile (5 ml) and the reaction was monitored at room temperature (Figure 3.17). At an aqueous  $\text{H}_2\text{O}_2$  : substrate ratio of 2:1, a maximum of 85.5% conversion of methyl phenyl sulfide was achieved in 2.5 h of reaction time. Decreasing this ratio to 1:1 decreases the conversion of methyl phenyl sulfide considerably, while increasing this ratio to 3:1 improves the conversion but not much (Figure 3.17), and facilitates the reaction to achieve equilibrium in a shorter time. However, aqueous  $\text{H}_2\text{O}_2$  : substrate ratio of 2:1 may be considered adequate to obtain maximum conversion of methyl phenyl sulfide.

Similarly, three different amounts of catalyst precursors – viz. 0.005, 0.010, and 0.015 g were taken while keeping methyl phenyl sulfide (1.242 g, 10 mmol) and 30%  $\text{H}_2\text{O}_2$  (2.27 g, 20 mmol) in acetonitrile (5 ml) to check the effect of amount of catalyst on the reaction. As may be seen in Figure 3.18, increasing its

amount from 0.005 g to 0.010 g increases the conversion from 82.4% to 85.5% while 0.015 g catalyst gave a marginal increase to 87.0 % conversion. Thus, 0.010 g of catalyst precursor is adequate to obtain an optimum methyl phenyl sulfide conversion of 85.5% in ca. 2.5 h of contact time.

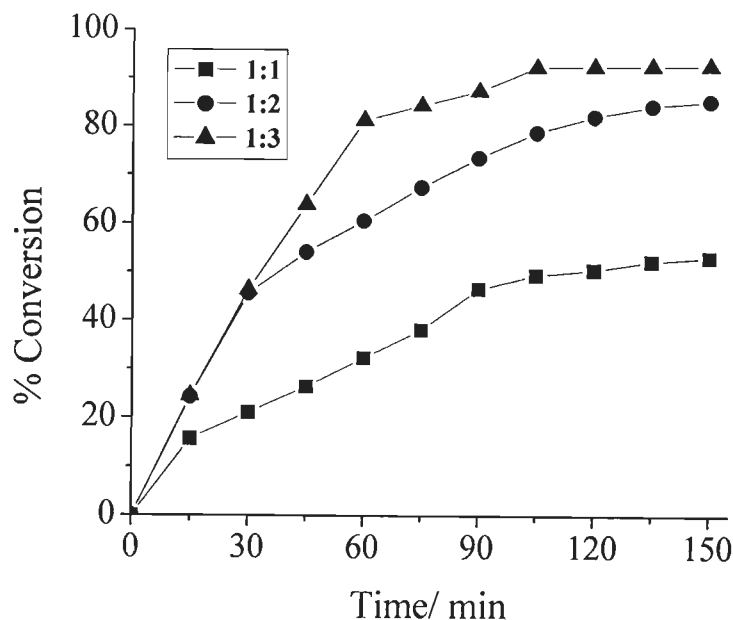


**Figure 3.17.** Effect of the amount of  $\text{H}_2\text{O}_2$  on the oxidation of methyl phenyl sulfide as a function of time. Reaction conditions: methyl phenyl sulfide (1.242 g, 10 mmol),  $[\text{V}^{\text{IV}}\text{O}(\text{pydx-en})]\text{-Y}$  (10 mg) and acetonitrile (5 ml).

In this reaction the volume of solvent again has a remarkable role in the oxidation of methyl phenyl sulfide. As may be seen in Figure 3.19, the use of 5 ml of acetonitrile gives much better conversion under above optimized reaction conditions of catalyst and oxidant than 10 or 15 ml. This may possibly be due to a much higher concentration gradient of reagents between the outside and inside of the zeolite cavities when the volume of solvent is lower.

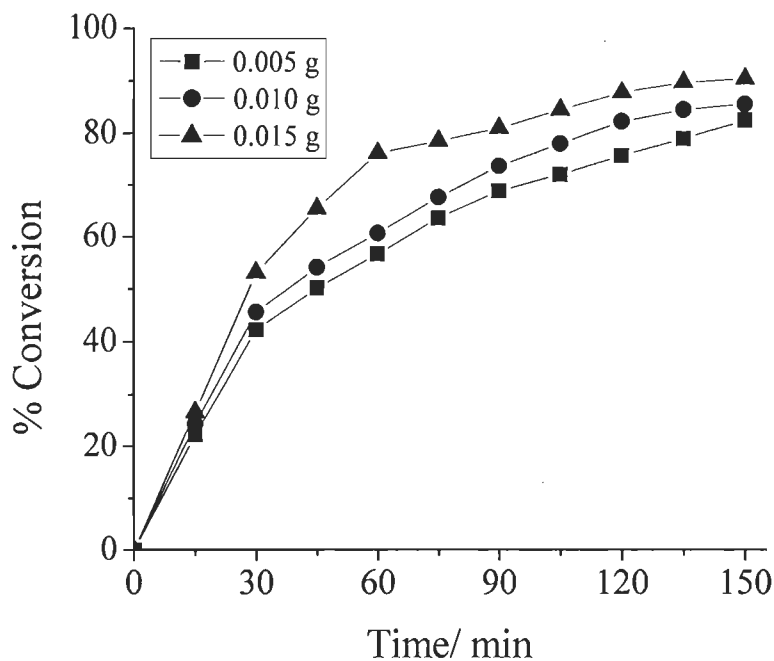


**Figure 3.18.** Effect of catalyst  $[V^{IV}O(pydx-en)]-Y$  on the oxidation of methyl phenyl sulfoxide at room temperature. Reaction conditions: methyl phenyl sulfide (1.24 g, 10 mmol),  $H_2O_2$  (2.27 g, 20 mmol) and acetonitrile (5 ml).

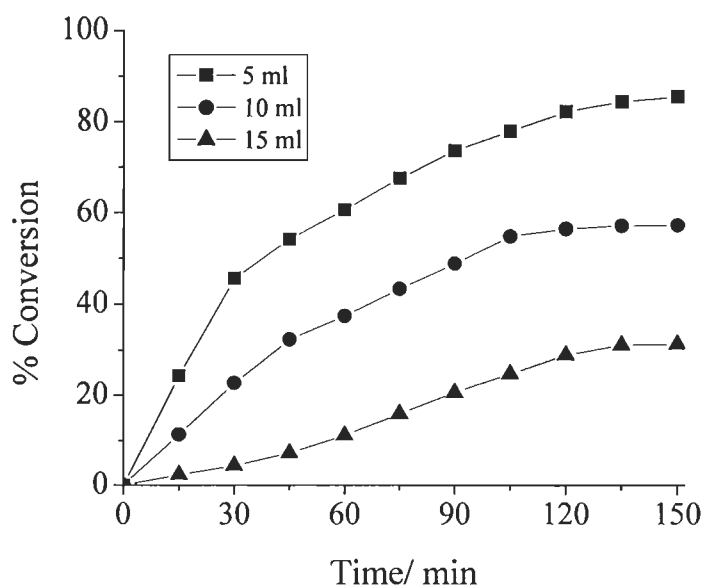


**Figure 3.19.** Effect of volume of solvent on the oxidation of methyl phenyl sulfide at room temperature as a function of time. Reaction conditions: methyl phenyl sulfide (1.24 g, 10 mmol),  $H_2O_2$  (2.2 g, 20 mmol) and  $[V^{IV}O(pydx-en)]-Y$  (0.01 g).

Therefore, from these experiments the more adequate reaction conditions for the maximum oxidation of methyl phenyl sulfide at room temperature are considered to be: catalyst (0.010 g), methyl phenyl sulfide (1.242 g, 10 mmol),  $\text{H}_2\text{O}_2$  (2.27 g, 20 mmol) and acetonitrile (5 ml). The other catalyst precursors  $[\text{V}^{\text{IV}}\text{O}(\text{pydx-1,3-pn})]\text{-Y}$  (3.5) and  $[\text{V}^{\text{IV}}\text{O}(\text{pydx-1,2-pn})]\text{-Y}$  (3.6) were also tested under the above reaction conditions and the corresponding results are summarized in Figure 3.20 and selectivity details are presented in Table 3.7.

From Table 3.7, it is clear that 80.0 - 85.5% of methyl phenyl sulfide is converted into products using all catalysts where the percentage conversion varied in the order:  $[\text{V}^{\text{IV}}\text{O}(\text{pydx-en})]\text{-Y}$  (85.5 %) >  $[\text{V}^{\text{IV}}\text{O}(\text{pydx-1,3-pn})]\text{-Y}$  (82.1%) >  $[\text{V}^{\text{IV}}\text{O}(\text{pydx-1,2-pn})]\text{-Y}$  (80.0%). The selectivity of the major product i.e. sulfone is similar but varies in the order:  $[\text{V}^{\text{IV}}\text{O}(\text{pydx-en})]\text{-Y}$  (79.6 %) >  $[\text{V}^{\text{IV}}\text{O}(\text{pydx-1,3-pn})]\text{-Y}$  (75.2%) >  $[\text{V}^{\text{IV}}\text{O}(\text{pydx-1,2-pn})]\text{-Y}$  (73.6%).

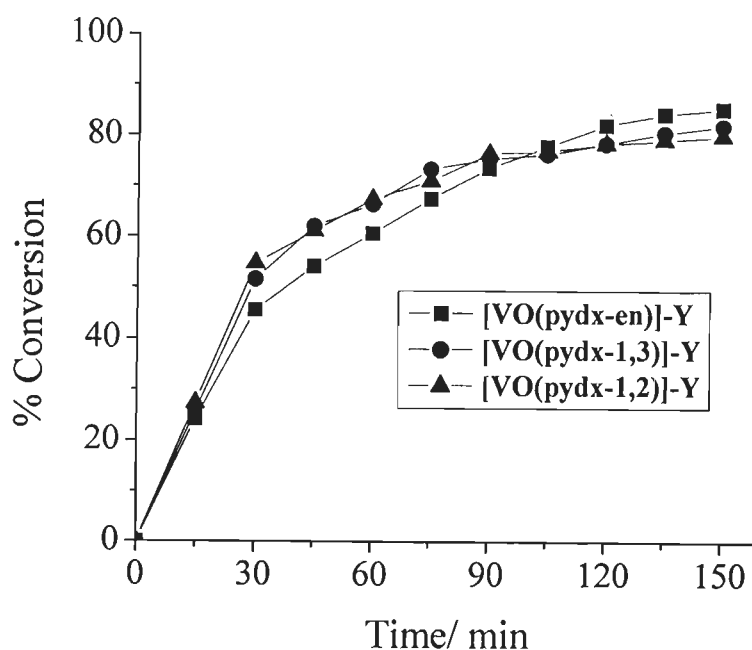


**Figure 3.20.** Effect of different catalyst on the oxidation of methyl phenyl sulfide at room temperature. Reaction conditions: catalyst (0.010 g), methyl phenyl sulfide (1.242 g, 10 mmol),  $\text{H}_2\text{O}_2$  (2.27 g, 20 mmol) and acetonitrile (5 ml).

The conversion of methyl phenyl sulfide and the selectivity of different reaction products using  $[V^{IV}O(\text{pydx-en})]-Y$  (**3.4**) as catalyst under the optimized reaction conditions were obtained as a function of time and are presented in Figure 3.21. It is clear from the plot that conversion of methyl phenyl sulfide starts with the good selectivity (ca. 90 %) for the formation of methyl phenyl sulfoxide, but this is slowly converted to the sulfone. The initial selectivity of methyl phenyl sulfone is ca. 10 % and reaches ca. 20 % after ca. 2.5 h. Very similar trends were also obtained with the catalyst precursors  $[V^{IV}O(\text{pydx-1,3-pn})]-Y$  (**3.5**) and  $[V^{IV}O(\text{pydx-1,2-pn})]-Y$  (**6**).

**Table 3.7.** Conversion percentage of methyl phenyl sulfide in 2.5 h and selectivity of sulfoxide and sulfone.

Catalyst	% Conversion	TOF ( $\text{h}^{-1}$ )	% Selectivity	
			Sulfoxide	Sulfone
$[V^{IV}O(\text{pydx-en})]-Y$	85.5	1980	79.6	20.4
$[V^{IV}O(\text{pydx-en})]-Y^a$	83.5	-	75.7	24.3
$[V^{IV}O(\text{pydx-1,3-pn})]-Y$	82.1	3160	75.2	24.8
$[V^{IV}O(\text{pydx-1,3-pn})]-Y^a$	80.4	-	73.2	26.8
$[V^{IV}O(\text{pydx-1,2-pn})]-Y$	80.0	1920	73.6	26.4
$[V^{IV}O(\text{pydx-1,2-pn})]-Y^a$	77.8	-	73.4	26.6
No solid <sup>b</sup>	ca. 3	-	ca. 3	ca. 0
Na-Y <sup>b</sup>	ca. 3	-	ca. 3	ca. 0
$[V^{IV}O(\text{pydx-en})]$	80.3	906	82.5	17.5
$[V^{IV}O(\text{pydx-1,2-pn})]$	75.8	884	80.8	19.2
$[V^{IV}O(\text{pydx-1,3-pn})]$	78.5	916	81.3	18.7

<sup>a</sup> First cycle of used catalyst.

<sup>b</sup> 10 ml of acetonitrile

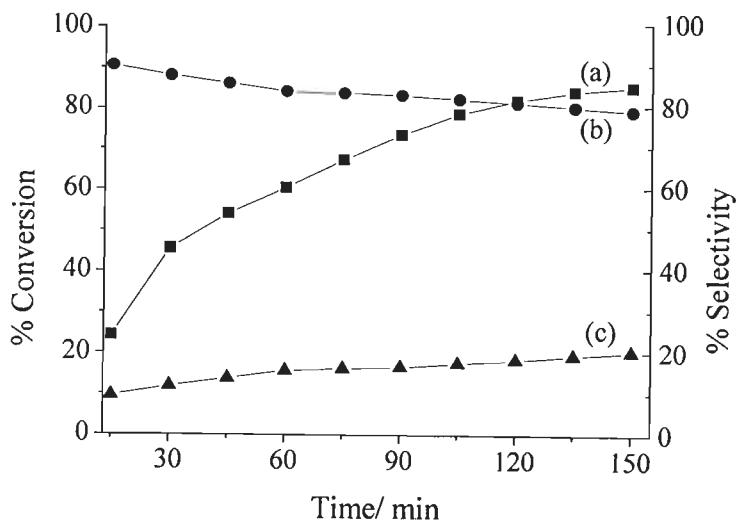


**Figure 3.21.** Conversion of methyl phenyl sulfide and variation in the selectivity of the reaction products as a function of time using  $[V^{IV}O(\text{pydx-en})]\text{-Y}$  (3.4) as catalyst: (a) conversion of methyl phenyl sulfide (●), (b) selectivity of methyl phenyl sulfoxide (■) and (c) selectivity of methyl phenyl sulfone (▲).

Considering same mole concentration of neat catalyst precursors,  $[V^{IV}O(\text{pydx-en})]$  (3.1),  $[V^{IV}O(\text{pydx-1,3-pn})]$  (3.2) and  $[V^{IV}O(\text{pydx-1,2-pn})]$  (3.3) under reaction conditions approximately equivalent to those above [i.e. catalyst (0.001 g for all), methyl phenyl sulfide (1.242 g, 10 mmol),  $H_2O_2$  (2.27 g, 20 mmol) and acetonitrile (5 ml)], 75.8 – 80.3 % conversion of methyl phenyl sulfide was achieved after 2.5 h where selectivity of sulfoxide is ca. 82 % which is slightly higher than obtained for the encapsulated complexes. Thus, both neat as well as encapsulated complexes are good catalysts for the oxidation of the organic sulfide; however, the stability and recyclable nature of zeolite-Y encapsulated complexes make them better over neat ones.

### 3.3.9. Tests of recycle ability and heterogeneity of the zeolite-Y encapsulated catalytic reactions

The recycle ability of encapsulated complexes was examined considering the oxidation of styrene. After contact for 6 h, the reaction mixture was filtered, the solid was washed with acetonitrile and dried at ca. 120 °C. It was subjected to further catalytic reaction under similar conditions. As may be checked in Table 3.5

not much loss in catalytic activity was observed, this indicating that most of the complex is still present in the cavity of the zeolite-Y. In another experiment, after ca. 6 h of reaction time the filtrate collected after separating the used catalyst was placed into the reaction flask and the reaction was continued after adding fresh oxidant for another 4 h. The gas chromatographic analysis showed no significant improvement in conversion and this confirms that the reaction did not proceed upon removal of the solid catalyst. The oxidation of styrene is, therefore, heterogeneous in nature. Similar experiments were done for the oxidation of cyclohexene (Table 3.6) and methyl phenyl sulphide (Table 3.7). The recycle experiments for cyclohexene show not much loss in catalytic activity, while in the case of methyl phenyl sulfide it gave ca. 2 % less conversion compared to original catalyst.

### **3.3.10. Reactivity of complexes and possible catalytic reaction pathway**

It is known that several  $V^VO_2L$  compounds react with  $H_2O_2$  to give  $V^VO(O_2)L$ , and it is normally assumed that the corresponding hydroperoxido-complex is the active catalyst which mediates oxygenations, including the oxidation of sulfides to sulfoxides and sulfones and the epoxidation of alkenes and allylic alcohols [160, 161].

The reactivity of  $[V^{IV}O(pydx-en)]$  (3.1) with  $H_2O_2$  in DMSO was monitored by electronic absorption spectroscopy and the observed spectral changes are presented in Figure. 3.22. Thus, the progressive addition of a dilute  $H_2O_2$  solution in DMSO to a solution of  $[V^{IV}O(pydx-en)]$  in DMSO results in the flattening of bands appearing at 776 and 650 nm. The intensity of the band at ca. 385 nm slowly decreases with a slight shift towards lower wavelength, stabilizing with the formation of a band at ca. 380 nm, while the intensity of other bands appearing in the UV region (at ca. 260 and ca. 280 nm) increases. These changes indicate the interaction of  $[V^{IV}O(pydx-en)]$  with  $H_2O_2$  in methanol, forming  $[V^VO(O)_2(pydx-en)]$ , where bands at ca. 360-450 nm are expected to appear [87 and references therein]. The disappearance of d-d bands is in accordance with the oxidation of the  $V^{IV}O$ -complex to an oxidoperoxovanadium(V).

Similar features were observed with  $[V^{IV}O(pydx-1,2-pn)]$  (3.3) upon similar treatment (Figures 3.23).

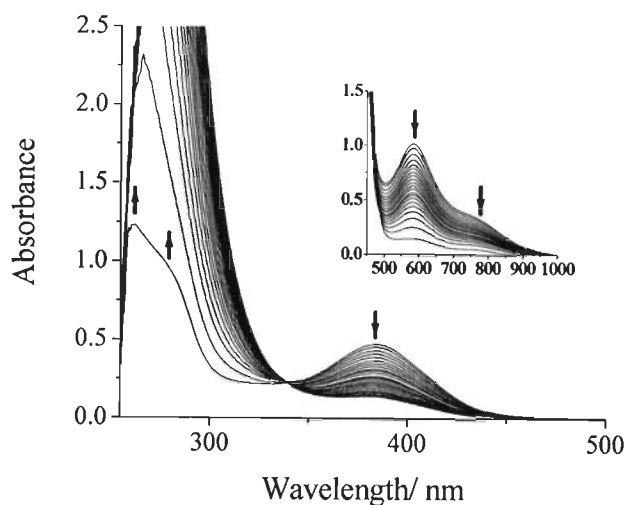


**Figure 3.22.** UV-Vis spectral changes observed during titration of  $[V^{IV}O(\text{pydx-en})]$  (**3.1**) with  $H_2O_2$ . The spectra were recorded upon stepwise additions of five drops portions of  $H_2O_2$  [1.178 g (10.39 mmol) of 30%  $H_2O_2$  dissolved in 5 ml of DMSO] to 10 ml of  $1.6 \times 10^{-4}$  M solution in DMSO. The inset shows similar spectra recorded with ca.  $7.55 \times 10^{-3}$  M solution of **3.1** in DMSO.

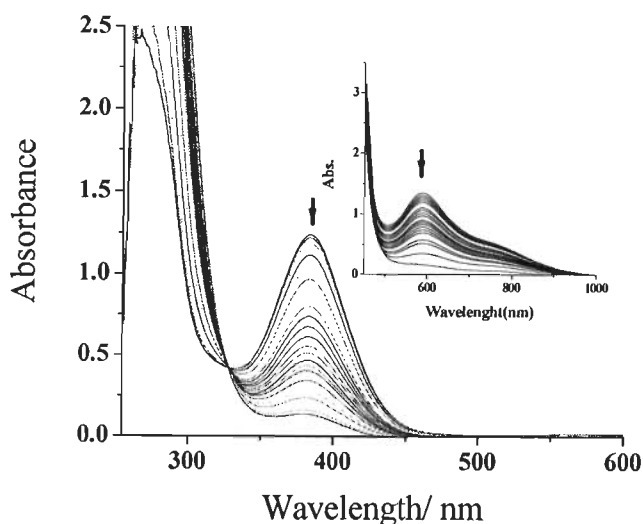
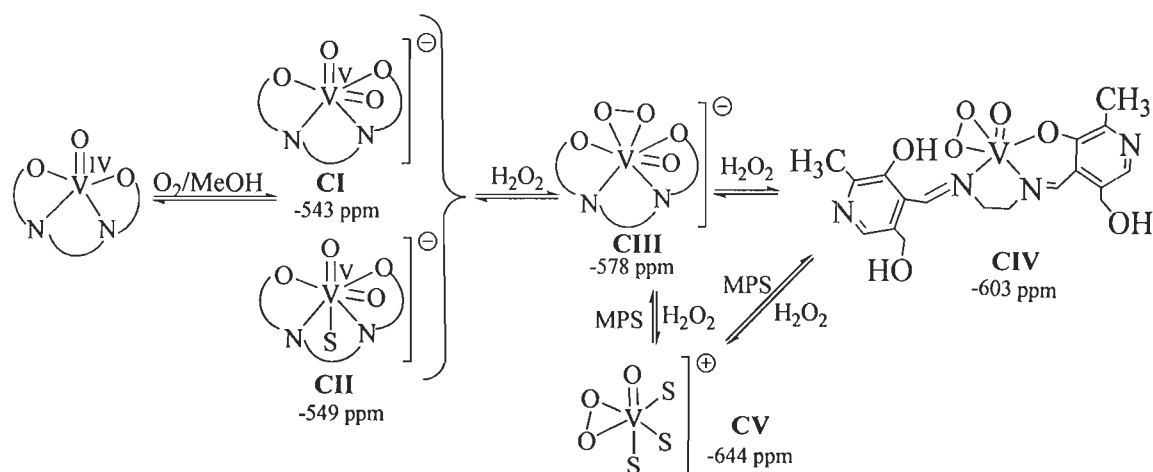


**Figure 3.23.** UV-Vis spectral changes observed during titration of  $[V^{IV}O(\text{pydx-1,2-pn})]$  (**3.3**) with  $H_2O_2$ . The spectra were recorded after stepwise additions of five drops portions of  $H_2O_2$  (1.178 g (10.39 mmol) of 30%  $H_2O_2$  dissolved in 5 ml of DMSO) to 10 ml of  $1.6 \times 10^{-4}$  M solution in DMSO. The inset shows similar spectra recorded with ca.  $1 \times 10^{-3}$  M solution of **3.3** in DMSO.



The  $^{51}\text{V}$  NMR of  $[\text{V}^{\text{IV}}\text{O}(\text{pydx-en})]$  (**3.1**) were recorded to establish their behaviour in solution and their speciation upon modifying the composition of the solutions (see Figure 3.24). A fresh methanolic solution of  $[\text{V}^{\text{IV}}\text{O}(\text{pydx-en})]$  (**3.1**) (ca. 4 mM) does not show any  $^{51}\text{V}$  NMR peak but after ca. 15 min resonances at -543 and -549 ppm build up, which we tentatively assign to species **CI** and **CII** (see Scheme 3.6). Upon successive additions of portions of a 30%  $\text{H}_2\text{O}_2$  aqueous solution the relative intensity of the -543 and -549 ppm peaks decrease and several new peaks build up. Namely, after addition of ca. 0.5 equiv. of  $\text{H}_2\text{O}_2$ , a peak at -578 ppm emerges; it corresponds to the monoperoxido **CIII**, and upon further additions of (1.0, 2.0 and 3.0 equiv.) of the 30%  $\text{H}_2\text{O}_2$  solution, new peaks appear at -603 (**CIV**) and -644 (**CV**), which increase intensity at the expense of the resonances of **CI** and **CII**. Upon addition of methyl phenyl sulphide, after ca. 3 h the peaks at -644 and -578 ppm corresponding to the peroxide complexes **CIII** and **CIV** disappear and the spectrum [Figure 3.24(g)] shows the resonances at -543 and -549 ppm corresponding to **CI** and **CII** as the main peaks.



**Scheme 3.6.** Tentative assignments of  $\text{V}^{\text{V}}$ -species formed in methanolic solutions of  $[\text{V}^{\text{IV}}\text{O}(\text{pydx-en})]$  (**3.1**), upon addition of aqueous  $\text{H}_2\text{O}_2$  solution, and upon addition of methyl phenyl sulphide.

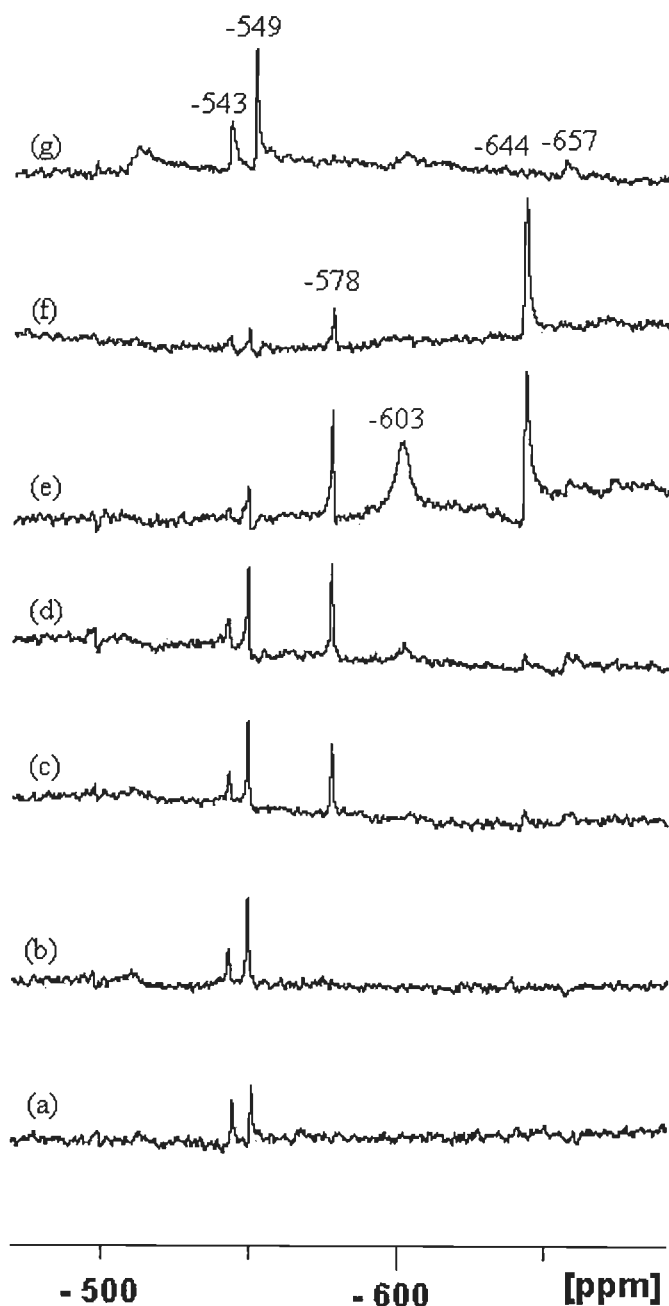


**Figure 3.24.**  $^{51}\text{V}$  NMR spectra (a) of a methanolic solution of  $[\text{V}^{\text{IV}}\text{O}(\text{pydx-en})]$  (3.1) (ca. 4 mM) the pH is ca. 7.5; (b) solution of (a) after 1 hr; (c) addition of 0.5 equiv. of aqueous 30%  $\text{H}_2\text{O}_2$  (total) to the solution of (b); (d) after addition of 1.0 equiv. of 30%  $\text{H}_2\text{O}_2$  (total) to the solution of (c); (e) after addition of 2.0 equiv. of 30%  $\text{H}_2\text{O}_2$  (total) to the solution of (d) the pH is ca. 6.5; (f) after addition of 3.0 equiv. (30%)  $\text{H}_2\text{O}_2$  (total) to the solution of (e) the pH is ca. 6.5; (g) addition of methyl phenyl sulphide (10 equiv.) to the solution of (f) after 3hr at room temperature.

These results indicate that during the catalytic reactions by peroxide, intermediate peroxido species indeed form. After addition of methyl phenyl sulphide (10 equiv.) besides the changes occurring in the  $^{51}\text{V}$  NMR spectra, where the peroxido-complexes disappear, a more intense EPR spectrum is recorded and the spin Hamiltonian parameters are almost identical to those of fresh solutions of  $[\text{V}^{\text{IV}}\text{O}\{(\text{pydx})_2\text{-en}\}]$  (3.1), indicating the reversibility of the processes. The EPR spectra measured (Figure 3.25 and Table 3.8 indicates that this solution also contains  $[\text{V}^{\text{IV}}\text{O}(\text{pydx-en})]$  (3.1).

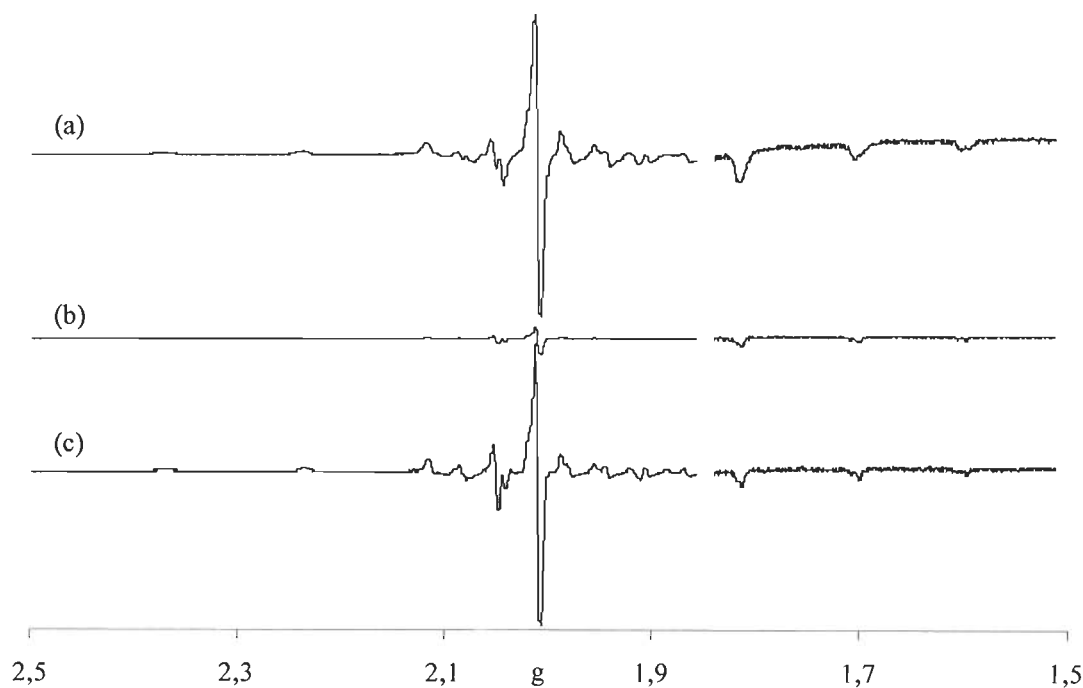


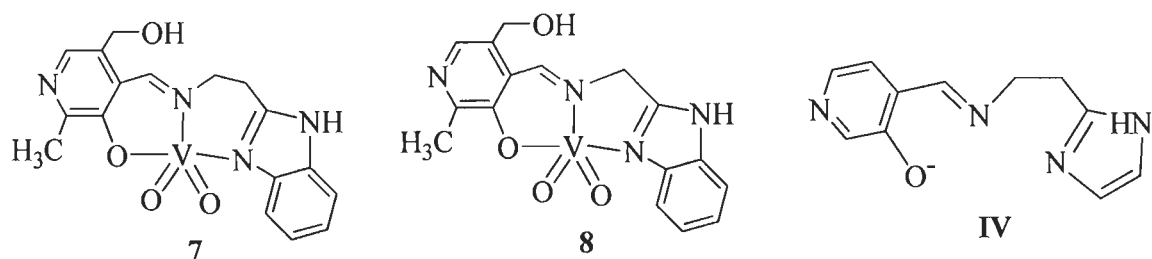
**Figure 3.25.** First derivative EPR spectra of frozen (77 K) solutions of (a) a methanolic solution of  $[\text{V}^{\text{IV}}\text{O}\{(\text{pydx})_2\text{-en}\}]$  (3.1) (c.a 4 mM); (b) after addition of 3.0 equiv (30%)  $\text{H}_2\text{O}_2$  (total) to the solution of (a); (c) after 24 h of addition of methyl phenyl sulphide (10 equiv) to the solution of (b). The high field ranges of the spectra are amplified.

**Table 3.8.** EPR spectral data after addition of H<sub>2</sub>O<sub>2</sub> and H<sub>2</sub>O<sub>2</sub> followed by methyl phenyl sulphide.

	$g_z$	$A_z$ $\times 10^4 \text{ cm}^{-1}$	$A_x, A_y$ $\times 10^4 \text{ cm}^{-1}$	$g_x, g_y$
(3.1) 4 mM solution in MeOH	1.957	158.5	55	1.979
Addition of 3 equiv. H <sub>2</sub> O <sub>2</sub>	1.956	158.0	58	1.974
After 24 h of addition of methyl phenyl sulphide (10 equiv.)	1.956	157.8	59	1.976

Thus, overall these UV-Vis and <sup>51</sup>V NMR experiments show that upon addition of aqueous H<sub>2</sub>O<sub>2</sub>, V<sup>V</sup>O(O)<sub>2</sub>L species form, supporting the possibility of hydroperoxide complexes being the active catalyst. After addition of the substrate (e.g. methyl phenyl sulphide) both V<sup>V</sup>- and V<sup>IV</sup>-L complexes are the only V-containing species detected, indicating that the integrity of the ligand is preserved. Thus, recycle ability of the catalyst precursors mainly depends on the more or less easy separation of the complex from the reaction mixture containing the products.

Catalytic oxidation of styrene by [V<sup>V</sup>O<sub>2</sub>(pydx-aebmz)] (3.7) and [V<sup>V</sup>O<sub>2</sub>(pydx-ambmz)] (3.8) (Scheme 3.7: aebmz = 2-aminoethylbenzimidazole and ambmz = 2-aminomethylbenzimidazole) [87], as well as with two catalyst precursors similar to 3.4 where the diamines were: 1,2-diaminocyclohexane (chen) and 1,2-diphenylethylenediamine (dpen) instead of ethylenediamine: [V<sup>IV</sup>O(pydx-chen)] (3.9) and [V<sup>IV</sup>O(pydx-dpen)] (3.10) have been recently reported [140]. The reaction gave identical products with similar selectivity, although for the present systems the relative amounts of benzaldehyde is significantly higher than in the case of 3.7 and 3.8 (ca. 55 % against ca. 75 % in this study), and lower than in the case of 3.9 and 3.10 (ca. 85 % and 92%, respectively [140]). Benzaldehyde is the product of the C–C bond cleavage of styrene which usually forms under free radical conditions [160, 161]. This may be considered an indication that in the present systems the mechanism follows a similar pathway.



Scheme 3.7.

For the oxidation of hydrocarbons with transition metal complexes as catalysts in the presence of  $\text{H}_2\text{O}_2$  two general groups of mechanisms usually considered: the radical and non-radical ones, both involving metal-peroxido intermediates. The radical mechanism [162-165], is based on the formation of the free  $\text{HOO}^\bullet$  and  $\text{HO}^\bullet$  radicals, the latter directly oxidizing hydrocarbons giving alkylperoxides, which then undergo decomposition to the final oxidation products. Among the non-radical pathways, the Sharpless mechanism is usually considered as the most favorable one for the epoxidation of olefins [166, 167].

The radical and non-radical (Sharpless-type) mechanism of epoxidation were recently studied by DFT methods for a model complex of **3.7** (ligand **3.IV**) and ethene as substrate. The radical pathway was found to be more favorable compared to the non-radical route. It is indeed possible that in the present systems the radical route might also be more favorable than the non-radical (Sharpless) pathway.

### 3.4. Conclusions

Oxidovanadium(IV)-exchanged zeolite-Y complexes  $[\text{V}^{\text{IV}}\text{O}(\text{pydx-en})]\text{-Y}$  (**3.4**),  $[\text{V}^{\text{IV}}\text{O}(\text{pydx-1,3-pn})]\text{-Y}$  (**3.5**) and  $[\text{V}^{\text{IV}}\text{O}(\text{pydx-1,2-pn})]\text{-Y}$  (**3.6**) were synthesized and characterized by IR, UV/Vis and EPR, elemental analyses, thermal studies, field emission scanning electron micrographs (FE-SEM) and X-ray diffraction patterns. The corresponding neat complexes,  $[\text{V}^{\text{IV}}\text{O}(\text{pydx-en})]$  (**3.1**) and  $[\text{V}^{\text{IV}}\text{O}(\text{pydx-1,3-pn})]$  (**3.2**),  $[\text{V}^{\text{IV}}\text{O}(\text{pydx-1,2-pn})]$  (**3.3**), were also prepared.

The encapsulated complexes  $[\text{V}^{\text{IV}}\text{O}(\text{pydx-en})]\text{-Y}$  (**3.4**),  $[\text{V}^{\text{IV}}\text{O}(\text{pydx-1,3-pn})]\text{-Y}$  (**3.5**) and  $[\text{V}^{\text{IV}}\text{O}(\text{pydx-1,2-pn})]\text{-Y}$  (**3.6**) efficiently catalyze the oxidation of

styrene by  $\text{H}_2\text{O}_2$  and with higher conversions, the corresponding neat complexes  $[\text{V}^{\text{IV}}\text{O}(\text{pydx-en})]$  (3.1) and  $[\text{V}^{\text{IV}}\text{O}(\text{pydx-1,3-pn})]$  (3.2),  $[\text{V}^{\text{IV}}\text{O}(\text{pydx-1,2-pn})]$  (3.3) and the related neat complexes  $[\text{V}^{\text{IV}}\text{O}(\text{pydx-chen})]$  (3.9) and  $[\text{V}^{\text{IV}}\text{O}(\text{pydx-dpen})]$  (3.10) [140], benzaldehyde being the main product formed (ca. 75 % under the ‘optimized’ conditions). The encapsulated complexes 3.4-3.6 are also efficient catalysts for the oxidation of cyclohexene, by  $\text{H}_2\text{O}_2$ , and under the ‘optimized’ conditions cyclohexane-1,2-one (ca. 45 %) and cyclohexene-1-ol (ca. 40 %) are the main products formed, followed by cyclohexane-1,2-diol. The encapsulated complexes  $[\text{V}^{\text{IV}}\text{O}(\text{pydx-en})\text{-Y}]$  (3.4),  $[\text{V}^{\text{IV}}\text{O}(\text{pydx-1,3-pn})\text{-Y}]$  (3.5) and  $[\text{V}^{\text{IV}}\text{O}(\text{pydx-1,2-pn})\text{-Y}]$  (3.6) again show much higher conversions than the corresponding neat complexes  $[\text{V}^{\text{IV}}\text{O}(\text{pydx-en})]$  (3.1) and  $[\text{V}^{\text{IV}}\text{O}(\text{pydx-1,3-pn})]$  (3.2),  $[\text{V}^{\text{IV}}\text{O}(\text{pydx-1,2-pn})]$  (3.3) and the related neat complexes  $[\text{V}^{\text{IV}}\text{O}(\text{pydx-chen})]$  (3.9) and  $[\text{V}^{\text{IV}}\text{O}(\text{pydx-dpen})]$  (3.10), as well as distinct selectivity. Neat complexes 3.9 and 3.10 gave mainly cyclohexane-1,2-diol (ca. 70-75 %), followed by cyclohexene-1-ol (ca. 14-18 %) and cyclohexane-1,2-one (ca. 4-9 %).<sup>[25]</sup> The neat complexes  $[\text{V}^{\text{IV}}\text{O}(\text{pydx-en})]$  (3.1) and  $[\text{V}^{\text{IV}}\text{O}(\text{pydx-1,3-pn})]$  (3.2),  $[\text{V}^{\text{IV}}\text{O}(\text{pydx-1,2-pn})]$  (3.3) gave higher selectivity for 2-cyclohexene-1-ol and lower for 2-cyclohexene-1-ol.

The encapsulated complexes  $[\text{V}^{\text{IV}}\text{O}(\text{pydx-en})\text{-Y}]$  (3.4),  $[\text{V}^{\text{IV}}\text{O}(\text{pydx-1,3-pn})\text{-Y}]$  (3.5) and  $[\text{V}^{\text{IV}}\text{O}(\text{pydx-1,2-pn})\text{-Y}]$  (3.6) catalyze the oxidation, by  $\text{H}_2\text{O}_2$  of methyl phenyl sulfide efficiently. Under the conditions studied, the encapsulated complexes gave conversions of ca. 80-85 %, with formation of the corresponding sulfoxide (ca. 75 %) and sulfone (ca. 25 %).

The catalytic reactions probably proceed via the formation of  $[\text{V}^{\text{V}}\text{O}(\text{O})_2(\text{Schiff base})]$  intermediates, followed by the corresponding hydroperoxido complexes. At least in the case of styrene, by comparison with a previous mechanistic study with a distinct system [87] it is suggested that a radical pathway is preferred for the epoxidation step, this being compatible with the preferred formation of benzaldehyde.

# *CHAPTER 4*

## Synthesis of manganese (III) complex of tribasic pentadentate ligand, its encapsulation in zeolite-Y, characterization and catalytic activity

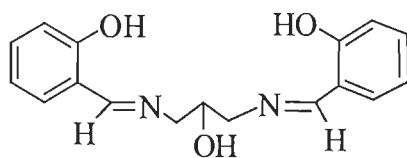
### 4.1. Introduction

Amongst tetradentate ligands, salen type ( $H_2\text{salen} = N,N'$ -bis(salicylidene)ethane-1,2-diamine) ligands find a key place in the literature as complexes of such ligands have great potentials as catalysts for oxo transfer reactions and other processes [96, 168, 169]. Manganese complexes having tetradentate ONNO donor ligands are found to be artificial mimics of manganese containing enzymes [88]. Manganese complexes of salen type ligands have also shown good catalytic reactions for oxygen transfers and E-H activations [96, 169]. The flexible nature of salen-type ligands has also provided opportunities to encapsulate various transition-metal complexes in the nanocavity of zeolites and to develop catalytic processes for various reactions. Ratnasamy and co-workers have used manganese(III) complexes of salen derivatives encapsulated in the cavity of zeolite-X and zeolite-Y for the oxidation of styrene under aerobic conditions using *tert*-butylhydroperoxide as an oxidant. These complexes also catalyze the oxidation of phenol and *p*-xylene [55-58]. Poltowicz et al. have encapsulated a whole range of metallosalen complexes including  $[Mn^{II}(\text{salen})]$  in the zeolite-X to study their catalytic activity for the oxidation of cyclooctane [48].

We have selected ligand systems similar to salen type but with one additional coordinating site while maintaining their flexible nature; Scheme 4.1. The deprotonating behaviour of additional functional group and its participation or non-participation in coordination to metal ions controls the oxidation state of central metal ions [170].

In this chapter, we report manganese (III) complex of Schiff base derived from salicylaldehyde and 1,3-diamino-2-hydroxypropane (Scheme 4.1:  $H_3\text{sal-dahp}$ , **4.I**) and its encapsulation in the super cages of zeolite-Y. The catalytic activity of neat as well as encapsulated complexes has been tested for the liquid phase oxidation of benzoin.





H<sub>3</sub>sal-dahp (4.I)

**Scheme 4.1.** Structure of ligand.

## 4.2. Experimental Section

### 4.2.1. Materials

Salicylaldehyde (Sisco research, India) and 1,3-diamino-2-hydroxypropane (Aldrich, U.S.A.) were used as obtained. Details of other chemicals, solvents details are given in Chapter 2.

### 4.2.2. Methods

Details of instrumentation are given in chapter 2.

### 4.2.3. Preparations

#### 4.2.3.1. Preparation of H<sub>3</sub>sal-dahp (4.I)

Ligand H<sub>3</sub>sal-dahp was prepared as reported previously [170]. Salicylaldehyde (2.44 g, 20 mmol) was dissolved in 50 ml of methanol. A solution of 1,3-diamino-2-hydroxypropane (0.90 g, 10 mmol) dissolved in 10 ml methanol was added drop wise to the above solution and the reaction mixture was stirred for 2 h. On standing the yellow solid slowly separated out which was filtered, washed with minimum of methanol and dried in a vacuum desiccator over silica gel. Yield 5.36 g (90%) Anal. calcd. for C<sub>17</sub>H<sub>18</sub>N<sub>2</sub>O<sub>3</sub> (298.34): C, 68.4; H, 6.1; N, 9.4. Found: C, 68.0; H, 6.9; N, 9.5. <sup>1</sup>H NMR (DMSO-d<sub>6</sub>, δ/ppm): 13.56 (br, 2H, phenolic OH), 8.54 (s, 2H, -CH=N-), 7.47-6.90 (m, 8H), 5.24 (br, 1H, -OH), 4.03 (s, 1H, -CH), 3.77 (q, 2H, -CH<sub>2</sub>), 3.56 (q, 2H, -CH<sub>2</sub>).

#### 4.2.3.2. Preparation of [Mn<sup>III</sup>(sal-dahp)H<sub>2</sub>O](4.1)

A filtered solution of manganese acetate (0.735 g, 3 mmol) in methanol (15 ml) was added to a solution of H<sub>3</sub>sal-dahp (0.895 g, 3 mmol) in methanol (15 ml) and the obtained reaction mixture was stirred for 5 h. Air was passed slowly through the solution for ca. 12 h and then volume was reduced to ca. 10 ml. Upon

cooling the solution to ca. 10 °C for over night complex **4.1** separated out which was filtered, washed with methanol and dried in vacuum over silica gel. Yield: 0.645 g (58.3%). Anal. Calc. for  $C_{17}H_{17}N_2O_2Mn$ (368.27): C, 55.58; H, 4.39; N, 7.63 %. Found: C, 55.2; H, 4.5; N, 7.4%.

#### **4.2.3.3. Preparation of $[Mn^{III}(sal-dahp)H_2O]-Y$ (4.2)**

A mixture of  $[Mn^{II}]-Y$  (3.0 g) and  $H_3sal-dahp$  (3.0 g) was mixed in methanol (40 ml) and the reaction mixture was refluxed for 15 h in an oil bath with stirring. The resulting material was suction filtered and washed with water thoroughly. It was then extracted with methanol using Soxhlet extractor until the complex was free from unreacted ligand. After filtering, the solid was suspended in aqueous 0.01M NaCl solution and stirred while passing air for 15 h. The resulting solid was filtered, washed with water till no precipitate of AgCl was observed in the filtrate on treating with  $AgNO_3$ . Finally it was dried at 120 °C for several hours. Yield: 3.1 g. Found (AAS): Mn, 1.34% (0.24 mmol/ g).

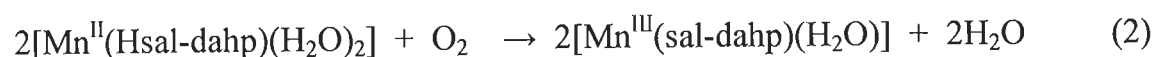
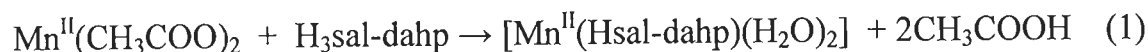
#### **4.2.4. Catalytic activity study: Oxidation of Benzoin**

Complexes  $[Mn^{III}(sal-dahp)(H_2O)]$  (**4.1**) and  $[Mn^{III}(sal-dahp)(H_2O)]-Y$  (**4.2**) have been used as catalyst to carry out the oxidation of benzoin. All reactions were carried out in a 50 ml two-neck glass reaction flask fitted with a water circulated condenser. In a typical reaction, benzoin (1.06 g, 5 mmol), aqueous 30%  $H_2O_2$  (1.14 g, 10 mmol) and catalyst (0.020 g) were mixed in methanol (20 ml) and the reaction mixture was heated at reflux with continuous stirring. The reaction was monitored by withdrawing small aliquots of the reaction mixture at every 30 min and analyzing them quantitatively by gas chromatography. The identities of the products were confirmed by GC-MS. The effects of various parameters, such as amounts of oxidant, catalyst and solvent were studied in order to see their effect on the conversion and selectivity of the reaction products.

### 4.3. Results and Discussion

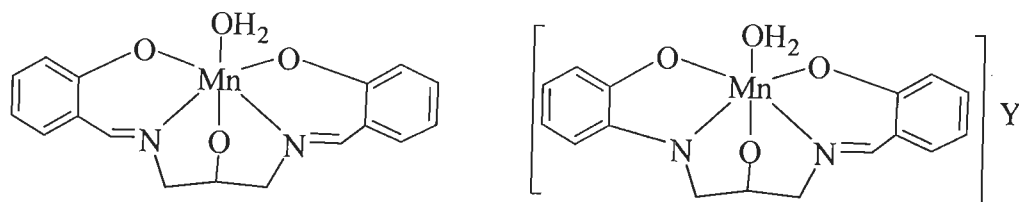
#### 4.3.1. Synthesis and solid state characteristics

Reaction of  $\text{Mn}^{\text{II}}(\text{CH}_3\text{COO})_2$  with  $\text{H}_3\text{sal-dahp}$  (**4.I**) in refluxing methanol followed by aerial oxidation yielded complex  $[\text{Mn}^{\text{III}}(\text{sal-dahp})(\text{H}_2\text{O})]$  (**4.1**). Equations (1) and (2) present the reactions involved:



Encapsulation of  $[\text{Mn}^{\text{III}}(\text{sal-dahp})(\text{H}_2\text{O})]$  (**4.1**) in the cavity of zeolite-Y involved the exchange of  $\text{Mn}^{2+}$  with  $\text{Na}^+$  of Na-Y in water to form zeolite- $[\text{Mn}^{\text{II}}]$ -Y species which is followed by the reaction of metal exchanged zeolite-Y with  $\text{H}_3\text{sal-dahp}$  (**4.I**) in methanol to give  $[\text{Mn}^{\text{II}}(\text{Hsal-dahp})(\text{H}_2\text{O})_2]$ -Y. Oxidation of  $[\text{Mn}^{\text{II}}(\text{Hsal-dahp})(\text{H}_2\text{O})_2]$ -Y in methanol finally provides  $[\text{Mn}^{\text{III}}(\text{sal-dahp})(\text{H}_2\text{O})]$ -Y (**4.1**). The remaining uncomplexed metal ions in zeolite were removed by ion-exchange with aqueous 0.01 M NaCl solution. Extraction of impurities with methanol was carried out by Soxhlet extraction, thus removing the excess free ligand as well as metal complex formed on the surface of the zeolite-Y if any. As the crude mass was extensively extracted, the metal content found (1.34%) after encapsulation is only due to the presence of Mn(III) complex in the cavities of the zeolite-Y. The diagonal dimension of the closely related complex,  $[\text{Cu}^{\text{II}}(\text{pydx-en})]$ [28] and  $[\text{Mn}^{\text{III}}(\text{pydx-en})\text{Cl}(\text{H}_2\text{O})]$  (see chapter 2) is ca. 12 Å which suggests that they will fit well into the super cages of the zeolite-Y and will not pass through the apertures of ca. 7.4 Å [77].  $[\text{Mn}^{\text{III}}(\text{sal-dahp})(\text{H}_2\text{O})]$  (**4.1**) was characterized by elemental analysis, IR and electronic spectroscopic studies. Encapsulated complex was additionally characterized by Field-Emission-Scanning Electron Micrograph (FE-SEM), Energy Dispersive X-Ray analysis (EDX) and powder X-ray Diffraction (XRD) Studies. The molecular formula of the

encapsulated complex is based on the corresponding neat complexes. Scheme 4.2 presents the structural formula and binding sets proposed for these complexes



Scheme 4.2. Proposed structures of complexes.

### 4.3.2. IR spectral studies

Table 4.1 summarizes IR data for the compounds discussed in this work. The IR spectra of H<sub>3</sub>sal-dahp (**4.I**) exhibits a sharp band due to  $\nu(\text{C}=\text{N})$  (azomethine) stretch at  $1633\text{ cm}^{-1}$ . This band shifts to lower wave number in complexes, indicating coordination of the azomethine nitrogen to the manganese. The presence of several medium intensity bands between  $3000$  and  $2500\text{ cm}^{-1}$  in the ligands as well as in the complexes suggest the existence of hydrogen bonding and C-H stretching due to  $-\text{CH}_2$ . The coordination of the phenolic oxygen could not be ascertained from IR data but it is considered coordinated based on the structurally characterized similar complex  $[\text{V}^{\text{IV}}\text{O}(\text{Hsal-dahp})]$ [170]. However, the presence of two medium intensity bands at  $574\text{--}587$  and  $457\text{--}462\text{ cm}^{-1}$  due to  $\nu(\text{Mn-O})$  and  $\nu(\text{Mn-N})$ , respectively should suggest the coordination of phenolic as well azomethine nitrogen atoms.

Table 4.1. IR spectral data of ligand and complexes

Compounds	IR / $\text{cm}^{-1}$		
	$\nu(\text{C}=\text{N})$	$\nu(\text{Mn-O})$	$\nu(\text{Mn-N})$
H <sub>3</sub> sal-dahp ( <b>4.I</b> )	1633		
$[\text{Mn}^{\text{III}}(\text{sal-dahp})(\text{H}_2\text{O})]$ ( <b>4.1</b> )	1625	587	462
$[\text{Mn}^{\text{III}}(\text{sal-dahp})(\text{H}_2\text{O})]\text{-Y}$ ( <b>4.2</b> )	1631	574	457

### 4.3.3. Electronic absorption studies

Electronic spectral data of ligand and complexes are presented in Table 4.2 and spectra of  $[\text{Mn}^{\text{III}}(\text{sal-dahp})(\text{H}_2\text{O})]$  (4.1) and  $[\text{Mn}^{\text{III}}(\text{sal-dahp})(\text{H}_2\text{O})]\text{-Y}$  (4.2) are reproduced in Figures 4.1 and 4.2, respectively. The UV spectra of the  $\text{H}_3\text{sal-dahp}$  (4.1) shows four sharp absorption maxima at 215, 256, 282 and 316 nm (see Table 4.2). First two bands are assignable due to  $\phi \rightarrow \phi^*$ , and  $\pi \rightarrow \pi^*$  transitions, respectively while last two are split bands of  $n \rightarrow \pi^*$  transition. Electronic spectrum of  $[\text{Mn}^{\text{III}}(\text{sal-dahp})(\text{H}_2\text{O})]$  (4.1) recorded in methanol exhibits a weak band at 574 nm in the visible region. For partially distorted  $d^4$  system, such  $d-d$  transition has been assigned to  ${}^5\text{E} \rightarrow {}^5\text{T}$  transition. The band at ca. 380 nm is attributable to phenolate  $\text{O}(p_\pi) \rightarrow \text{Mn}(d_{\pi^*})$  ligand to metal charge transfer transition. The remaining UV bands are similar to those appearing in the ligand. Only two bands in the UV region could be observed for encapsulated complex  $[\text{Mn}^{\text{III}}(\text{sal-dahp})(\text{H}_2\text{O})]\text{-Y}$  (4.2). Band due to either charge transfer or  $d-d$  transition could not be located due to poor loading of complex in Zeolite-Y.

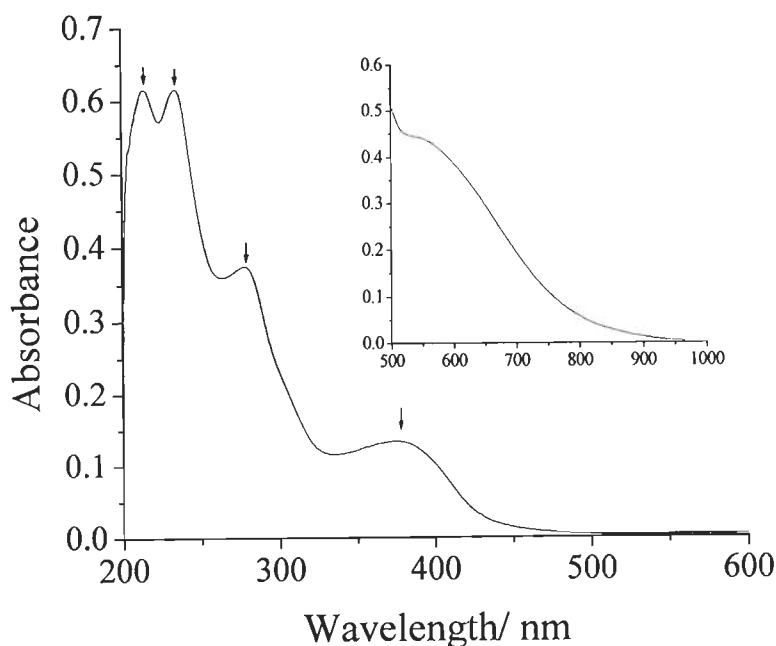


Figure 4.1. Electronic spectrum of  $[\text{Mn}^{\text{III}}(\text{sal-dahp})(\text{H}_2\text{O})]$  (4.1).

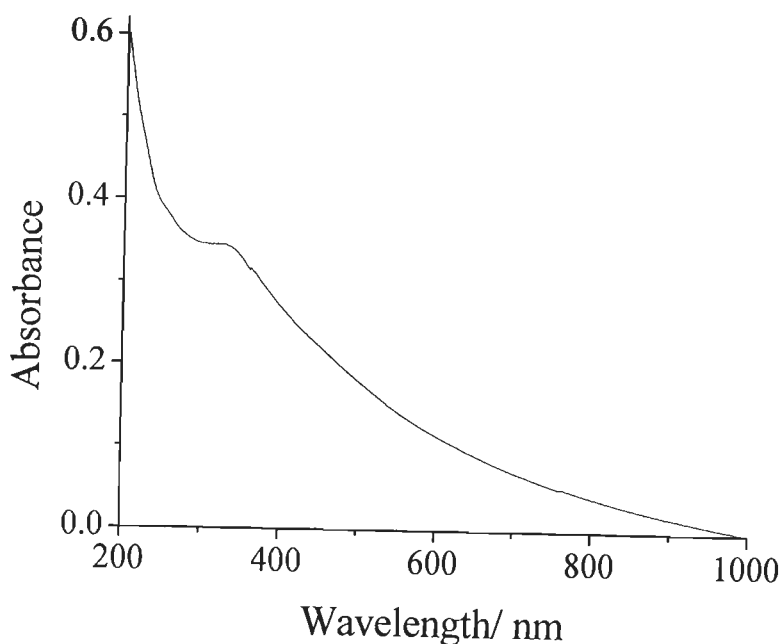


Figure 4.2. Electronic spectrum of  $[\text{Mn}^{\text{III}}(\text{sal-dahp})(\text{H}_2\text{O})]\text{-Y}$  (4.2)

Table 4.2. Electronic spectral data of ligand and complexes.

Compound	Solvent	$\lambda(\text{nm})$
$\text{H}_3\text{sal-dahp}$	MeOH	215, 256, 282, 316
$[\text{Mn}^{\text{III}}(\text{sal-dahp})(\text{H}_2\text{O})]$ (4.1)	MeOH	215, 235, 280, 380, 574
$[\text{Mn}^{\text{III}}(\text{sal-dahp})(\text{H}_2\text{O})]\text{-Y}$ (4.2)	MeOH	250, 330

#### 4.3.4. Powder X-ray Diffraction Studies

The powder X-ray diffraction patterns of Na-Y,  $[\text{Mn}^{\text{II}}]\text{-Y}$  and encapsulated complex  $[\text{Mn}^{\text{III}}(\text{sal-dahp})(\text{H}_2\text{O})]\text{-Y}$  (4.2) were recorded at  $2\theta$  values between  $5^\circ$  and  $70^\circ$ , and patterns are presented in Figure 4.3. Essentially similar diffraction patterns for all three samples were observed except a slightly weaker intensity for the zeolite having metal complex encapsulated. These observations indicate that the framework of the zeolite has not undergone any structural change during incorporation of the catalyst and hence crystallinity of the zeolite-Y is preserved during encapsulation. This is expected as  $[\text{Mn}^{\text{III}}(\text{sal-dahp})(\text{H}_2\text{O})]\text{-Y}$  (4.2) will fit nicely without any strain into the cavity of zeolite-Y. No new peaks due to

encapsulated complex were detected in the zeolite encapsulated sample possibly due to very low percentage loading of metal complex.

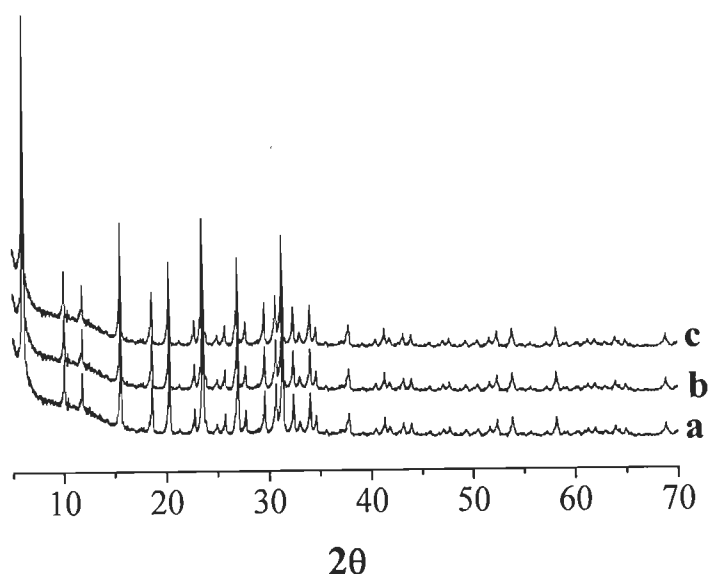


**Figure 4.3.** XRD patterns of Na-Y (a),  $[\text{Mn}^{\text{II}}]\text{-Y}$  (b) and  $[\text{Mn}^{\text{III}}(\text{sal-dahp})(\text{H}_2\text{O})]\text{-Y}$  (c).

#### 4.3.5. Field-Emission-Scanning Electron Micrograph (FE-SEM) and Energy Dispersive X-Ray analysis (EDX) studies

The field emission scanning electron micrograph (FE-SEM) of  $[\text{Mn}^{\text{III}}(\text{sal-dahp})(\text{H}_2\text{O})]$  (4.1) along with their energy dispersive X-ray analysis (EDX) profile are presented in Figure 4.4. Accurate information on the morphological changes in terms of exact orientation of ligand coordinated to the metal ion has not been possible due to poor loading of the metal complex. However, it is clear from the micrograph that zeolite having encapsulated manganese complex has well defined crystals and there is no indication of the presence of any metal ion or complex on the surface. Energy dispersive X-ray analysis plot, evaluated semi-quantitatively, supports this conclusion as no manganese or nitrogen contents were noted on the spotted surface in the plot for  $[\text{Mn}^{\text{III}}(\text{sal-dahp})(\text{H}_2\text{O})]$ . Only small amount of

carbon (ca. 26 %) but no nitrogen on the spotted surfaces suggest the presence of trace amount of adsorbed solvent (methanol) from which it was finally washed after Soxhlet extraction. An amount of ca. 2% sodium suggests the exchange of remaining free vanadium ion by sodium ion during re-exchange process. The average silicon and aluminium percentage obtained were ca. 7 % and ca. 3%, respectively.

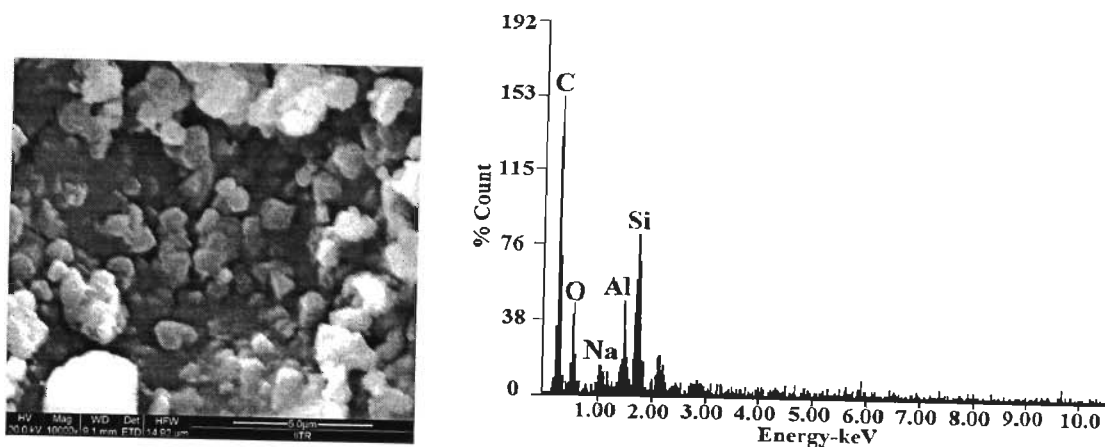
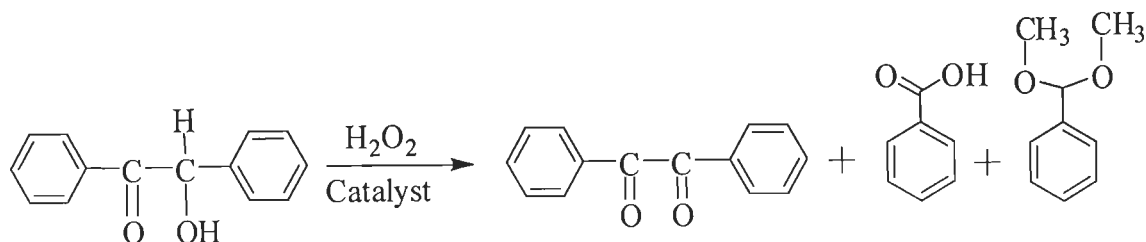


**Figure 4.4.** Field emission-scanning electron micrograph of  $[\text{Mn}^{\text{III}}(\text{sal-dahp})\text{H}_2\text{O}]\cdot\text{Y}$  and the corresponding energy dispersive X-ray analysis plot .

#### 4.3.6. Oxidation of benzoin

Oxidation of benzoin, a secondary alcohol, has attracted attention in recent years because one of its oxidized products, benzil, is a useful intermediate for the synthesis of heterocyclic compounds and benzylic acid rearrangements [128]. The catalytic activity of neat as well as encapsulated manganese complexes was studied here for the oxidation of benzoin using  $\text{H}_2\text{O}_2$  as oxidant. Three main oxidation products obtained are benzil, benzoic acid and benzaldehyde-dimethylacetal (Scheme 4.3). These are the same products obtained earlier using catalysts reported in Chapter 2.





**Scheme 4.3.** Oxidized products of benzoin.

The reaction conditions were optimized for the maximum oxidation of benzoin by studying three different parameters viz. the effect of amount of oxidant (moles of  $\text{H}_2\text{O}_2$  per mole of benzoin), catalyst (amount of catalyst per mole of benzoin) and solvent volume of the reaction mixture in detail.

The effect of  $\text{H}_2\text{O}_2$  was studied by considering substrate to oxidant ratios of 1:1, 1:2 and 1:3 for the fixed amount of benzoin (1.06 g, 5 mmol) and  $[\text{Mn}^{\text{III}}(\text{sal-dahp})(\text{H}_2\text{O})]\text{-Y}$  (0.020 g) in refluxing methanol (20 ml). Figure 4.5 presents the conversion obtained as a function of time in each case. As shown in figure, the conversion increases from 72.6% to 86.1% on increasing substrate to oxidant ratios from 1:1 to 1:2. Further increment of  $\text{H}_2\text{O}_2$  has no effect on the net oxidation of benzoin.

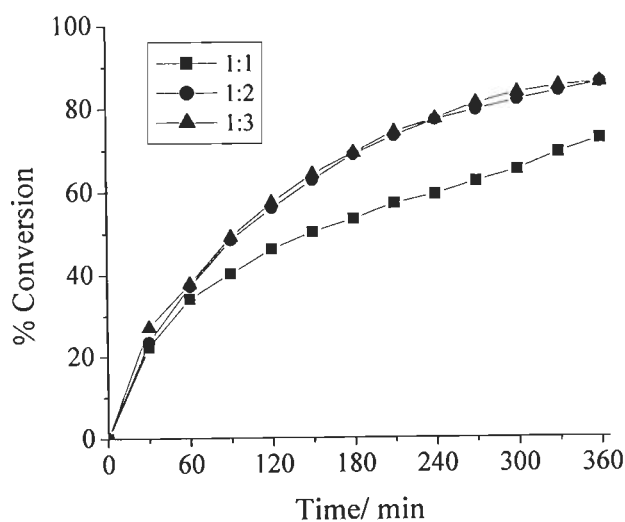


**Figure 4.5.** Effect of amount of  $\text{H}_2\text{O}_2$  on the oxidation of benzoin as a function of time. Other reaction conditions: benzoin (1.06 g, 5 mmol),  $[\text{Mn}^{\text{III}}(\text{sal-dahp})(\text{H}_2\text{O})]\text{-Y}$  (0.020 g) and methanol (20 mL).

Similarly, three different amounts of catalysts i.e. 0.015, 0.020 and 0.025 were considered for the fixed amount of benzoin (1.06 g, 5 mmol) and 30% H<sub>2</sub>O<sub>2</sub> (1.13 g, 10 mmol) methanol (20 mL) to see their effect on the conversion of benzoin. As illustrated in Figure 4.6, 0.020 g catalyst was sufficient to effect 86.1 % conversion while increasing the amount of catalyst (0.025 g) did not show improvement in the oxidation of benzoin except slight reduction in time to reach the steady-state of the reaction and 0.015 g catalyst gave only 79.5% conversion. Thus, higher amount of catalyst is not required to obtain maximum oxidation of benzoin.

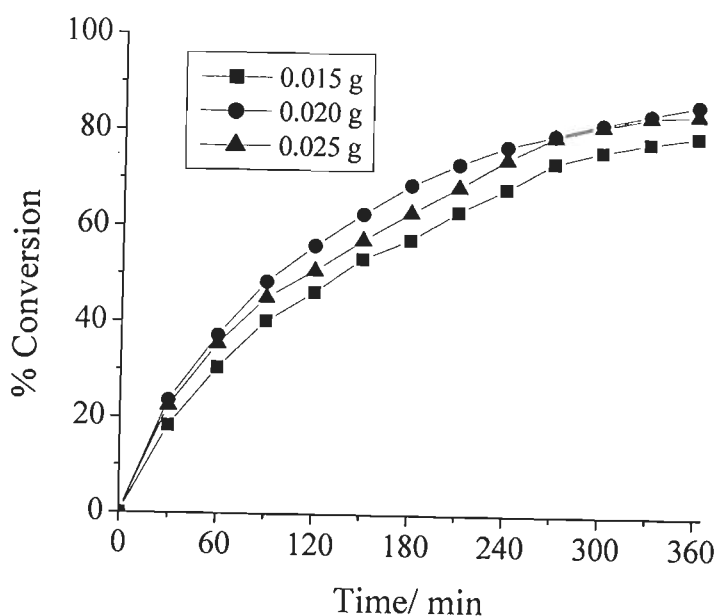


**Figure 4.6.** Effect of amount of catalyst on the oxidation of benzoin as a function of time. Other reaction conditions: benzoin (1.06 g, 5 mmol), H<sub>2</sub>O<sub>2</sub> (1.13 g, 10 mmol) and methanol (20 mL).

Variation in the volume of the solvent was also studied by taking 20, 25 and 30 ml of methanol. It was observed that 20 ml of methanol was sufficient enough for benzoin (1.06 g, 5 mmol), [Mn<sup>III</sup>(sal-dahp)(H<sub>2</sub>O)]-Y (0.020 g) and H<sub>2</sub>O<sub>2</sub> (1.13 g, 10 mmol) to give good transformation of benzoin while running the reaction at reflux temperature; Figure 4.7.

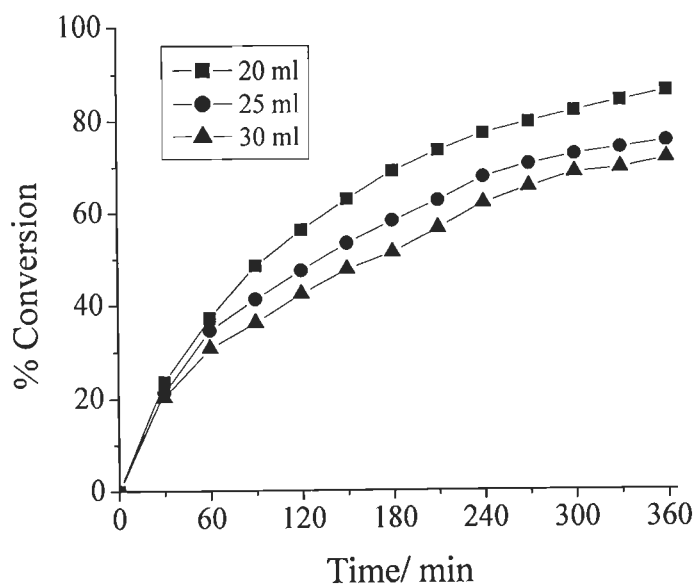


**Figure 4.7.** Effect of amount of solvent on the oxidation of benzoin as a function of time. Other reaction conditions: benzoin (1.06 g, 5 mmol),  $[\text{Mn}^{\text{III}}(\text{sal-dahp})(\text{H}_2\text{O})]\text{-Y}$  (0.020 g) and  $\text{H}_2\text{O}_2$  (1.13 g, 10 mmol).

All reaction conditions along with conversion of benzoin are summarized in Table 4.3.

**Table 4.3.** Conversion of benzoin (1.06 g, 5 mmol) using  $[\text{Mn}^{\text{III}}(\text{sal-dahp})(\text{H}_2\text{O})]\text{-Y}$  as catalyst in 6 h of reaction time under different reaction conditions.

Entry No.	Catalyst (g)	$\text{H}_2\text{O}_2$ (g, mmol)	Acetonitrile (ml)	% Conversion
1	0.020	0.565, 5	20	72.6
2	0.020	1.13, 10	20	86.1
3	0.020	1.695, 15	20	86.0
4	0.015	1.13, 10	20	79.5
5	0.025	1.13, 10	20	84.0
6	0.020	1.13, 10	25	75.2
7	0.020	1.13, 10	30	71.4

Thus, the optimized reaction conditions concluded for the oxidation of 5 mmol (1.06 g) of benzoin are:  $[\text{Mn}^{\text{III}}(\text{sal-dahp})(\text{H}_2\text{O})]\text{-Y}$  (0.020 g),  $\text{H}_2\text{O}_2$  (1.13 g, 10 mmol) and methanol (20 ml) (entry no. 2 of Table 4.3). This condition is almost same to that optimized in Chapter 2. Under these conditions, a maximum of 86.1 % oxidation of benzoin with turn over frequency of 152 was obtained after 6 h of reaction time. At this conversion the selectivity of various products obtained are presented in Table 4.4. The encapsulated catalyst separated from the reaction mixture after catalytic action was washed with acetonitrile, dried and subjected to further catalytic reaction for the oxidation of benzoin under similar conditions. The obtained results are also presented in Table 4.4. It is clear from the table that catalyst is still active after recycle and exhibits 84.8% conversion.

**Table 4.4.** Conversion of benzoin, TOF and selectivity data of products

Catalyst	% Conv.	TOF ( $\text{h}^{-1}$ )	% Selectivity		
			Benzil	Benzoic acid	Dimethyl-aetal
$[\text{Mn}^{\text{III}}(\text{sal-dahp})(\text{H}_2\text{O})]\text{-Y}$	86.1	152	28.6	59.2	12.2
$[\text{Mn}^{\text{III}}(\text{sal-dahp})(\text{H}_2\text{O})]\text{-Y}^{\text{a}}$	84.8		23.8	62.7	13.5
$[\text{Mn}^{\text{III}}(\text{sal-dahp})(\text{H}_2\text{O})]$	91.8	188	79.1	14.5	5.8
Without catalyst	8.7	-		7.1	27.3

<sup>a</sup> First cycle of used catalyst.

Figure 4.8 presents the selectivity of various products along with the conversion of benzoin as a function of time for catalyst  $[\text{Mn}^{\text{III}}(\text{sal-dahp})(\text{H}_2\text{O})]\text{-Y}$  under the best suited experimental conditions. It is clear from the plot that three reaction products form after 30 min of reaction time in the selectivity order: benzil (55.9%) > benzoic acid (42.7%) > benzaldehyde-dimethylacetal (1.3%). The selectivity of benzil decreases slowly but continuously with time and reaches 22.3 % after 6 h while the selectivity of benzoic acid follows just opposite trend and reaches 64.3%. The selectivity of benzaldehyde-dimethylacetal, which is much

less in the beginning, improves slowly and reaches 13.4 % at the end of 6 h. Thus, with the maximum benzoin oxidation of 86.1% after 6 h of reaction time, the selectivity of the reaction products varies in the order: benzoic acid (64.3 %) > benzil (22.3 %) > benzaldehyde-dimethylacetal (13.4 %).

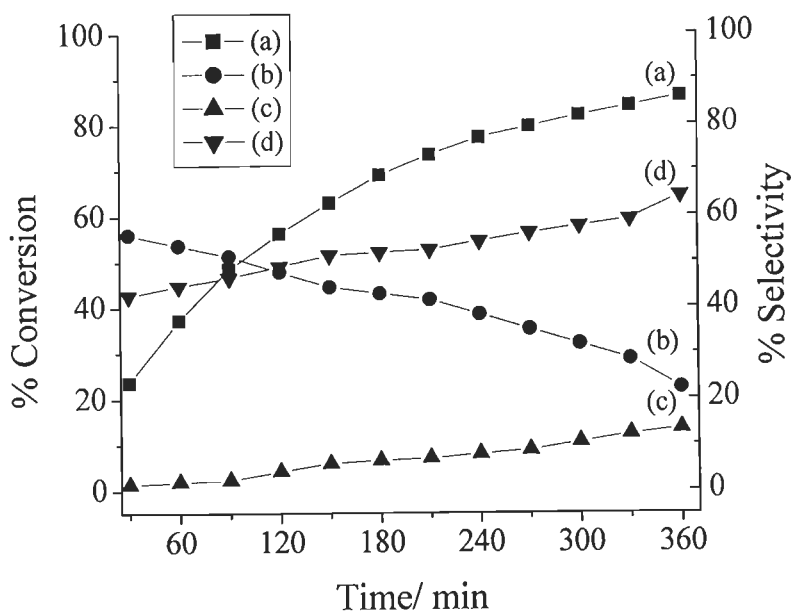


**Figure 4.8.** Conversion of benzoin and variation in the selectivity of different reaction products as a function of time using  $[\text{Mn}^{\text{III}}(\text{sal-dahp})(\text{H}_2\text{O})]\text{-Y}$  as a catalyst: conversion of benzoin (a), selectivity of benzil (b), benzaldehyde-dimethylacetal (c) and benzoic acid (d).

The performance of neat complex  $[\text{Mn}^{\text{III}}(\text{sal-dahp})(\text{H}_2\text{O})]$  using the same mole concentration as used for zeolite-Y encapsulated complex  $[\text{Mn}^{\text{III}}(\text{sal-dahp})(\text{H}_2\text{O})]\text{-Y}$  has also been studied under the above optimized conditions. It was observed that the neat complex is also very active and gave 91.8% conversion in 6 h of reaction time. Here, the selectivity of the products follow different order: benzil (79.1%) >> benzoic acid (14.5%) > benzaldehyde-dimethylacetal (5.8%). The turn over frequency for the neat complex is higher than the encapsulated

complex. However, the easy removal of the encapsulated catalysts makes them better compared to their neat analogues.

Blank reaction under similar conditions gave only 8.7% conversion.

#### **4.3.7. Reactivity of complexes with H<sub>2</sub>O<sub>2</sub> and possible reaction mechanism**

In order to identify the intermediate form and possible reaction mechanism during catalytic reaction, the interaction of [Mn<sup>III</sup>(sal-dahp)(H<sub>2</sub>O)] (4.1) in methanol was studied with H<sub>2</sub>O<sub>2</sub> by electronic absorption spectroscopy; Figure 4.9. Thus, the stepwise additions of one drops portions of aqueous 30% H<sub>2</sub>O<sub>2</sub> (0.227 g, 2.003 mmol) dissolved in 5 mL of MeOH to 5 mL of ca.  $6.8 \times 10^{-4}$  M solution of [Mn<sup>III</sup>(sal-dahp)(H<sub>2</sub>O)] in MeOH results in the decrease in intensity of the 363 nm band without changing its position. The band appearing at 322 nm slowly flattens and finally disappears. Simultaneously, a band at 270 nm develops. The band at 220 nm also moves slowly to 210 nm with partial decrease in intensity. The change in visible region could only be observed with concentrated solution (see in set of Figure 4.9). Thus the d – d band appearing at 670 nm slowly loses its intensity with slight shift towards lower wavelength and finally appears as a weak shoulder at 570 nm. All these changes in spectra have been interpreted as the formation of Mn<sup>IV</sup>=O compound [117, 118]. Similar features have also been observed earlier for Mn(III) complexes (see Chapter 2). Interestingly, solutions of all complexes acquire original spectral patterns on keeping for long time.

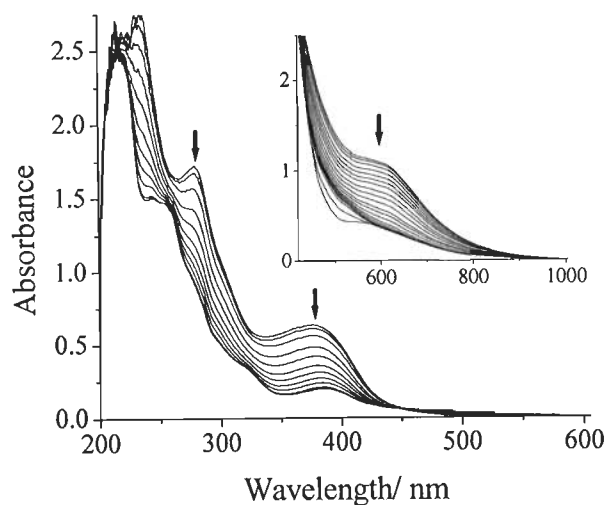


**Figure 4.9.** UV-Vis spectral changes observed during titration of  $[\text{Mn}^{\text{III}}(\text{sal-dahp})(\text{H}_2\text{O})]$  (**4.1**) with  $\text{H}_2\text{O}_2$ . The spectra were recorded after stepwise addition of one drops portions of aqueous 30%  $\text{H}_2\text{O}_2$  (0.227 g, 2.0 mmol) dissolved in 5 mL of MeOH to 5 mL of ca.  $6.8 \times 10^{-4}$  M solution of  $[\text{Mn}^{\text{III}}(\text{sal-dahp})(\text{H}_2\text{O})]$  (**4.1**) in MeOH. In set shows similar spectra recorded with 5 mL of  $1.36 \times 10^{-3}$  M solution of **4.1** in MeOH.

Based on the oxidation products obtained using tert-butylhydroperoxide (TBHP) and experiments carried out for vanadium complexes, at least two different pathways have been proposed to exist in solution [171]. In the first pathway, vanadium complex interacts with TBHP to give tert-butylperoxo complex which finally catalyzes abstraction of hydrogen from alcoholic group of benzoin to give benzil. By oxidative cleavage benzil produces benzoic acid which on subsequent esterification gives methylbenzoate. The acid produced by tert-butylhydroperoxide during catalytic reaction catalyzes the esterification. In the second pathway, benzoin reacts itself with vanadium complex to give benzoin coordinated vanadium complex where coordinated carbonyl oxygen takes up  $\text{H}^+$  ion produced by TBHP followed by detachment of vanadium complex to give

cationic species. This positively charged species on rearrangement followed by oxidative cleavage produces benzaldehyde and benzoic acid. Since benzaldehyde was not observed in the reaction mixture, it was speculated that benzaldehyde reacts with methanol in presence of  $H^+$  to give dimethylacetal. Benzoic acid may partly convert into methylbenzoate also. The formation of methylbenzoate by both mechanisms has been proposed as this form in highest yield. Both types of mechanism may also be considered to follow by manganese complex reported here as (i) it interacts with  $H_2O_2$  to give  $Mn^{IV}=O$  containing intermediate compound and (ii) it has one weakly coordinated water site where substrate can interact to give intermediate complex.

#### 4.4. Conclusions

Tribasic pentadentate ligand ( $H_3sal-dahp$ ) obtained by the condensation of salicylaldehyde and 1,3-diamino-2-hydroxypropane has been used to prepare complex  $[Mn^{III}(sal-dahp)(H_2O)]$  (4.1). Its encapsulation in the nano-cavity of zeolite-Y has also been achieved by interacting ligand with manganese (II)-exchange zeolite-Y followed by oxidation. These complexes have been characterized by elemental analysis, spectroscopic (IR and electronic) studies, scanning electron micrographs and X-ray diffraction patterns. The interaction of  $[Mn^{III}(sal-dahp)(H_2O)]$  (4.1) with  $H_2O_2$  has also been demonstrated in solution by treating 4.1 with  $H_2O_2$  in methanol. Under optimized reaction conditions, the oxidation of benzoin, catalyzed by  $[Mn^{III}(sal-dahp)(H_2O)]-Y$  (4.2) in refluxing methanol using  $H_2O_2$  as oxidant gave 86.1% conversion after 6 h of reaction time where selectivity of reaction products follow the order: benzoic acid (64.3 %) > benzil (22.3 %) > benzaldehyde-dimethylacetal (13.4 %). Neat complex is equally active and its oxidation products also follow the same order of selectivity. Two possible mechanisms, one via  $Mn^{IV}=O$  containing intermediate compound formation and second via direct interaction of benzoin with manganese through weakly water coordinated site have been proposed through which various substrates form.



# *CHAPTER 5*

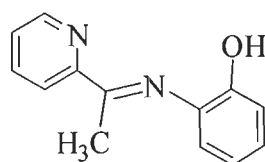
## **Oxidation of styrene and cyclohexene with TBHP catalyzed by copper(II) complex encapsulated in Zeolite-Y**

### **5.1. Introduction**

Catalytic properties of the transition metal complexes are generally controlled by metal ions present and their electronic and structural properties [172, 173]. The oxygen transformations catalyzed by transition metal complexes to produce more valuable organic compounds such as alcohols, aldehydes, and ketones, requires the selective oxidation of strong C–H bonds. In homogeneous systems the catalytic activity of the complexes slowly decreases with time which is normally due to their slow decomposition or dimerization and formation of dimeric oxo- or peroxy-bridged complexes. Heterogenization of the homogeneous catalysts (metal complexes) has been sought to avoid such complications [5, 6, 174]. Amongst heterogeneous catalysts, zeolite encapsulated metal complexes (ZEMC) hold a key place and is suggested as model compounds for enzyme mimicking [71, 175]. Encapsulations of complexes in the nano-cavity of zeolite-Y is a process that does not require interactions between the catalyst and the support, and thus maintain their inherent advantages of homogeneous catalytic systems [6]. Such zeolite encapsulated metal complexes (ZEMC) have provided the opportunity to develop catalytic processes for the selective oxidation of various substrates and are able to produce important intermediates as well as most industrial products [6, 56, 71, 174, 176–179]. In many cases these are more active, easily recyclable and maintain their activity after several cycles of catalytic use.

In the present investigation, we have encapsulated copper(II) complex of Schiff base derived from 2-acetylpyridine and o-aminophenol (Scheme 5.1) in the super cages of zeolite-Y and characterized. Its catalytic potential has been tested for the oxidation of styrene and cyclohexene. Selective oxidation of styrene has been reported using various homogeneous catalysts e.g. metal complexes [180–183] and supported heterogeneous catalysts such as mixed metal oxides [184],

zeolites [185], zeolite encapsulated metal complexes [51], metal complexes supported on mesoporous materials, etc. [31, 186]. Copper complexes encapsulated in the cavity of zeolite-Y have been used as catalyst for the oxidation of cyclohexene where various oxidation products such as cyclohexene oxide, 2-cyclohexene-1-one, 2-cyclohexene-1-ol, cyclohexane-1,2-diol etc. have been identified [74, 187–189].



**Scheme 5.1.** Structure of ligand: (Hacpy-oap; **5.I**)

## 5.2. Experimental

### 5.2.1. Materials and methods

Copper(II) nitrate (Qualigens, India), 2-acetylpyridine, *o*-aminophenol, cyclohexene (Himedia, India), styrene (Acros Organics, USA), 70% (w/v) *tert*-butylhydroperoxide (TBHP) (E. Merck, India), styrene (Acros Organics, U.S.A) was used as obtained. Y-zeolite (Si/Al = 10) was obtained from Indian Oil Corporation (R&D), Faridabad, India. All other chemical and solvent used were also of AR grade.

Instrumental details for this chapter are also presented in Chapter 2.

### 5.2.2. Preparations

#### 5.2.2.1. Preparation of Hacpy-oap (**5.I**)

A filtered solution of *o*-aminophenol (0.504 g, 5 mmol) in methanol (25 ml) was added to a solution of 2-acetylpyridine (0.605 g, 5 mmol) in methanol (25 ml) with stirring and the resulting reaction mixture was refluxed for 4 h. The volume of solvent was reduced to ca. 20 ml and in situ formed light brown ligand was used as such for further reaction.

#### **5.2.2.2. Preparation of [Cu<sup>II</sup>(acpy-oap)Cl] (5.1)**

A solution of ligand (equivalent to 5 mmol) was prepared as mentioned above in 50 ml of methanol. A filtered solution of CuCl<sub>2</sub>·2H<sub>2</sub>O (0.852 g, 5 mmol) prepared in 100 ml methanol was added to the above solution and the resulting reaction mixture was stirred at room temperature for 4 h. After reducing the solvent volume to ca. 20 ml, the flask was kept at ambient temperature for over night where brown mass separated out. This was filtered, washed with methanol and dried in vacuum over silica gel. Yield: 56%. Anal. Calc. for C<sub>13</sub>H<sub>11</sub>N<sub>2</sub>OCuCl (310.04): C, 50.32; H, 3.55; N, 9.03; Cl, 11.45%. Found: C, 50.5; H, 3.4; N, 9.2 ; Cl, 11.3%.

#### **5.2.2.3. Preparation of [Cu<sup>II</sup>]-Y**

An aqueous solution of Copper(II) nitrate (2.9 g, 12 mmol in 50 ml) was added to a suspension of Na-Y zeolite (5.0 g) in 250 ml of distilled water and the mixture was stirred at 90 °C for 24 h. The resulting bluish solid was filtered, washed with hot distilled water until filtrate was free from any metal ion content, and dried at 120 °C in air oven for 24 h. Found: Cu (ICP-MS), 7.6%.

#### **5.2.2.4. Preparation of [Cu<sup>II</sup>(acpy-oap)Cl]-Y (5.2)**

A methanolic solution of *o*-aminophenol (1.64 g, 15 mmol) in 15 ml was added to a solution of 2-acetylpyridine (1.82 g, 15 mmol) already dissolved in 25 ml of methanol. The obtained reaction mixture was refluxed for 4 h in an oil bath. An amount of 1.0 g of [Cu<sup>II</sup>]-Y was suspended to the above solution and the reaction mixture was heated under reflux for 15 h in an oil bath while stirring. The resulting light brown material was filtered, dried and soxhlet extracted with methanol followed by acetone to remove excess ligand and metal complex on the surface of the zeolite if any. The uncomplexed metal ions in zeolite were removed by treating with aqueous 0.01M NaCl solution (200 ml) with stirring for 8 h. It was then washed with double distilled water till no precipitate of AgCl was

observed in the filtrate on treating with  $\text{AgNO}_3$ . Finally it was dried at  $120^\circ\text{C}$  till constant weight. Found: Cu (ICP-MS), 2.6%.

### **5.2.3. Catalytic activity studies**

#### **5.2.3.1. Oxidation of styrene**

The catalytic oxidation of styrene was carried out in a 50 ml flask fitted with a water circulated condenser. An aqueous solution of 70 % *tert*-butylhydroperoxide (TBHP) (2.56 g, 20 mmol) and styrene (1.04 g, 10 mmol) were mixed in 20 ml of  $\text{CH}_3\text{CN}$  and the reaction mixture was heated at  $80^\circ\text{C}$  with continuous stirring in an oil bath. The reaction was considered to begin after addition of  $[\text{Cu}^{\text{II}}(\text{acpy-oap})\text{Cl}]\text{-Y}$  (0.035 g). During the reaction, the products were analyzed quantitatively by gas chromatography by withdrawing small aliquots after specific interval of time. The identities of the products were confirmed by GC-MS.

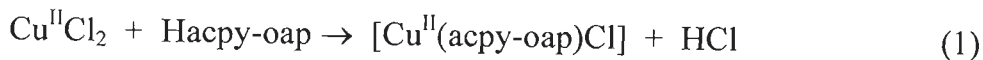
#### **5.2.3.2. Oxidation of cyclohexene**

An aqueous solution of 70% *tert*-butylhydroperoxide (TBHP) (2.56 g, 20 mmol), cyclohexene (0.82 g, 10 mmol) and catalyst (0.035 g) were mixed in 20 ml of  $\text{CH}_3\text{CN}$  and the reaction mixture was heated at  $75^\circ\text{C}$  with continuous stirring in an oil bath. The progress of the reaction was monitored as mentioned above and identity of the various products was confirmed by GC-MS.

## **5.3. Results and discussion**

### **5.3.1. Characterization of catalysts**

Reaction between equimolar amounts of  $\text{Cu}^{\text{II}}\text{Cl}_2$  and the ligand Hacpy-oap (5.1) in dry, refluxing methanol yields the brown complex  $[\text{Cu}^{\text{II}}(\text{acpy-oap})\text{Cl}]$  (5.1). The ligand coordinates out of its monoanionic (ONN(1-)) form; equation (1).



Encapsulation of  $[\text{Cu}^{\text{II}}(\text{acpy-oap})\text{Cl}]$  (**5.1**) in the nano cavity of the zeolite-Y involved the interaction of  $[\text{Cu}^{\text{II}}]\text{-Y}$  with excess Hacpy-oap in methanol where ligand slowly enters into the cavity of zeolite-Y due to its flexible nature and interacts with metal ions. Soxhlet extraction using methanol/ acetone finally purified the impure complex. The remaining uncomplexed metal ions in zeolite were removed by exchanging with aqueous 0.01 M NaCl solution. As one extra anionic ligand would be required to balance the overall charges on the  $\text{Cu}^{\text{II}}$ ,  $\text{Cl}^-$  of NaCl used during exchanged process fulfills this requirement. The presence of chloride ion in complex has been confirmed qualitatively. Hence, the formula of the encapsulated  $\text{Cu}^{\text{II}}$  complex may also be written as  $[\text{Cu}^{\text{II}}(\text{acpy-oap})\text{Cl}]$ ; the encapsulated complex is then abbreviated as  $[\text{Cu}^{\text{II}}(\text{acpy-oap})\text{Cl}]\text{-Y}$  (**5.2**). As impure sample of **5.2** was extracted with methanol and acetone, the copper content (2.6%) found after encapsulation is only due to the presence of  $[\text{Cu}^{\text{II}}(\text{acpy-oap})\text{Cl}]$  in the super cages of the zeolite-Y. Due to space constraint in the cavity of the zeolite-Y, **5.1** will exist in its monomeric form only in the nano cavity. Similarity in the spectral properties of neat as well as encapsulated complex (vide infra) suggests a square planar structure for encapsulated complex as well.

Scheme 5.2 provides structures of the complexes described here and characterized on the basis of spectroscopic (IR and UV/Vis) data, elemental analysis, FE-SEM, X-ray powder diffraction pattern and thermogravimetric analysis.

### **5.3.2. Powder X-ray diffraction studies**

The powder X-ray diffraction patterns of Na-Y,  $[\text{Cu}^{\text{II}}]\text{-Y}$  and encapsulated metal complex  $[\text{Cu}^{\text{II}}(\text{acpy-oap})\text{Cl}]\text{-Y}$  (**5.2**) were recorded at  $2\theta$  values between 5 and  $40^\circ$ . Figure 5.1 shows X-ray diffraction patterns of all these. The diffraction

patterns of encapsulated metal complex,  $[\text{Cu}^{\text{II}}]\text{-Y}$  and  $\text{Na-Y}$  are essentially similar except a slight change in the intensity of the bands in encapsulated complex. These observations indicate that the framework of the zeolite has not undergone any significant structural change during encapsulation. No new peaks were detected in the zeolite having encapsulated complex due to poor loading of metal complex in the nano cavity of zeolite-Y.

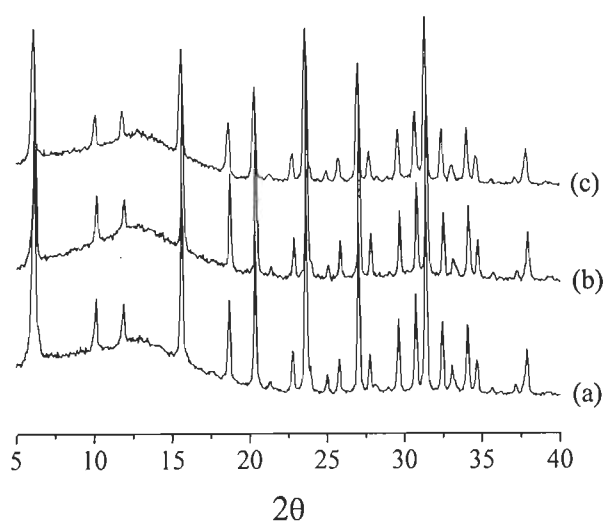


**Figure 5.1.** XRD patterns of (a)  $\text{Na-Y}$ , (b)  $\text{Cu}^{\text{II}}\text{-Y}$  and (c)  $[\text{Cu}^{\text{II}}(\text{acpy-oap})\text{Cl}]\text{-Y}$

### 5.3.3. Thermogravimetric analysis

The thermogravimetric analysis data of  $[\text{Cu}^{\text{II}}(\text{acpy-oap})\text{Cl}]\text{-Y}$  (5.2) along with the percent weight loss at different steps and their assignments are presented here. The thermogram of encapsulated complex indicates its decomposition in three steps, though these steps are overlapping. The first step involves the removal of just trapped water of ca. 3.8 % up to 150° C, while loss of water of ca. 9.8 % is associated with the structural frame work occurs in the temperature range 170–350 °C. The third step involves the slow but exothermic weight loss of ca. 19.2 % in a wider temperature range (350–800 °C) due to decomposition of the chelating ligand.

### 5.3.4. IR spectral studies

A partial list of IR spectral data is presented in Table 5.1. The intensity of the peaks in encapsulated complex is, though weak due to their low concentration in zeolite matrix, spectra of neat as well as encapsulated complexes show essentially similar bands. Comparison of spectra of these catalysts with ligand provides evidence for the coordination mode of the ligand in catalyst. IR spectrum of ligand exhibits  $\nu(\text{C}=\text{N})$  (azomethine) at  $1587\text{ cm}^{-1}$  and this band moves towards lower wave numbers ( $1583\text{ cm}^{-1}$  in **5.1** and  $1585\text{ cm}^{-1}$  in **5.2**) in complexes, indicating the participation of the azomethine nitrogen atom in coordination. A weak band appearing at ca.  $1633\text{ cm}^{-1}$  is assigned due to the coordinated pyridine nitrogen. Absence of band due to hydroxyl group in complex  $[\text{Cu}^{\text{II}}(\text{acpy-oap})\text{Cl}]$  (**5.1**) indicates its deprotonation followed by coordination of oxygen to the metal while presence of such band in complex  $[\text{Cu}^{\text{II}}(\text{acpy-oap})\text{Cl}]\text{-Y}$  (**5.2**) is due to the presence of intra-zeolite water.

**Table 5.1.** IR and electronic spectral data of ligand, pure and encapsulated complexes

Compound	IR ( $\text{cm}^{-1}$ ) $\nu(\text{C}=\text{N})$	$\lambda_{\text{max}}$ (nm)
Hacpy-oap ( <b>5.1</b> )	1587	208, 236, 273, 428
$[\text{Cu}^{\text{II}}(\text{acpy-oap})\text{Cl}]$ ( <b>5.1</b> )	1633, 1583	235, 268, 432, 500
$[\text{Cu}^{\text{II}}(\text{acpy-oap})\text{Cl}]\text{-Y}$ ( <b>5.2</b> )	1631, 1585	235, 270, 440

### 5.3.5. Electronic spectral studies

Table 5.1 also presents electronic spectral data of ligand and complexes. The electronic spectrum of the ligand exhibits four bands at 208, 236, 273 and 428 nm. The low energy band (428 nm) is assigned to  $n - \pi^*$  transition, the bands at 236 and 273 nm are due to split band of  $\pi - \pi^*$  while 208 nm band is due to  $\phi - \phi^*$

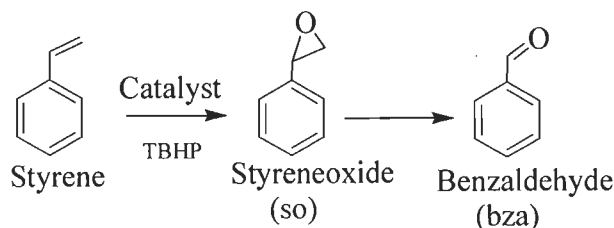


transition. All these bands are also present in the complex  $[\text{Cu}^{\text{II}}(\text{acpy-oap})\text{Cl}]$  (**5.1**) with slight variations. A broad band at 432 nm is assigned due to the ligand-to-metal charge transfer (LMCT) from the phenolate oxygen to an empty d orbital of copper. The  $n - \pi^*$  band merges with this band. In addition, a broad band at ca. 500 nm also appears and is assigned due to d – d transition of  $\text{Cu}^{\text{II}}$  ion. Encapsulated complex  $[\text{Cu}^{\text{II}}(\text{acpy-oap})\text{Cl}]\text{-Y}$  (**5.2**) displays only two bands at 206 and 270 nm in Nujol in the UV region and a LMCT band at 440 nm in the visible region. The d-d transition band could not be located due to poor loading of **5.1** in the zeolite-Y.

### 5.3.6. Catalytic activity studies

#### 5.3.6.1. Oxidation of styrene

The oxidation of styrene, catalyzed by  $[\text{Cu}^{\text{II}}(\text{acpy-oap})\text{Cl}]\text{-Y}$  was carried out using 70% tert-butylhydroperoxide (TBHP) as an oxidant to give styrene oxide and benzaldehyde along with only minor amounts of unidentified products; Scheme 5.2. These are common products and have been identified by others as well [56, 176–179]. In the presence of  $\text{H}_2\text{O}_2$ , further oxidation of styrene oxide to other products have also been reported [ see Chapters 2 and 3 and references there in].



**Scheme 5.2.** Oxidation products of styrene

In search of suitable reaction conditions to achieve the maximum oxidation of styrene, the effect of three different reaction parameters viz. amount of oxidant

(moles of TBHP per mole of styrene) and catalyst (amount of catalyst per mole of styrene), and temperature of the reaction were studied in detail.

The effect of TBHP on the oxidation of styrene is illustrated in Figure 5.2. Three different styrene/ TBHP molar ratios of 1:1, 1:2 and 1:3 were considered where the mixture of styrene (1.04 g, 10 mmol), catalyst (0.050 g) and oxidant were taken in 20 ml of CH<sub>3</sub>CN and the reaction was carried out at 80 °C (entry no. 1, 2 and 3 of Table 5.2). Increasing the styrene/ TBHP ratio from 1:1 to 1:2 increases the conversion from 34.7 % to 50.8 %. Further increasing the ratio to 1:3 brings the conversion down to 47.5 %. The reason for this may be due to the dilution of the reaction mixture by the presence of larger amount of water molecules in TBHP solution. It is, therefore, concluded that the 1:2 molar ratio is the best one to obtain the maximum styrene conversion of 50.8% in 7 h reaction time.

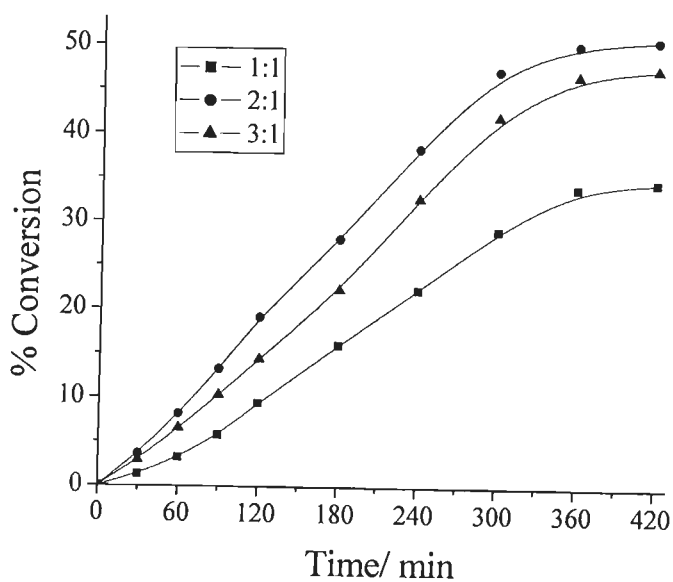


**Figure 5.2.** Effect of TBHP concentration (TBHP : styrene) on oxidation of styrene. Reaction conditions: styrene (1.04 g, 10 mmol), catalyst (0.050 g), CH<sub>3</sub>CN (20 ml) and temperature (80 °C).

Amount of catalyst also affects on the conversion. In order to optimize it, four different amounts of catalyst viz. 0.020, 0.035, 0.050 and 0.075 g were taken for the fixed operating conditions of styrene (1.04 g, 10 mmol) and TBHP (2.56 g, 20 mmol) in 20 ml of CH<sub>3</sub>CN at 80 °C. As shown in Figure 5.3 (entry no. 2, 5, 6 and 7 of Table 5.2), increasing the catalyst amount from 0.020 g to 0.035 g improved the styrene conversion from 36.6 to 60.2%. However, increasing the catalyst amount to 0.050 g and 0.075 g did not improve the conversion, thereby suggesting that 0.035 g of catalyst is sufficient to effect maximum conversion. The reason for lower conversion at higher catalyst amount may possibly be due to adsorption/chemisorptions of two reactants on separate catalyst particles, thereby reducing the chance to interact.

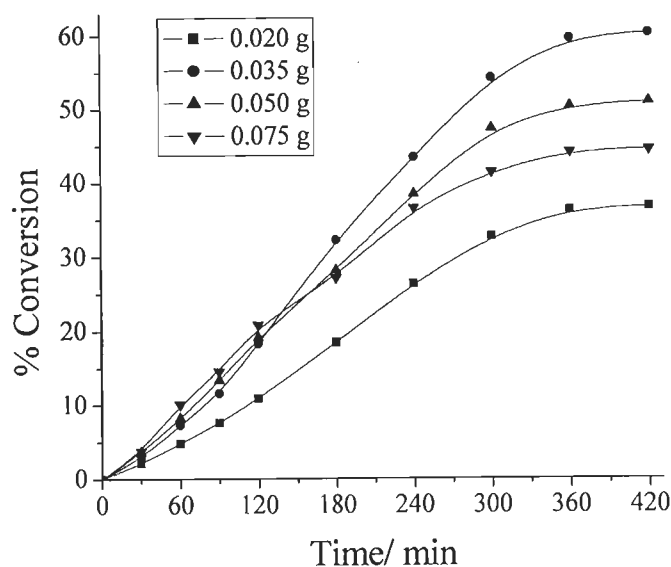


**Figure 5.3.** Effect of amount of catalyst per unit weight of styrene. Reaction conditions: styrene (1.04 g, 10 mmol), TBHP (2.56 g, 20 mmol), CH<sub>3</sub>CN (20 ml) and temperature (80 °C).

Figure 5.4 and entry no. 5, 7 and 8 of Table 5.2) show the effect of temperature on the oxidation of styrene while keeping amount of catalyst and

styrene/TBHP ratio optimized as above in 20 ml of CH<sub>3</sub>CN. From figure it is clear that increasing the temperature increase the conversion and running the reaction at 80 °C is the best to obtain 60.2% conversion in 7 h of reaction time.

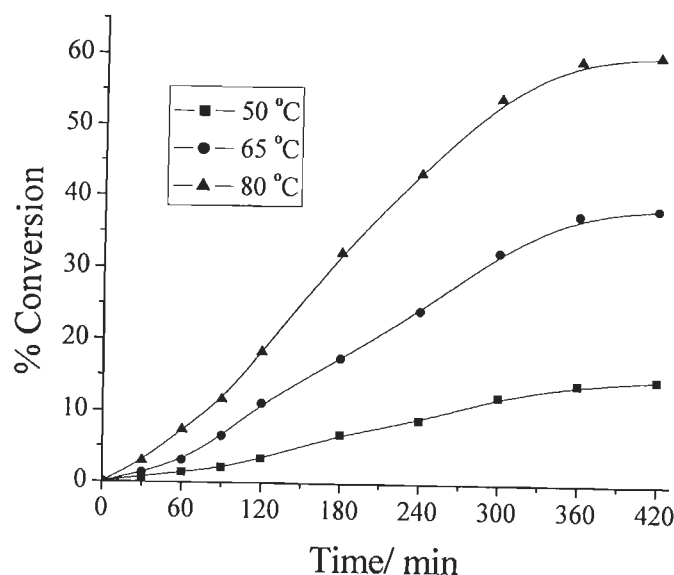


**Figure 5.4.** Effect of temperature on the oxidation of styrene. Reaction conditions: styrene (1.04 g, 10 mmol), catalyst (0.035 g), TBHP (2.56 g, 20 mmol) and CH<sub>3</sub>CN (20 ml).

**Table 5.2.** Conversion of styrene (1.04 g, 10 mmol) using [Cu<sup>II</sup>(acpy-oap)Cl]-Y as catalyst in 7 h of reaction time under different reaction conditions.

Entry No.	Catalyst (g)	TBHP (g, mmol)	Temp. (° C)	MeCN (ml)	Conv. %
1	0.050	1.28, 10	80	20	34.7
2	0.050	2.56, 20	80	20	50.8
3	0.050	3.84, 30	80	20	47.5
4	0.020	2.56, 20	80	20	36.6
5	0.035	2.56, 20	80	20	60.2
6	0.075	2.56, 20	80	20	44.4
7	0.035	2.56, 20	50	20	14.7
8	0.035	2.56, 20	65	20	38.6

Thus, for the maximum oxidation of 10 mmol of styrene other optimized parameters as concluded above (entry no. 5 of Table 5.2) are:  $[\text{Cu}^{\text{II}}(\text{acpy-oap})\text{Cl}]\text{-Y}$  (0.035 g), TBHP (2.56 g, 20 mmol),  $\text{CH}_3\text{CN}$  (20 ml) and temperature (80 °C).

The conversion of styrene along with TOF and selectivity of different reaction products under the optimized reaction conditions after 7 h of reaction time are presented in Table 5.3. It clear from table that styrene oxide an important product is obtained in major amount (78.2%) while benzaldehyde is obtained in minor amount (18.2%). Higher selectivity of styrene oxide can be explained from the fact that TBHP is milder oxidant, thus leads to the formation of styrene oxide in better yield and does not go to further oxidation considerably. After washing with acetonitrile and drying, the used catalyst was further used under similar conditions as mentioned above to check its recyclability. About 59.6% conversion of styrene obtained at the end of 7 h with similar selectivity order of products suggests its recyclability.

Neat complex  $[\text{Cu}^{\text{II}}(\text{acpy-oap})\text{Cl}]$  has been used as a catalyst precursor using same mole concentration of copper as in its zeolite encapsulated complex to compare its catalytic activity. Interestingly, this exhibited 38.6% conversion (Figure 5.5) when complex (0.0028 g, 0.009 mmol), styrene (1.04 g, 10 mmol), TBHP (2.56 g, 20 mmol),  $\text{CH}_3\text{CN}$  (20 ml) and the reaction was carried out at 80 °C. Here, the selectivity of different products follow the order: styrene oxide (73.4%) > benzaldehyde (20.7%). Thus, the order is same as obtained by encapsulated complex and the selectivity of individual products differs only slightly. Blank reaction under above reaction conditions gave 3% conversion. Thus, neat as well as encapsulated complexes both are good in catalytic activity. However, the recyclable nature and no leaching of  $[\text{Cu}(\text{acpy-oap})\text{Cl}]\text{-Y}$  makes it better over neat one.

**Table 5.3.** Percent conversion of styrene along with TOF and selectivity of different reaction products after 7 h of reaction time

Catalyst	% Conv.	TOF <sup>a</sup> (h <sup>-1</sup> )	% Selectivity <sup>b</sup>		
			so	bza	Other
[Cu <sup>II</sup> (acpy-oap)Cl]-Y	60.2	61	78.2	18.2	3.6
[Cu <sup>II</sup> (acpy-oap)Cl]-Y <sup>c</sup>	59.6	-	78.0	18.5	3.5
[Cu <sup>II</sup> (acpy-oap)Cl]	38.6	40	73.4	20.7	5.9

<sup>a</sup>TOF h<sup>-1</sup> (Turnover frequency): moles of substrate converted per mole of metal (in the solid state catalyst) per hour.

<sup>b</sup>For abbreviations see Scheme 5.2.

<sup>c</sup>First cycle of used catalyst.

Catalytic activity of the encapsulated complex [Cu<sup>II</sup>(acpy-oap)Cl]-Y compares well with other catalysts. Metal complex [Mn<sup>II</sup>(salen)] encapsulated in zeolite-Y exhibits ca. 30 % conversion of styrene using molecular oxygen as an oxidant in excess of *tert*-butylhydroperoxide as initiator [180]. Zeolite-Y encapsulated [V<sup>IV</sup>O(salphen)] exhibits 34.8 % conversion of styrene using TBHP as an oxidant [181]. Other zeolite encapsulated catalysts such as [Mn<sup>II</sup>(3-MeOsalen)]-Y (H<sub>2</sub>salen = bis(salicylaldehyde)-1,2-diaminoethane), [Mn<sup>II</sup>(3-MeOsalp<sub>n</sub>)]-Y and [Mn<sup>II</sup>(salp<sub>n</sub>)]-Y (H<sub>2</sub>salp<sub>d</sub> = bis(salicylaldehyde)-1,3-diaminopropane) exhibit only 17%, 8.7% and 7.4% conversions, respectively, using *tert*-butylhydroperoxide as oxidant [123]. A maximum of 56.7% conversion of styrene was reported using closely related catalyst [Cu<sup>II</sup>(sal-ambmz)Cl]-Y (Hsal-ambmz = Schiff base derived from salicylaldehyde and 2-aminomethylbenzimidazole) using H<sub>2</sub>O<sub>2</sub> as oxidant while [VO<sub>2</sub>(sal-ambmz)] showed much better conversion of ca. 97% [73].

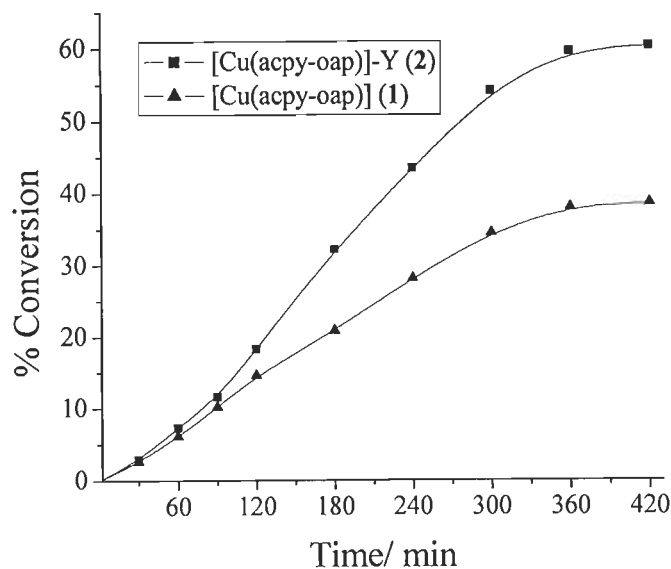
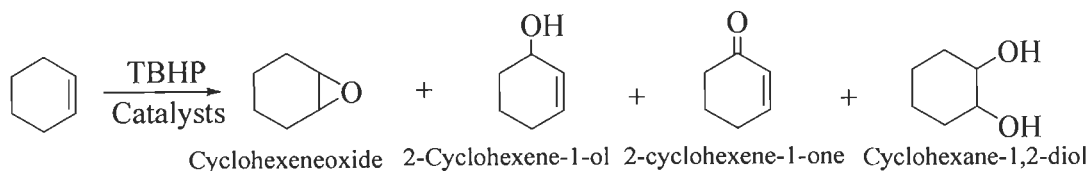


**Figure 5.5.** Effect of different catalysts  $[\text{Cu}(\text{acpy-oap})\text{Cl}]$  (5.1) and  $[\text{Cu}(\text{acpy-oap})\text{Cl}]\text{-Y}$  (5.2) on the oxidation of styrene.

### 5.3.6.2. Oxidation of cyclohexene

Complex  $[\text{Cu}^{\text{II}}(\text{acpy-oap})\text{Cl}]\text{-Y}$  also catalyzes the oxidation of cyclohexene by 70% tert-butylhydroperoxide (TBHP) as oxidant to give cyclohexene oxide, 2-cyclohexene-1-ol, 2-cyclohexene-1-one and cyclohexane-1,2-diol as presented in Scheme 5.3. Reaction conditions have also been optimized for the maximum oxidation of cyclohexene by varying different parameters.



**Scheme 5.3.** Oxidation products of cyclohexene.

In order to achieve suitable reaction conditions for a maximum oxidation of cyclohexene, four different cyclohexene to aqueous 70 % TBHP molar ratios viz 1:1, 1:2 and 1:3 were considered for the fixed amount of cyclohexene (0.82 g, 10

mmol) and catalyst (0.035 g) in 20 ml of MeCN and reaction was carried out at 75 °C. As illustrated in Figure 5.6 and entry no. 1, 2 and 3 of Table 5.4, a maximum of 41.1 % conversion was achieved in 6 h of contact time at a cyclohexene to TBHP molar ratio of 1:1. Increasing the ratio to 1:2 improved the conversion to 61.3 %, while further increasing the ratio to 1:3 brings the conversion back to 58.5 %.

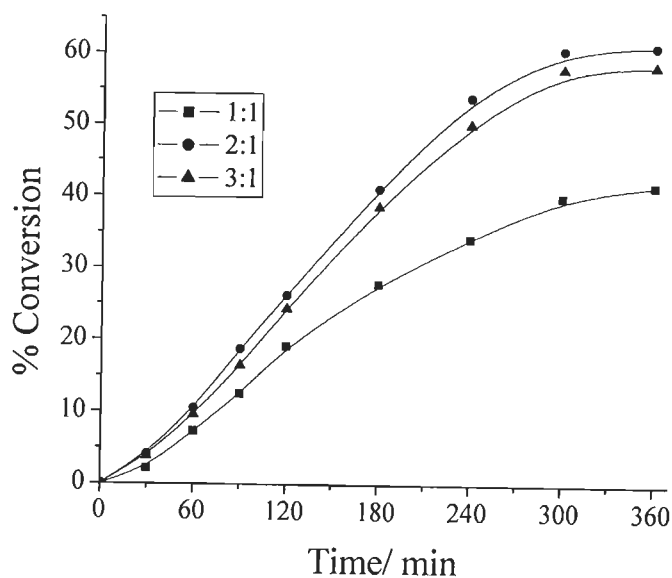
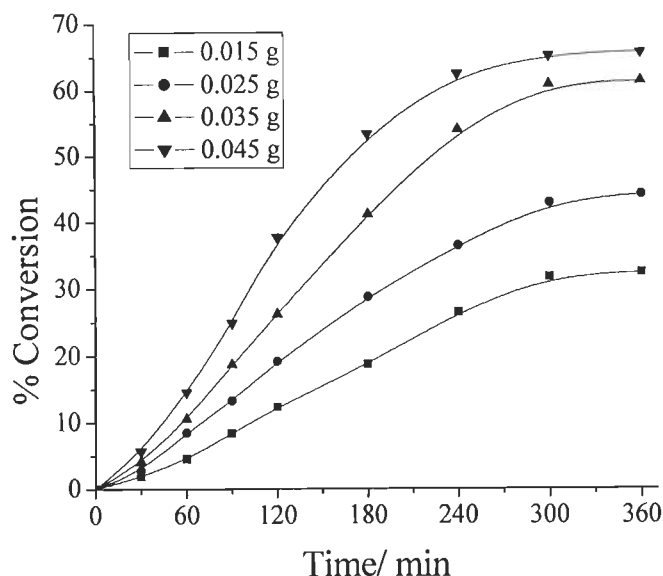


**Figure 5.6.** Effect of TBHP concentration (TBHP : cyclohexene) on oxidation of cyclohexene. Reaction conditions: cyclohexene (0.82 g, 10 mmol), catalyst (0.035 g), CH<sub>3</sub>CN (20 ml) and temperature (75 °C).

Under the operating conditions as fixed above i.e. cyclohexene (0.82 g, 10 mmol), TBHP (2.56 g, 20 mmol), MeCN (20 ml) and temperature (75 °C), the effect of catalyst considering three different amounts viz. 0.015, 0.025, 0.035 and 0.045 g as a function of time was studied ((entry no. 2, 4 - 6 of Table 5.4) and results are illustrated in Figure 5.7. A maximum of 32.3 % oxidative conversion was achieved in 6 h of reaction time with 0.015 g of catalyst. This conversion takes up increasing trend on further increasing the catalyst amount i.e. 44.1 % with

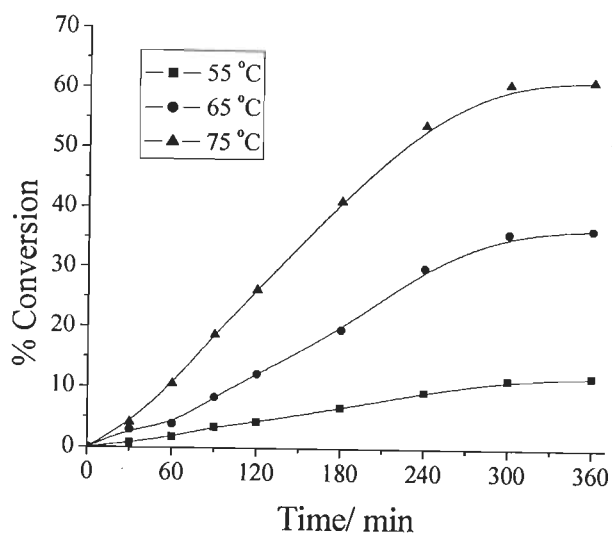


0.025 g, 61.3% with 0.035 g and 65.6 % with 0.045 g. However, 0.035 g of catalyst can be considered the suitable one as increasing the amount further increases the conversion as well as turn over rates only marginally.



**Figure 5.7.** Effect of amount of catalyst on oxidation of cyclohexene. Reaction conditions: cyclohexene (0.82 g, 10 mmol), TBHP (2.56 g, 20 mmol), CH<sub>3</sub>CN (20 ml) and temperature (75 °C).

After optimizing the cyclohexene to TBHP molar ratio and catalyst amount, temperature of the reaction medium was also varied in the range 55 - 75 °C (entry no. 2, 7 and 8 of Table 5.4) while keeping other parameters as optimized above. It is evident from Figure 5.8 that increasing the temperatures increase the conversion and 75 °C is the best one to obtain 61.3 % conversion in 6 h of reaction time.



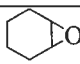
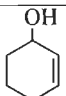
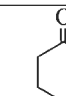

**Figure 5.8.** Effect of reaction temperature on the oxidation of cyclohexene. Reaction conditions: cyclohexene (0.82 g, 10 mmol), catalyst (0.035 g), TBHP (2.56 g, 20 mmol) and CH<sub>3</sub>CN (20 ml).

Table 5.4. Conversion of cyclohexene (0.82 g, 10 mmol) using [Cu<sup>II</sup>(acpy-oap)Cl]-Y as catalyst in 6 h of reaction time under different reaction conditions.

Entry No.	Catalyst (g)	TBHP (g, mmol)	Temp. (°C)	MeCN (ml)	Conv. %
1	0.035	1.28, 10	75	20	41.4
2	0.035	2.56, 20	75	20	61.3
3	0.035	3.84, 30	75	20	58.5
4	0.015	2.56, 20	75	20	32.3
5	0.025	2.56, 20	75	20	44.1
6	0.045	2.56, 20	75	20	65.3
7	0.035	2.56, 20	55	20	11.9
8	0.035	2.56, 20	65	20	36.5

Thus, for the maximum oxidation of 10 mmol of cyclohexene other optimized parameters as concluded are:  $[\text{Cu}^{\text{II}}(\text{acpy-oap})\text{Cl}]\text{-Y}$  (0.035 g), TBHP (2.56 g, 20 mmol),  $\text{CH}_3\text{CN}$  (20 ml) and temperature (75 °C). The conversion of cyclohexene along with TOF and selectivity of different reaction products under the optimized reaction conditions after 6 h of reaction time are presented in Table 5.5. At the end of 6 h, the selectivity of different products follows the order: cyclohexane-1,2-diol (77.7 %) > 2-cyclohexene-1-ol (11.1 %) > cyclohexene epoxide (4.7 %) > 2-cyclohexene-1-one (4.6%). After washing with acetonitrile and drying, the used catalyst was further used under similar conditions as mentioned above. About 60% conversion of cyclohexene was obtained at the end of 6 h and selectivity of reaction products is maintained. A maximum of 42.1 % conversion of cyclohexene was obtained with neat catalyst precursor  $[\text{Cu}^{\text{II}}(\text{acpy-oap})\text{Cl}]$  under similar conditions (Figure 5.9) where products selectivity varied in the order: cyclohexane-1,2-diol (73.5 %) > 2-cyclohexene-1-ol (9.2 %) > cyclohexene epoxide (6.8 %) > 2-cyclohexene-1-one (3.4%). Thus neat complex also maintains the selectivity order as obtained for the encapsulated complex, though conversion is relatively lower.

**Table 5.5.** Effect of different catalysts on the oxidation of cyclohexene and product selectivity

Catalyst	Conv. %	TOF ( $\text{h}^{-1}$ )	% Product selectivity				
							Others
$[\text{Cu}^{\text{II}}(\text{acpy-oap})\text{Cl}]\text{-Y}$	61.3	72	4.6	11.1	4.7	77.7	1.9
$[\text{Cu}^{\text{II}}(\text{acpy-oap})\text{Cl}]\text{-Y}^{\text{a}}$	60.2	-	4.5	11.3	4.8	77.9	1.5
$[\text{Cu}^{\text{II}}(\text{acpy-oap})\text{Cl}]$	42.1	46	3.4	9.2	6.8	73.5	7.1

<sup>a</sup>First cycle of used catalyst.

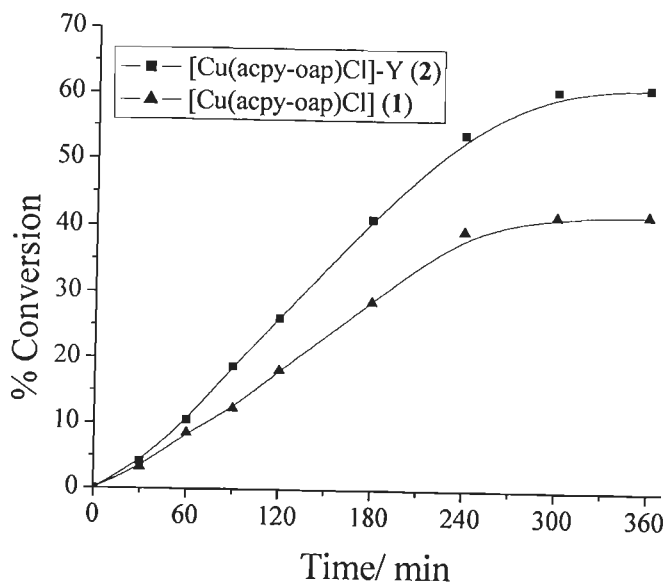


**Figure 5.9.** Effect of different catalysts [Cu(acpy-oap)Cl] (5.1) and [Cu(acpy-oap)Cl]-Y (5.2) on the oxidation of cyclohexene.

Catalytic potential of the encapsulated complex presented here compares well with similar encapsulated complexes. For example, [Cu(2-pyrazinecarboxylate)<sub>2</sub>]-Y exhibited as high as 90.5 % conversion of cyclohexene at a substrate to oxidant (30 % H<sub>2</sub>O<sub>2</sub>) ratio of 1:2 where no formation of cyclohexene epoxide was observed and the selectivity of the other oxidation products varied in the order: 2-cyclohexene-1-one (51%) > 2-cyclohexene-1-ol (42.4%) > cyclohexane-1,2-diol (6.6%) [187]. Complex [Cu(sal-oaba)(H<sub>2</sub>O)]-Y, however, exhibited only 45.8% conversion with the formation of only two products, 2-cyclohexene-1-one and 2-cyclohexene-1-ol [74]. Cyclohexene was oxidized very slowly by *tert*-butylhydroperoxide using similar catalyst [Cu(pan)Cl]-Y (where Hpan = 1-(2-pyridylazo)-2-naphthol) under aerobic conditions and only 28% conversion was obtained Here, the percent selectivity of products varied in the order: 1-*tert*-butylperoxy-2-cyclohexene 89% > 2-cyclohexene-1-one (11%) [188]. Under optimized conditions nearly quantitative

oxidation (99.6%) of cyclohexene was achieved using  $H_2O_2$  as oxidant where the selectivity of different products followed the order: 2-cyclohexene-1-ol (44%) > 2-cyclohexene-1-one (40%) cyclohexene epoxide (12%) > cyclohexane-1, 2-diol (4%) [189].

### 5.3.7. Possible reaction mechanism

In order to propose mechanism for the catalytic reaction, we have studied the interaction of  $[Cu^{II}(\text{acpy-oap})Cl]$  (5.1) with TBHP. Thus, the addition of one drop portions of TBHP in minimum amount of methanol to 10 ml of ca.  $10^{-4}$  M solution of  $[Cu^{II}(\text{acpy-oap})Cl]$  in methanol results in the slow reduction of the intensity of the d-d band at 500 nm without changing its position. The charge transfer band at 432 nm also experienced decrease in intensity, while a shoulder appearing at 228 nm slightly moves towards higher wave length with slight decrease in intensity. Other band at 235 nm slowly gains intensity without changing its position. Figure 5.10 presents spectral changes observed. All these suggest the interaction of TBHP with Cu(II) centre.

At least three types of intermediates having copper-oxygen interaction viz. side-on  $Cu^{III}-(\mu-\eta^2\text{-peroxo})-Cu^{III}$ , bis( $\mu\text{-oxo}-Cu^{III}$ ) and  $Cu^{III}-O-O-H$  (copper-hydroperoxide) have been discussed in the literature during catalytic action [190, 191]. As copper complex  $[Cu^{II}(\text{acpy-oap})Cl]$  will exist as monomeric in the cavity of the zeolite-Y due to space constraints, the facile formation of  $[(HOO)-Cu^{III}(\text{acpy-oap})Cl]$  intermediate is expected in the cavity due to the vacant available site on copper complex. A decrease in the intensity of d-d band at 500 nm and of UV bands at 270 and 250 nm may possibly be due to the formation of hydroperoxide  $[HOO)-Cu^{III}(\text{acpy-oap})Cl]$  intermediate of the neat complex. Similar observations have also been noted earlier for complex  $[Cu^{II}(\text{sal-aebmz})Cl]$  [73]. Hydroperoxocopper complexes are known to exhibit a charge transfer band at ca. 600 nm [192]. The intermediate finally transfers coordinated oxygen atoms to the substrates to give the products. Thus, the catalytic

performance of encapsulated catalyst could be attributed to the formation of facile and reversible intermediate species.

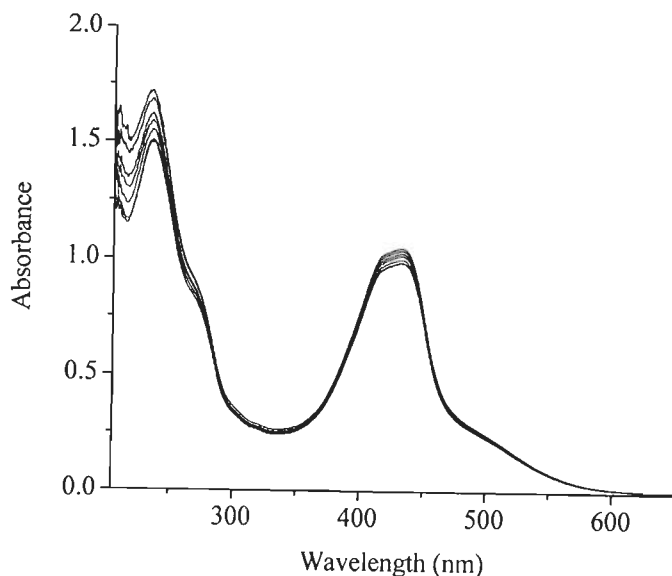


**Figure 5.10.** UV-Vis spectral changes observed during titration of  $[\text{Cu}^{\text{II}}(\text{acpy-oap})\text{Cl}]$  with TBHP. The spectra were recorded after successive addition of one drop portions of TBHP in minimum amount of methanol to 10 ml of ca.  $10^{-4}$  M solution of  $[\text{Cu}^{\text{II}}(\text{acpy-oap})\text{Cl}]$  in methanol

#### 5.4. Conclusions

Schiff base Hacpy-oap, an ONN donor ligand has been used to prepare complex  $[\text{Cu}^{\text{II}}(\text{acpy-oap})\text{Cl}]$ . Its encapsulation in the super cages of zeolite-Y by flexible ligand method gave  $[\text{Cu}(\text{acpy-oap})\text{Cl}]\text{-Y}$ . Spectroscopic along with chemical and thermal studies confirmed their structures. The encapsulated complex has been found active for the oxidation of styrene and cyclohexene. Oxidation of styrene gives 60.2 % conversion in 7 h where the selectivity of two main products follows the order: styrene oxide (78.2%) > benzaldehyde (18.2%). Oxidation of cyclohexene requires 6 h to attain the equilibrium with 61.3% conversion and the selectivity of different products follows the order:

cyclohexane-1,2-diol (77.7 %) > 2-cyclohexene-1-ol (11.1 %) > cyclohexene epoxide (4.7 %) > 2-cyclohexene-1-one (4.6%). No leaching of metal ion during catalytic reactions, recyclability and heterogeneous nature are added advantages of the catalyst. Neat analogue  $[\text{Cu}^{\text{II}}(\text{acpy-oap})\text{Cl}]$  is also active but exhibits less conversion than obtained for the encapsulated one. Oxidation of cyclohexene proceeds through intermediate  $[(\text{HOO})\text{-Cu}^{\text{III}}(\text{acpy-oap})\text{Cl}]$  species, formation of which has been demonstrated by electronic absorption spectroscopy.

*SUMMARY*

*&*

*CONCLUSIONS*



## Summary and Conclusions

Modern catalytic science faces big challenges as most of the catalytic processes, which are widely engaged in the manufacture of bulk as well as fine chemicals, are homogeneous in nature. Homogeneous catalysts also face the problem of separation from the substrate and products, and very often decompose or polymerize during catalytic action. Present thesis highlighted the importance of supported metal complexes and their catalytic potentials for various organic transformations. The applications of zeolite-Y encapsulated metal complexes have further been extended in this thesis. The main objective of the thesis set out was to synthesize new zeolite-Y encapsulated metal complexes and study their catalytic utility for various oxidation reactions. This goal has been achieved by synthesizing zeolite-Y encapsulated vanadium, manganese and copper complexes of tridentate, tetradentate and pentadentate O and N donor ligands. Thus, zeolite-Y encapsulated manganese(III) complexes  $[\text{Mn}^{\text{III}}(\text{pydx-en})\text{Cl}(\text{H}_2\text{O})]\text{-Y}$  (2.4) ( $\text{H}_2\text{pydx-en} = N,N'$ -ethylenebis (pyridoxylideneiminato)),  $[\text{Mn}^{\text{III}}(\text{pydx-1,3-pn})\text{Cl}(\text{H}_2\text{O})]\text{-Y}$  (2.5) ( $\text{H}_2\text{pydx-1,3-pn} = N,N'$ -propylenebis(pyridoxylideneiminato)),  $[\text{Mn}^{\text{III}}(\text{pydx-1,2-pn})\text{Cl}(\text{H}_2\text{O})]\text{-Y}$  (2.6) ( $\text{H}_2\text{pydx-1,2-pn} = 1\text{-methyl-}N,N'$ -ethylenebis(pyridoxylidene iminato) and  $[\text{Mn}^{\text{III}}(\text{sal-dahp})(\text{H}_2\text{O})]\text{-Y}$  (4.2) ( $\text{H}_3\text{sal-dahp} =$  Schiff base obtained by the condensation of salicylaldehyde and 1,3-diamino-2-hydroxypropane), oxidovanadium(IV) complexes  $[\text{V}^{\text{IV}}\text{O}(\text{pydx-en})]\text{-Y}$  (3.4),  $[\text{V}^{\text{IV}}\text{O}(\text{pydx-1,3-pn})]\text{-Y}$  (3.5) and  $[\text{V}^{\text{IV}}\text{O}(\text{pydx-1,2-pn})]\text{-Y}$  (3.6), and copper(II) complex  $[\text{Cu}^{\text{II}}(\text{acpy-oap})\text{Cl}]\text{-Y}$  (5.2) ( $\text{Hacpy-oap} =$  Schiff base derived from 2-acetylpyridine and o-aminophenol) have been prepared using suitable metal precursors and ligands. These complexes have been characterized with the help of various physico-chemical techniques such as elemental, spectral (FT-IR, electronic,  $^{51}\text{V}$  NMR and EPR (for vanadium complexes)), scanning electron micrograph and thermal analysis patterns. The respective neat complexes have also been prepared and characterized. The formulations of the encapsulated complexes are based on the

respective neat complexes and conclusions drawn from the various characterization studies.

Catalytic abilities of these encapsulated complexes have also been explored considering various organic substrates. Oxidation of methyl phenyl sulphide catalyzed by manganese complexes under the optimized reaction conditions gave ca. 86 % conversion with two major products methyl phenyl sulfoxide and methyl phenyl sulfone in the ca. 70 % and 30 % selectivity, respectively. Oxidation of styrene catalyzed by these complexes gave at least five products namely styrene oxide, benzaldehyde, benzoic acid, 1-phenylethane-1,2-diol and phenylacetaldehyde with a maximum of 76.9 % conversion of styrene by  $[\text{Mn}^{\text{III}}(\text{pydx-en})\text{Cl}(\text{H}_2\text{O})]\text{-Y}$  (**2.4**), 76.3 % by  $[\text{Mn}^{\text{III}}(\text{pydx-1,3-pn})\text{Cl}(\text{H}_2\text{O})]\text{-Y}$  (**2.5**) and 76.0 % by  $[\text{Mn}^{\text{III}}(\text{pydx-1,2-pn})\text{Cl}(\text{H}_2\text{O})]\text{-Y}$  (**2.6**) under optimized conditions. Similarly, ca. 93% conversion of benzoin has been obtained by these catalysts, where the selectivity of the products followed the order: benzil > benzoic acid > benzaldehyde-dimethylacetal. Under optimized reaction conditions  $[\text{Mn}^{\text{III}}(\text{sal-dahp})(\text{H}_2\text{O})]\text{-Y}$  (**4.2**) gave a maximum of 86.1% conversion of benzoin in 6 h of reaction time. The selectivity of the various products follows the order: benzoic acid (64.3 %) > benzil (22.3 %) > benzaldehyde-dimethylacetal (13.4 %).

Oxidations of styrene, cyclohexene and methyl phenyl sulfide have been investigated using vanadium complexes as catalyst precursors in the presence of  $\text{H}_2\text{O}_2$  as oxidant. Under the optimized reaction conditions, a maximum of 85.5 % conversion of styrene has been obtained with **3.4**, 84.6 % conversion with **3.5** and 82.9 % conversion with **3.6** in 6 h of reaction time. The selectivity of the various products is similar for the catalyst precursors (i.e. complexes **3.4** to **3.6**) and follows the order: benzaldehyde > 1-phenylethane-1,2-diol > benzoic acid > phenyl acetaldehyde. With cyclohexene, a maximum conversion of 95.9 % has been achieved with **3.4**, 94.5 % with **3.5** and 94.2 % conversion with **3.6**, also in 6 h of reaction time. The selectivity of the various products is similar for the three catalysts: 2-cyclohexene-1-one > 2-cyclohexene-1-ol > cyclohexane-1,2-diol. The

oxidation of methyl phenyl sulfide is achieved with **3.4**, **3.5** and **3.6** in 2.5 h of reaction time with 85.5 %, 82.1% and 80% conversion, with higher selectivity towards sulfoxide. UV-Vis and  $^{51}\text{V}$  NMR experiments with **3.1** confirm the plausible formation of  $\text{V}^{\text{V}}\text{O}(\text{O}_2)\text{L}$  as intermediates in the catalytic oxidations.

Oxidation of styrene by *tert*-butylhydroperoxide using  $[\text{Cu}^{\text{II}}(\text{acpy-oap})\text{Cl}]$  as catalyst gave a maximum of 60.2% conversion in 7 h with mainly two reaction products namely styrene oxide and benzaldehyde. Here, the selectivity of different products follow the order: styrene oxide (73.4%) > benzaldehyde (20.7%). Thus, obtained products and their selectivity mainly depend on the oxidant used. Oxidation of cyclohexene required 6 h to give 61.3% conversion where cyclohexene epoxide, 2-cyclohexene-1-one, 2-cyclohexene-1-ol and cyclohexane-1,2-diol are obtained as major oxidation products.

Keeping in mind the industrial usage of the heterogeneous catalysts, the leaching and recycle ability of all encapsulated complexes reported here have also been tested. All these catalysts are stable and do not leach during the catalytic reactions.

The catalytic activities of these complexes have also been compared with the corresponding neat complexes and it has been observed that some of these complexes have comparable catalytic activities. However, the recycle ability and easy separation of the zeolite-encapsulated metal catalysts from the reaction mixture make them better catalysts over neat ones.

Thus, synthesis and characterization of zeolite-encapsulated metal complexes and their catalytic potentials achieved in the thesis contribute significantly to the existing knowledge. It is hoped that these catalysts may find industrial applications in near future.

# *REFERENCES*

## References

1. S. Sivasanker, "Recent developments in catalysis: Principles and Applications", Edited by: B. Viswanathan, S. Sivasanker and A.V. Ramaswamy, Narosa Publishing House, New Delhi, 2002, p.272.
2. V. Conte and B. Floris, "Vanadium catalyzed oxidation with hydrogen peroxide", *Inorg. Chim. Acta*, 363 (2010)1935–1946.
3. E.R. Hartley, "Catalysis by metal complexes: Supported metal reagents" Reidel, Dordrecht, 1984.
4. T.M. Suzuki and T. Yokoyama, "Preparation and chelation properties of the polystyrene resins containing pendant multidentate ligands", *Polyhedron*, 2 (1983) 127–128.
5. R.B. Merrifield, "Solid phase peptide synthesis: The synthesis of a tetrapeptide", *J. Am. Chem. Soc.*, 85 (1963) 2149 – 2154.
6. M.R. Maurya and J. Costa Pessoa, "Polymer-bound metal complexes as catalysts: Synthesis, characterization, reactivity and catalytic activity in E-H bond activation", *J. Organometal. Chem.*, 696 (2011) 244–254
7. M.R. Maurya, A. Kumar and J. Costa Pessoa, "Vanadium complexes immobilized on solid supports and their use as catalysts for oxidation and functionalization of alkanes and alkenes", *Coord. Chem. Rev.*, xxx (2011) xxx–xxx. DOI: 10.1016/j.ccr. 2011.01.050.
8. D. C. Sherrington, "Polymer-supported metal complex alkene epoxidation catalysts", *Catal. Today*, 57 (2000) 87–104.
9. D.C. Sherrington, "Preparation, structure and morphology of polymer supports", *Chem. Commun.*, 21 (1998) 2275–2286.
10. A. Syamal and M.M. Singh, "Novel polystyrene-anchored copper(II), nickel(II), cobalt(II), iron(III), zinc(II), cadmium(II), zirconium(IV), molybdenum(V), molybdenum(VI) and uranium(VI) complexes of the chelating resin containing the Schiff base derived from salicylaldehyde and 1-amino-2-naphthol-4-sulfonic acid", *React. Polym.*, 21 (1993) 149–158.
11. R. Ando, T. Yagyu and M. Maeda, "Characterization of oxovanadium(IV)-Schiff-base complexes and those bound on resin, and their use in sulfide oxidation", *Inorg. Chim. Acta*, 357 (2004) 2237–2244.

12. M.R. Maurya, U. Kumar, I. Correia, P. Adão, J.C. Pessoa, "A polymer-bound oxidovanadium(IV) complex prepared from an L-cysteine-derived ligand for the oxidative amination of styrene", *Eur. J. Inorg. Chem.*, (2008) 577–587.
13. M.R. Maurya, U. Kumar and P. Manikandan, "Polymer supported vanadium and molybdenum complexes as potential catalysts for the oxidation and oxidative bromination of organic substrates", *Dalton. Trans.*, (2006) 3561–3575.
14. M. R. Maurya, U. Kumar and P. Manikandan, Synthesis and characterisation of polymer-anchored oxidovanadium(IV) complexes and their use for the oxidation of styrene and cumene, *Eur. J. Inorg. Chem.*, (2007) 2303–2314.
15. M.R. Maurya, A. Arya, U. Kumar, A. Kumar, F. Avecilla and J. Costa Pessoa, "Polymer-bound oxidovanadium(IV) and dioxovanadium(V) complexes: synthesis, characterization and catalytic application for the hydroamination of styrene and vinyl pyridine", *Dalton Trans.*, (2009) 9555–9566.
16. D. Kumar, A. Syamal and A.K. Singh, "Synthesis and characterization of manganese(II), cobalt(II), nickel(II), copper(II), zinc(II), cadmium(II), iron(III), zirconium(IV), dioxomolybdenum(VI) and dioxouranium(VI) coordination compounds of polystyrene-supported tridentate dibasic Schiff base derived from semicarbazide and 3-formylsalicylic acid", *Indian J. Chem.*, 42A (2003) 280–286.
17. M.R. Maurya, M. Kumar and S. Sikarwar, "Model dioxovanadium(V) complexes through direct immobilization on polymer support, their characterization and catalytic activities", *Catal. Commun.*, 10 (2008) 187–191.
18. S. Tangestaninejad, M.H. Habibi, V. Mirkhani, M. Moghadam, G. Grivani, Readily prepared polymer-supported molybdenum carbonyls as novel reusable and highly active epoxidation catalysts. *Inorg. Chem. Commun.*, 9 (2006) 575–578.
19. G. Grivani, S. Tangestaninejad, M.H. Habibi, V. Mirkhani and M. Moghadam, "Epoxidation of alkenes by a readily prepared and highly active and reusable heterogeneous molybdenum-based catalyst", *Appl. Catal. A: Gen.*, 299 (2006) 131–136.

## References

---

20. G. Grivani, S. Tangestaninejad, A. Halili, "A readily prepared, highly reusable and active polymer-supported molybdenum carbonyl Schiff base complex as epoxidation catalyst", *Inorg. Chem. Commun.*, 10 (2007) 914–917.
21. S. Chavan, W. Maes, J. Wahlen, P. Jacobs, D. De Vos and W. Dehaen, "Benzimidazole-functionalized dendrons as molybdenum supports for selective epoxidation catalysis", *Catal. Commun.*, 6 (2005) 241–246.
22. M.M. Miller and D.C. Sherrington, "Alkene epoxidation catalysed by Mo(VI) on imidazole-containing polymers: Recycling of polybenzimidazole-supported Mo(VI) in the epoxidation of cyclohexene". *J. Catal.*, 152 (1995) 377–383.
23. G.H. Mahdavinia, S. Rostamizadeh, A.M. Amani and Z. Emdadi, "Ultrasound-promoted greener synthesis of aryl-14-H dibenzo[a,j]xanthenes catalyzed by  $\text{NH}_4\text{H}_2\text{PO}_4/\text{SiO}_2$  in water", *Ultrason. Sonochem.*, 16 (2009) 7–10.
24. H. Naeimi and M. Moradian, "Alumina-supported metal(II) Schiff base complexes as heterogeneous catalysts in the high-regioselective cleavage of epoxides to halohydrins by using elemental halogen", *Polyhedron*, 27 (2008) 3639–3645.
25. G.S. Mishra and A. Kumar, "Liquid phase oxidation of n-octane catalyzed by silica gel supported vanadium ( $\text{VO}^{2+}$ ) complex using molecular oxygen", *React. Kinet. Cata. Lett.*, 80 (2003) 223–231.
26. M.J.L. Kishore, G.S. Mishra and A. Kumar, "Synthesis of hetero binuclear macrocyclic CoV complex bonded to chemically modified alumina support for oxidation of cyclohexane using oxygen", *J. Mol. Catal. A: Chem.*, 230 (2005) 35–42.
27. K. Soai, M. Watanabe and A. Yamamoto, "Enantioselective addition of dialkylzinc to aldehyde using heterogeneous chiral catalysts immobilized on alumina and silica gel", *J. Org. Chem.*, 55 (1990) 4832–4835.
28. P. Barbaro, C. Bianchini, V.D. Santoro, A. Meli, S. Moneti, R. Psaro, A. Scaffidi, L. Sordelli and F. Vizza, "Hydrogenation of arenes over silica-supported catalysts that combine a grafted rhodium complex and palladium nanoparticles: Evidence for substrate activation on  $\text{Rh}_{\text{single-site}}-\text{Pd}_{\text{metal}}$  moieties", *J. Am. Chem. Soc.*, 128 (2006) 7065–7076.

29. H.G. Alt, P. Schertl and A. Köppl, "Polymerization of ethylene with metallocene/methylaluminoxane catalysts supported on polysiloxane microgels and silica", *J. Organomet. Chem.*, 568 (1998) 263–269.
30. T. Joseph, S.S. Deshpande, S.B. Halligudi, A. Vinu, S. Ernst and M. Hartmann, "Hydrogenation of olefins over hydridochlorocarbonyl tris(triphenylphosphine) ruthenium(II) complex immobilized on MCM-41 and SBA-15", *J. Mol. Catal. A: Chem.*, 206 (2003) 13–21.
31. T. Joseph and S.B. Halligudi, "Oxyfunctionalization of limonene using vanadium complex anchored on functionalized SBA-15", *J. Mol. Catal. A: Chem.*, 229 (2005) 241–247.
32. S.L. Jain, J.K. Joseph, F.E. Kühn and O. Reiser, "An efficient synthesis of poly(ethylene glycol)-supported Iron(II) porphyrin using a click reaction and its application for the catalytic olefination of aldehydes", *Adv. Synth. Catal.*, 351 (2009) 230–234.
33. R. Wang, B. Gao and W. Jiao, "A novel method for immobilization of Co tetraphenylporphyrins on P(4VP-co-St)/SiO<sub>2</sub>: Efficient catalysts for aerobic oxidation of ethylbenzenes", *Appl. Surf. Sci.*, 255 (2009) 4109–4113.
34. C.T. Kresge, M.F. Leonowicz, W.J. Roth, J.C. Vartuli and J.S. Beck, "Ordered mesoporous molecular sieves synthesized by a liquid-crystal template mechanism", *Nature*, 359 (1992) 710–712.
35. M. Masteri-Farahani, F. Farzaneh and M. Ghandi, "Synthesis of tetradentate N<sub>4</sub> Schiff base dioxomolybdenum(VI) complex within MCM-41 as selective catalyst for epoxidation of olefins", *Catal. Commun.*, 8 (2007) 6–10.
36. S. Singhal, S.L. Jain and B. Sain, "Alumina-supported molybdenum(VI) oxide: An efficient and recyclable heterogeneous catalyst for regioselective ring opening of epoxides with thiols, acetic anhydride, and alcohols under solvent-free conditions", *Chem. Lett.*, 37 (2008) 620–621.
37. S. Sahoo, P. Kumar, F. Lefebvre and S.B. Halligudi, "Synthesis of chiral sulfoxides by enantioselective sulfide oxidation and subsequent oxidative kinetic resolution using immobilized Ti–binol complex", *J. Catal.*, 262 (2009) 111–118.
38. S. Sahoo, P. Kumar, F. Lefebvre and S.B. Halligudi, "Enantioselective hydrogenation of olefins by chiral iridium phosphorothioite complex covalently anchored on mesoporous silica", *J. Catal.*, 254 (2008) 91–100.



## References

---

39. G. Liu, Y. Gao, X. Lu, M. Liu, F. Zhang and H. Li, "Microwave-assisted catalytic allylation of aldehydes promoted by a mesoporous silica-supported BINOL ligand in solid media", *Chem. Commun.*, 27 (2008) 3184–3186.
40. A.R. McDonald, C. Müller, D. Vogt, G.P.M. van Klink and G. van Koten, "BINAP-Ru and -Rh catalysts covalently immobilized on silica and their repeated application in asymmetric hydrogenation", *Green Chem.*, 10 (2008) 424–432.
41. Y. Yang, Y. Zhang, S. Hao, J. Guan, H. Ding, F. Shang, P. Qiu and Q. Kana "Heterogenization of functionalized Cu(II) and VO(IV) Schiff base complexes by direct immobilization onto amino-modified SBA-15: Styrene oxidation catalysts with enhanced reactivity", *Appl. Catal. A: Gen.*, 381 (2010) 274–281.
42. A. Stamatis, D. Giasafaki, K.C. Christoforidis, Y. Deligiannakis and M. Louloudi, "The catalytic function of SiO<sub>2</sub>-immobilized Mn(II)-complexes for alkene epoxidation with H<sub>2</sub>O<sub>2</sub>", *J. Mol. Catal. A: Chem.*, 319 (2010) 58–65.
43. M. Moghadam, V. Mirkhani, S. Tangestaninejad, I. Mohammadpoor-Baltork and H. Kargar, "Silica supported Mn(Br8TPP)Cl and Mn(TPP)Cl as efficient and reusable catalysts for selective hydrocarbon oxidation under various reaction conditions: The effect of substituted bromines on the catalytic activity and reusability", *J. Mol. Catal. A: Chem.*, 288 (2008) 116–124.
44. P. Das, I. Kúzniarska-Biernacka, A.R. Silva, A.P. Carvalho, J. Pires and C. Freire, "Encapsulation of chiral Mn(III) *salen* complexes into aluminium pillared clays: Application as heterogeneous catalysts in the epoxidation of styrene", *J. Mol. Catal. A: Chem.*, 248 (2006) 135–143.
45. S. Tangestaninejad, M. Moghadam, V. Mirkhani, I. Mohammadpoor-Baltork and M.S. Saeedi, "Efficient epoxidation of alkenes with sodium periodate catalyzed by reusable manganese(III) salophen supported on multi-wall carbon nanotubes", *Appl. Catal. A: Gen.*, 381 (2010) 233–241.
46. B.V. Romanovskii, "Zeolite-encapsulated compounds: synthesis, physico-chemical properties, and applications in catalysis", *Kinetics Catal.*, 40 (1999) 673–681.
47. N.S. Finney, P.J. Pospisil, S. Chang, M. Palucki, R.G. Konsler, K.B. Hansen, E.N. Jacobsen, "On the Viability of Oxametallacyclic Intermediates in the

- (salen)Mn-Catalyzed Asymmetric Epoxidation”, *Angew. Chem. Int. Ed.* 1997, 36, 1720 – 1723.
48. J. Poltowicz, K. Pamin, E. Tabor, J. Haber, A. Adamski and Z. Sojka, “Metallosalen complexes immobilized in zeolite NaX as catalysts of aerobic oxidation of cyclooctane”, *Appl. Catal. A: Gen.*, 299 (2006) 235–242.
49. M. S. Niasari, M. R. Ganjali and P. Norouzi, “Host (nanopores of zeolite Y)-guest (oxovanadium(IV) tetradentate schiff-base complexes) nanocomposite materials: synthesis, characterization and liquid phase hydroxylation of phenol with hydrogen peroxide” *J. Porous Mater.*, 14 (2007) 423–432.
50. A. Kozlov, K. Asakura and Y. Iwasawa, “Synthesis and characterization of vanadium (IV) complexes in NaY zeolite supercages”, *Micropor. Mesopor. Mater.*, 21 (1998,) 571–579.
51. T. Joseph, D. Srinivas, C. S. Gopinath and S. B. Halligudi, “Spectroscopic and catalytic activity studies of VO(Saloph) complexes encapsulated in zeolite-Y and Al-MCM-41 molecular sieves”, *Catal Lett.*, 83 (2002) 209–214.
52. A. P. A. Marques, E. R. Dockal, F. C. Skrobot and I. L. V. Rosa, “Synthesis and characterization of vanadium (IV) complexes in Na-Y zeolite supercages”, *Inorg. Chem. Commun.*, 10 (2007) 255–261.
53. M. R. Maurya, A. K. Chandrakar and S. Chand, “Oxovanadium(IV) and copper(II) complexes of 1,2-diaminocyclohexane based ligand encapsulated in zeolite-Y for the catalytic oxidation of styrene, cyclohexene and cyclohexane”, *J. Mol. Catal. A: Chem.* 270 (2007) 225–235.
54. M. R. Maurya, M. Kumar, S. J. J. Titinchi, H. S. Abbo and S. Chand. “Oxovanadium(IV) Schiff Base Complexes Encapsulated in Zeolite-Y as Catalysts for the Liquid-Phase Hydroxylation of Phenol”, *Catal. Lett.*, 86 (2003) 97–105.
55. S.P. Verkey, C. Ratnasamy and P. Ratnasamy, “Zeolite-encapsulated manganese(III) salen complexes”, *J. Mol. Catal. A: Chem.*, 135 (1998) 295 – 306.
56. S.P. Verkey, C. Ratnasamy and P. Ratnasamy, “Selective oxidation over copper and manganese salens encapsulated in zeolites”, *Micropor. Mesopor. Mater.*, 22 (1998) 465 – 474.

## References

---

57. S.P. Verkey, C. Ratnasamy and P. Ratnasamy, "Oxidation of p-xylene over zeolite-encapsulated copper and manganese complexes", *Appl. Catal. A: Gen.*, 182 (1999) 91–96.
58. S. Deshpande, D. Srinivas and P. Ratnasamy, "EPR and catalytic investigation of Cu(salen) complexes encapsulated in zeolites", *J. Catal.*, 188 (1999) 261–269.
59. M.R. Maurya, M. Kumar, S.J.J. Titinchi, H. S. Abbo and S. Chand, "Oxovanadium(IV) Schiff base complexes encapsulated in zeolite-Y as catalyst for the liquid-phase hydroxylation of phenol", *Catal. Lett.*, 86 (2003) 97–105.
60. K.J. Balkus Jr., A.K. Khanmamedova, K.M. Dixon and F. Bedioui, "Oxidations catalyzed by zeolite ship-in-a-bottle complexes", *Appl. Catal. A: Gen.*, 143 (1996) 159–173.
61. G.S. Mishra and A. Kumar, "Preparation of heterogeneous vanadium ( $\text{VO}_2^+$ ) catalyst for selective hydroxylation of cyclohexane by molecular oxygen", *Catal. Lett.*, 81 (2002) 113–117.
62. C.R. Jacob, S.P. Varkey and P. Ratnasamy, "Selective oxidation over copper and manganese salens encapsulated in zeolites", *Micropor. Mesopor. Mater.*, 22 (1998) 465–474.
63. M.R. Maurya, S. J. J. Titinchi and S. Chand, "Spectroscopic and catalytic activity study of N,N'-bis(salicylidene)propane-1,3-diamine copper(II) encapsulated in zeolite-Y", *Appl. Catal. A: Gen.*, 228 (2002) 177–187.
64. M.R. Maurya, S. J. J. Titinchi, S. Chand and I.M. Mishra, "Zeolite-encapsulated Cr(III), Fe(III), Ni(II), Zn(II) and Bi(III) salpn complexes as catalysts for the decomposition of  $\text{H}_2\text{O}_2$  and oxidation of phenol", *J. Mol. Catal. A: Chem.*, 180 (2002) 201–209.
65. M.R. Maurya, S.J.J. Titinchi and S. Chand, "Oxidation of phenol with  $\text{H}_2\text{O}_2$  catalysed by Cr(III), Fe(III) or Bi(III) N, N'-bis-(salicylidene)diethylenetriamine ( $\text{H}_2\text{saldien}$ ) complexes encapsulated in Zeolite-Y", *J. Mol. Catal. A: Chem.*, 193 (2003) 165–176.
66. M.R. Maurya, S.J.J. Titinchi and S. Chand, "Oxidation of phenol with  $\text{H}_2\text{O}_2$  catalysed by Cu(II), Ni(II) and Zn(II) complexes of N, N'-bis-(salicylidene) diethylenetriamine ( $\text{H}_2\text{saldien}$ ) encapsulated in Y-zeolite", *J. Mol. Catal. A: Chem.*, 201 (2003) 119–130.

67. T. A. Alsalim, J. S. Hadi, E. A. Al-Nasir, H. S. Abbo, S. J. J. Titinchi, "Hydroxylation of phenol catalyzed by oxovanadium(IV) of salen type Schiff base complexes with hydrogen peroxide", *Catal. Lett.*, 136 (2010) 228–233.
68. S. Seelan and A. K. Sinha, "Phenol hydroxylation activity of metal phthalocyanine complexes encapsulated in zeolite-Y", *Appl. Catal. A: Gen.*, 238 (2003) 201–209.
69. M. R. Maurya, H. Saklani, A. Kumar and S. Chand; "Dioxovanadium(V) complexes of dibasic tridentate ligands encapsulated in zeolite-Y for the liquid phase catalytic hydroxylation of phenol using H<sub>2</sub>O<sub>2</sub> as oxidant", *Catal. Lett.*, 87 (2004) 121–127.
70. M. R. Maurya, H. Saklani and S. Agarwal, "Oxidative bromination of salicylaldehyde by potassium bromide/H<sub>2</sub>O<sub>2</sub> catalysed by dioxovanadium(V) complexes encapsulated in zeolite-Y: a functional model of haloperoxidases", *Catal. Commun.*, 5 (2004) 563–568.
71. P.P. Knops-Gerrits, D. De Vos, F. Thibault-Starzyk and P.A. Jacobs, "Zeolite-encapsulated Mn(II) complexes as catalyst for selective alkene oxidation", *Nature*, 369 (1994) 543–546.
72. M.S. Niassary, F. Farzaneh and M. Ghandi, "Selective hydroxylation of cyclic ethers with tert-butylhydroperoxide and hydrogen peroxide catalyzed by iron(III) and manganese(II) bipyridine complexes included in zeolite Y and bentonite", *J. Mol. Catal. A: Chem.*, 175 (2001) 105 – 110.
73. M. R. Maurya, A. K. Chandrakar and S. Chand, "Oxidation of phenol, styrene and methyl phenyl sulfide with H<sub>2</sub>O<sub>2</sub> catalysed by dioxovanadium(V) and copper(II) complexes of 2-aminomethylbenzimidazole-based ligand encapsulated in zeolite-Y", *J. Mol. Catal. A: Chem.*, 263 (2007) 227–237.
74. M. R. Maurya, A. K. Chandrakar and S. Chand. "Zeolite-Y encapsulated metal complexes of oxovanadium(VI), copper(II) and nickel(II) as catalyst for the oxidation of styrene, cyclohexane and methyl phenyl sulfide", *J. Mol. Catal. A: Chem.*, 274 (2007) 192–201.
75. M. R. Maurya, A. K. Chandrakar and S. Chand, "Oxidation of methyl phenyl sulfide, diphenyl sulfide and styrene by oxovanadium(IV) and copper(II) complexes of NS donor ligand encapsulated in zeolite-Y", *J. Mol. Catal. A: Chem.*, 278 (2007) 12–21.

## References

---

76. M.S. Niasari, "Synthesis, characterization and liquid-phase hydroxylation of phenol with hydrogen peroxide over host (nanopores of zeolite-Y)/ guest (oxovanadium(IV) complexes of tetraaza macrocyclic ligands) nanocatalyst", *Inorg. Chim. Acta*, 362 (2009) 2159–2166.
77. M.S. Niasari, "Flexible ligand synthesis, characterization and liquid phase hydroxylation of phenol by H<sub>2</sub>O<sub>2</sub> with host (nanopores of zeolite-Y)/guest [VO([R]<sub>2</sub>-N<sub>2</sub>X<sub>2</sub>)]<sup>2+</sup> (R = H, CH<sub>3</sub>; X = NH, O, S) nanocomposite materials", *J. Incl. Phenom. Macrocycl. Chem.*, 65 (2009) 349–360.
78. A. P. A. Marques, E. R. Dockal, F. C. Skrobot and I. L. V. Rosa, "Synthesis and characterization of vanadium (IV) complexes in NaY zeolite supercages", *Inorg. Chem. Commun.*, 10 (2007) 255–261.
79. V.K. Bansal, P.P. Thankachan and R. Prasad, "Oxidation of benzyl alcohol and styrene using H<sub>2</sub>O<sub>2</sub> catalyzed by tetraazamacrocyclic complexes of Cu(II) and Ni(II) encapsulated in zeolite-Y", *Appl. Catal. A: Gen.*, 381 (2010) 8–17.
80. M.S. Niasari and A. Sobhani, "Ship-in-a-bottle synthesis, characterization and catalytic oxidation of cyclohexane by Host (nanopores of zeolite-Y)/guest (Mn(II), Co(II), Ni(II) and Cu(II) complexes of bis(salicylaldehyde)oxaloyldihydrazone) nanocomposite materials", *J. Mol. Catal. A: Chem.*, 285 (2008) 58–67.
81. M.S. Niasari, "Host (nanocage of zeolite-Y)/guest (manganese(II), cobalt(II), nickel(II) and copper(II) complexes of 12-membered macrocyclic Schiff-base ligand derived from thiosemicarbazide and glyoxal) nanocomposite materials: Synthesis, characterization and catalytic oxidation of cyclohexene", *J. Mol. Catal. A: Chem.*, 283 (2008) 120–128.
82. T. Joseph, S.B. Halligudi, C. Satyanarayan, D.P. Sawant and S. Gopinathan, "Oxidation by molecular oxygen using zeolite encapsulated Co(II)saloph complexes", *J. Mol. Catal. A: Chem.*, 168 (2001) 87–97.
83. K.O. Xavier, J. Chacko and K.K.M. Yusuff, "Intrazeolite cobalt(II), nickel(II) and copper(II) complexes of 3-formylsalicylic acid for oxidation reactions", *J. Mol. Catal. A: Chem.*, 178 (2002) 275–281.
84. K.K.M. Yusuff and J. Mathew, "Ascorbic acid oxidation by a new zeolite encapsulated copper(II) complex", *Indian J. Chem.*, 36A (1997) 303–306.

85. H. M. Alvarez, L. F. B. Malta, M. H. Herbst, A. Horn Jr. and O. A. C. Antunes, "Catalytic isosafrol oxidation mediated by impregnated and encapsulated vanadyl-Y-zeolite under microwave irradiation", *Appl. Catal. A: Gen.*, 326 (2007) 82–88.
86. M.R. Maurya, M. Bisht and F. Avecilla, "Synthesis, characterization and catalytic activities of vanadium complexes containing ONN donor ligand derived from 2-aminoethylpyridine", *J. Mol. Catal. A: Chem.*, 344 (2011) 18–27.
87. M.R. Maurya, M. Bisht, A. Kumar M.L. Kuznetsov, F. Avecilla and J. Costa Pessoa, "Synthesis, characterization, reactivity and catalytic activity of oxidovanadium(IV), oxidovanadium(V) and dioxidovanadium(V) complexes of benzimidazole modified ligands", *Dalton Trans.*, (2011) 6968–6983.
88. N. A. Law, M. T. Caudle and V. L. Pecoraro, "Manganese redox enzymes and model systems: properties, structures, and reactivity", *Adv. Inorg. Chem.*, 46 (1998) 305–440.
89. H. Sigel, A. Sigel, in *Metal Ions in Biological Systems*, (Eds: H. Sigel, A. Sigel), Marcel Dekker, Inc. 2000.
90. G. C. Dismukes, "Manganese enzymes with binuclear active Sites", *Chem. Rev.*, 96 (1996) 2909–2926.
91. M. S. Lah, M. M. Dixon, K. A. Patridge, W. C. Stallings, J. A. Fee and M. L. Ludwig, "Structure-function in Escherichia coli iron superoxide dismutase: Comparisons with the manganese enzyme from Thermus thermophilus", *Biochemistry*, 34 (1995) 1646–1660.
92. J. E. Penner-Hahn, in *Metal Sites in Proteins and Models*, (Eds: H. A. O. Hill, P. J. Sadler, A. J. Thomson), Springer-Verlag 1998, p. 1.
93. J. Limburg, V. A. Szalai and G. W. Brudvig, "A mechanistic and structural model for the formation and reactivity of a MnV:O species in photosynthetic water oxidation", *J. Chem. Soc., Dalton Trans.*, (1999) 1353–1362.
94. V. K. Yachandra, V. J. DeRose, M. J. Latimer, I. Mukerji, K. Sauer and M. P. Klein, "Where plants make oxygen: a structural model for the photosynthetic oxygen-evolving manganese cluster", *Science*, 260 (1993) 675–679.

## References

---

95. M. Sundaramoorthy, K. Kishi, M. H. Gold and T. L. Poulos, "The crystal structure of manganese peroxidase from *Phanerochaete chrysosporium* at 2.06-Å resolution", *J. Biol. Chem.*, 269 (1994) 32759–32767.
96. L. Canali and D.C. Sherrington, "Utilization of homogeneous and supported chiral metal(salen) complexes in asymmetric catalysis", *Chem. Soc. Rev.*, 28 (1999) 85 – 93.
97. M. Maneiro, M.R. Bermejo, M.I. Fernández, E. Gómez-Fórneas, A. M. González-Noya and A.M. Tyryshkin, "A new type of manganese-Schiff base complex, catalysts for the disproportionation of hydrogen peroxide as peroxidase mimics", *New J. Chem.*, 27 (2003) 727–733.
98. N.A. W.F. Holderich and F. Kollmer, "Oxidation reactions in the synthesis of fine and intermediate chemicals using environmentally benign oxidants and the right reactor system", *Pure Appl. Chem.*, 72 (2000) 1273–1287.
99. M.H. Valkenberg and W.F. Holderich, "Preparation and use of hybrid organic-inorganic catalysts", *Catal. Rev.*, 44 (2002) 321–374.
100. D.E. De Vos, B.F. Sels and P.A. Jacobs, "Practical heterogeneous catalysts for epoxide production", *Adv. Synth. Catal.*, 345 (2003) 457–473.
101. D.E. De Vos, M. Dams, B.F. Sels and P.A. Jacobs, "Ordered mesoporous and microporous molecular sieves functionalized with transition metal complexes as catalysts for selective organic transformations", *Chem. Rev.*, 102 (2002) 3615–3640.
102. P. Das, I. Kuźniarska-Biernacka, A.R. Silva, A.P. Carvalho, J. Pires and C. Freire, "Encapsulation of chiral Mn(III) salen complexes into aluminium pillared clays: Application as heterogeneous catalysts in the epoxidation of styrene", *J. Mol. Catal. A: Chem.*, 248 (2006) 135–143.
103. I. Kuźniarska-Biernacka, A.R. Silva, A.P. Carvalho, J. Pires and C. Freire, "Direct immobilisation versus covalent attachment of a Mn(III)salen complex onto an Al-pillared clay and influence in the catalytic epoxidation of styrene", *J. Mol. Catal. A: Chem.*, 278 (2007) 82–91.
104. H. Zhang, S. Xiang, J. Xiao and C. Li, "Heterogeneous enantioselective epoxidation catalyzed by Mn(salen) complexes grafted onto mesoporous materials by phenoxy group", *J. Mol. Catal. A: Chem.*, 238 (2005) 175–184.



105. M. Moghadam, S. Tangestaninejad, V. Mirkhani, I. Mohammadpoor-Baltork and M. Moosavifar, "Host (nanocavity of zeolite-Y or X)-guest (manganese (III) tetrakis[4-N-methylpyridinium]porphyrin) nanocomposite materials as efficient catalysts for biomimetic alkene epoxidation with sodium periodate: Shape-selective epoxidation of linear alkenes", *J. Mol. Catal. A: Chem.*, 302 (2009) 68–75.
106. I. Correia, J. Costa Pessoa, M.T. Duarte, R.T. Henriques, M.F.M. Piedade, L.F. Veiros, T. Jackusch, A. Dornyei, T. Kiss, M.M.C.A. Castro, C.F.G.C. Geraldes and F. Avecilla, "N,N'-Ethylenebis(pyridoxylideneiminato) and N,N'-ethylenebis (pyridoxylaminato): Synthesis, characterization, potentiometric, spectroscopic, and DFT studies of their vanadium(IV) and vanadium(V) complexes", *Chem. Eur. J.*, 10 (2004) 2301 – 2317
107. G. M. Sheldrick, SHELXL-97: An integrated system for solving and refining crystal structures from diffraction data (Revision 5.1); University of Göttingen, Germany, 1997.
108. L. Sabater, C. Hureau, R. Guillot and A. Aukauloo, "Influence of the Electrochemical Conversion of  $[(LH)Mn^{II}Cl_2]$  into  $[(L)Mn^{III}Cl]^+$  on the protonic state of a phenol-containing ligand", *Inorg. Chem.*, 45 (2006) 2373–2375.
109. J. Lin, C. Tu, H. Lin, P. Jiang, J. Ding and Z. Guo, "Crystal structure and superoxide dismutase activity of a six-coordinate manganese(III) complex", *Inorg. Chem. Commun.*, 6 (2003) 262–265.
110. M.R. Maurya, B. Singh, P. Adão, F. Avecilla and J. Costa Pessoa, "Zeolite-encapsulated copper(II) complexes of pyridoxal-based tetradentate ligands for the oxidation of styrene, cyclohexene and methyl phenyl sulphide", *Eur. J. Inorg. Chem.*, (2007) 5720–5734.
111. A. Syamal and M. R. Maurya, "Salicylaldehyde-2-furoic acid hydrazide as a chelating ligand: complexes with nickel(II), cobalt(II), copper(II), zinc(II), zirconium(IV), oxomolybdenum(V) and dioxouranium(VI)", *Indian J. Chem.*, 24A (1985) 836–840.
112. H. Torayama, T. Nishide, H. Asada, M. Fujiwara and T. Matsushita, "Preparation and characterization of different two types of di- $\mu$ -oxo dimanganese(IV) complexes with tetradentate Schiff bases", *Polyhedron*, 17 (1998) 105–118.



## References

---

113. L.J. Boucher and V.W. Day, "Manganese Schiff base complexes. 5. Synthesis and spectroscopy of some anion complexes of N,N'-ethylenebis(acetylacetonimine)manganese(III)", *Inorg. Chem.*, 16 (1977) 1360–1367.
114. S.B. Kumar, S. Bhattacharyya, S.K. Dutta, E.T. Tiekink and M. Chaudhury, "Mononuclear manganese(III) complexes of a heterodonor (N<sub>2</sub>OS) ligand containing thiolate-type sulfur: synthesis, structure, redox and spectroscopic properties", *J. Chem. Soc. Dalton Trans.*, (1995) 2619–2626.
115. S. Biswas, K. Mitra, C.H. Schwalbe, C.R. Lucas, S.K. Chattopadhyay and B. Adhikari, "Synthesis and characterization of some Mn(II) and Mn(III) complexes of N,N'-o-phenylenebis(salicylideneimine) (LH<sub>2</sub>) and N,N'-o-phenylenebis(5-bromosalicylideneimine) (L<sup>1</sup>H<sub>2</sub>). Crystal structures of [Mn(L)(H<sub>2</sub>O)(ClO<sub>4</sub>)], [Mn(L)(NCS)] and an infinite linear chain of [Mn(L)(OAc)]", *Inorg. Chim Acta*, 358 (2005) 2473–2481.
116. P.P. Knops-Gerrits, D.E. de Vos and P.A. Jacobs, "Oxidation catalysis with semi-inorganic zeolite-based Mn catalysts", *J. Mol. Catal. A: Chem.*, 117 (1997) 57–70.
117. K. Srinivasan, S. Perrier and J.K. Kochi, "Dual pathways for manganese catalysis of olefin oxidation with alkyl hydroperoxides", *J. Mol. Catal.*, 36 (1986) 297–317.
118. I. Fernandez and N. Khair, "Recent Developments in the Synthesis and Utilization of Chiral Sulfoxides", *Chem. Rev.*, 103 (2003) 3651–3706.
119. F.M. Collins, A.R. Lucy and C. Sharp, "Oxidative desulfurization of oils via hydrogen peroxide and heteropolyanion catalysis", *J. Mol. Catal. A: Chem.*, 117 (1997) 397–403.
120. I.V. Babich and J.A. Moulijn, "Science and technology of novel processes for deep desulfurization of oil refinery streams: a review", *Fuel*, 82 (2003) 607–631.
121. X. M. Feng, Z. Wang, N.S. Bian and Z.L. Wang, "Sulfide oxidation with H<sub>2</sub>O<sub>2</sub> catalyzed by manganese complex of N,N',N''-tris(2-hydroxypropyl)-1,4,7-triazacyclononane", *Inorg. Chim. Acta*, 360 (2007) 4103–4110.
122. M. R. Maurya, A. K. Chandrakar and S. Chand, "Oxovanadium(IV) and copper(II) complexes of 1,2-diaminocyclohexane based ligand encapsulated

- in zeolite-Y for the catalytic oxidation of styrene, cyclohexene and cyclohexane”, *J. Mol. Catal. A: Chem.*, 270 (2007) 225–235.
123. M. Silva, C. Freire, B. de Castro and J.L. Figueiredo, “Styrene oxidation by manganese Schiff base complexes in zeolite structures”, *J. Mol. Catal. A: Chem.*, 258 (2006) 327–333.
124. V. Hulea and E. Dumitriu, “Styrene oxidation with H<sub>2</sub>O<sub>2</sub> over Ti-containing molecular sieves with MFI, BEA and MCM-41 topologies”, *Appl. Catal. A Gen.*, 277 (2004) 99–106.
125. S.B. Halligudi, N.K. Kala Raj, S.S. Deshpande and S. Gopinathan, “Kinetics of oxidation of  $\beta$ -isophorone to keto-isophorone catalyzed by manganese Schiff base complex using molecular oxygen”, *J. Mol. Catal. A: Chem.*, 157 (2000) 9–14.
126. M. R. Maurya, U. Kumar and P. Manikandan, “Polymer-supported vanadium and molybdenum complexes as potential catalysts for the oxidation and oxidative bromination of organic substrates”, *Dalton Trans.*, (2006) 3561–3575.
127. M. R. Maurya, U. Kumar and P. Manikandan, “Synthesis and characterisation of polymer-anchored oxidovanadium(IV) complexes and their use for the oxidation of styrene and cumene”, *Eur. J. Inorg. Chem.*, (2007) 2303–2314.
128. G. B. Gill, in *Comprehensive Organic Synthesis*, (Eds: G. Pattenden), vol. 3, Pergamon Press, New York, 1991, p. 821–838.
129. C. Bowers and P.K. Dutta, “Olefin oxidation by zeolite-encapsulated manganese(salen)<sup>+</sup> complexes under ambient conditions”, *J. Catal.*, 122 (1990) 127–279.
130. R. Raja and P. Ratnasamy, “Selective oxidation of phenols using copper complexes encapsulated in zeolites”, *Appl. Catal. Gen.*, 143 (1996) 145–158.
131. E. Paez-Mozo, N. Gabriunas, R. Maggi, D. Acosta, P. Ruiz, and B. Delmon, “Selective olefin oxidation with cobalt phthalocyanine encapsulated in Y-zeolite” *J. Mol. Catal. A: Chem.*, 91 (1994) 251–258.
132. C.R. Jacob, S.P. Varkey and P. Ratnasamy, “Oxidation of para-xylene over zeolite-encapsulated copper and manganese complexes”, *Appl. Catal.: Gen.*, 182 (1999) 91–96.

133. D. Chatterjee and A. Mitra, "Olefin epoxidation catalysed by Schiff-base complexes of Mn and Ni in heterogenized-homogeneous systems", *J. Mol. Catal. A: Chem.*, 144 (1999) 363–367.
134. M.S. Niassary, F. Farzaneh, M. Ghandi and L. Turkian, "Oxidation of cyclohexene with tert-butylhydroperoxide catalyzed by manganese(II) complexes included in zeolite Y", *J. Mol. Catal. A: Chem.*, 157 (2000) 183–188.
135. M. Silva, C. Freire, B. de Castro and J.L. Figueiredo, "Styrene oxidation by manganese Schiff base complexes in zeolite structures", *J. Mol. Catal. A: Chem.*, 257 (2006) 327 – 333.
136. S. Rayati, M. Koliaei, F. Ashouri, S. Mohebbi, A. Wojtczak and A. Kozakiewicz, "Oxovanadium(IV) Schiff base complexes derived from 2,2'-dimethylpropanediamine: A homogeneous catalyst for cyclooctene and styrene oxidation", *Appl. Catal. A: Gen.*, 346 (2008) 65–71.
137. C.C. McLauchlan, M.P. Weberski Jr. and B.A. Greiner, "Synthesis, catalytic activity, phosphatase inhibition activity, and X-ray structural characterization of vanadium scorpionate complexes, (Tpms)VCl<sub>2</sub>(DMF) and (Tpms)VOCl(DMF)", *Inorg. Chim. Acta*, 362 (2009) 2662–2666.
138. R. Bai, X. Fu, H. Bao and W. Ren, "Chiral salen Mn(III) complex axial coordination immobilized on diamine modified ZSPP and their catalytic epoxidation of styrene", *Catal. Commun.*, 9 (2008) 1588–1594.
139. P. Adão, J. C. Pessoa, R. T. Henriques, M. L. Kuznetsov, F. Avecilla, M. R. Maurya, U. Kumar and I. Correia, "Synthesis, characterization and application of vanadium-salan complexes in oxygen transfer reactions", *Inorg. Chem.*, 48 (2009) 3542–3561.
140. P. Adão, M.R. Maurya, U. Kumar, F. Avecilla, R.T. Henriques, M.L. Kuznetsov, J. Costa Pessoa and I. Correia, "Vanadium-salen and -salan complexes: characterization and application in oxygen transfer reactions", *Pure Appl. Chem.*, 81 (2009) 1279-1296.
141. A. Rockenbauer and L. Korecz, "Automatic computer simulations of ESR spectra", *Appl. Magn. Reson.*, 10 (1996) 29–43.
142. M.R. Maurya, "Development of the coordination chemistry of vanadium through bis(acetylacetonato)oxovanadium(IV): Synthesis, reactivity and structural aspects", *Coord. Chem. Rev.*, 237 (2003) 163–181.

143. D.H. Williams and I. Fleming, *Spectroscopic Methods in Organic Chemistry*, McGraw-Hill, London, 5<sup>th</sup> Ed. 1995, p. 18–21.
144. L.F. Vilas Boas and J. Costa Pessoa in *Comprehensive Coordination Chemistry*; G. Wilkinson; R.D. Gillard and J.A. McCleverty, Eds., Oxford, Pergamon, 1987, p. 453–583.
145. N.D. Chasteen, in: J. Reuben (Ed.), *Biological Magnetic Resonance*, Plenum, New York 1981, 53.
146. K. Wüthrich, “Elektronenspinresonanz-untersuchungenvon  $\text{VO}^{2+}$ -komplexverbindungen in wässriger Lösung II”, *Helv. Chim. Acta.*, 48 (1965) 1012–1017.
147. D. Rehder, C. Weidemann, A. Duch and W. Pribsch, “Vanadium-51 shielding in vanadium(V) complexes: a reference scale for vanadium binding sites in biomolecules”, *Inorg. Chem.*, 27 (1988) 584–587.
148. N. Butenko, I. Tomaz, O. Nouri, E. Escribano, V. Moreno, S. Gama, V. Ribeiro, J.P. Telo, J. Costa Pessoa and I. Cavaco, “DNA cleavage activity of  $\text{V}^{\text{IV}}\text{O}(\text{acac})_2$  and derivatives”, *J. Inorg. Biochem.*, 103 (2009) 622–632.
149. I. Cavaco, J. Costa Pessoa, D. Costa, M.T.L. Duarte, R.D. Gillard and P.M. Matias, “N-Salicylideneamino acidate complexes of oxovanadium(IV). Part 1. Crystal and molecular structures and spectroscopic properties”, *J. Chem. Soc. Dalton Trans.*, (1994) 149–157.
150. J. Costa Pessoa, M.J. Calhorda, I. Cavaco, I. Correia, M.T. Duarte, V. Felix, R.T. Henriques, M. F.M. Piedade and I. Tomaz, “Molecular modeling studies of N-salicylideneamino acidato complexes of oxovanadium(IV). Molecular and crystal structure of a new dinuclear  $\text{LOV}^{\text{IV}}\text{-O-V}^{\text{V}}\text{OL}$  mixed valence complex”, *J. Chem., Soc. Dalton Trans.*, (2002) 4407–4415.
151. G. Martini, M.F. Ottaviani and G.L. Seravalli, “Electron spin resonance study of vanadyl complexes adsorbed on synthetic zeolites”, *J. Phys. Chem.*, 79 (1975) 1716–1720.
152. D. C. Crans, A. D. Keramidis, S. S. Amin, O. P. Anderson and S. M. Miller, “Six-coordinated vanadium(IV) and (V) complexes of benzimidazole and pyridyl containing ligands”, *J. Chem. Soc., Dalton Tans.*, (1997) 2799 – 2812.

## References

---

153. K. Srinivasan, P. Michaud and J. K. Kochi, "Epoxidation of olefins with cationic (salen)manganese(III) complexes. The modulation of catalytic activity by substituents", *J. Am. Chem. Soc.*, 108 (1986) 2309–2320.
154. R. Irie, Y. Ito and T. Katsuki, "Donor ligand effect in asymmetric epoxidation of unfunctionalized olefins with chiral Salen complexes", *Synlett.*, (1991) 265–266.
155. S.B. Kumar, S.P. Mirajkar, G.C.G. Pais, P. Kumar and R. Kumar, "Epoxidation of styrene over a titanium silicate molecular sieve TS-1 using dilute H<sub>2</sub>O<sub>2</sub> as Oxidizing Agent", *J. Catal.*, 156 (1995) 163–166.
156. J.D. Koola and J.K. Kochi, "Charge-transfer interactions of amines with tetrahalomethanes. X-ray crystal structures of the donor-acceptor complexes of quinuclidine and diazabicyclo[2.2.2]octane with carbon tetrabromide", *J. Org. Chem.*, 52 (1987) 4545 – 4553.
157. D. Rehder, *Bioinorganic Vanadium Chemistry*, John Wiley & Sons, New York, 2008.
158. M.A. Anderson, A. Willets and S. Allenmark, "Asymmetric Sulfoxidation Catalyzed by a Vanadium-Containing Bromoperoxidase", *J. Org. Chem.*, 62 (1997) 8455–8458.
159. H. B. ten Brink, H. E. Schoemaker and R. Wever, "Sulfoxidation mechanism of vanadium bromoperoxidase from *Ascophyllum nodosum*", *Eur. J. Biochem.*, 268 (2001) 132–138.
160. A.G.J. Ligtenberg, R. Hage and B.L. Feringa, "Catalytic oxidations by vanadium complexes", *Coord. Chem. Rev.*, 237 (2003) 89–101.
161. A. Butler, M. J. Clague and G. E. Meister, "Vanadium peroxide complexes", *Chem. Rev.*, 94 (1994) 625–638.
162. A. Kitaygorodskiy and V.S. Kulikova, "Alkane oxygenation with H<sub>2</sub>O<sub>2</sub> catalysed by FeCl<sub>3</sub> and 2,2'-bipyridine", *J. Chem. Soc., Perkin Trans. 2* (2001) 1351–1371.
163. Y.N. Kozlov, V.B. Romakh, A. Kitaygorodskiy, P. Buglyóo, G. Süss-Fink and G. B. Shul'pin, "Oxidation of 2-propanol and cyclohexane by the reagent "hydrogen peroxide-vanadate anion-pyrazine-2-carboxylic acid": Kinetics and mechanism", *J. Phys. Chem. A*, 111 (2007) 7736–7752.

164. R.Z. Khaliullin, A.T. Bell and M. Head-Gordon, "A Density Functional theory study of the mechanism of free radical generation in the system vanadate/PCA/H<sub>2</sub>O<sub>2</sub>", *J. Phys. Chem. B*, 109 (2005) 17984–17992.
165. M.V. Kirillova, M.L. Kuznetsov, V.B. Romakh, L.S. Shul'pina, J.J.R. Fraústo da Silva, A.J.L. Pombeiro and G. B. Shul'pin, "Mechanism of oxidations with H<sub>2</sub>O<sub>2</sub> catalyzed by vanadate anion or oxovanadium(V) triethanolamine (vanadatrane) in combination with pyrazine-2-carboxylic acid (PCA): Kinetic and DFT studies", *J. Catal.*, 267 (2009) 140–157.
166. D. V. Deubel, G. Frenking, P. Gisdakis, W. A. Herrmann, N. Rosch, J. Sundermeyer, "Olefin epoxidation with inorganic peroxides. Solutions to four long-standing controversies on the mechanism of oxygen transfer", *Acc. Chem. Res.*, 37 (2004) 645–652.
167. M.L. Kuznetsov and J. Costa Pessoa, "Epoxidation of olefins catalysed by vanadium-salan complexes: a theoretical mechanistic study", *Dalton Trans.*, 2009, 5460–5468.
168. H. Gröger, "Catalytic enantioselective strecker reactions and analogous syntheses", *Chem. Rev.*, 103 (2003) 2795–2828.
169. P. G. Cozzi, "Metal–Salen Schiff base complexes in catalysis: Practical aspects", *Chem. Soc. Rev.*, 33 (2004) 410–421.
170. K. I. Smith, L. L. Borer, and M. M. Olmstead "Vanadium(IV) and Vanadium(V) Complexes of Salicyladimine Ligands", *Inorg. Chem.*, 42 (2003) 7410–7415.
171. M.R. Maurya, S. Sikarwar and P. Manikandan, "Oxovanadium(IV) complex of 2-( $\alpha$ -hydroxyethyl)benzimidazole covalently bonded to chloromethylated polystyrene for oxidation of benzoin", *Appl. Catal., A: Gen.*, 315 (2006) 74–82.
172. E.N. Jacobsen, W. Zhang, M. G'uler, "Electronic tuning of asymmetric catalysis", *J. Am. Chem. Soc.*, 113 (1991) 6703–6704.
173. M. S. Niasari, "Nanoscale microreactor-encapsulation of 16-membered hexaaza macrocycle nickel(II) complexes: In situ one-pot template synthesis (IOPTS), characterization and catalytic activity", *Micropor. Mesopor. Mater.*, 92 (2006) 173 - 180.

## References

---

174. K.C. Gupta, A.K. Sutar and C.-C. Lin, "Polymer-supported Schiff base complexes in oxidation reactions", *Coord. Chem. Rev.*, 253 (2009) 1926–1946.
175. N. Herron, "A cobalt oxygen carrier in zeolite-Y. A molecular ship in a bottle", *Inorg. Chem.* 25 (1986) 4714–4717.
176. G.S. Rafelt and J.H. Clark, "Recent advances in the partial oxidation of organic molecules using heterogeneous catalysis", *Catal. Today*, 57 (2000) 33–44 and references there in.
177. R.A. Sheldon, I.W.C.E. Arends and A. Dijkstra, "New developments in catalytic alcohol oxidations for fine chemicals synthesis", *Catal. Today*, 57 (2000) 157–166.
178. G.J. Hutchings, "New approaches to rate enhancement in heterogeneous catalysis", *Chem. Commun.*, (1999) 301–306.
179. M.R. Maurya, S.J.J. Titinchi and S. Chand, "Catalytic activity of chromium(III), iron(III) and bismuth(III) complexes of 1,2-bis(2-hydroxybenzamido)ethane (H<sub>2</sub>hybe) encapsulated in zeolite-Y for liquid phase hydroxylation of phenol", *J. Mol. Catal. A: Chem.*, 214 (2004) 257–264.
180. W. Zeng, J. Li and S. Qin, "The effect of aza crown ring bearing salicylaldimine Schiff bases Mn(III) complexes as catalysts in the presence of molecular oxygen on the catalytic oxidation of styrene", *Inorg. Chem. Commun.* 9 (2006) 10–12.
181. B.M. Choudary and P.N. Reddy, "A new peroxo vanadium catalyst for selective oxidation of aralkenes to benzaldehyde", *J. Mol. Catal. A: Chem.*, 103 (1995) L1–L3.
182. S.S. Kurek, P. Michorczyk and A.-M. Balisz, "The oxidation of styrene in the presence of thiols and porphyrin", *J. Mol. Catal. A: Chem.*, 194 (2003) 237–248.
183. J.-Y. Liu, X.-F. Li, Y.-Z. Li, W.-B. Chang and A.-J. Huang, "Oxidation of styrene by various oxidants with different kinds of metalloporphyrins", *J. Mol. Catal. A: Chem.*, 187 (2002) 163–167.



184. N. Ma, Y. Yue, W. Hua and Z. Gao, "Selective oxidation of styrene over nanosized spinel-type  $Mg_xFe_{3-x}O_4$  complex oxide catalysts", *Appl. Catal. A: Gen.*, 251 (2003) 39–47.
185. L.M. Kustov, A.L. Tarasov, V.I. Bogdan, A.A. Tyrlov and J.W. Fulmer, "Selective oxidation of aromatic compounds on zeolites using  $N_2O$  as a mild oxidant: A new approach to design active sites", *Catal. Today*, 61 (2000) 123–128.
186. Y. Luo and J. Lin, "Synthesis and characterization of Co(II) salen functionalized MCM-41-type hybrid mesoporous silicas and their applications in catalysis for styrene oxidation with  $H_2O_2$ ", *Microbor. Mesopor. Mater.* 86 (2005) 23–30.
187. P. Chutia, S. Kato, T. Kojima and S. Satokawa, "Synthesis and characterization of Co(II) and Cu(II) supported complexes of 2-pyrazinecarboxylic acid for cyclohexene oxidation", *Polyhedron*, 28 (2009) 370–380.
188. I. Kuźniarska-Biernacka, K. Biernacki, A.L. Magalhães, A.M. Fonseca and I.C. Neves, "Synthesis of a new type of immobilized chiral salen Mn(III) complex as effective catalysts for asymmetric epoxidation of unfunctionalized olefins", *J. Catal.*, 278 (2011) 102–110.
189. M.R. Maurya, C. Haldar, S. Behl, N. Babu and F. Avecilla, "Copper(II) Complex of Monobasic Tridentate ONN Donor Ligand: Synthesis, Encapsulation in Zeolite-Y, Characterization and Catalytic Activity", *J. Coord. Chem.*, (2011) In press.
190. E.I. Solomon, P. Chen, M. Metz, S.-K. Lee and A.E. Palmer, "Oxygen binding, activation, and reduction to water by copper proteins", *Angew. Chem. Int. Ed.*, 40 (2001) 4570 – 4590.
191. J.P. Klinman, "Mechanisms whereby mononuclear copper proteins functionalize organic substrates", *Chem. Rev.*, 96 (1996) 2541 – 2561.
192. K.D. Karlin, J.C. Hayes, Y. Gultneh, R.W. Cruse, J.W. McKown, J.P. Hutchinson and J. Zubieta, "Copper-mediated hydroxylation of an arene: Model system for the action of copper monooxygenases. Structures of a binuclear copper(I) complex and its oxygenated product", *J. Am. Chem. Soc.*, 106 (1984) 2121 – 2128.